DOT/FAA/CT-94/11

FAA Technical Center
Atlantic City International Airport,
N.J. 08405

Emerging Nondestructive Inspection for Aging Aircraft

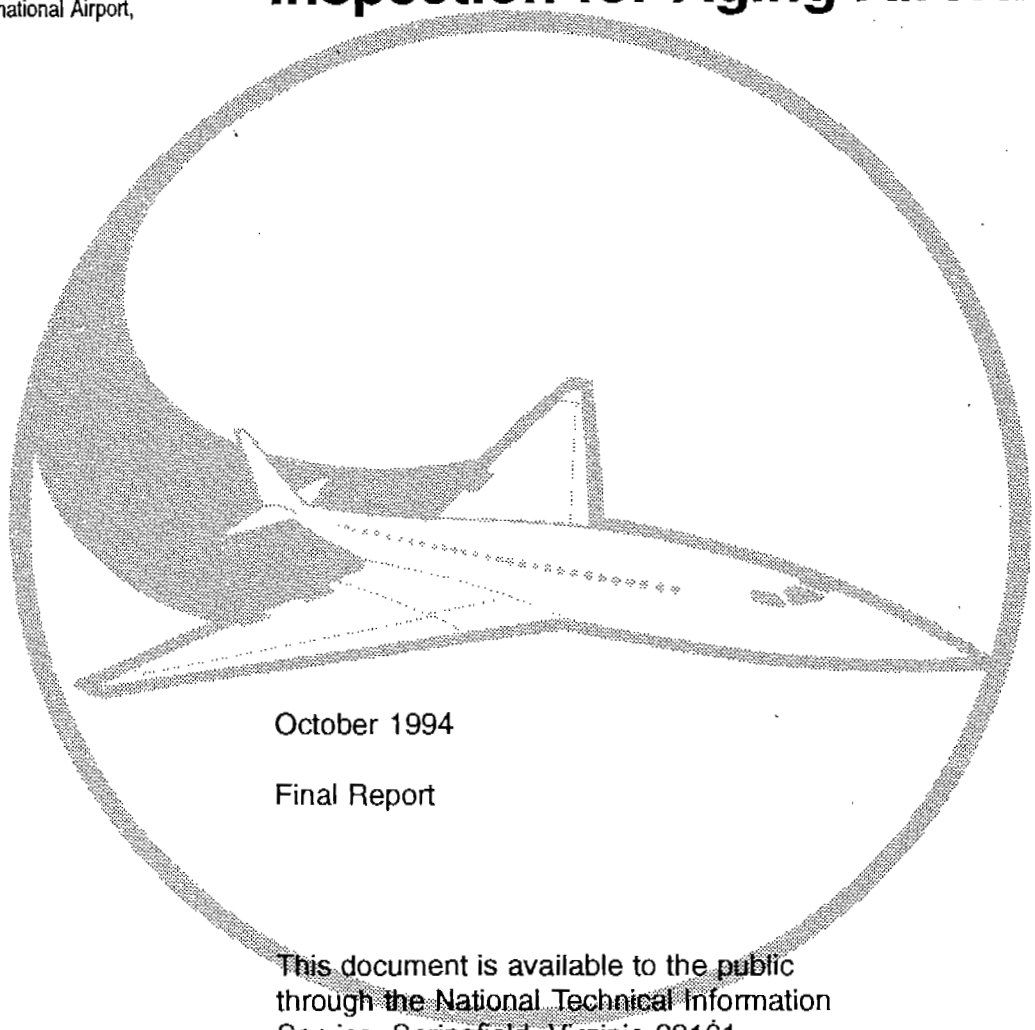

October 1994

Final Report

U.S. Department of Transportation
Federal Aviation Administration

NOTICE

This document is disseminated under the sponsorship of the U. S. Department of Transportation in the interest of information exchange. The United States Government assumes no liability for the contents or use thereof.

The United States Government does not endorse products or manufacturers. Trade or manufacturers' names appear herein solely because they are considered essential to the objective of this report.

Technical Report Documentation Page

1. Report No.	2. Government Accession No.	3. Recipient's Catalog No.
DOT/FAA/CT-94/11		

4. Title and Subtitle	5. Report Date
Emerging Nondestructive Inspection Methods for Aging Aircraft	October 1994
	6. Performing Organization Code

7. Author(s)	8. Performing Organization Report No.
Allan Beattie, Lutz Dahlke, John Gieske, Bruce Hansche, Gary Phipps, Dennis Roach, Rich Shagam, & Kyle Thompson	

9. Performing Organization Name and Address	10. Work Unit No. (TRAIS)
Sandia National Laboratories Aging Aircraft NDI Validation Center Albuquerque New Mexico 87185	11. Contract or Grant No.

12. Sponsoring Agency Name and Address	13. Type of Report and Period Covered
U.S. Department of Transportation Federal Aviation Administration Technical Center Atlantic City International Airport, NJ 08405	Final Report
	14. Sponsoring Agency Code ACD-220

15. Supplementary Notes

Dennis Roach, Sandia National Laboratories, Aging Aircraft Project Engineer
Dave Galella, FAA Technical Monitor

16. Abstract

This report identifies and describes emerging nondestructive inspection (NDI) methods that can potentially be used to inspect commercial transport and commuter aircraft for structural damage. The nine categories of emerging NDI techniques are acoustic emission, x-ray computed tomography, backscatter radiation, reverse geometry x-ray, advanced electromagnetics (including magneto-optic imaging and advanced eddy current techniques), coherent optics, advanced ultrasonics, advanced visual and infrared thermography. The physical principles, generalized performance characteristics, and typical applications associated with each method are described. In addition, aircraft inspection applications are discussed along with the associated technical considerations. Finally, each technique's status is presented with a discussion on when they may be available for use in actual aircraft maintenance programs. It should be noted that is a companion document to DOT/FAA/CT-91/5, "Current Nondestructive Inspection Methods for Aging Aircraft."

17. Key Words	18. Distribution Statement
Acoustic Emission, Reverse Geometry X-ray, Backscatter Radiation, Coherent Optics, X-ray Computed Tomography, Magneto-optic Eddy Current, Advanced Eddy Current, Advanced Ultrasonic, Advanced Visual, Infrared Thermography, Nondestructive Inspection	Document is available to the public through the National Technical Information Service, Springfield, Virginia 22161

19. Security Classif. (of this report)	20. Security Classif. (of this page)	21. No. of Pages	22. Price
Unclassified	Unclassified	166	

Form DOT F1700.7 (8-72) Reproduction of completed page authorized

Preface

In August 1991, a major center with emphasis on validation of nondestructive inspection (NDI) techniques for aging aircraft was established at Sandia National Laboratories by the Federal Aviation Administration (FAA). This center, called the Aging Aircraft NDI Validation Center (AANC), is tasked through FAA Interagency Agreement DTFA-03-91-A-00018. This agreement provided the following tasking statement: "The task assignments call for Sandia to support technology transfer, technology assessment, technology validation, data correlation, and automation adaptation as ongoing processes." Key to accomplishing this tasking is the FAA/AANC, which resides in a hangar at the Albuquerque International Airport. Other contributors to the AANC consortium include Science Applications International Corporation, New Mexico State University, and AEA Technology.

In association with this general charter, the AANC was tasked with producing this document describing emerging NDI techniques for aging aircraft inspections. Each chapter was authored by appropriate NDI technical experts in each of the different disciplines. Input was also provided by various researchers throughout the NDI industry. The purpose of this report is to present a detailed, consolidated description of the prevalent emerging NDI techniques and to discuss their potential applications to the inspection demands brought about by the expanding fleet of aging aircraft. "Emerging Nondestructive Inspection Methods for Aging Aircraft" is an overview document that is intended to provide a backdrop for future NDI development and validation.

TABLE OF CONTENTS

LIST OF ILLUSTRATIONS

LIST OF TABLES

ACRONYMS

AANC	Aging Aircraft NDI Validation Center
AEA	Atomic Energy Authority (UK)
AEMS	Acoustic Emission Monitoring Service
ANN	artificial neural network
ASME	American Society of Mechanical Engineers
ASTM	American Society for Testing Materials
AU	acousto-ultrasonics
CAD	computer-aided design
CASR	Center for Aviation System Reliability
CBI	Compton backscatter imaging; Compton backscatter inspection
CCD	charge-coupled device
CNDE	Center for Nondestructive Evaluation
CPU	central processing unit
CRT	cathode ray tube
CT	computed tomography
DSTO	Defense Science and Technology Organization (Australia)
EDM	electron discharge machining; electrical discharge machining
EMAT	electromagnetic acoustic transducer
ESPI	electronic speckle-pattern interferometry
FAA	Federal Aviation Administration
FAATC	Federal Aviation Administration Technical Center (Atlantic City, NJ)
FFT	Fast Fourier Transform
F-map	feature mapping
LLW	leaky Lamb wave
MAUS	mobile automated ultrasonic scanner
MOI	magneto-optic eddy current imager
NAARP	National Aging Aircraft Research Program
NADC	Naval Air Development Center
NASA	National Aeronautics and Space Administration (US)
NDE	nondestructive evaluation
NDI	nondestructive inspection
NDT	nondestructive testing
NTSC	National Transportation Systems Center
OEM	original equipment manufacturer
PAC	Physical Acoustics Corporation
POD	probability of detection
PRI	Physical Research Instrumentation, Inc.
QA	quality assurance
RAF	Royal Air Force
RGX	reverse geometry X-ray
SAIC	Science Applications International Corporation
SH	shear horizontal
SMOOPI	Shadow Moiré Out-of-Plane Interferometric (Damage Detector)
SSID	Supplemental Structural Inspection Document
SV	shear vertical
SWF	stress-wave-factor
TOF	time-of-flight
2D	two-dimensional
3D	three-dimensional

EXECUTIVE SUMMARY

This report investigates the major emerging NDI techniques that are currently available or are being developed for application to the detection and evaluation of flaws in aging aircraft. The information has been taken primarily from research laboratories and from open literature publications of development centers and private industry and has been reinforced in many instances by private communication with the companies.

As applied to aircraft inspections, many of the techniques are still in the developmental stage. The objective of this report is to present the technical background of the major emerging NDI techniques, discuss their generic applications and, in particular, their real and potential applications to NDI of aging aircraft, discuss the technical considerations for their use (listing advantages and disadvantages), give the status of each with respect to nondestructive inspection of aging aircraft, and discuss what might be expected of each technique in the future. The major emerging NDI technologies for aging aircraft are discussed in this report.

Acoustic emission testing detects bursts of high-frequency sound generated by flaws in a material under stress and for some applications can locate flaws in a structure and evaluate their growth rate in a single test. Although it cannot size the flaw, its locating capabilities may have the potential to greatly reduce the area that must be scanned by other NDI methods.

X-ray computed tomography (CT) collects X-ray transmissions from many angles around a component to digitally map the relative linear attenuation coefficient of small-interior volume elements. It provides cross-sectional views of the component's internal structure that are free of the shadowing and superposition of film radiographs. CT provides quantitative spatial and material/density assessments from which inaccessible regions of a component can be measured and flaw sizes gauged; however, component size limitations do exist.

Reverse geometry X-radiography uses an electronic point detector and a raster-scanned large-area X-ray source. Unlike conventional radiography, the radiographic object need be only in the proximity of the X-ray source. This "reverse radiography" technique provides scatter-free digital radiographic images in seconds. The system's contrast sensitivity is superior to that of standard radiography, and its spatial resolution is comparable. Its greatest potential lies in the detection of corrosion in aircraft aluminum and small density changes in composite materials.

Two ***advanced electromagnetic techniques*** are presented: Magneto-optic eddy current imaging and advanced eddy current techniques. ***Magneto-optic eddy current imaging (MOI)*** does real-time visual imaging of airframe fatigue cracks and corrosion. Evaluations of MOI by both airplane manufacturers and airlines has shown that inspection of large areas for cracks and corrosion is rapid and can be performed through paint and airline decals. Its use requires little training, and interpretation of the visual image is fairly intuitive. One limitation is its inability to inspect raised surfaces, such as button-head rivets.

Advanced eddy current techniques employ multiple-frequency and pulsed eddy current phenomena. These techniques improve inspection capabilities for fatigue crack and corrosion detection, particularly in subsurface or second-layer structures. Computerization and signal processing of eddy current signals are advancing the interpretation of low-level detection of cracks and corrosion that cannot be detected by manual techniques alone. Eddy current C-scan imaging is becoming available through the use of encoded scanning devices. The capability of these techniques to inspect multiple layers with a single scan reduces inspection time.

Coherent optic methods include holographic interferometry (holometry), electronic speckle pattern interferometry, and shearography. These are all wide-area interferometric imaging techniques that are capable of detecting micron-sized displacements of the surface of an object such as the skin of an aircraft. The object under test must be stressed to cause the surface to deform anomalously where a flaw is present. Coherent optics techniques are most useful for detecting debonds or delaminations; flaws that do not bulge under stress, such as cracks, are difficult to detect. Shearography's relative insensitivity to object motion provides an advantage over holometry for field inspections.

The two ***advanced ultrasonic techniques*** presented are ***laser ultrasonic methods*** and methods that use ***electromagnetic acoustic transducers*** (EMATs). The development of laser pulse generation and laser beam detection methods has reached the stage where both methods can be applied to the inspection of aircraft structures. Both are non-contact and remote—features that lend themselves to fast and wide-area scanning. The wide variety of wave propagation modes available with EMATs enable the inspector to choose the mode most sensitive to detection of the particular type of flaw of interest in a specific aircraft structure. Portable computer systems have become available that can be applied to aircraft NDI inspections to increase reliability and effectiveness.

Advanced visual inspection methods are moiré and structured-light-based optical profilometry, Diffracto Sight (a patented process developed by Diffracto, Ltd.), and video image enhancement analysis. Moiré and structured light are methods to visualize and quantify surface height irregularities, Diffracto Sight is a surface slope visualization technique, and video image processing is a computer-based methodology for enhancing and analyzing video images for flaw detection. The most promising applications for these advanced visual techniques are detection and classification of corrosion-induced paint liftoff and pillowing induced by corrosion between faying surfaces and in areas that would normally require disassembly. Diffracto sight and video image enhancement and analysis are being investigated for commercialization.

Infrared thermography is being investigated by several entities for detecting such flaws as corrosion and debonds. By the judicious application of external heat sources, thermography systems can monitor the temperature distribution on an aircraft component. This information is then used to characterize the thermal properties, and thus flaws of the structure being tested. The more advanced systems are in the prototype stage, and their design and operational feasibility for use on transport aircraft is being evaluated.

INTRODUCTION

Background

Over the past decade, the commercial aviation industry has experienced a substantial growth in its aging aircraft fleet due to increasing airlift demands coupled with the high cost of aircraft replacement. In 1989, the average age of the commercial fleet was 12.7 years with 25 percent of the fleet exceeding the estimated economical design life of 20 years. If this trend continues, 60 percent of the current commercial aircraft fleet will exceed their economic design life by the year 2000.

Chronological age alone is not an effective measure of aircraft condition. The most important indicator is the number of flights; other factors include flight time, environmental exposure, and usage patterns. It is clear that the total usage of the U.S. fleet is increasing to unprecedented levels in every aspect: age, number of flights, and flight hours.

In 1978, fail-safe design requirements gave way to the damage tolerance approach. Damage tolerance requires that the structure be capable of sustaining small cracks without failure, and that an inspection program be instituted to detect such cracks before they grow to a critical length. This damage tolerance philosophy recognizes the impossibility of establishing complete structural redundancy (the fail-safe premise) and places greater emphasis on inspection. The FAA issued Advisory Circular (AC) 91-56 in 1981 which provided a means for aircraft maintenance and inspection procedures to meet damage tolerance criteria. It required the evaluation of structures using fracture mechanics analyses to develop supplemental structural inspections. Through the resulting Supplemental Structural Inspection Document (SSID) program, fail-safe designed aircraft were brought into conformance with the damage tolerance approach by means of an updated inspection program.

Maintenance programs, which include Airworthiness Directives, Service Bulletin Compliance Documents, Supplemental Structural Inspection Documents, and Corrosion Prevention and Control Programs, are essential to ensure a continuous high level of safety. Existing NDI techniques play a critical role in these programs through the detection of cracks, corrosion, and disbonds. However, the extended usage of aircraft means that the occurrence of fatigue cracks and other flaws can be expected to increase, thus increasing the probability that some will escape detection. In addition, known problem areas, which are subjected to "directed inspections," use labor intensive NDI techniques in order to achieve high probabilities of detection. It is not economically desirable to apply these methods to an entire airplane. This situation highlights the need for improved and more cost effective NDI methods.

The three main potential causes of structural failure in aging aircraft are cracks, corrosion, and structural debonds. ***Fatigue cracks*** occur in structures that have been subjected to repeated stress cycles. These cracks typically initiate where the design or surface conditions provide points of stress concentration. Original fatigue goals based on the initial design life estimates of the aircraft may, at some point, not adequately cover older aircraft. Thus, new inspection techniques, with the ability to inspect large areas while still retaining the ability to resolve small details, are needed.

Corrosion is neither new nor limited to aging aircraft. Corrosion is highly operator dependent and is widespread in aircraft that have not had the benefit of a program for inhibiting corrosion during early in-service life. It tends to occur in hidden areas and, unlike cracks, may have poorly defined boundaries. Inspection problems associated with this type of defect are exacerbated by the fact that corrosion is not always time dependent.

Debonds may lead to adhesive joint failures and/or cracking in cases where rivets are also present, due to higher-than-anticipated stresses at those sites. Disbonding by its nature occurs at an interface and is, therefore, always hidden. The interactions at the bond interface are extremely complex, with the result that the strength of the bond is difficult to predict or measure. Even a partial debond may compromise the integrity of a structural assembly. Therefore, it is necessary to detect all areas of disbonding as early as possible before joint failures or fatigue cracking can occur.

Purpose

Developments in NDI technology need to keep pace with an increasing number of SSID-directed inspections along with a possible increase in aircraft flaws brought on by extended aircraft use. The purpose of this document is to describe emerging NDI techniques under consideration by the FAA. The FAA's National Aging Aircraft Research Program (NAARP) addresses current and future commercial aircraft inspection requirements.

Scope

This document describes several emerging NDI techniques that are applicable to aging aircraft inspection issues. All chapters have been structured in a similar format that shows the reader the basis for assessing the technology for a particular NDI application. The "Technical Background" section provides the physical principles on which the technique is based. The "Applications" section describes how the technique is currently being applied in industry and how it may be applied if, after suitable evaluation, it appears to meet specific aircraft inspection needs. "Technical Considerations" are presented to discuss the issues that must be considered when applying a particular technique to an aircraft inspection task. The "Status" section, divided into Present and Future, summarizes the state of ongoing research and development and possible timelines to actual aircraft use. Finally, a list of references are included at the end of each section.

The following NDI methods are presented:

1. Acoustic Emission Testing
2. X-ray Computed Tomography
3. Backscatter Radiation
4. Reverse Geometry X-ray
5. Advanced Electromagnetics—including Magneto-optic Imaging and Advanced Eddy Current Techniques
6. Coherent Optics
7. Advanced Ultrasonics
8. Advanced Visual
9. Infrared Thermography.

This document does not discuss advances in peripheral technology that may benefit NDI techniques. Development of automated scanners and robotic manipulators, for example, will permit increased reliability of detailed inspection using several of the methods described in this paper. Advanced image processing and artificial intelligence methods such as neural networks, as well as computer based information management systems, will enhance existing systems and extend the value of these emerging NDI technologies.

1. ACOUSTIC EMISSION TESTING.

1.1 SUMMARY.

Acoustic emission is a NDE technique that detects bursts of high-frequency sound generated by flaws in a material under stress. These acoustic emission bursts can be used both to locate flaws and to evaluate their rate of growth as a function of applied stress. Acoustic emission testing has an advantage over other NDE methods, in that it can detect and locate all of the activated flaws in a structure in one test. Acoustic emission does not now have the ability to size flaws but it can greatly reduce the area needed to be scanned by other NDE methods. Acoustic emission technology has been applied quite successfully in monitoring proof tests of pressure vessels and tests of fiber-reinforced plastic structures of all kinds. There are now ASTM standards and ASME codes applying to its use in testing gas cylinders, and both metal and fiber-reinforced plastic vessels, tanks, and piping. The application of acoustic emission testing to aircraft has required a new level of sophistication, both in testing techniques and data interpretation, because of the complexity of aircraft structures. The technology has progressed to the state where there are currently two acoustic emission testing programs being applied to fleets of aircraft. These are the US and Australian F-111 fighter/bomber fleet and the English Royal Air Force fleet of VC-10 transport aircraft. Though not available at the time of this document publication, a study of the results of these two programs along with the results of research programs in Canada and Australia should give a good estimate of the increase in testing reliability and decrease in testing costs possible with acoustic emission testing of aircraft.

1.2 TECHNICAL BACKGROUND.

1.2.1 Introduction.

In contrast with most NDI techniques, acoustic emission testing is passive, not active. No external energy is introduced into the test object to probe its components as is done with ultrasonic, radiographic, and eddy current testing. Instead, the test object is usually stressed to a level 10 percent or more above its normal working load. Any defects that are induced to grow on even a microscopic level by this overload generate acoustic signals. Detection and analysis of these signals allow identification and location of the defects. Because there is no searching energy to be injected into the structure, there are no inaccessible areas due to its geometry. Acoustic emission testing gives information on defects throughout the entire volume of a structure. If the applied stress field on the structure duplicates the normal working stress fields, then acoustic emission detects only "pathological" defects, flaws that can grow under normal loads. Flaws that are not affected by working loads will not be detected. For a welded structure such as a pressure vessel, acoustic emission testing works well with relatively simple instrumentation. However, slight movement of bolted or riveted joints can also generate acoustic signals. Thus, a complex structure may have many acoustic sources besides flaws in its components. These unwanted emission sources greatly complicate acoustic emission tests of complex structures, such as aircraft. The difficulties are not prohibitive, but they put a premium on the intelligent use of signal processing and interpretation.

1.2.2 Description.

The terminology "acoustic emission" is widely used to describe both the testing technique and the acoustic waves emitted by a material. (However, in this section, the term "acoustic emission

testing" is used to refer to the testing technique.) Acoustic waves are generated when a small region of a material undergoes a rapid change in its local stress state. Such a change can be associated with a large number of mechanisms. Examples of such mechanisms are twining, local yielding, transgranular and intergranular fracture of crystallites, and the propagation of cracks in engineering materials. A phase transformation of a crystallite producing a volume mismatch with the surrounding material is another common emission source. In composites, the fracture of the matrix, fiber, or the fiber-matrix interface all generate acoustic waves. In general, most irreversible changes in the microscopic or macroscopic structure of a material will generate acoustic waves.

The acoustic signals created by these processes are initially impulsive in nature, usually being short bursts on the order of microseconds in length. As these signals propagate through the material, they result in transient acoustic waves that are hundreds of microseconds to tens of milliseconds in length. The impulsive nature of the mechanism generates a wide band of frequency components, extending from low audio frequencies up to a few megahertz. The upper frequency limit of the acoustic bursts is usually determined not by the generating mechanism but by the frequency-dependent attenuation of the material. For example, steel and aluminum may transmit acoustic waves with frequencies up to several megahertz, whereas some composites may attenuate most acoustic energy above 50 kHz. The acoustic bursts occur with random spacings in time between bursts. The average time between bursts can range from centuries in the case of earthquakes to less than microseconds during catastrophic failure. If the average time separating bursts is shorter than the burst length, the bursts will overlap and create a noise-like signal known as continuous emission.

The polarizations and amplitudes of the acoustic waves are strongly influenced by the microscopic environment of the region of generation. Thus, there may not be strong correlation between the characteristics of two acoustic waves generated by adjacent crystallites or even subsequent extensions of the same crack. There is a randomness in the characteristics of acoustic emission signals from the same test or even the same micro region. To further complicate the problem, solids have many modes of acoustic propagation, some of which are geometry dependent. The result is that by the time an acoustic wave propagates from its source to the detecting sensor, the original wave form may be drastically distorted and contain far more information about the path traveled than about the source of the wave. The relevant information conveyed by all acoustic emissions is that an event of measurable amplitude did happen, an approximate time when it happened, and some measure of the strength of the source.

1.2.3 Detection.

In practice, acoustic emission signals are normally detected by piezoelectric crystals or ceramics, which transform the acoustic wave into an electrical signal. These electrical signals are then amplified and analyzed by standard electronic techniques. Piezoelectric sensors are quite sensitive and can detect average displacements of a surface to within a small fraction of an atomic spacing. They are inexpensive and relatively rugged, but they do have limitations. The first is that they average the displacement over their entire surface area. This can significantly distort the signal from a high-frequency wave traveling parallel to the surface (surface wave). They also have mechanical resonances determined by their geometries which, at the least, distorts their response to the acoustic wave and, at the worst, removes almost all information except the amplitude and the existence of the wave. However, their ruggedness, simplicity, and ease of use make them the preferred sensor for most acoustic emission applications.

The size range of commercial acoustic emission sensors extends from a cylinder about 3 mm in diameter and 3 mm high to a cylinder 30 mm in diameter and 40 mm high. Their frequency responses cover the range from about 30 kHz to 1 MHz. The sensors often designated as "resonant" will have a dominant frequency response band but will also respond with lesser sensitivity to most other frequencies. Broad-band sensors have a smoother response over an extended frequency band, but their response is not "flat." Broad-band sensors are usually about an order of magnitude less sensitive than resonant sensors. In a single test, the dynamic range of the acoustic emission usually covers at least three orders of magnitude. As a result, even resonant sensors respond to a great many frequencies outside their resonant band.

Other methods of detecting acoustic emission exist. These include optical detection of a surface displacement, capacitative sensors, and magnetic detectors such as a phonograph pickup. All lack sensitivity compared to piezoelectric sensors. Laser interferometers have recently been developed into a useful laboratory tool that has the advantage of a large frequency range and a very small detection area. They can be high-fidelity sensors that almost eliminate the problem of averaging the surface displacement over the sensor area. However, at this time their expense, size, and complexity make them impractical for a large multi-channel test. Capacitance sensors, which also have a high-fidelity response, are confined to the laboratory and have several characteristics that make them of little use in field tests. Magnetic detectors generally do not have the necessary high-frequency response.

1.2.4 Signal Parameters.

A general introduction to the physics and electronics of acoustic emission is given in Reference 1-1. Figure 1-1 is from this reference and illustrates some commonly measured signal parameters. The most useful parameters in testing aircraft are (1) the time of arrival at a sensor to the nearest microsecond, (2) the acoustic emission count, which is the number of times the signal crosses a preset threshold in one direction, (3) the peak amplitude, defined as the maximum rectified voltage that a signal achieves, (4) the signal rise time, which is often defined as the time between the initial detection and the occurrence of the peak amplitude, (5) the signal length, which is the time between the initial detection of the signal and the time when it disappears into the background noise, (6) the signal strength (sometimes designated as energy), defined as the area under the envelope of the voltage-versus-time curve, and (7) the signal energy, defined as the area under the voltage squared versus time curve. A combination of these parameters from one or more sensors can allow the detection of a flaw, the determination of its location to various degrees of accuracy, and an estimate of its severity.

1.2.5 Instrumentation.

Acoustic emission instrumentation ranges from a sensor, an amplifier, and an oscilloscope or counter to sophisticated computerized instruments. At the high end, a system currently being used on the VC-10 aircraft consists of four linked 72-channel systems. Data acquisition and analysis speeds vary with both the system and the test setup. As an example, a current 24-channel system can record and process data in real time at input rates of up to ~50 burst emissions per second. Most systems have dynamic ranges for variations in signal energies up to

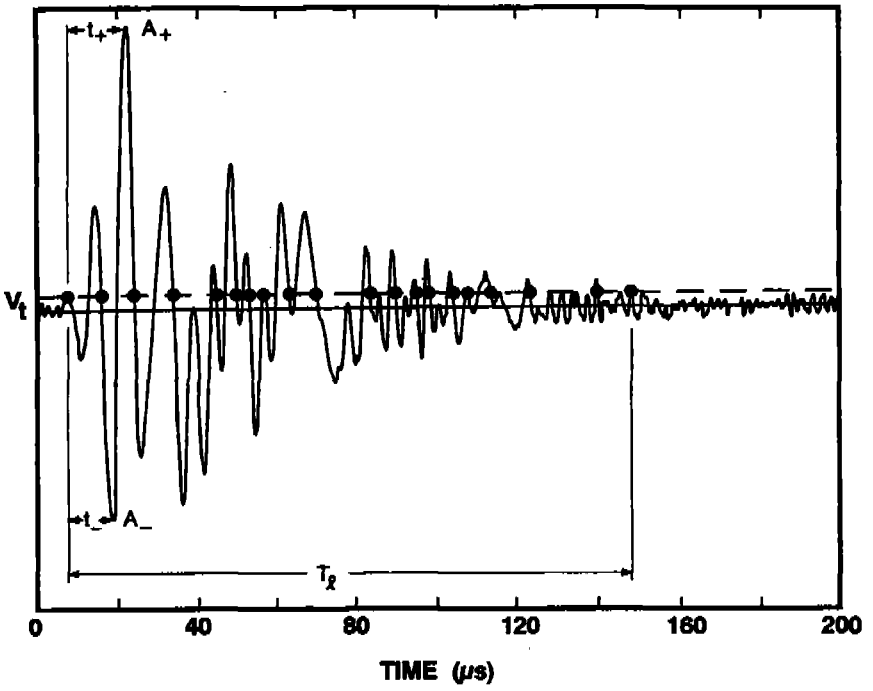

Figure 1-1. Simulated Acoustic Emission Signal Showing the Triggering Points for the Acoustic Emission Count. For this threshold, V_t, the count, N, is 20. Also shown are the rise times, t_+ and t_-; the peak amplitudes, A_+ and A_-; and the signal length, T_ℓ. In modern systems the maximum of the two rise times and of the two peak amplitudes is the one used.

~70 dB (variations in signal amplitudes up to a factor of ~3200). Current large systems are capable of acquiring the necessary data to test complex structures such as aircraft. The main problems are the difficulty of designing the test setup on complex structures and the difficulty in interpreting the data from field tests on real structures.

A single-channel acoustic emission system will record a set of signal parameters from one sensor. However, the recorded time of signal occurrence typically has less than millisecond accuracy. Multi-channel systems record the same parameters from each channel, but they also record either the absolute time or the relative time of arrival between different channels with sufficient accuracy to allow source location by triangulation. Triangulation is a calculation of the location of the emission source on a plane using the arrival times of the acoustic wave at three sensors, the locations of the three sensors, and the acoustic velocity in the plate. The location accuracy on a plane is affected by several factors, some of them being the thickness of the plate, the size of the sensors, and the feature of the wave form that triggers the system. Current systems are capable of locating a source to within one centimeter under favorable conditions and to within a few inches on many metal structures. Sources on structural members below the surface will be detected and an approximate location on the surface will be calculated; however, the accuracy of the location will be dependent on the exact geometry around the source.

1.2.6 Overall View of Acoustic Emission Testing.

Like all other NDE techniques, acoustic emission testing has its strengths and weaknesses. (These are enumerated in more detailed form in Section 1.5, Technical Considerations.) In

general, some of its strengths are the capability to do global monitoring, to both detect and locate flaws, and to detect all flaws affected by loading without regard to geometry. It also has the capability to detect flaw growth in real time and estimate relative flaw severity, thereby warning of an impending failure. The tests are often computerized, which allows the use of relatively untrained personnel after the initial design and setup and provides a permanent record of the results.

Acoustic emission testing also has some weaknesses. Although it is able to detect flaw growth, it is unable to assess the size of a flaw. It is capable of very high sensitivity which may allow the detection of flaws much smaller than the critical size, which can lead to worry or unnecessary repairs. The test object, such as an airplane, may be very complex and require highly skilled operators to design the test and carry out the initial setup. Finally, acoustic emission testing is primarily a negative test in that sound parts generate little or no emission. Therefore, a bad part which shows no emission because of an incompetent test may be declared good.

Where acoustic emission testing programs have been conducted by trained personnel fully aware of both the strengths and weaknesses, they have been remarkably successful. Acoustic emission testing has also succeeded in situations where other test methods are difficult to apply, such as finding flaws in fiber-reinforced plastic structures. The ability to test a whole structure at one time makes acoustic emission testing both time and cost effective.

1.3 PRESENT APPLICATIONS.

The field of acoustic emissions has developed into a maturing NDE technology over the last ten years, as reflected by the growing number of ASTM standards on acoustic emission and its incorporation into some ASME codes. It is now the NDE method of choice for most proof testing of structures made of fiber-reinforced composites and is widely used to test metal pressure vessels, storage tanks, and other potentially hazardous structures. Also, it has become an invaluable tool in material science laboratories; it is used in the electronics industry to detect loose particles in semiconductor packages, and has proven useful in weld and other process monitoring. Reference 1-2 gives an extensive review of current uses of acoustic emission testing.

1.4 AIRCRAFT APPLICATIONS.

Much experimentation with acoustic emission has been done in the aerospace industry, and some successful applications have been made to military aircraft. However, the technology has not been applied to the commercial aircraft fleet. One of the first successful applications was the testing of Polaris missile cases in the early 1960s. In the 1970s, many experimental programs applied acoustic emission testing to aerospace problems. Some of the early programs that should be mentioned are those by Lockheed-Georgia on structures and on in-flight tests on the C-5A,[1-3] by Battelle Northwest on in-flight monitoring on the Maccahi jet trainer,[1-4] and by McClellan Air Force Base work on testing honeycomb panels in the F-111 fighter.[1-5] The first acoustic emission testing on the ground of a fleet of airplanes was also on the F-111 using instrumentation developed by Dr. J. M. Carlyle of Physical Acoustics Corporation (PAC). The first in-flight acoustic monitoring of a fleet of airplanes was performed by Dr. S. L. McBride of the Royal Military College of Canada on the CF-100. Dr. Carlyle and PAC have now applied acoustic emission tests to a variety of transport aircraft. Dr. McBride (now with Acoustic Emission Monitoring Services Inc., AEMS) and his co-workers at the Royal Military College of Canada have a continuing program on in-flight and structural monitoring of mostly military aircraft. Drs. C. M. Scala and I. G. Scott of The Aeronautical Research

Laboratory, DSTO, Australia, have also done extensive work on applying acoustic emission testing to fighter aircraft.

1.4.1 Testing by Private Industry.

The Physical Acoustics Corporation has applied acoustic emission testing to three types of aircraft: the F-111 fighter/bomber, transport aircraft, and the VC-10 fleet.

1.4.1.1 F-111 Fighter/Bomber.

The F-111 has a variable-sweep wing, which is supported by a D6AC steel structure called a carry-through box. D6AC steel has both high strength and toughness, but it also has a small critical crack size,[1-6] as well as a rather high ductile-to-brittle transition temperature. This high-transition temperature, although normally not desirable, is used to advantage in acoustic emission testing. If the aircraft is cooled to −40°F (which is below the transition temperature) and loads are applied to the wings, any small cracks present in the steel will propagate. This crack propagation is detected by the acoustic emission it generates.

The Physical Acoustics Corporation was awarded a contract to implement acoustic emission monitoring of the F-111 during load testing at −40°F. The loads used are +7.3 g and −3.0 g at two different sweeps of the wings. Data was taken and analyzed. A commercial acoustic emission system was modified and then tested. More modifications were made and the system was then installed in the cold proof-testing chamber at McClellan AFB, Sacramento, CA. This system uses 28 sensors and is completely computerized. Because of complex geometries and acoustic noise sources such as slight movement under bolts, several types of signal processing were used. Guard sensors to exclude signals that did not originate in a predefined area, location by arrival times at different sensors, and location by the zone of sensitivity of the individual sensors were all used. The severity of the flaws was determined from the location, the signal amplitude, and the signal strength (called "energy" in PAC systems, also called MARSE in some papers and standards). One of the design criteria for the system was that it could be used by Air Force personnel and not require PAC engineers to run it. To this end, attempts were made to make the system user friendly. This included a color computer graphics display that shows the approximate location and severity of the flaws in real time. This display is shown in black and white in Figure 1-2.

Because of security restrictions, the results of this series of inspections are not available. However, it is reported that all U.S. and Australian F-111 aircraft are being inspected in this facility, and that cracks have been found by the acoustic emission system.

1.4.1.2 Transport Aircraft.

During the past several years, PAC has inspected several transport aircraft.[1-7] The program has been partially experimental with a large learn-as-you-test component included. Because most of these inspections have been performed for private companies, the detailed results are proprietary. Therefore, only brief descriptions of these inspections follow.

F-111 CPTS Acoustic Emission Monitoring System

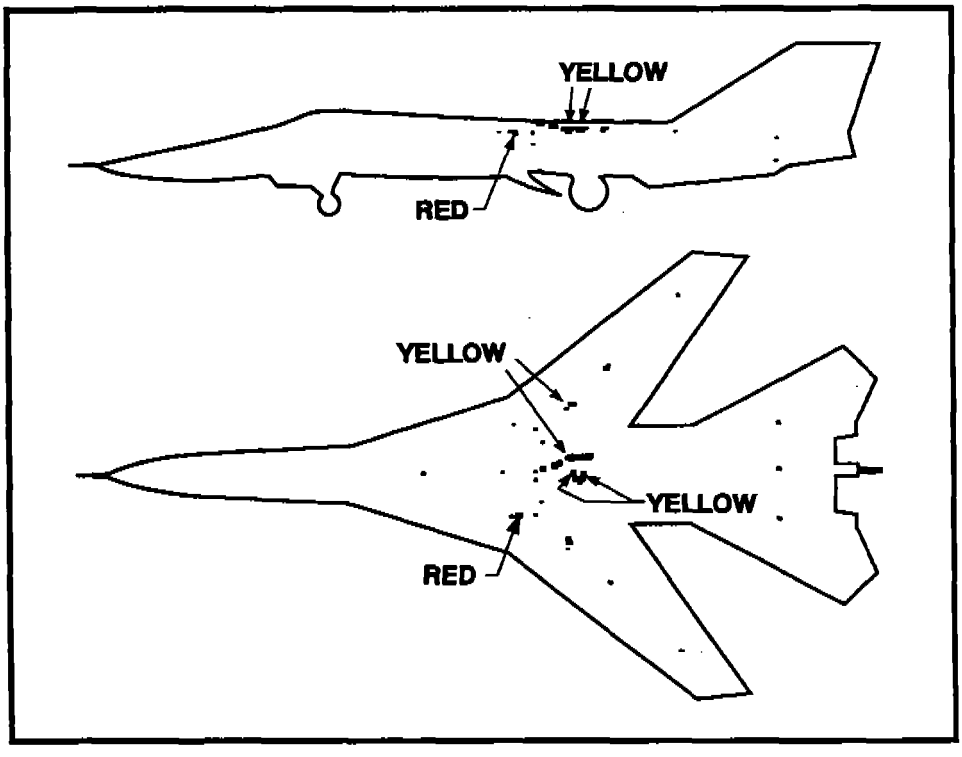

Figure 1-2. Color CRT Screen Showing Approximate Locations and Severity of Located Emissions on the F-111. Note the yellow events from a cracked tunnel truss, a yellow event from a disbonded wing joint, and the red event from a broken bolt in the wing carry-through box. The severity of the events is color coded. Green is least severe, yellow is moderately severe, and red is most severe. [Source: Physical Acoustics Corporation, Princeton, NJ. Printed with permission of John M. Carlyle.]

1.4.1.2.1 C-141 Test.

The aircraft had cracks in the right wing spar joint, and acoustic emission indicated that the left wing was also suspect. A posttest tear-down confirmed cracking in the left wing spar joint.

1.4.1.2.2 Boeing 707 Test.

Acoustic emission testing just before this aircraft was converted into a private business jet showed high-amplitude sources in both wings and at a site in the fuselage. During the rework, cracks were found in a wing joint and in an engine thrust link at the wing locations. Also, an improper repair in the pressure bulkhead was found at the indicated fuselage location.

1.4.1.2.3 Boeing 720 Test.

This was an early use of pressurization of the fuselage as the loading mechanism for an acoustic emission test. One of the cockpit window posts produced high-amplitude emission. Upon

disassembly, a 3/4-inch-long crack was found in the window-post forging. This crack had not been seen by radiography performed 100 flight hours before the acoustic emission test.

1.4.1.2.4 Boeing 727 Tests.

The upper lobe of a 727 was tested using fuselage pressurization for loading and 64 sensors applied to the upper fuselage. Twenty-eight emission sites were located. To check these sites for cracks in the skin, two different organizations performed eddy current tests. These tests gave quite different results—one reported cracks and approximate flaw lengths at 14 of the 28 sites; the other reported no cracks at any site. The eddy current measurements were hindered by layers of paint thick enough to visually hide the rivet lines. To the best of PAC's knowledge, these sites have not been further investigated.

Two more 727s have had acoustic emission tests with internal fuselage pressure loads. Both of these tests were designed to investigate the feasibility of detecting corrosion with acoustic emission. The results on the first test indicated that pressurization did not cause corrosion sites to produce acoustic emission. The results of the second test have not yet been released.

1.4.1.2.5 Boeing 737 Test.

This test was designed to look for problems in the belly area aft of the nose wheel. The test was performed just before several skin panels were replaced. No problems were found by the acoustic emission test, and none were found during the reskinning.

1.4.1.3 VC-10 Fleet.

In 1990, British Aerospace recommended to the Royal Air Force that they requalify the fuselages of their VC-10 fleet by pressure proof testing. PAC received a contract in conjunction with this proof testing to evaluate the effectiveness of using acoustic emission monitoring to detect structural damage. During this evaluation, it was determined that 288 sensors would be needed to perform source location on the complete fuselage. The evaluation showed the value of acoustic emission monitoring, and a contract was awarded PAC in 1991 to build a system and train Royal Air Force personnel to use it. The system was delivered in November 1991 and the first inspection was completed successfully in December. Eight aircraft were inspected in the first year. Figure 1-3 shows one of the VC-10s under test. By correlating the acoustic emission results with posttest structural findings, a data base will be built up which will both aid in the routine maintenance of the VC-10 and provide solid data on the value of acoustic emission monitoring of fuselages.

1.4.2 Canadian Program.

For almost twenty years, Professor S. L. McBride and his co-workers at the Royal Military College of Canada have been studying the use of acoustic emission to detect cracking in Canadian military aircraft.[1-8,1-9] This program has now been commercialized by AEMS. Most of the work has been aimed at in-flight monitoring of aircraft, but much of what has been learned can be applied to structural testing. The problem of how to distinguish a crack advancement signal from other acoustic signals present in the air frame is basic to any form of acoustic emission testing on aerospace structures.

These studies involved laboratory experiments and data recorded in flight. Sensors were attached to structural components of the aircraft, such as the forward wing trunnions, and the waveforms of the detected signals were recorded. Also recorded were the G loads on the plane

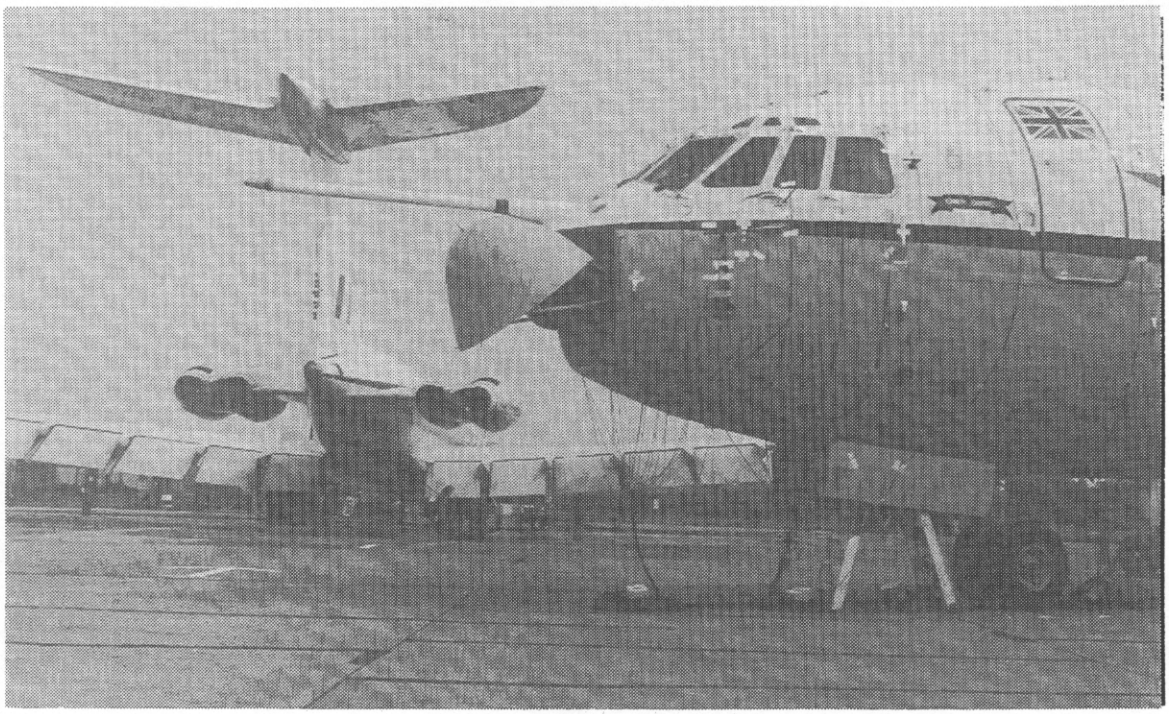

Figure 1-3. The Nose of a VC-10 Undergoing an Acoustic Emission Test of the Fuselage. Note the sensors and coaxial cables.

at the time the signals occurred. In some tests, one trunnion was deliberately cracked to provide a comparison between good and defective parts. The results of these experiments showed that crack signals could be identified by using a rigorously defined signal rise time, the relative arrival times at the different sensors that give the location of the source, and the force on the component when the emission occurred. Studies were also done on the in-flight noise environment. A wide variety of aircraft were used in these tests. The following aircraft were involved in this program: CC-115, CC-130, CF-5, CF-100, CF-104, CF-116, CT-114, UK-Tornado, and the US Navy A-7.

These studies led to the design and construction of a specialized acoustic emission instrument specifically for in-flight monitoring. Shortly after the development of this instrument, a long-term fatigue test on durability and damage tolerance was started on a CF-5 fighter aircraft. Several of the in-flight monitoring acoustic emission systems were combined to make a large multi-channel monitoring system. Sensors were applied to the lower wing skin of the aircraft at locations suggested by the fatigue test engineers. The intent of the test was to subject the aircraft to several lifetimes of fatigue, or stop the test if a major failure occurred before completion. The maximum loading was the equivalent of 7 g. There were 6.5 loadings per equivalent flying hour and 1.3 percent of these were to 7 g. Figure 1-4 gives some of the results. The upper bars show the number of emissions that occurred at each location, approximately at the maximum load. The lower bars show the number of defects at each position. Initially, other NDE techniques failed to show some of the cracks indicated by the acoustic emission. It was only after the wing was removed, turned upside down, and loaded that the cracks were found by these other NDE methods. The cracks had been under such high compressive stress that they were not seen by eddy current testing or liquid penetrants in the resting position of the wing. In further testing acoustic emission was able to detect cracks as much as 3000 effective

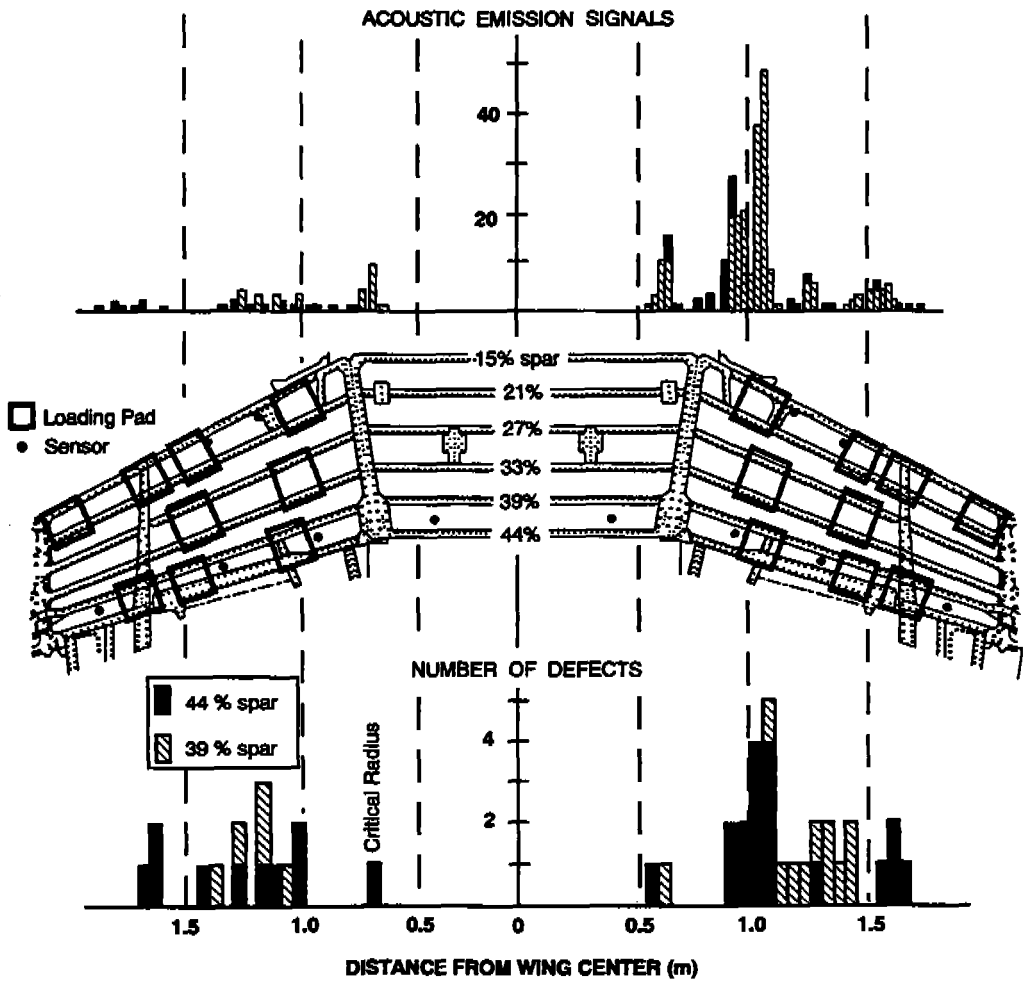

Figure 1-4. Comparison of the Acoustic Emission Event Histogram with the Defect Histogram from a Fatigue Test of a Jet Fighter. The acoustic emission data shows the number of events that occurred on the 39 percent and 44 percent wing spars during sixty-eight 7-g loadings. These events were collected only when the load was above 95 percent of maximum. The defects are those measured inside fastener holes using eddy current and liquid penetrant inspection. The percentages are the spar locations in percentage of wing chord. [Source: Acoustic Emission Monitoring Services, Inc., Ontario K7G 2V4, CANADA. Reprinted with permission of Dr. S. L. McBride, President.]

flying hours (out of 12,000) before other NDE techniques. It was also found that continuous monitoring during the fatigue test enhanced crack detection. Non-crack noise tended to average itself over the whole region whereas crack-produced noise always appeared at the same location. This observation tends to stress the value of in-flight monitoring of critical areas.

1.4.3 Australian Program.

The Australian DSTO Aeronautical Research Laboratory, under the direction of Drs. C. M. Scala and I. G. Scott, has been studying the application of acoustic emission testing to military aircraft for the past decade.[1-10,1-11] Their main programs included in-flight monitoring of the Macchi jet trainer, a full-scale fatigue test of a Mirage jet fighter, and a fatigue test of a wing attachment bulkhead of an F/A-18 aircraft. In the process of successfully detecting and locating

the cracks that formed in the Mirage wing spar and the F/A-18 bulkhead, they tried a variety of signal processing techniques to separate crack-produced emission signals from all of the other emission detected during the tests.

Adaptive signal-processing techniques were tried with little success. In adaptive processing, a training set of data that contains signals from known crack growth in the tested parts is needed. This data is hard to obtain for real aircraft both due to the complexity of the structure and the difficulty of knowing beforehand where these cracks will occur. (One must know not just which part will fail but also where in the part the crack will develop.) The general conclusion of the Australian group was that the more adaptive the signal processing was, the poorer the location and detection of real cracks. Therefore, they developed what they called semi-adaptive processing in which some predetermined data was used along with a few carefully selected signal parameters. The level and direction of the load was also included.

The parameter set that the Australian group finally chose included the load, the relative arrival times at different sensors, and the signal rise times. With this set, they were able to detect and locate most cracks at a depth of ~1 mm in the F/A-18 bulkhead, and all cracks could be located by the time they reached a depth of 2 mm.

1.5 TECHNICAL CONSIDERATIONS.

The location and evaluation of acoustic emission sources on an aircraft structure has several complications not usually found on simpler structures, such as pressure vessels. Acoustic transmission across riveted joints is, at best, variable. The presence of a highly anisotropic underlying structure can also complicate acoustic transmission. A third complication is that often the ideal location for a sensor is under a faring or is otherwise inaccessible. This puts a premium on a careful study of the structure of the airplane before the sensor locations are chosen. Even then, during the actual application of sensors the chosen locations may have to be modified because of features not seen on the blueprints.

Another problem in actual tests on the fuselage of the aircraft is air leaks. A new aircraft should have a minimum of leaks, but aging aircraft may be in quite a different state. Leaks can generate large acoustic signals which, in some cases, can completely saturate one or more channels of a source location system. In such cases, all signals from sources within the triangles involving these sensors may be ignored by the system. For this reason any leaks seen during the preliminary stages of the pressurization should be fixed before the higher pressure stages are reached.

The following lists of advantages and disadvantages are characteristic of acoustic emission testing in general and apply equally well to nondestructive testing of aging aircraft.

1.5.1 Advantages.

Some advantages of acoustic emission testing are included below:

- It is a global monitoring technique; an entire structure can be tested in one loading.
- It both detects and locates flaws.
- It can detect all flaws in a structure that are affected by the loading, regardless of the geometry.
- It can detect flaw growth in real time and estimate relative flaw severity, thus warning of an impending failure.
- It can find defects that are not readily detected by other NDE methods.

- It is often computerized, allowing tests to be conducted by relatively untrained personnel once the design and interpretation of the test have been determined. This also gives a permanent record of the test.

1.5.2 Disadvantages.

Some weaknesses of acoustic emission are included below:

- It is unable to size flaws accurately. (Flaw size is harder to assess than flaw severity.)
- It can detect flaws that are much smaller than the critical size, causing unnecessary repairs or worry.
- The design of the test can be complex and the interpretation of the results is not always straightforward. Highly trained operators are needed for the initial test design and setup.
- It is a negative test in that a good part generates little or no acoustic emission. Thus an incompetent test can declare bad parts to be good.

1.5.3 Discussion.

Acoustic emission testing is now in limited use on military fighter and transport aircraft. The RAF operates a system specifically designed to test aircraft fuselages. A similar system could be used on a commercial fleet. The problem of using such a system on other parts of an aircraft, such as the wings, is more a problem of providing realistic loads than of using acoustic emission.

Once a system was in place with a setup designed for one type of aircraft, the inspections could be fairly fast and inexpensive. A trained crew should be able to test one 727-size aircraft in less than a week. Most of the time would be taken in the application of the sensors, in checking their response, and in applying internal pressure loads to the aircraft. This could be sped up by using electronics that allowed the computer to pulse each sensor and receive the pulse at the surrounding sensors. The actual pressurization would take about two hours. The rest of the time would be used in test tear-down and in inspection of the located flaws with other NDE methods.

1.6 STATUS.

1.6.1 Present.

Two fleet-wide acoustic emission testing programs are currently in progress. They are the F-111 inspection program on the swing-wing mounting structure and the fuselage inspections of the VC-10s. The technology used by PAC in these two programs is satisfactory for the current programs but certainly is capable of improvement.

A major problem in acoustic emission testing is how to select the significant signals from the huge number of emission signals that can be produced by an aircraft. The programs in Canada and Australia have shown that the intelligent selection and use of signal parameters greatly aids in determining which acoustic emission signals are produced by cracks. It is interesting to note that both programs arrived at approximately the same set of parameters. The PAC systems also use various signal parameters to filter the incoming data. Further investigation of filtering techniques, especially with respect to specific aircraft structures or construction methods, should result in improved performance.

Several companies are developing pure digital acoustic emission systems. These systems digitize every emission signal and calculate the desired parameters from the digitized signal. At

present, the data acquisition, storage, and processing rate for these systems are still too slow for use in aircraft testing. However, the increase in speed and capability in computer technology has been phenomenal. In a few years, a pure digital system may be able to process data fast enough for use in aircraft testing. One digital system uses material characteristics and wave propagation characteristics to measure the wave arrival time for a specified velocity at a known frequency and plate wave propagation mode.[1-12,13] This technology can increase the accuracy of locating the emission sources on the skin of aircraft, and it should be able to provide new information about the problem of acoustic wave propagation through bolted or lap joints.

1.6.2 Future.

1.6.2.1 New Technology.

The Australian program found that various types of signal processing worked much better with broad-band rather than resonant sensors. The ideal sensor would have the sensitivity of the best resonant sensors, a perfectly flat frequency response from 10 kHz to 1 MHz, and a contact area of $\sim$1 mm^2. It should be a differential sensor to help eliminate electrical noise, physically small, relatively inexpensive, and rugged. Although the sensor should have a flat response, it should be used with a system with variable filtering ranges to help in the reduction of acoustic noise from the aircraft.

Faster digital electronics and display processing would be an asset to any acoustic emission system designed to inspect aircraft, but any concrete specifications given here would probably be rapidly outdated. More research is needed on acoustic propagation through real structures, particularly with welded, bolted, riveted, and glued joints.

Major improvements in location and analysis software are both needed and possi- ble. Algorithms that could improve the location and analysis are those that address location on some parts of the three-dimensional structure, that use over-determined data sets (data from more sensors than the minimum needed to locate the emission source), and that use the acoustic attenuation to back-calculate the energy of the emission at its source.

1.6.2.2 Future Use.

Although present systems can be used, definite improvements could be made. Some of the signal acceptance logic developed by the Canadian and Australian teams could be built into the system hardware. More sophisticated analysis algorithms can be developed. Displays such as that used on the F-111 should be available for the complete aircraft fuselage. These would show the entire fuselage, and the operator could zoom in on any trouble area. Sensors with smaller contact areas and flatter frequency response should be developed specifically for aerospace applications. If digital signal-acquisition technology improves sufficiently, it should be used. A true all-digital system would give much greater flexibility because even drastic changes in the analysis could be implemented in the software.

Acoustic emission testing of transport aircraft is possible today. However, it will not be implemented on a commercial fleet until there is a good, publicly available data base that shows its effectiveness on a fleet of transport airplanes. The best chance to get such a data base quickly would be for the RAF to release to the public the entire data base that they collect on the VC-10 fleet. This must include the posttest inspections, which list how many of the acoustic emissions found were defects, the size or severity of the defects, how many false positive indications there were, and whether any defects were found that had been missed by acoustic

emission. It would also be desirable to give the manpower requirements for conducting these tests. Currently, in the United States few programs apply acoustic emission testing to aircraft.

Acoustic emission testing has great potential to improve the effective inspection of aging aircraft and to reduce the costs. However, several years of hard work are needed before such an inspection system can or will be accepted for inspection of commercial aircraft in the United States.

1.7 REFERENCES.

1-1. A. G. Beattie, "Acoustic Emission, Principles and Instrumentation," *Journal of Acoustic Emission* **2**,95, 1983

1-2. Nondestructive Testing Handbook, Vol. **5**, *Acoustic Emission Testing*, R. K. Miller and P. McIntire, eds., American Society for Nondestructive Testing, 1987.

1-3. C. M. Breevoort, C. D. Bailey, and W. M. Pless, "Acoustic Emission Structure-Borne Noise Measurements on Aircraft During Flight," *Acoustical Imaging, Proceedings 14th International Symposium, 22-25 April, 1985,* Plenum Press, New York, pp. 643-48, 1985.

1-4. P. H. Hutton, D. K. Lemon, R. B. Melton, and P. G. Doctor, "Develop In-Flight Acoustic Emission Monitoring of Aircraft to Detect Fatigue Crack Growth," *Review of Progress in Quantitative NDE*, Vol. **1** Plenum Press, pp. 459-62, 1982.

1-5. J. M. Rodgers, "The Developing Role of Acoustic Emission in Aircraft Main- tenance and Structural Integrity," *Proceedings of the 5th International Symposium on Acoustic Emission*, pp. 537-49, 1980.

1-6. J. M. Carlyle, "Acoustic Emission Testing the F-111," *NDT International* 22:67, 1989.

1-7. J. M. Carlyle, *Physical Acoustics Corp.*, private communication.

1-8. S. L. McBride, M. R. Viner, and M. D. Pollard, "Acoustic Emission Monitoring of a Ground Durability and Damage Tolerance Test," *Review of Progress in Quantitative NDE*, Vol. **10b** Plenum Press, New York, p. 1913, 1991.

1-9. S. L. McBride, Y. Hong, and M. D. Pollard, "Enhanced Fatigue Crack Detection in Aging Aircraft Using Continuous Acoustic Emission Monitoring," to be published in *Review of Progress in Quantitative NDE*, Vol. **12**, pp. 2191-97, 1992.

1-10. C. M. Scala, S. J. Bowles, and I. G. Scott, "The Development of Acoustic Emission for Structural Integrity Monitoring of Aircraft," *International Advances in Nondestructive Testing*, Vol. **14**, ed. McGonnagle, W. M., Gordon and Breach, Montreux, Switzerland, p. 219, 1989.

1-11. C. M. Scala, J. F. McCardle, and S. J. Bowles, "Acoustic Emission Monitoring of a Fatigue Test on an F/A-18 Bulkhead," to be published in *Journal of Acoustic Emission.* Vol. **10**, 1991/92, p49.

1-12. M. E. Gorman, "Determining Fatigue Crack Growth in Aircraft by Monitoring Acoustic Emission," *Naval Research Review* **Vol. 1**:24, 1992.

1-13. M. E. Gorman, Digital Wave Corp., private communication.

2. X-RAY COMPUTED TOMOGRAPHY.

2.1 SUMMARY.

X-ray computed tomography (CT) is a nondestructive evaluation technique developed originally for medical diagnosis. It has also proved to be a valuable tool in industry, complementing and sometimes replacing conventional nondestructive evaluation methods. CT collects X-ray transmission measurements from many angles around a component to digitally reconstruct a map of the relative linear attenuation coefficient of small-interior-volume elements and view them as cross-sectional images.[2-1] These images provide clear and easy-to-interpret cross sectional views of the component's internal structure that do not have the shadowing and superposition found in film radiographs. CT provides quantitative spatial and material/density assessments. Based on these quantitative assessments, inaccessible regions of the component can be measured and flaw sizes gauged. Although the use of CT is currently concentrated in component engineering, materials research, and failure analysis, it has great potential for a variety of aircraft applications.

2.2 TECHNICAL BACKGROUND.

Originally developed in the 1970s, CT was built on the foundations of X-ray radiography and axial tomography.[2-2] CT can be thought of as a high-tech extension of standard X-ray radiography. In radiography, an object is placed between an X-ray machine and an X-ray measurement device, usually film. When the X-ray machine is turned on, X-rays are emitted, traveling toward the film. As the X-rays travel toward the film, they interact with the object, causing some of the X-rays to be absorbed or scattered in different directions. Typically, dense areas of the object absorb or scatter more X-rays than less dense areas. The film is exposed by the X-rays that make it through the object. When the film is processed, the resultant image is a radiograph of the object that shows the internal structure of the object with its different features superimposed upon one another.

CT expands on radiography by using electronic detectors instead of film and by measuring the X-rays transmitted through the object from several different angles. The CT detector readings are then processed on a computer to produce a cross-sectional image of the inside of the object, without the superposition inherent in radiography.

As an example, consider an object composed of two cylinders of material embedded inside a third larger cylinder of material, as illustrated in Figure 2-1. Let the three cylinders each be made of different-density materials. If the object is aligned so that the axes of the two interior cylinders are collinear with a line from the X-ray source to the film, then the radiograph will show all the cylinders superimposed upon one another. A CT image obtained by rotating the object about the axis of the large outer cylinder would result in a cross-sectional image of all three cylinders with no superposition (see Figure 2-2). This is a very simplistic example, but it illustrates the differences between radiography and CT, as well as some of the advantages a CT image presents.

As CT equipment has evolved through its many developmental stages, the principal driving factors have been scan-time or X-ray dose to the object, image resolution, and image quality. The original CT systems consisted of a single X-ray detector and source. Today's CT systems, which encompass five generations of hardware design and scan geometry, span a broad range in

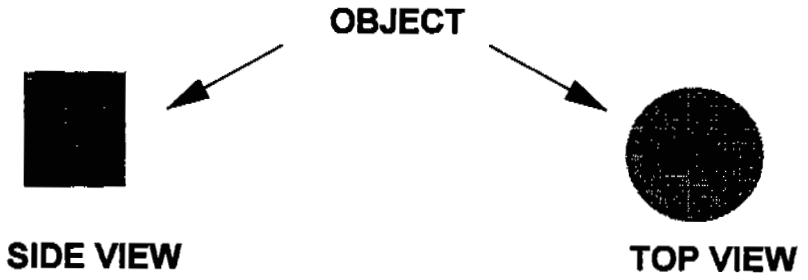

FIGURE 2-1. Views of Example Cylindrical Object.

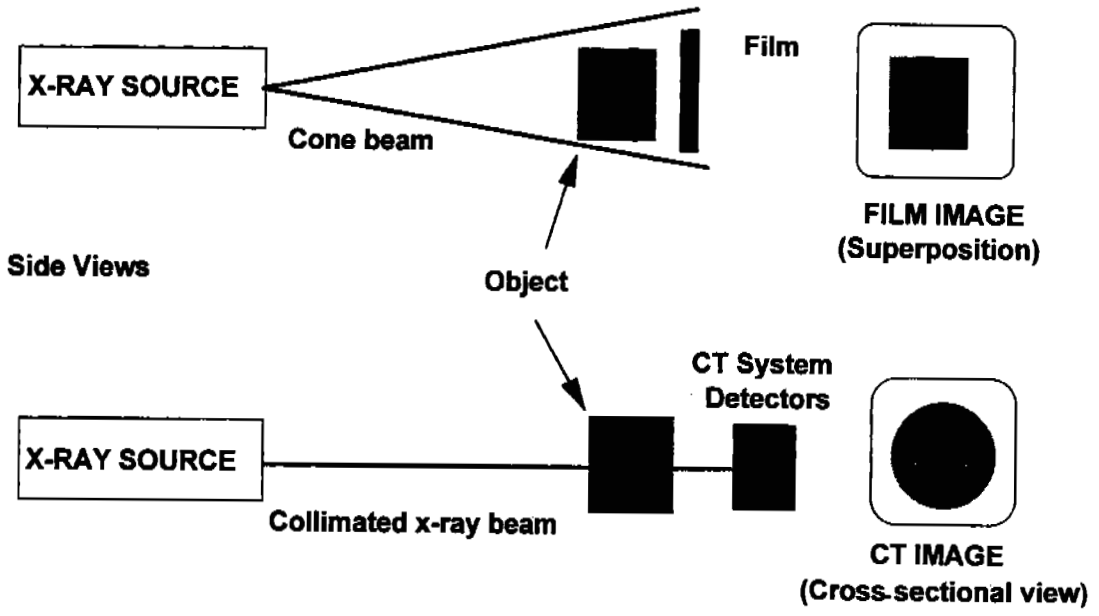

Figure 2-2. Difference Between Film Radiography and CT Images of the Same Object.

their complexity. Figure 2-3 shows each of the five CT scanner generations. Each new generation reduced the time required to obtain an image. The quality and resolution of a CT image are directly related to scan time and, at long scan times, approach the design limitations of the scanner. Thus, as new generations of scanners have evolved, the image quality and resolution have improved for a given scan time. A detailed description of the different CT scanner generations will not be addressed in this text. Because of the high cost of fourth- and fifth-generation scanners (several million dollars) almost all commercial industrial scanners are of the second and third generation.

There is a trade-off between spatial or density resolution and scan time. High-resolution images require longer scan times than lower resolution images. The resolution and scan time of

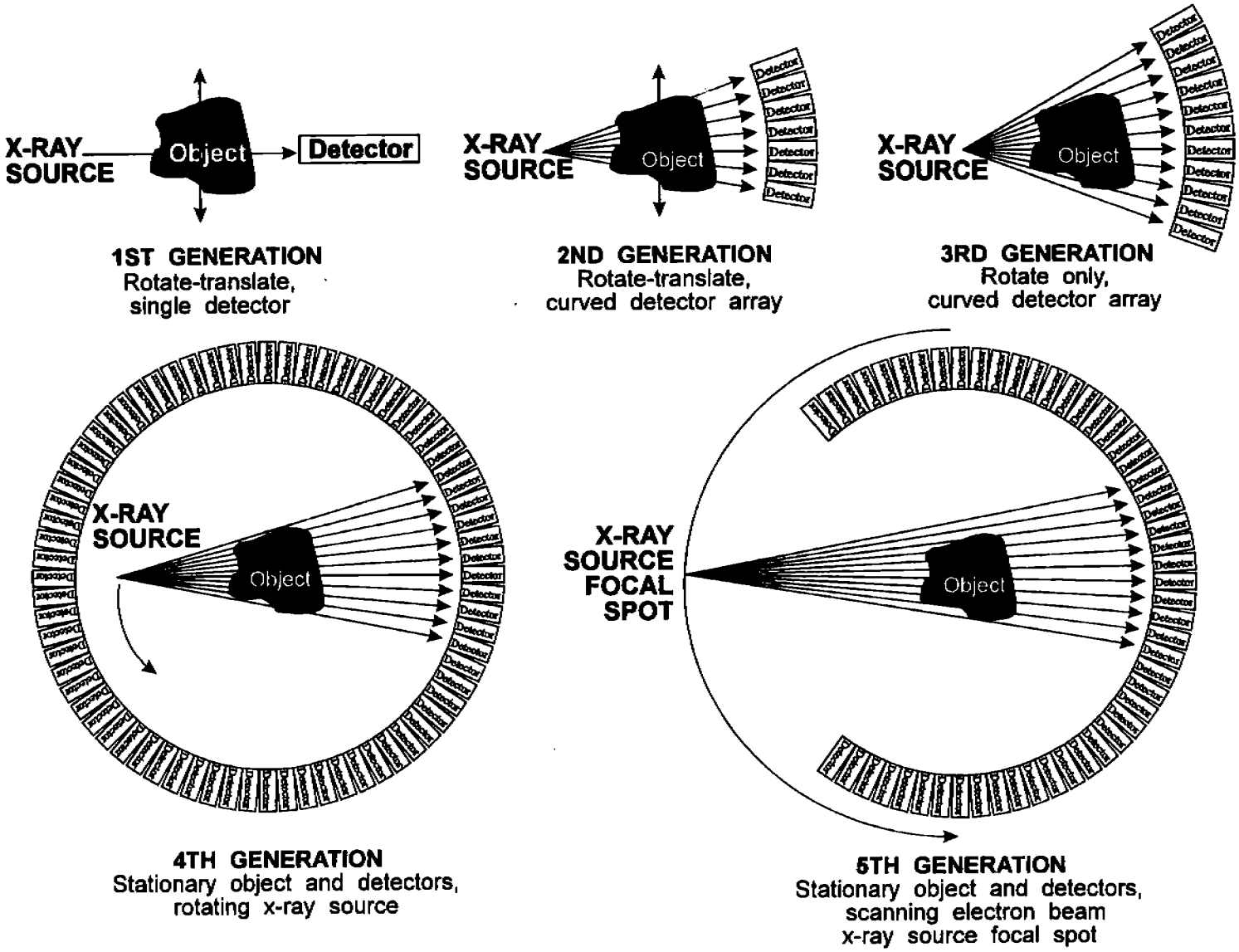

Figure 2-3. Illustrations of the Different Generations of CT Scanners.

industrial CT scanners are limited primarily by the physics of the X-ray sources available. The spatial resolution of a scanner is a function of the size of the X-ray focal spot (the point in the X-ray machine where the X-rays are created), and the scan time is a function of the rate at which X-rays are emitted from the X-ray machine. To obtain a signal-to-noise ratio sufficient to generate high-quality CT images, a certain number of X-rays must be detected. The physical properties of X-ray machines dictate how high the rate of X-ray generation (current of the X-ray machine) can be for a given focal spot size—at high currents, the X-ray machine can be damaged. Another consideration is the energy of the X-rays emitted from the X-ray machine. Higher energy X-ray machines tend to have larger focal spots. Industrial CT scanners have scan times varying from a few minutes to hours and have spatial resolutions varying from a few tens of microns to a few millimeters.

The X-ray energy of a CT scanner needs to be high enough so that the X-rays can penetrate the object being scanned. Thus, scanners that are designed for the inspection of large objects (over a meter in diameter), such as rocket motors, have relatively high energy X-ray machines, typically in the megaelectron-volt range. Given that the size of the focal spot in high-energy X-ray machines is in the millimeter range, high-energy CT scanners or scanners capable of scanning large objects result in resolution in the millimeter range. Small objects or low-density objects can be scanned on CT systems with lower energy X-ray sources. In microfocus (or small-spot) X-ray machines, the size of focal spots is in the range of ten microns, and maximum X-ray energies range from 160 to 200 keV. Medium-energy CT systems have maximum X-ray energies of 420 to 450 keV, with resolutions in fractions of millimeters.

CT is a computationally intensive inspection method that requires high-performance computer hardware. Typical CT scans acquire millions of detector readings and require billions of calculations to generate an image. In the past, the computational performance of a CT system contributed significantly to the price and time needed to generate an image. With the recent advances in computing technology, the computer components of a CT system are not the limiting factor in the performance of 2D or single-slice CT systems. However, CT systems that generate full 3D images and data sets still require leading-edge computing technology.

2.3 PRESENT APPLICATIONS.

Industry currently uses CT for a wide variety of applications. Below is a brief description of some of the current applications.

Composites. CT is being employed in several advanced material development activities. Carbon-fiber- and glass-fiber-reinforced plastics developed by NASA and the aerospace industry are being inspected with CT scanners to locate flaws and manufacturing process deficiencies. CT has also provided valuable information about how to produce new components from ceramic materials. Examples are ceramic drill bits and rotors.

Castings. Automobile manufacturers are using CT during the prototype development stages to inspect engine block, gear box, and aluminum wheel castings. Foundries are also investigating CT as a development tool.

Explosive material inspection. The performance and safe operation of devices containing explosives can be seriously affected by flaws in the explosive materials. CT is used to detect inhomogeneities, voids, cracks, and inclusions in explosive material before, during, and after the manufacturing process.

Rocket motors. Flaws in rocket motors can have disastrous effects when the motor is used. Thus, many manufacturers and military establishments use CT to inspect rocket motors for propellant voids, delaminations, inclusions, and other anomalies.

Cruise missile engines. CT equipment vendors have demonstrated that complete cruise missile engines can be inspected using CT.

Electronic parts. Most equipment manufactured today has some electronic components. These components are often very complicated and difficult to inspect. CT is proving to be a valuable tool for many such inspections. Examples are:

- circuit boards—for bad or missing components and damaged areas
- switches—for closure conditions (i.e., on or off)
- capacitors and transformers—for failed components and windings.

Space shuttle fuel system components. Defective valves used in space shuttle fuel systems are inspected with CT as part of failure analysis testing.

Thermal batteries. CT is used for failure analysis of thermal batteries where electrical tests do not provide adequate information.

Characterization tool used in the development of advanced materials. The development of advanced materials often requires that knowledge about material interaction and manufacturing be extended to new levels. The properties of the materials and the definition of what a flaw is are sometimes not known. CT scanners are providing important contributions in advanced material development because of the large amount of quantitative data that can be obtained from a CT image.

Measurements. CT is often used to quantify flaws in components. The size of a flaw and how it is manifested plays a crucial part in determining the condition of the component. In some cases small flaws do not render the component unusable. CT allows spatial and density measurements of flaws or flawed areas.

Reverse engineering. In many cases drawings do not exist for parts. Sometimes the drawings are lost or inaccessible, or they were never created. Drawings for these parts may be needed to make new parts or fix old parts, or to determine how to safely dispose of old parts. The images obtained from CT scanners are dimensionally accurate and therefore can be used to generate computer-aided design (CAD) drawings. This capability is in limited use today but should be a common tool in the future.

Closed systems. In systems or components where information is needed about internal structures or component orientations, CT is often employed. The CT scanner provides clear images of the internal structures without the superposition found in other radiographic techniques.

Failure analysis. Failure analysis is a difficult process involving many nondestructive tools. CT provides additional information that is very valuable in failure analysis.

Switching components and valves. Critical switching components and valves play a significant role in the safety of some systems. CT provides accurate information as to their status or condition.

3D visualization of components. By acquiring multiple CT slices or images of a part and stacking this data together, a 3D data set can be obtained. By using specialized visualization

software, a 3D image of the part can be generated. These 3D images provide valuable insight into the part structure and design that is sometimes difficult if not impossible to perceive by other means.

Trees and wood. CT is being investigated as a tool for inspecting trees and wood. Two examples of CT for this purpose are (1) to determine the presence of rot or decay in electrical power poles before the poles break, which saves money and provides a greater margin of safety, and (2) to determine the quality of the lumber that can be obtained from trees prior to cutting logs.

2.4 AIRCRAFT APPLICATIONS.

Current applications of CT in the aerospace industry have been limited to relatively small or medium-sized component pieces. Most of the applications discussed in the previous section have been developed in the aerospace and related industries. Jet engine manufacturers are investigating the use of CT to inspect turbine blades. CT can be used to measure internal turbine blade dimensions including wall thickness and point-to-point distances. Failure analysis of components that cannot be disassembled is also a common application area for CT.

Turbine blades. Because of the high cost of turbine blade manufacturing and the high cost of turbine blade failure, significant effort is being extended to inspect turbine blades for inclusions, voids, wear, and dimensional compliance with design specifications. CT is a valuable tool in these difficult inspection tasks. Figures 2-4 and 2-5 show CT images of turbine blades.

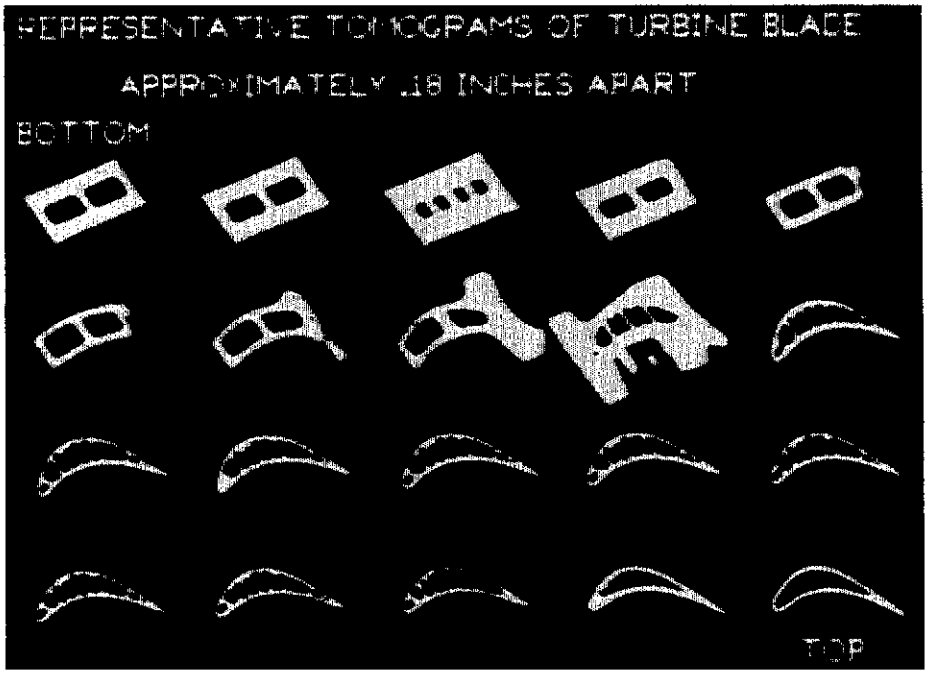

Figure 2-4. A Series of CT Images from a Turbine Blade. [Source: Keith Jezek, Scientific Measurement Systems, Inc., Austin, Texas. Printed with permission of Keith Jezek.]

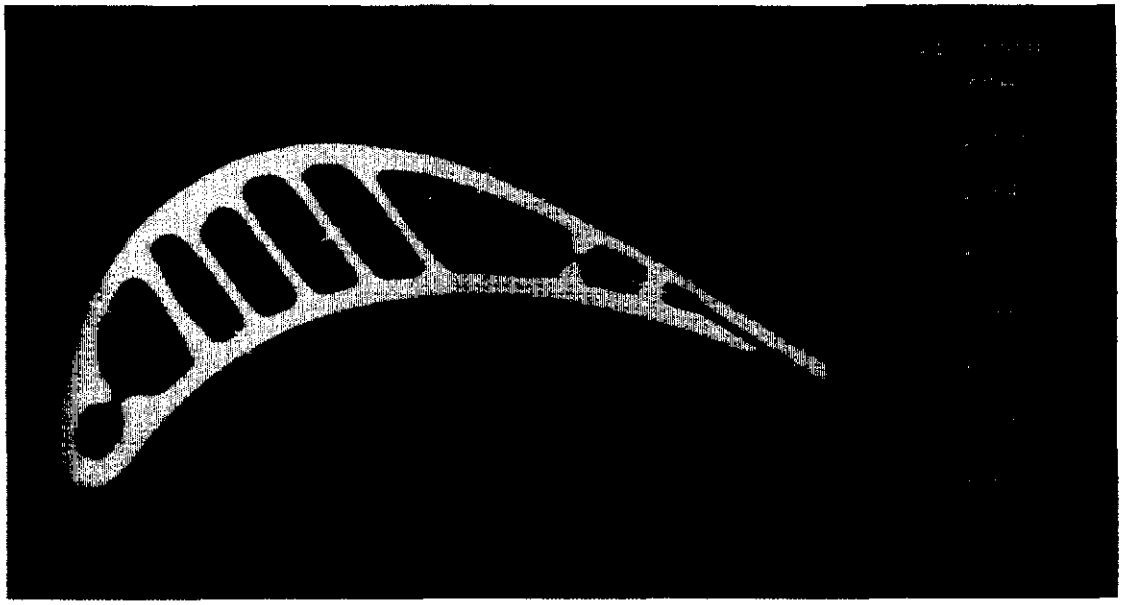

Figure 2-5. A CT Image of a Turbine Blade Illustrating the Measurement Features that CT Can Provide. [Source: Keith Jezek, Scientific Measurement Systems, Inc., Austin, Texas. Printed with permission by Keith Jezek.]

Characterization tool. At the Boeing Defense & Space Group aircraft development site, CT is used as a material characterization tool in the advanced materials development cycle.[2-3] Conventional qualitative inspection methodologies (ultrasonics, radiography, and visual) are proving inadequate to fully characterize and understand properties and defects of advanced materials and processes.[2-4] CT can provide information about the size and location of flaws in new materials under development that allows development engineers and scientists to gain a better understanding of the manufacturing processes. Using the CT data, fabrication processes can be optimized, reducing the time required to develop new materials.

2.5 TECHNICAL CONSIDERATIONS.

CT is a relatively complicated inspection methodology that requires extensive equipment and computer resources. Applying CT to the inspection of aging aircraft is quite possible. Following is a brief summary of the advantages and disadvantages of CT.

2.5.1 Advantages.

- The images and data are readily interpretable, providing density and geometric information not available with other types of inspection.
- CT can provide quantitative measures of density (0.1 percent to 1.0 percent).
- CT can provide quantitative 3D dimensional measurements (with resolution of 0.025 mm to 0.25 mm) of the interior of objects.
- Volumetric defects, such as voids and inclusions, can be easily detected.
- The size and location of defects can be readily measured.

2.5.2 Disadvantages.

- CT equipment is very expensive, typically costing one million to several million dollars for a single CT scanner.

- The size of part that can be inspected is usually limited to approximately two cubic meters in volume. This is due to the large range of motion and part access required. CT systems designed for high spatial resolution are usually limited to scanning parts ranging in size from a few millimeters to a few centimeters.
- The resolution of image (spatial or density resolution) generated by a CT scanner is governed by the scan time. The image quality improves with longer scan times, asymptotically approaching the physical limitation of the CT scanner.
- CT scanners are typically non-portable systems that require large X-ray–shielding enclosures or rooms.
- Current commercial CT systems require 360° access to the object under inspection. Usually the parts must be brought to the CT scanner rather than moving the scanner to the parts.

2.6 STATUS.

2.6.1 Present.

CT scanners are useful for small-component inspections or failure analysis of assemblies that can fit within the object-handling capabilities of the scanners. Many aerospace companies use CT to support their development testing and inspection efforts. Because of the high cost of equipment and facilities, CT has not yet been employed to a large degree for routine aircraft inspections.

CT systems could be developed, and are currently being considered, for inspecting large sections of aircraft structures. Some of the obstacles to overcome are the limitations of the X-ray machine and the size of the CT scanner. Current X-ray machines that have sufficient energy to penetrate large aircraft structures have focal-spot sizes that limit the resolution of the CT system beyond what is required. Also, the output flux of an X-ray machine with a sufficiently small focal spot would force the scan times of the CT system to be unacceptably long for commercial inspections.

2.6.2 Future.

No CT systems have been built to the size and geometry requirements for a complete aircraft scanner; therefore, an adequate CT system would have to be prototyped and developed before CT scanning could become a viable inspection technique.

2.7 REFERENCES.

2-1. Richard H. Bossi, Gary E. Georgeson, *Computed Tomography Analysis of Castings,* Wright Laboratory Interim Report WL-TR-91-4121, January 1992, p. 1.

2-2. John F. Moore, "Evolution of Computed Tomography," *Materials Evaluation,* Vol. **48**, May 1990, p. 630.

2-3. Richard H. Bossi, Gary E. Georgeson, "The Application of X-Ray Computed Tomography to Materials Development," *The Journal of The Minerals, Metals & Materials Society,* Vol. **43**, No. 9, September, 1991, pp. 8-15.

2-4. Gary E. Georgeson, Richard H. Bossi, *X-Ray Computed Tomography for Advanced Materials and Processes,* Wright Laboratory Interim Report WL-TR-91-4101, June 1992, p. 2.

3. COMPTON X-RAY BACKSCATTER IMAGING.

3.1 SUMMARY.

Many NDI tools are available to the airline maintenance industry for the detection of near surface or first-layer flaws such as fatigue cracks or massive skin corrosion. However, only a few techniques, such as radiography or visual inspection combined with airframe disassembly, can detect subsurface flaws in layered structures. Compton backscatter imaging (CBI), a re-emerging near surface NDI measurement and imaging technique based on Compton X-ray backscatter principles, can detect critical imbedded flaws such as cracks, corrosion, and delaminations in metal and composite aircraft structures and offers exciting possibilities for solving many of the most critical flaw-detection requirements encountered by the aging aircraft industry.

CBI yields a point-by-point measurement of material density. A beam of radiation penetrating an object will be attenuated by absorption and scatter. A collimated radiation detector located on the source side of the part measures some of the scattered radiation from a small region or inspection volume within the object. The inspection volume element is defined by the intersection between the collimated detector's field of view and the collimated X-ray beam. When the object is scanned with the collimated source-detector assembly and the measured signal strength is stored as a function of position in digital memory, a 2D or 3D density map of the inspection volume is obtained. Software analysis and display of this data completes the inspection process.

The technical advantages of CBI technology, especially when used for aircraft inspection, are many. Like pulse echo ultrasonics and eddy current testing, CBI is a single-sided inspection technique capable of obtaining quantitative material information about the volume being inspected. CBI responds to material electron density, which is directly proportional to its physical density and composition. The information can be presented in forms ranging from a simple accept-repair gage for corrosion-induced aircraft skin thinning to the more sophisticated 3D tomographic-like digital flaw image displays.

Unlike eddy current and ultrasonic NDI, CBI is unaffected by variations in lift off, surface roughness variations or paint, metal conductivity, delamination, and air gaps. CBI can inspect solid aluminum or composite materials to depths of 5 cm (2 in.) or more. If the structure is layered with intervening air gaps, information can be obtained at greater depths.

Although many of the technical capabilities of CBI in solving flaw detection problems in aging aircraft have been successfully demonstrated, its use by the aircraft industry has been almost nonexistent—possibly because no practical, cost-effective industrial CBI instrument has been designed that is specific to the commercial airline industry. Other deterrents to its acceptance may be the reluctance of aircraft maintenance facilities to use radiation-based technology unless it is required and the high cost of the custom-made technologically complex inspection systems. However, cost-effective CBI systems can be developed.

3.2 TECHNICAL BACKGROUND.

3.2.1 Introduction.

Conventional transmission radiographic inspection of an aircraft and its components is often limited because of restricted equipment access and the inability of conventional transmission radiography to reliably detect critical aged aircraft defects such as corrosion and delaminations. An alternate radioscopic inspection technique that images backscattered X-rays to create a digital density image of the area being inspected is Compton backscatter imaging (CBI). By utilizing the backscattered X-ray signals, the X-ray detector can be located next to the shielded X-ray source (Figure 3-1) so that radioscopic inspection may be accomplished from a single side, similar to pulse-echo ultrasonic testing. This configuration is based on Compton backscatter principles (Figure 3-2) and can greatly simplify the inspection of an aircraft and its components where rear-side access is difficult. Equipment setup is also simplified, since only the combined X-ray source-detector assembly must be manipulated, rather than a separate X-ray source system and a separate detector system. Compared to conventional radiography where the whole area is flooded with X-rays, backscatter imaging equipment has a highly collimated, pencil-like X-ray beam and detector geometry and exposes only a very small volume of the inspection area. This significantly reduces the stray radiation and minimizes additional shielding requirements (i.e., time, distance, shielding material) for maintenance personnel.

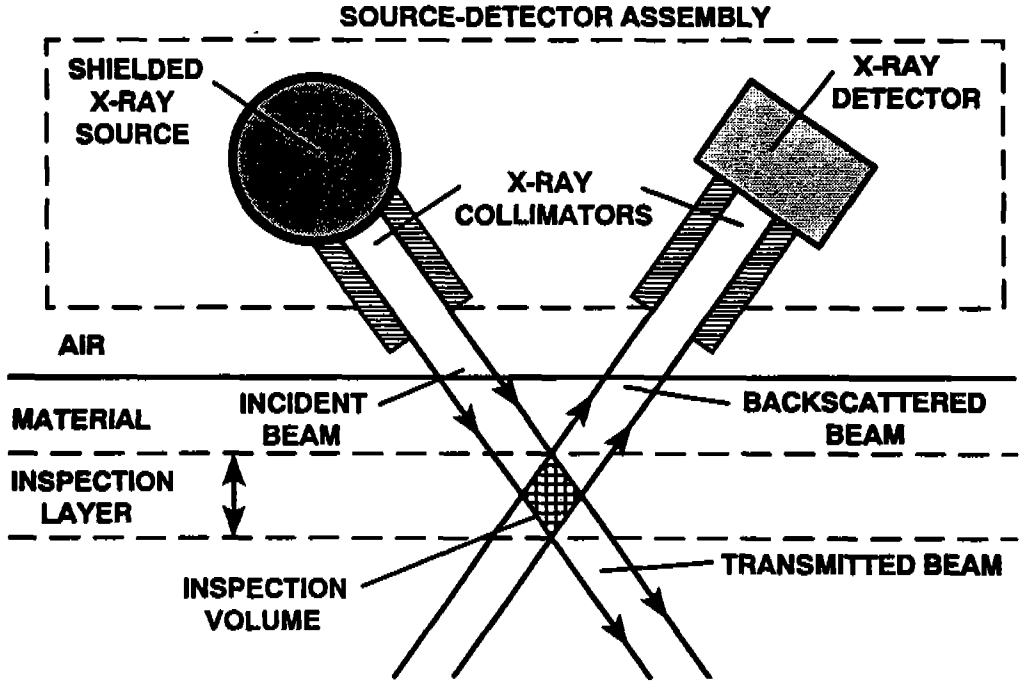

Figure 3-1. Diagram Showing the Essential Elements of a Compton Backscatter X-ray Measuring System. A tomographic image of the inspection layer is obtained by raster scanning the collimated source-detector assembly over the object and storing the measured signal as a function of position in a computer.

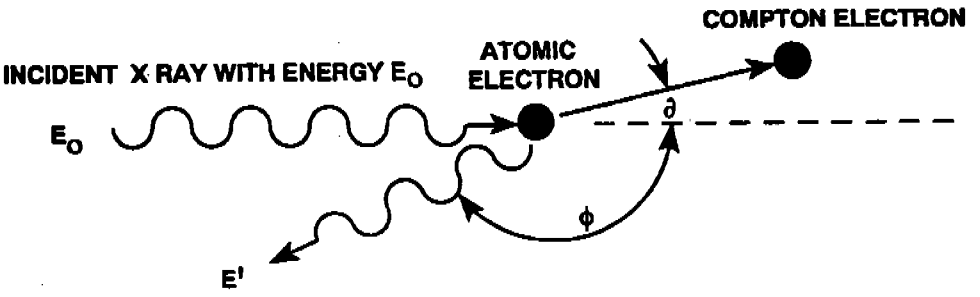

$$E' \text{ (keV)} = \frac{511 \text{ (keV)} * E_O \text{ (keV)}}{[511 \text{ (keV)} - E_O \text{ (keV)} * (1 - \cos \phi)]}$$

Figure 3-2. Diagram Showing the X-ray and Electron Trajectories Before and After a Compton Backscatter Interaction. The Compton equation relates the energy of the Compton scattered X-ray (E′) as a function of its incident energy (E_o) and its scattering angle ϕ.

Most important, for many applications the images produced with CBI techniques are superior to images produced with transmitted X-ray beam techniques. This is especially true for low X-ray absorption materials such as thin sections of aluminum or composite structures where subject contrast is often very low. The radioscopic detectability of small voids and laminar defects such as unbonds is also significantly enhanced.

Compton backscatter imaging is a radioscopy technique (radiography with an electronic X-ray detector and imager) that utilizes the physical principles of Compton scattering to yield a point-by-point measurement of material density (Figures 3-1 and 3-2). A beam of radiation penetrating an object will be attenuated by absorption and scatter. A collimated radiation detector located on the source side of the part measures some of the radiation scattered from a small region or inspection volume within the object. The inspection volume element (voxel) is defined by the intersection between the collimated detector's field of view and the collimated X-ray beam. By raster-scanning the object with the collimated source-detector assembly and storing the measured signal strength as a function of position in digital memory, a two- or three-dimensional density map of the inspection volume can be obtained.

CBI images are digital tomographic images that represent a slice parallel to the scanning plane. The depth and thickness of the image slice is determined by the position and design of the source-detector assembly. A 3D volumetric object image can be obtained by scanning the same area at different image slice depths. Unlike computed tomography (CT), which provides reconstructed tomographic slice images from a sufficiently large number of X-ray transmission measurements at different orientations of the object, backscatter imaging uses a single imaging orientation of the object and is totally one-sided. This opens up many inspection possibilities that are difficult or impossible to perform with conventional radiography and CT.

3.2.2 X-ray Interactions.

X-rays interact with materials through absorption and scattering processes. At energies less than 1 MeV, photons are attenuated by photoelectric absorption and scattering. The scattering processes are (1) Rayleigh (elastic) scattering and (2) Compton (inelastic) scattering. Depending on the photon energy and material, some of these interaction processes tend to dominate, as shown in Figure 3-3.

For energies below 100 kV, for example, the predominant mode of photon interaction in all medium-to-high atomic number (Z) absorbers (i.e., steel to tungsten) is the photoelectric process. This absorption may be described as an interaction of the incident photon with the atom in which the entire photon energy is absorbed and one electron, usually from the atom's K- or L-shell, is ejected. This vacancy in the electron shell is filled by an upper orbital electron. A low-energy Auger electron or characteristic fluorescence X-ray is emitted from the atom during this electron transition.

Rayleigh scattering is the elastic scattering of photons by tightly bound electrons. In this interaction, X-rays lose no energy and are scattered primarily in the forward direction. The only contribution of Rayleigh scattering to backscatter imaging is that it assists X-ray attenuation; it never dominates X-ray interactions. However, depending on photon energy and material, Rayleigh scattering interactions can exceed photoelectric absorption or Compton scatter interactions.

The intensity of characteristic fluorescence X-rays produced by photoelectric interactions in a material can be comparable to or greater than the intensity of the Compton scatter X-rays. Fluorescence is an important consideration when inspecting materials with atomic numbers greater than 18 (e.g., titanium and steel) and can be removed from the backscattered radiation with the appropriate K-edge filters. For aircraft materials (low atomic number) X-ray fluorescence and Rayleigh X-ray scatter do not contribute to the backscatter intensity. However, for high atomic number materials (e.g., tungsten and uranium) Rayleigh scattering in the back direction may be significant relative to Compton backscatter and cannot be removed by filtering.

3.2.3 Compton X-ray Scatter.

Of the several processes which may occur when X-rays interact with matter, Compton scattering is dominant for most materials over a wide range of industrial radiographic energies (Figure 3-3). Compton scattering is a scatter process whereby an X-ray photon interacts with a free or outer-shell electron of an atom.[3-1] The Compton interaction causes the electron to recoil and the photon to propagate in a new direction with a reduced energy. The mechanistics of the Compton scattering process are illustrated in Figure 3-2. The energy of the scattered photon (E′) is only a function of its incident energy and its scattering angle and is independent of the scattering material.

The energy of the scattered photon (E′) as a function of incident photon energy (E_o) for various backscatter angles is plotted in Figure 3-4. This figure shows that (1) the energies of Compton backscattered photons from 135° to 180° fall in a tight energy band ranging from 100 to 150 keV for industrial radiographic energies, and (2) the energies of 180° backscattered Compton scattered photons approaches a 250-keV maximum for higher incident X-ray energies. It is interesting to note at this time that the energy and hence the maximum range of the backscatter photons in the material being inspected impose an inspection depth limit of backscatter imaging (Table 3-1).

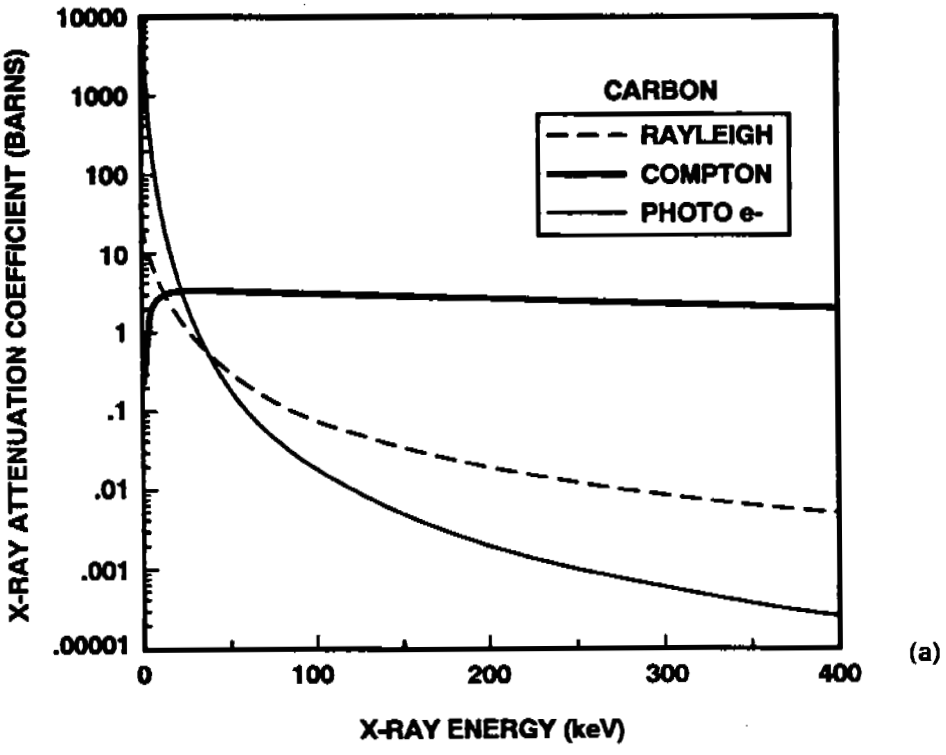

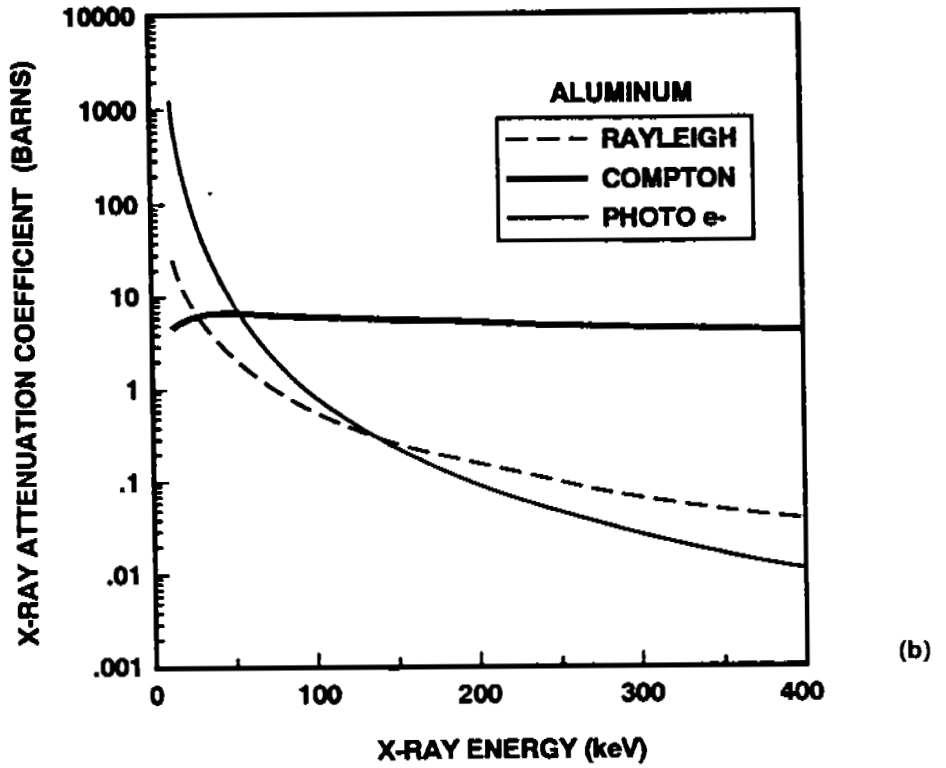

Figure 3-3. X-ray Interaction Processes as a Function of Photon Energy with Carbon (a) and Aluminum (b). Shows that the Compton scattering interaction is the dominant process over a wide range of industrial radiographic energies.

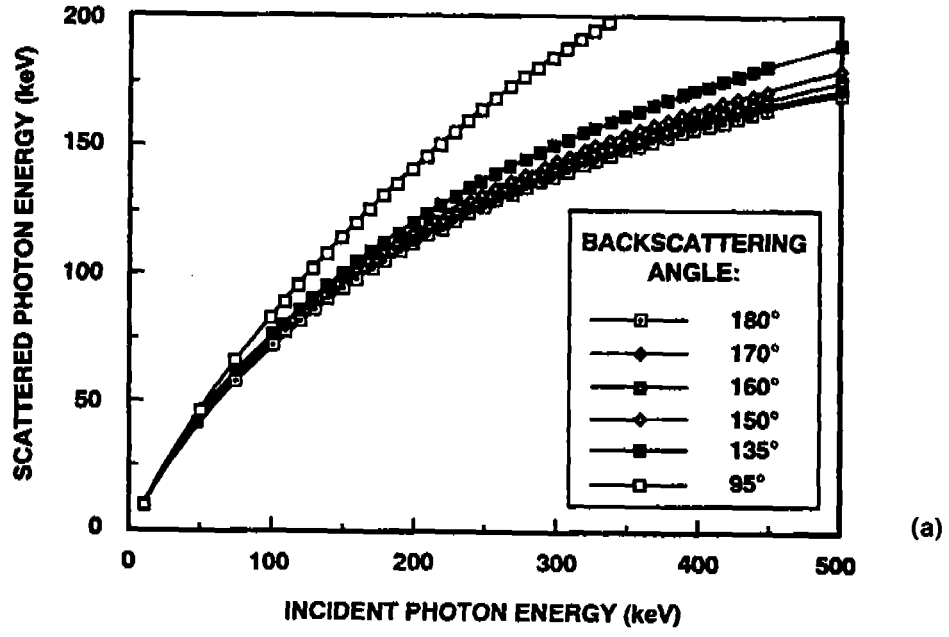

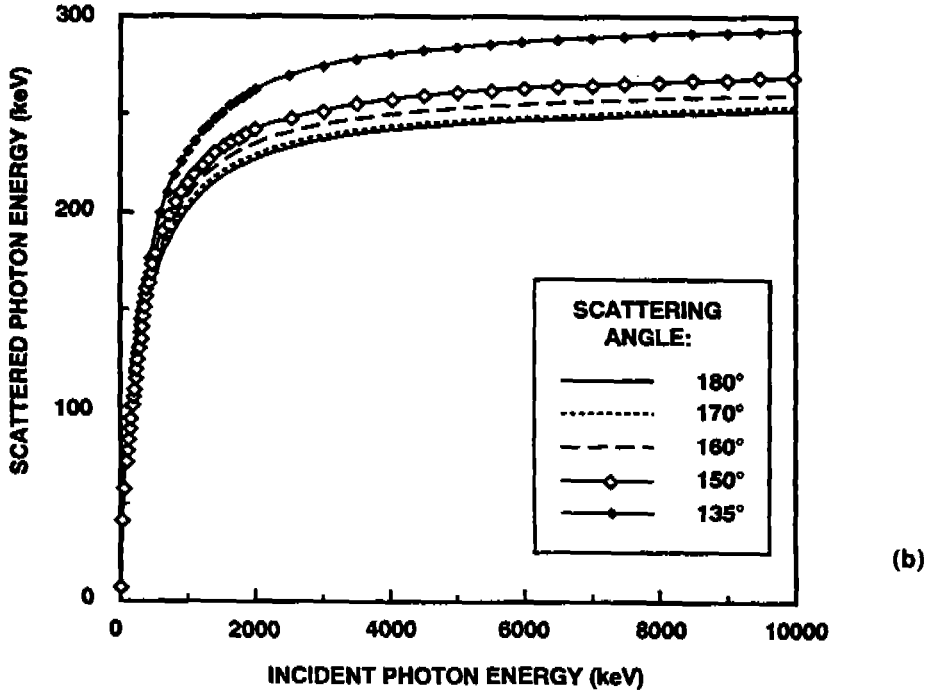

Figure 3-4. Calculated Compton Backscattered Photon Energies (a) for Various Scattering Angles (b) as a Function of Incident X-ray Energy. Note that the backscattered X-rays (ϕ = 135° to 180°) for industrial inspection systems (160–400 kV peak) fall into a narrow energy band of 100 to 175 keV. This backscatter energy band increases to 250–290 keV with inspection energies up to 10 MeV.

The probability for a Compton scatter interaction is given by the material's Compton scattering cross section, which is shown for carbon and aluminum in Figure 3-3 as a function of X-ray energy. These graphs illustrate that Compton scattering is the dominant contribution to the total X-ray attenuation in aerospace and aircraft materials of interest.

Compton scattering in a material is directly proportional to its electron density. Material electron density, tabulated in Table 3-2, is directly proportional to its material density times the ratio of its atomic number (Z) to its atomic weight (A). Therefore, a measure of the scatter intensity from a given material volume element is proportional to its material density or composition. Any change in density or composition of the scattering material will result in a change in the intensity of scattered X-rays. Thus it is possible to use Compton backscatter measurements to detect variations in these material properties where conventional radiography is not practical.

TABLE 3-1. Calculated Mean Free Path of Compton Backscattered X-rays (ϕ = 135° to 180°) in Some Aircraft Materials of Interest as a Function of Peak X-ray Machine Energy. The practical maximum material thickness that can be inspected with Compton backscatter imaging is estimated to be 3 to 5 mean free paths.

Peak Radiographic Energy (keV)	Backscattered X-ray Energy (keV)	X-ray Range (cm)			
		Carbon	Aluminum	Titanium	Steel
160	100	2.5	2.2	0.8	0.35
300	130 – 150	2.8	2.6	1.2	0.55
10,000	250 – 300	3.4	3.3	1.9	1.00

TABLE 3-2. Electron Densities of Materials and Compounds Tabulated in Ascending Order. The Compton X-ray scattering probability of a material is directly proportional to its electron density.

Material	Atom No.	Density (gm/cc)	e-/cc (N*Z)
Air		1.29^{-3}	3.88^{+20}
Polyethylene		9.25^{-1}	3.18^{+23}
Water		1.00	3.35^{+23}
Polystyrene		1.06	3.43^{+23}
Nylon		1.10	3.63^{+23}
Neoprene		1.23	3.85^{+23}
Lucite, Plexiglas		1.19	3.87^{+23}
Kapton		1.42	4.35^{+23}
Cellulose Nitrate		1.45	4.50^{+23}
Carbon	6	1.60	4.82^{+23}
Beryllium	4	1.84	4.92^{+23}
Saran		1.68	5.08^{+23}
Magnesium	12	1.74	5.18^{+23}
Silicone Rubber		1.70	5.53^{+23}
Teflon		2.20	6.36^{+23}

Material	Atom No.	Density (gm/cc)	e-/cc (N*Z)
Silicon	14	2.35	7.06^{+23}
Aluminum	13	2.70	7.84^{+23}
Concrete		2.35	1.18^{+24}
Titanium	22	4.50	1.25^{+24}
Tin	50	7.28	1.85^{+24}
Iron	26	7.86	2.20^{+24}
Cadmium	48	8.65	2.23^{+24}
Copper	29	8.94	2.46^{+24}
Nickel	28	8.90	2.56^{+24}
Lead	82	1.14^{+1}	2.72^{+24}
Silver	47	1.05^{+1}	2.76^{+24}
Palladium	46	1.22^{+1}	3.17^{+24}
Tantalum	73	1.66^{+1}	4.03^{+24}
Uranium	92	1.89^{+1}	4.40^{+24}
Gold	79	1.93^{+1}	4.66^{+24}
Tungsten	74	1.93^{+1}	4.68^{+24}
Platinum	78	2.14^{+1}	5.16^{+24}

Features of Compton scatter that bear on backscatter imaging are:

- The Compton scatter cross section is nearly constant over a broad range of energies. Thus inspection with high-energy X-rays, where the incident beam has negligible attenuation, is just as sensitive to material density or thickness variations as a lower- energy beam. This is not true for conventional transmission radiography.
- The CBI inspection depth is limited by attenuation and range of the backscattered photon, which is reduced in energy relative to the incident energy. The energy of the scattered photons is independent of the scattering material. It is only a function of the incident photon energy and scattering angle.
- The intensity measurement of the backscattered radiation can be complicated by the fact that the X-rays are attenuated going into and coming out of the sample by Rayleigh and Compton scatter and photoelectric absorption, and by the emission of fluorescence X-rays from the sample volume.
- Compton scattering sends radiation in all directions. At radiographic energies of about 300 kVp the scattering is fairly uniform. That is, backscattering (135° to 180°) is generally as strong as forward scattering. At higher energies the mean scatter direction moves toward the forward direction. Imaging of Compton scattered radiation emanating from other directions (i.e., side scatter imaging) is possible and sometimes desirable if the object's geometry permits it.
- Most scattered radiation leaving a test object has undergone multiple Compton scattering and has little to do with the location of the initial interaction. Therefore multiple-scattered radiation contains no image information and is an image contrast- degrading noise in conventional radiography. Image information from Compton scattered radiation signals can only be used if care is taken that just singly scattered radiation events are measured. This can be accomplished with a highly shielded and collimated source-detector assembly. The size of the sample volume or object slice being analyzed is defined by the intersecting volume of source and detector collimators. The imaging depth is controlled by the collimator's size and intersection angle and the position of the source-detector assembly relative to the surface of the test object.

3.2.4 Sensitivity.

Radiographic sensitivity is a measure of percent thickness change one can detect in an object of a given thickness. It is a function of the subject contrast of the thickness change. With good conventional radiographic techniques it is possible to achieve a 2 percent sensitivity over a wide range of material thickness by optimizing the radiographic energy. A 0.5 percent to 1 percent sensitivity can be demonstrated over a more limited range of material thickness. This implies that indications with a thickness or density change less than these values are not imaged. Laminar defects, such as disbonds and surface corrosion, are difficult to image. Since the lamination usually represents thicker sections, it is often necessary to increase the X-ray energy. As the energy increases, the X-ray attenuation of the sample material decreases, causing small features to be imaged with decreased sensitivity.

With CBI, the measured signal from a volume element being irradiated is directly proportional to its electron density. The change in scattered X-ray intensity is directly proportional to the change in material electron density as shown in Table 3-2. The contrast of a signal originating from a very small inspection volume can approach 100 percent. When material is present in the inspection volume to scatter the X-ray beam, a scattered signal will be present. When no

material or air is present, there will be very little or no scattering and no signal above background will be detected, so that nearly 100 percent subject contrast is provided.

To enhance the detectability of laminar flaws or skin corrosion with CBI, one can make the scattering volume thinner and increase its areal size. This is not possible with conventional radiography. In general, CBI competes with transmission radiography when the test object is thin. In many ways, Compton scatter imaging behaves somewhat like a pulse-echo ultrasonic testing technique, where discontinuities, or voids, act as reflectors of the incident ultrasonic energy.

In general, CBI works best on lower atomic number materials, such as plastics and light metal alloys, where Compton scatter dominates. CBI is especially useful for imaging low-contrast features in low atomic number materials. High atomic number materials can also be imaged if the part is sufficiently thin.

3.2.5 Comparison with Computed Tomography.

Computed tomography is a well-used technique for specific applications like the inspection of rocket motors and jet engine turbine blades. In most CT systems, the scanning system rotates around the object or the object rotates inside the scanning system. The acquired X-ray transmission data, obtained at many different transmission angles, is numerically reconstructed, and the resulting computer-generated image (tomogram) represents a slice image out of the object. CT does not work well for bulky objects like airframes because of rotational limitations. CT also does not work well for flat objects like aircraft wings because of very different object thicknesses in the different transmission directions. In addition, image reconstruction artifacts often affect the tomographic results.

In contrast, CBI is not affected by the object geometry and images can be generated in near real-time without the need for complicated, time-consuming back-projection algorithms. Unlike CT, which provides reconstructed tomographic slice images from a sufficiently large number of X-ray transmission measurements at different orientations of the object, backscatter imaging uses a single imaging orientation of the object and is totally one-sided. This opens up many inspection possibilities which are difficult or impossible to perform with conventional radiography and CT. CBI images, like CT images, show only the area of interest and are free from interfering image superimpositions encountered in transmission radiography.

CBI has the capability to obtain single-slice thickness images representing an X-ray plane at a specified depth below the test object's surface. Individual slices may be assembled into a 3D image in the same manner used with CT. Also, backscattered radiation images can be produced from limited inspection volumes in the immediate region of interest. Conventional CT techniques often require acquisition of data from other regions of the test part in order to compute the geometry of the region of interest.

3.3 PRESENT APPLICATIONS.

The application of CBI to industrial inspection problems has been almost nonexistent until very recently, although the CBI technology has been available for almost 40 years, when it was first used in the medical field.[3-2 to 3-6] Its reemergence was brought about by the U.S. Air Force's need for improved NDI techniques for composite aircraft assemblies and by the marketing effort launched by the Philips Electronics Instrument Company, Industrial Automation

Division of their ComScan Unit, aimed at the use of CDI to inspect automotive castings. The dormancy of this technology in the industrial arena was partly due to a general lack of awareness that the CBI technology existed and partly due to its being overshadowed by the rapid developments in computed tomography. However, during this industrial dormancy, the technology was being used in several other areas; e.g., in the chemical field, for process control, to nondestructively measure soil compaction densities for material level and fill measurements;[3-7] by the military for the detection of buried land mines;[3-8] and for the detection of small voids and case separations in artillery shells.[3-9]

The first reported industrial application of the Compton backscatter measurement technology was the one-sided quantitative measurement of glass-reinforced laminates reported in 1970.[3-10] During the last decade or so, CBI technology has been used for several nonindustrial applications: detection of subsurface defects in metals and castings;[3-11,3-12] inspection of composites for ply separations and density determination;[3-13 to 3-15] detection of solid propellant rocket motor to case unbonds and, in the automotive industry, for inspection of near surface regions of light metal alloys used in such parts as cylinder heads and motor blocks;[3-16] inspection of keel sonar domes;[3-17] and inspection of pipe thermal insulation.[3-18] References 3-11 and 3-19 to 3-25 describe the use of radiation backscatter measurement techniques for a variety of other techniques.

3.4 AIRCRAFT APPLICATIONS.

3.4.1 Technology.

Four aspects of CBI make its use desirable for inspecting aircraft. (1) CBI is a one-sided, near-surface planar inspection technique that is unaffected by aircraft paint or surface roughness. (2) In low-density materials such as composites, CBI can detect small variations in density or thickness that are unlikely to be detected by transmission radiography. (3) CBI is quantitative in measuring material density, depth, and areal size. (4) CBI is unaffected by the delaminations, unbonds, density striations, and electrical conductivity that limit the eddy current and ultrasonic techniques.

Some applications for which CBI is especially useful are (1) the inspection of composites for variations in density as a result of local compositional variations, voids, or delaminations,[3-15 to 3-24] (2) the detection of first-layer and second-layer corrosion in aircraft structures, (3) the quantitative determination of aluminum skin loss due to corrosion, (4) the imaging of moisture intrusion into honeycomb structures, (5) the imaging of cracks in metal and composite structures, (6) the detection of crushed core, (7) the imaging of sealants, gaskets, and O-rings even when these items are enclosed in thick sections of aluminum, and (8) the imaging of many aircraft fuselage and engine components, including castings, for anomalies.

Figure 3-5 illustrates the application of CBI to measurement of aluminum skin loss due to corrosion. Three Compton backscatter images (0.8 mm thick) of a 3-mm-thick aluminum skin from a military transport airplane with corrosion on its backside are shown in the figure. Other applications that are of interest *were* the successful imaging of simulated O-ring damage (i.e., cuts and nicks) when imbedded in aluminum 3 to 4 mm thick (Figure 3-6) and the imaging of sub-millimeter porosity and density changes in sintered ceramic tensile test specimen. The former example illustrates the power of this technique to image details in low-density materials even when covered by dense, thick metals. (It is possible that CBI inspection of space shuttle O-rings prior to launch could have averted a catastrophe. The images were obtained by the

author with the prototype ComScan unit, which was limited by design to a 4-mm maximum depth of focus and a 1-2 line pair per millimeter spatial resolution.)

Excellent Compton backscatter images of interest to the aircraft community can be found in Philips' literature advertising the ComScan Unit. Two of their illustrated brochures describing the ComScan Unit and its applications are available to the public.
The *ComScan X-ray Imaging* brochure[3-16] describes the technical operation of the unit and illustrates some of its applications, such as the backscatter images of simulated crushed honeycomb core, drilled holes in a complex aluminum casting, delaminations in a fiber-reinforced plastic, corrosion in a riveted airframe skin panel, and defects in a polypropylene weld. The other brochure, *Announcing A New Dimension In Aircraft Inspection*, is aimed directly at the aircraft industry. Figure 3-7 shows the ComScan Unit being used for aircraft inspection. Some aircraft applications that are highlighted include the quantitative determination, both in depth and areal size, of first- and second-layer corrosion, honeycomb impact damage, density variations in carbon composite sandwiches, water entrapment in honeycomb structures, and the detection of delaminations and cracks in stabilizer stringers in an all-carbon-reinforced wing which had escaped detection by traditional X-ray inspection methods. This brochure also shows how the ComScan unit is configured for airframe inspection on the hangar floor.

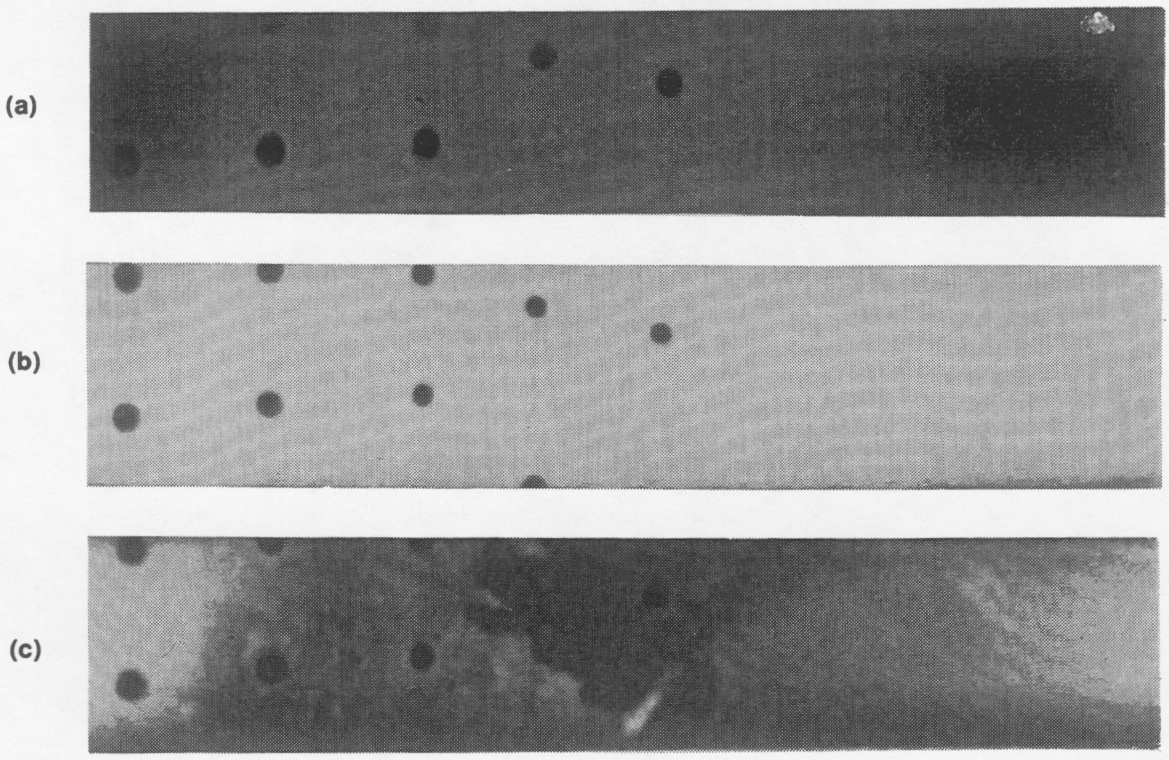

Figure 3-5. Three Compton Backscatter Image Slices Approximately 20 mm x 140 mm by 0.8 mm Thick of Military Aircraft Fuselage Skin Exhibiting Corrosion on Its Under Side. Slice (a) is of the surface; slice (b) is in the skin center of the 3-mm-thick aluminum sample; and slice (c) is of the backsurface showing metal thinning due to corrosion. Surface image slices (a) and (c) are darker (less X-ray backscatter) when compared to slice (b) because the backscatter volume consisted of air and aluminum. These three tomographic slices, as well as 27 others which are not shown, were obtained simultaneously with the 160 kVp prototype ComScan unit in 60 seconds.

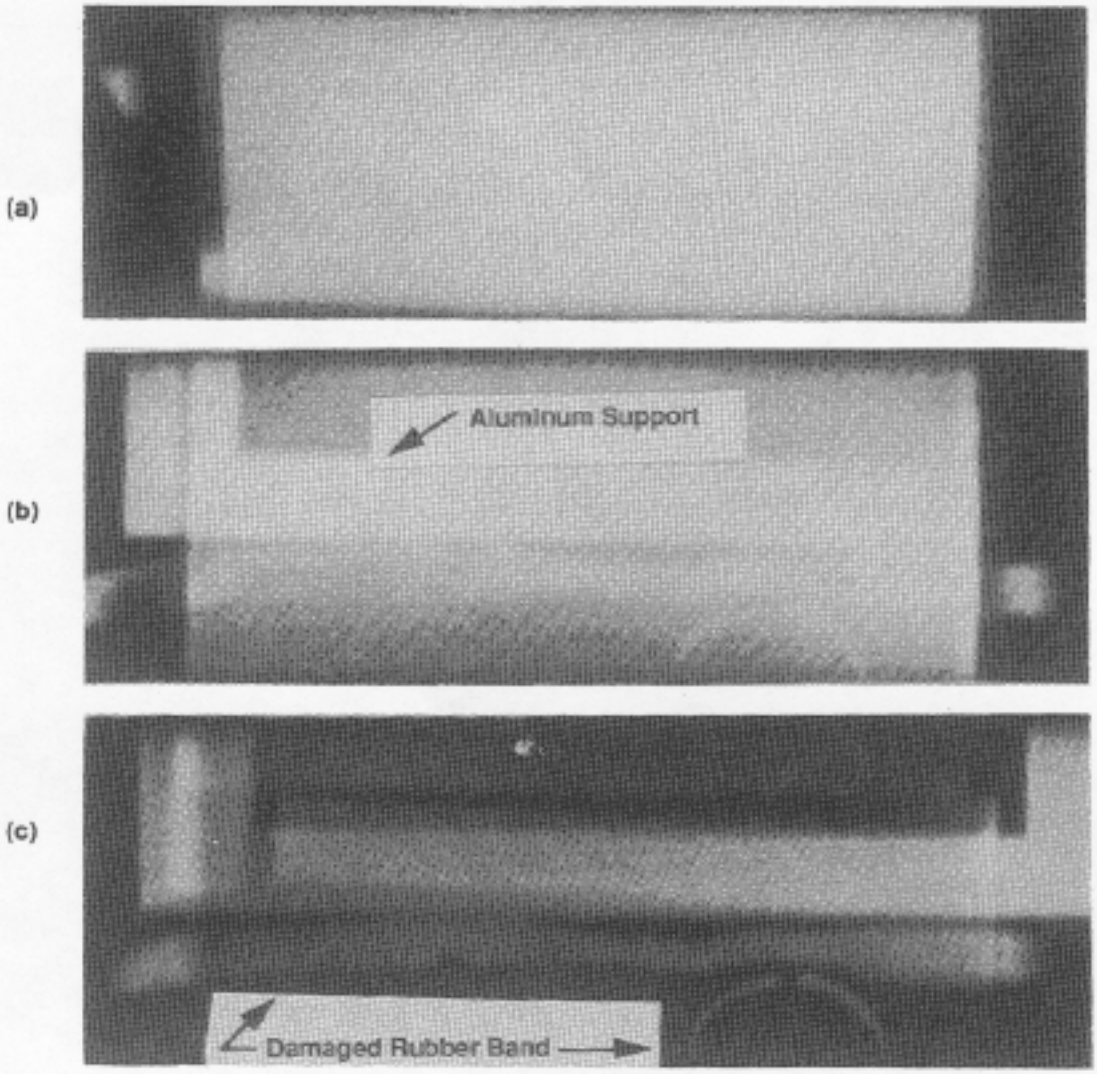

Figure 3-6. Compton Backscatter Image Slices Approximately 0.8 mm Thick Obtained with the Prototype ComScan Machine Showing Cut Rubber Bands Simulating Damaged O-rings Covered with 3 mm of Aluminum. Image slice (a) is inside the 3-mm-thick aluminum top layer; slice (b) contains the bottom side of the aluminum top layer, some underlying aluminum support structure, and partial image of the cut rubber bands; and slice (c) contains the simulated O-rings and the aluminum support structure.

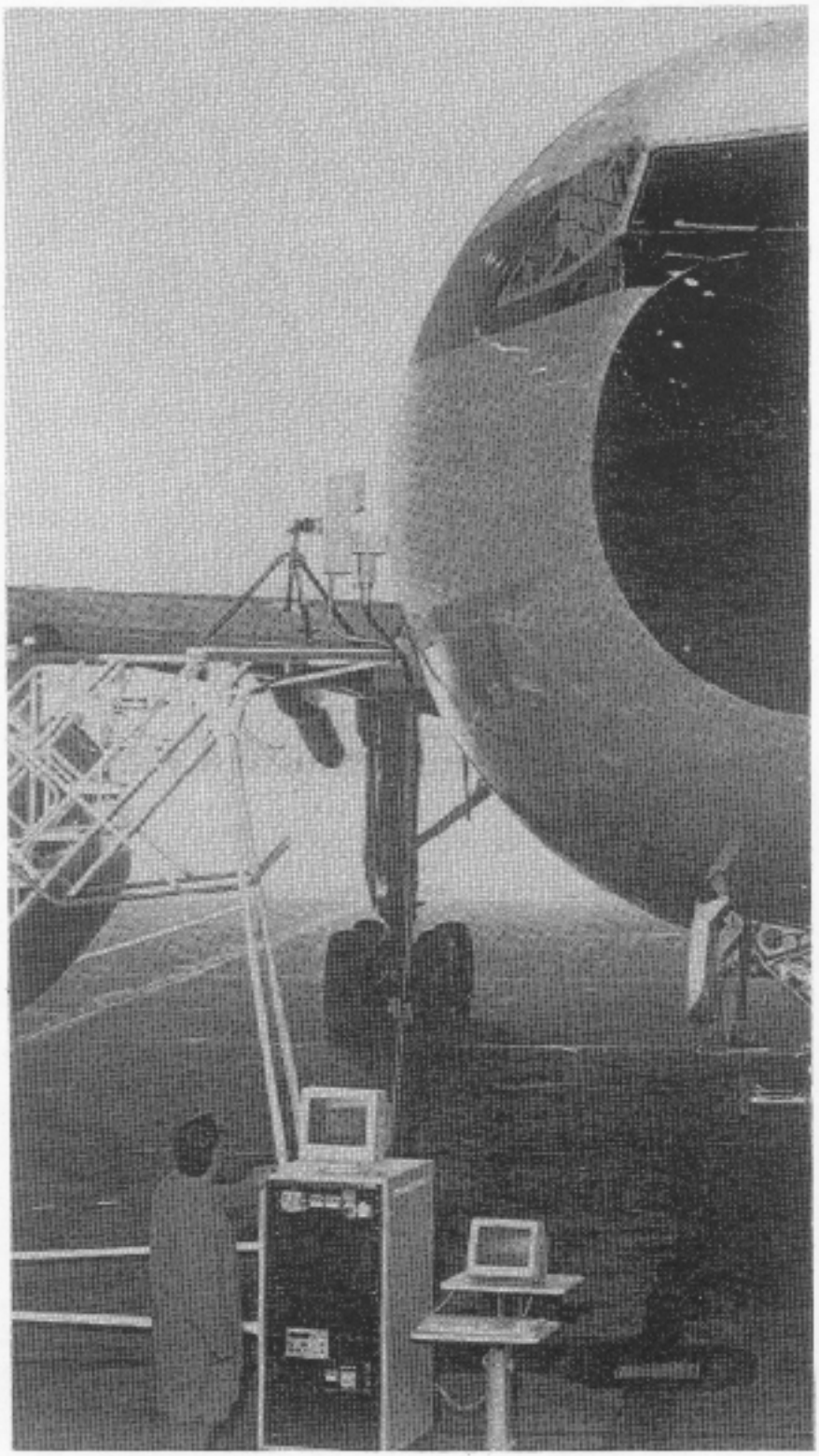

Figure 3-7. Aircraft Fuselage Inspection for First-Layer Corrosion with the ComScan Unit. [Source: Philips Electronic Instruments Company, Industrial Automation Division. By permission of Steve Zahorodny.]

3.4.2 Current Systems.

To date, none of the commercially produced systems were specifically designed and optimized for aircraft inspection. The successful application of CBI technology to the inspection of aged aircraft on the hangar floor will require custom-manufactured systems optimized for a specific inspection problem. For example, a model optimized for the quantitative measurement of localized material loss of aircraft skin with a ± 5 percent accuracy would be different in design from one that was optimized for the inspection and measurement of areal density variations in composites. Currently Philips has the only commercially available system that has been developed for use on aircraft, although it was not initially designed for that purpose. Two other one-of-a-kind imaging systems, the BIT and the ZT, have recently been developed for the U.S. Air Force.

3.4.2.1 The Philips ComScan System.

The Philips ComScan system is a commercially available unit built around a unique compact X-ray scanning head which combines an industrial X-ray source (160 kV) and a scanning collimator with a solid-state detector array and collimation system to provide planar tomographic-like images. Advertised image spatial resolution (for the 10-mm depth range) is 0.4 mm (0.016 in.) by 0.4 mm (0.016 in.), with a depth resolution of 0.45 mm (0.018 in.). All scanning motions are built into the shielded scanning head to provide an approximate X-Y image area of 5 cm by 10 cm (2×8 in.). To image larger areas the source-collimator assembly is indexed to an adjacent location on the object's surface. The system is capable of simultaneously imaging 22 individual parallel thickness slices to a maximum depth of 50 mm (2 in.) to obtain a 3D density map of the volume being inspected. The imaging depth is designed into the source-collimator assembly and can be optimized by the manufacturer for specific applications.

The unit can provide 3D information in the form of closely spaced planar images of the interior of the object being examined. Formation of these images is in real time since the images do not require computed reconstruction. The system is capable of detecting voids or high density inclusions of 0.025 mm, which indicates a 5 percent sensitivity to density changes from one volume element to the next.

The image data is pixelized (250 by 500 pixels by 16 bits deep) and stored in a frame buffer memory. The digital images can be analyzed with standard image processing and analysis software and viewed on a graphic display monitor.

The ComScan prototype unit, now located at the University of Houston, can simultaneously image as many as 30 overlapping tomographic object slices up to a depth of 4 mm in an object with a 5 cm by 20 cm area (2×8 in.) in a single scan of approximately 1 minute. Each tomographic slice image consists of 256 by 512 pixel elements, each 8 bits. Volume elements imaged with this prototype unit were nominally 0.5 mm wide by 1.0 mm long by 1.0 mm deep. The accuracy of the depth position is much better than the thickness of a volume element because of the overlapping slice information. Using X-ray resolution test patterns, the system spatial resolution was measured to be 1 line pair per millimeter. The images shown in Figures 3-5 and 3-6 were obtained with this system.

3.4.2.2 BIT and ZT Systems.

Two other one-of-a-kind backscatter imaging systems developed recently for the U.S. Air Force to inspect aerospace composites are the BIT and the ZT machines.[3-18,3-26] The BIT machine,

built by the Advanced Research and Application Corp., Inc., is used for inspecting structural foams as well as composite materials. The ZT system was manufactured by American Science and Engineering, Inc., who also market a Model 101ZZ backscatter X-ray baggage inspection system to detect explosives.

3.4.3 Possible Future Systems.

Aged aircraft inspection systems based on the Compton backscatter technology can be built by many of the X-ray inspection system manufacturers, computed tomography system suppliers, and experienced radiation-based NDI equipment manufacturers. Commercial suppliers who have demonstrated a CBI capability include Industrial Quality, Inc., Gaithersburg, MD; American Science and Engineering (AS&E), Cambridge, MA; Advanced Research and Application Corp (ARACOR), Sunnyvale, CA; and Bio-Imaging Research (BIR), Inc., Lincolnshire, IL.

3.5 TECHNICAL CONSIDERATIONS.

3.5.1 Advantages.

Compton backscatter imaging is a nondestructive inspection technique that offers many advantages for aircraft inspection. Most important, it allows radiographic inspection to be performed with access to only one side in much the same way that an eddy current or pulse-echo ultrasonic inspection might be conducted. Unlike these two commonly employed aircraft inspection techniques, CBI is a non-contact inspection technique that is unaffected by paint, airgaps, surface roughness variations, electrical conductivity, unbonds, and delaminations. Because of the penetrating power of X-rays, CBI can inspect first-layer, second-layer, and multi-layer aircraft structures to a depth of several inches. In addition to these positive attributes of Compton backscatter imaging, CBI offers many other advantages:

- Backscatter X-ray images can be quantitative in material density, thickness, and areal size.
- Compton backscatter images are digital and can be manipulated with a wide variety of commercial software for analysis, enhancement, and display.
- Compton backscatter images, like computed tomograms, are free of superimposed test object surface information and are easy to interpret.
- CBI depends on detecting the scattered radiation which is an image quality degrading noise in conventional transmission radiography.
- Depending on source and detector collimator geometries, CBI is capable of obtaining laminographic images parallel to the aircraft surface at a known depth. One commercial CBI machine can simultaneously image 22 parallel slices in a single one-minute scan to obtain a 3D volumetric image of the inspection region.
- Compared to conventional radiography, in which the whole inspection region is flooded with X-rays, CBI uses a tightly collimated pencil-like X-ray beam that minimizes the stray radiation, thus significantly reducing radiation shielding requirements (time, distance, or high-density shielding materials).
- Most important, CBI techniques produce superior X-ray imaging results for many applications compared to those achievable with transmitted beam techniques. This is especially true for low X-ray absorption materials like carbon, aerospace composites, explosives, and aluminum, even when they are encased with steel.

- CBI can detect laminar defects and very small amounts of material loss parallel to the inspection surface, for which the transmitted X-ray beam is not useful. It can provide very high contrast images of low-contrast features in low atomic number materials that are impossible to image with conventional radiographic techniques.
- CBI with the X-ray source and detector mounted into a single shielded assembly is an ideal sensor for the automated robotic scanning of the aircraft fuselage.
- CBI systems are easy to use and can be operated by technicians. Imaging is in near real time and does not require complex computationally intensive reconstruction as is required for computed tomography.

3.5.2 Disadvantages.

Like all inspection techniques, CBI has its shortcomings. Some are system specific and others are inherent in the technique. The system specific disadvantages could be overcome or mitigated by tailoring the inspection technology to industry needs.

3.5.2.1 System Specific Disadvantages

System specific disadvantages in current designs and configurations are the following:

- High cost. Currently, only one system is being commercially marketed. System costs are projected to decline as customer demand increases and other suppliers enter the market.
- Potential radiation hazard. Although a potential for radiation hazards exists, the danger is less than with transmission radiography, where the whole area is flooded with X-rays. CBI employs a small-diameter, collimated X-ray beam and detector geometry, which is easily shielded.
- Small inspection area and slow acquisition rates. These disadvantages could be overcome by building a system that measures large-area metal loss. This can be achieved by increasing the sample volume area while keeping the depth resolution the same, or simply by statistically sampling the inspection area. The high-resolution images of corrosion, which require a tremendous amount of time-consuming data acquisition, are not essential for corrosion detection.

3.5.2.2 Technique Limitations

Technique limitations are as follows:

- Reduced image contrast in high atomic number materials (e.g., tungsten).
- Limited depth of penetration. (See discussion below.)

3.5.2.3 Depth of Penetration.

CBI systems have an inspection depth limit. The CBI inspection depth is limited by the energy and hence the range of backscattered X-rays in the material being inspected. As shown in Figure 3-2, energy of the backscattered X-rays is a function of the incident X-ray energy and the cosine of its scattering angle. The calculated Compton backscattered X-ray energies for various scattering angles is shown in Figure 3-4. These graphs illustrate that (1) the maximum energy of backscattered X-rays for 160- to 400-kV industrial inspection systems falls into a

narrow energy range (i.e., 100 to 160 kV) and (2) the peak energies of backscattered photons are in the 250- to 290-kV range even when the inspection is being done with 10 MeV or more energetic X-rays. Thus the imaging depth of CBI is bounded by the maximum range of 250- to 290-keV backscattered X-rays in the material being inspected. The average range of Compton backscattered photons in some aircraft materials of interest are shown in Table 3-2. The practical upper inspection depth limit is approximately 3 to 5 times the average X-ray range in these materials. For example, the penetration depth in aluminum is approximately 7.5 to 13 cm (about 3 to 5 in.) when the inspection is being done with 300-kV X-rays. Because of signal-to-noise statistical limitations of the backscatter measurement, better flaw detection sensitivity is achieved when thinner sections are inspected.

Even though CBI offers technical solutions to some critical aging aircraft inspection problems, its disadvantages, especially in its present stage of development, appear to slow its acceptance by the industry.

3.6 STATUS.

3.6.1 Present.

Although many of the technical capabilities of CBI for solving aging aircraft flaw detection problems have been successfully demonstrated, industry acceptance of this technique has been almost nonexistent. The primary reason appears to be the absence of a practical, cost-effective industrial Compton backscatter imager that has been specifically designed for the commercial airline industry. Other deterrents to ready acceptance may be that aircraft maintenance facilities are reluctant to use radiation-based technology unless absolutely necessary and that the cost of custom-made, technologically complex inspection systems is very high.

Currently, the only CBI system commercially available is the ComScan System developed by Philips Industrial X-ray Supply Center in Hamburg, Germany, and marketed in the United States by the Philips Electronic Instruments Company, Norcross, Georgia. (See Section 3.4.2.) The cost of the ComScan CBI System competes with low-end CT systems and is approximately $500,000.[3-19 to 3-26]

Two other one-of-a-kind backscatter imaging systems developed recently for the U.S. Air Force to inspect aerospace composites are the BIT and ZT machines. The BIT machine, built by the Advanced Research and Application Corp., Inc., is used for inspecting structural foams as well as composite materials. The ZT system was manufactured by American Science and Engineering, Inc.

3.6.2 Future.

CBI equipment evaluations conducted by both the manufacturer and potential customers have shown the utility of CBI technology. It appears that CBI technology offers advantages, especially for the inspection of layered composites and detection of second-layer corrosion, when compared to currently employed NDI techniques such as pulse echo ultrasonics. These advantages imply that CBI offers a potential solution to numerous aging aircraft inspection problems that other currently employed NDI techniques fail to solve. Although CBI appears to offer a technical solution for some rather difficult inspection problems, its future acceptance by the airline industries will be tempered by its present state of development and its relatively high cost.

The successful implementation of CBI technology for the inspection of aged aircraft appears to rest with the customer, the airline industry, and the system manufacturers. The customer has to show a stronger interest in the development of this technology, while the manufacturer has to respond with cost-effective systems designed to address aged aircraft inspection areas of interest.

3.7 REFERENCES

3-1. A. H. Compton, "A Quantum Theory of the Scattering of X-rays by Light Elements." *Phys. Rev.*, Vol **21**, pp. 483–502, 1923.

3-2. J. Battista and M. Bronskill, "Compton-Scatter Tissue Densitometry: Calculation of Single and Multiple-Scatter Photon Fluences," *Phys. Med. Biol.*, Vol. **23**, pp. 1–23, 1978.

3-3. R. L. Clarke and G. Van Kyk, "New Method for Measurement of Bone Mineral Content Using Both Transmitted and Scattered Beams of Gamma-Rays," *Phys. Med. Biol.*, Vol. **18**, pp. 5342–539, 1973.

3-4. E. S. Garnett, T. J. Kennett, D. B. Kenyon, and C. E. Weaver, "A Photon Scattering Technique for Measurement of Absolute Bone Density in Man," *Radiol.*, Vol. **106**:209–13, 1973

3-5. P. G. Lalo, "The Examination of Internal Tissues Using Gamma-Ray Scatter with Possible Extension to Megavolt Radiography," *Phys. Med. Biol.*, Vol. **4**, pp. 159–67, 1959.

3-6. E. Odelblad, and A. Norhagen, "Electron Density in a Localized Volume by Compton Scattering," *Acta Radiologics*, Vol. **45**:161–167, 1956.

3-7. M. Kato, O. Sato, and H. Saito, "A Study on the Applications of Backscatter Gamma-Rays To Gauging," pp. 230–33, Proceedings of ERDA Symposium on X-and Gamma-Rays (Conference 760639), Ann Arbor, MI, May 19–21, 1976.

3-8. F. L. Roder and R. A. Van Konyenburg, *Theory and Application of X Ray and Gamma-Ray Backscatter to Landmine Detection*, Report 2134. Fort Belvoir, VA, U.S. Army Mobility Equipment Research and Development Center, 1975.

3-9. D. G. Costello, J. A. Stokes, and A. P. Trippe, "Theory and Applications of Collimated Photon Scattering," 14th Symposium on Nondestructive Evaluation, San Antonio, TX. 1983.

3-10. J. D. White, *Compton Scattering Technique for Measuring the Areal Density of Glass-Reinforced Structures*, TID-4500, Document Y-1714, Oak Ridge Y-12 Plant, Union Carbide Corp. Nuclear Division, May 7, 1970.

3-11. G. A. Arkhipov, E. G. Golukov, B. L. Dvinyaninov, P. P. Zol'nikov, Yu. Kovyazin, and K.A. Sukhanova, "Using Scattered Gamma Radiation for Detecting Subsurface Defects in Metals," *Soviet Journal of NDT*, Vol. **12**, No 3, pp. 272–75, 1976.

3-12. H. Strecker, "Scatter Imaging of Aluminum Castings Using an X-ray Fan Beam and a Pinhole Camera," *Materials Evaluation*, Vol. **40**: 1050–56, September 1982.

3-13. D. Babot, G. Peix, P. Duvauchelle, C. Le Floc'h and P. Sarrazin, "Thickness and Density Measurements of Advanced Materials by Using Backscattering of X-rays," *Review of Progress in Quantitative Nondestructive Evaluation*, Vol. **10A**, pp. 385–92, Plenum Press, NY, 1991.

3-14. H. Berger, Y. T. Cheng, and E. L. Criscuolo, *High Sensitivity, One-Sided X-ray Inspection System*, NSWC TR 85-292, July 1985.

3-15. T. S. Jones and H. Berger "Applications of Nondestructive Inspection Methods to Composites," *Materials Evaluation*, pp. 390–98, April 1989.

3-16. J. Kosanetzky, G. Harding, K. H. Fisher, A. Meyer, "Compton Backscatter Tomography of Low Atomic Number Materials With the COMSCAN System," *Philips ComScan X-Ray Imaging Technical Information Bulletin*, February 1988, Philips GmbH, Hamburg, Germany.

3-17. E. C. Greenwald, C. F. Poranski, and D. Schafer, "X-Ray Backscatter Tomography for NDE of Steel Reinforced Domes," *Review of Progress in Quantitative Nondestructive Evaluation*, Vol. **10A**, 469–76, Plenum Press, NY, 1991.

3-18. B. D. Cook, Z-H Xu, W. L. Anderson, and S. Nileshwar, "X-ray Backscattering in Thermal Insulation," Proceedings 1990 ASNT Spring Conference, San Antonio, TX, pp. 199–201, March 19–23, 1990.

3-19. Marin Annic, Paul Bjorkholm, and Richard Mastonardi, "ZT: A Tomographic Backscatter Technique for Nondestructive Evaluation," 16th Symposium on Nondestructive Evaluation, San Antonio, TX, April 1987.

3-20. R. T. Bernardi, M. D. Silver, and C. V. Uropas, "X-ray Backscatter Tomography Research at BIR," Bio-Imaging, Inc. (BIR) White Paper, June 22, 1991.

3-21. R. H. Bossi, K. D. Friddel, and J. M. Nelson, "Backscatter X-ray Imaging," *Materials Evaluation*, Vol. **46**, 1462–65, October 1988.

3-22. R. H. Bossi and J. L. Cline, "One Sided Radiographic Inspection Using Backscatter Imaging," *Review of Progress in Quantitative Nondestructive Evaluation*, Vol. **8A**; 465–71, Plenum Press, NY, 1989.

3-23. S. Bukshpan, D. Kedem, "Detection of Imperfections by Means of Narrow Beam Gamma Scattering," *Materials Evaluation*, Vol. **33**, No. 10, pp. 243–245, 1975.

3-24. G. Harding, "On the Sensitivity and Application Possibilities of a Novel Compton Scatter Imaging System," IEEE Transactions on Nuclear Science, Vol. NS-29, No. 3, June 1987.

3-25. D. W. Hill and J. C. Peak, "Development of a One Sided Gamma-Ray Tomography System," *Review of Progress in Quantitative Nondestructive Evaluation*, Vol. **7A**, pp. 415–23, Plenum Press, NY, 1988.

3-26. J. H. Stanley and J. J. Lepage, "Development of a Prototype Backscatter Tomograph," AFWAL-TR-85-4140, February 1986.

4. REVERSE GEOMETRY X-RADIOGRAPHY.

4.1 SUMMARY.

Unlike conventional industrial radiography, which utilizes a fixed-point X-ray source and a large-area detector (film or X-ray image intensifier), reverse geometry radiography (RGX) uses an electronic point detector and a raster-scanned large-area X-ray source. In conventional radiography, the radiographic object must be placed close to the large-area detector. With the Reverse Geometry X-ray (RGX)® system, the opposite is true. The object is placed in the proximity of the X-ray source. With this "reverse radiography" technique, scatter-free (high signal/noise) digital radiographic images are obtained in seconds.

System evaluations have shown that RGX images of aircraft materials and components exhibit contrast sensitivity (i.e., 1.25 percent and 0.2 percent thickness change in 0.04 and 0.5 in. of aluminum, respectively) that is superior to the sensitivity obtainable with standard radiography, and spatial resolution that is comparable to that obtainable with standard radiography. System performance characteristics such as these indicate that RGX is an excellent tool for detecting corrosion in aircraft aluminum and small density changes in composite materials. Digital image interpretation is assisted by RGX system software.

For the RGX system to be useful to the aircraft industry, its components must be modularized. If it is possible to place a shielded reverse geometry X-ray source outside the airplane against the fuselage and the X-ray detector(s) inside the cabin, cargo bay, or wing, many inspection possibilities are feasible.

4.2 TECHNICAL BACKGROUND.

4.2.1 The Concept of Reverse Geometry X-radiography.

Reverse geometry X-radiography is a new concept in radiography that was recently introduced to the radiography community by Digiray Corporation with the RGX® system. The RGX system provides high-quality 2D or stereoscopic (3D) digital radiographs with high resolution and high contrast sensitivity in near real-time. RGX provides images that are essentially free of scattered radiation (noise), which degrades image contrast. The system exhibits an exceptionally high ability to image very small differences in material thickness or density (subject contrast) over a wide range of material thicknesses when compared to conventional industrial radiography (film) and radioscopy (electronic imaging). Figure 4-1 shows these aspects of the RGX image. The ability of RGX to reject scattered radiation, which is a common occurrence in most X-ray interactions in light aerospace and aircraft materials such as composites and aluminum, makes reverse geometry digital radiography an important quality control tool for the air transportation industry. Figure 4-2 illustrates the dominant role that X-ray scattering interactions play in the radiography of aerospace materials.[4-1, 4-2]

Reverse geometry X-radiography, like conventional radiography, employs three components: an X-ray source, a radiographic object, and an X-ray detector. These components are shown in Figure 4-3. Instead of employing a point-source and a large-area radiation detector such as film, reverse geometry radiography is performed with a large-area raster scanning X-ray source and a small point radiation detector. The geometry is exactly reversed.

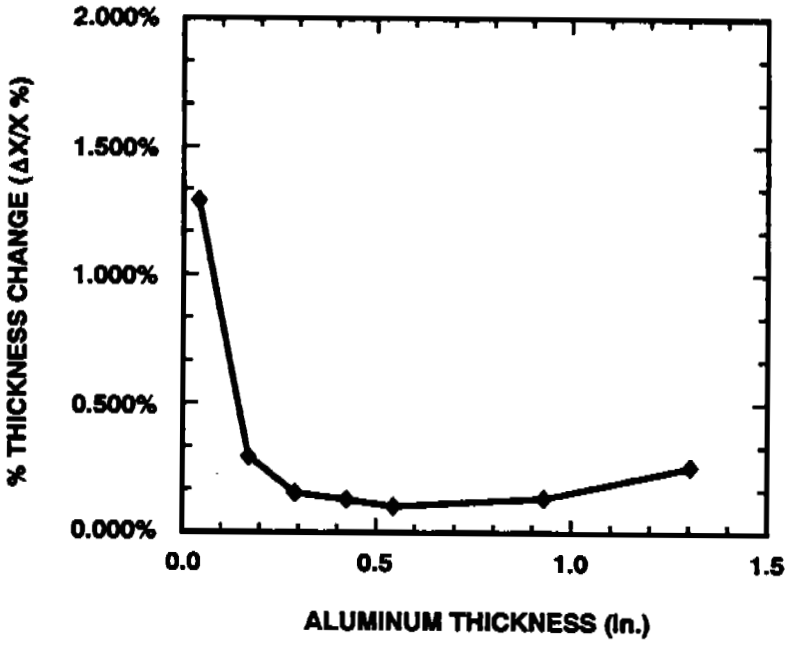

Figure 4-1. Graph of Aluminum Material Percentage Thickness Changes (Subject Contrast Sensitivity) as a Function of Aluminum Thickness that is Achievable with the Digiray RGX System. From this graph one can predict that corrosion thinning of 0.0005 in. or more should be detectable in a 0.040-in.-thick aircraft skin panel.

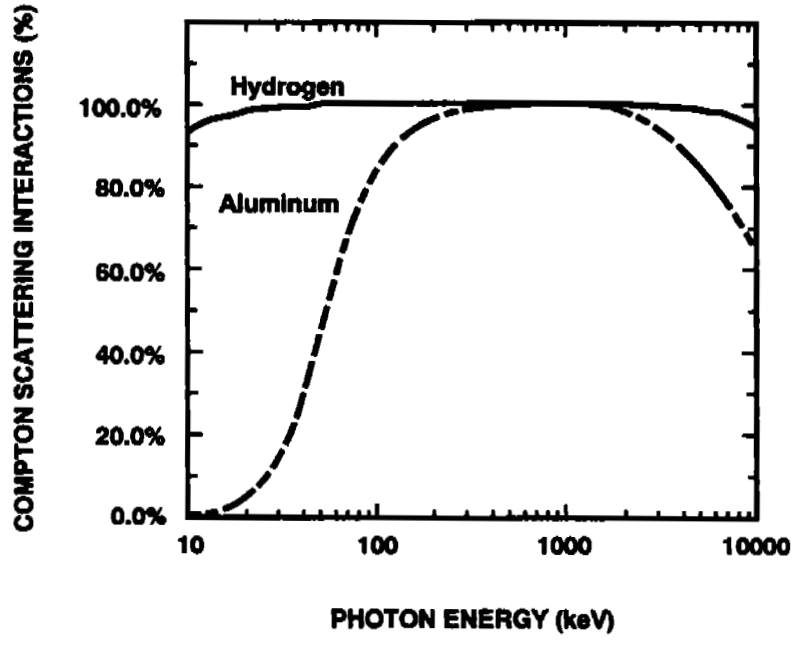

Figure 4-2. Graph of the X-ray Scattering Fraction of All X-ray Interactions in Hydrogen and Aluminum as a Function of X-ray Photon Energy. This graph shows that scattering is the dominant X-ray interaction in composites and light aerospace structural materials such as beryllium and aluminum over the radiographic energy range of interest.

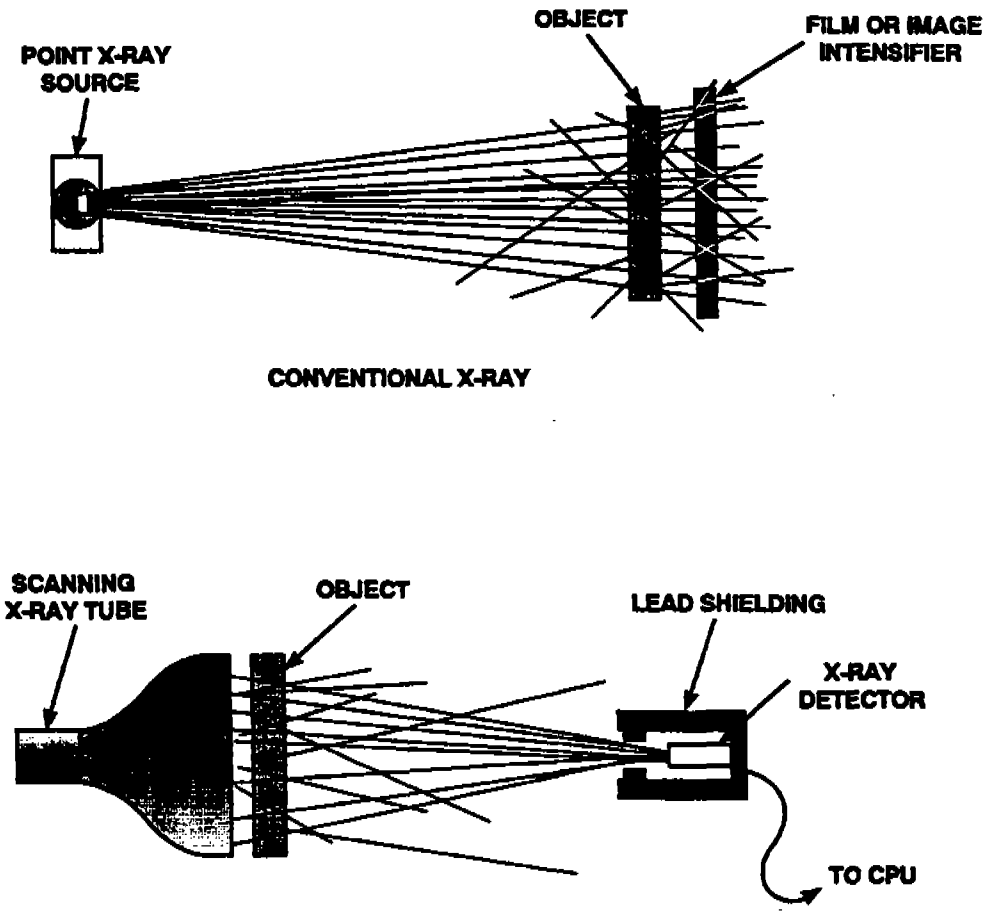

Figure 4-3. Schematic Concept of Conventional Radiography and Reverse Geometry X-radiography Illustrating Fundamental Differences Between the Two Techniques.

The reverse geometry X-ray source is a cathode ray tube in which a focused beam of energetic electrons is accelerated toward the face of the tube or anode. X-rays are produced in the target, which is a thin sheet of high-atomic-number metal such as tantalum. Some of the X-rays leave the transmission target, while others are absorbed in the target and in the X-ray tube housing.

The energetic electron beam scans the inside surface of the target in a manner similar to that employed in a television picture tube to produce a rapidly moving microfocus X-ray source. The electron beam is electromagnetically deflected to create a 512-, 1024-, or 2048-line pattern. Data from the collimated X-ray detector is synchronized with the raster data from the source and processed in a computer to produce an image on a monitor.

The radiographic object is placed next to the source while the X-ray beam scans through the object in a raster pattern. Some of the X-rays are absorbed in the object, some are scattered out of the beam by the object, and the others do not interact at all with the object but pass right through it. A fraction of these un-interacted transmitted X-rays (signal) and a much smaller fraction of the scattered X-rays (noise) reaches the radiation detector and generates a signal proportional to the number of X-rays detected. This signal is recorded in an array computer

memory as a function of X-ray source position or time. An image can be formed with a frame time as little as one-fourth of a second.

An identical radiation interaction process takes place during conventional radiography. However, in conventional radiography: (1) The total object is irradiated at any instant during the exposure compared to just a very small volume fraction with RGX, and (2) With the object being close to the large-area detector, a much larger fraction of the scattered radiation interacts with the detector, resulting in an image with reduced contrast. The reduction in radiographic image contrast results in a proportional loss in flaw detection sensitivity.

Another fundamental difference between the two radiographic processes lies in the performance characteristics of the imaging detectors. Compared to industrial X-ray film or X-ray image intensifiers, the small-point radiation detector, which is a scintillating crystal coupled to a photomultiplier tube, has a dynamic range at least ten times that of film. This permits the RGX detector to record and display smaller differences in material density or thickness over a wider range of materials and thicknesses than is possible with conventional radiographic imagers in a single exposure. Finally, since the RGX images are digital, a wide variety of standard image-processing tools such as averaging, filtering, image subtraction, and edge enhancement are easily and rapidly applied to assist in image interpretation.[4-3, 4-4]

The concept of reverse geometry radiography, although simple, is difficult for many radiographers to understand immediately because it initially appears to violate many of the principles of fundamental radiography. For example, in conventional radiography the radiographic object must be placed close to the X-ray detector to reduce image blur. With RGX the opposite is true: the image sharpness is maximized when the object is very close to the scanning X-ray source. The following paragraphs describe Digiray's RGX system and its features.

4.2.2 RGX System Description.

The basic RGX cabinet radiography system shown in Figure 4-4 consists of a shielded X-ray cabinet and an electronic equipment rack. The cabinet houses the high-voltage power supply and the reverse geometry 100-kV, 1.5-mA X-ray tube. The exposure area is in the center behind access doors that, for operational safety, are electronically interlocked with the source. The 1-in.-diameter, scintillation-crystal photomultiplier radiation detector is housed in the upper chamber. The source-to-detector distance is variable from 3 inches to 9 feet. The equipment rack holds an AT-386 CPU, an optional image storage disk, a pseudocolor video image processor, and a high-resolution display monitor.

RGX exposures for 8-bit data vary from 0.25 second to several minutes. 12-bit images can also be obtained with a longer image acquisition time. The data from the detector is digitized and sorted into a pixel array of 512×512, 1024×1024 or 2048×2048 lines. Images, up to 10 inches in diameter, are immediately available on a video monitor. The radiographer can choose among three levels of line resolution and frame time: 512×512 line imaging takes 0.25 second per frame, 1024×1024 line imaging takes 1 second per frame and 2048×2048 line imaging takes 4 seconds per frame. Multiple frames can be summed or averaged in the computer for contrast and resolution enhancement.

Other on-line image processing features available to the user include zoom and pan capabilities to enlarge features, pseudocolor to highlight areas of interest, tint rolling in black and white or color to bring out subtle image density differences, pseudo-3D density graphs that project object density as depth, pixel intensity graphs for feature analysis such as crack depth, image dimensional measurement, and annotation.

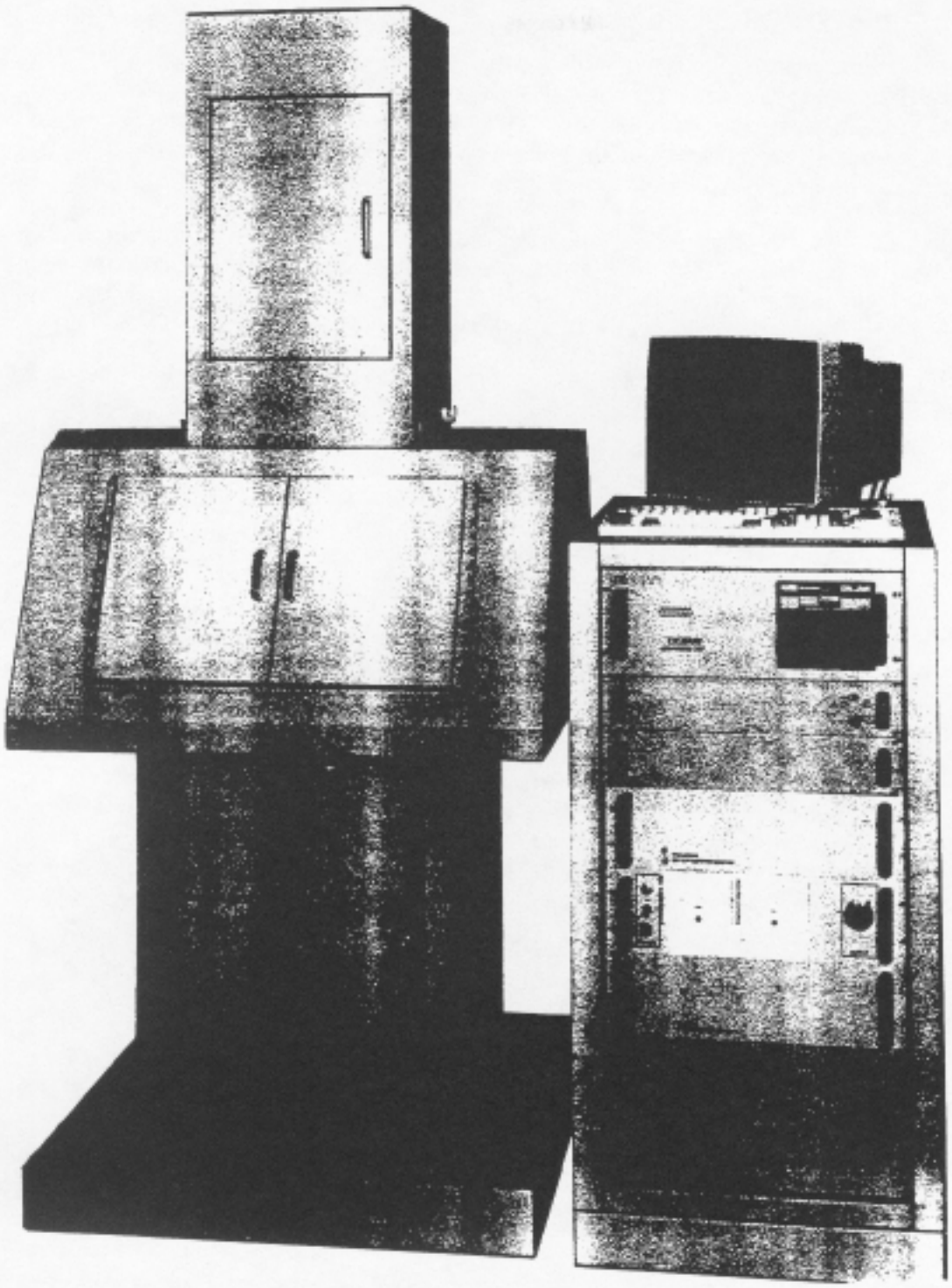

Figure 4-4. Photograph of a 100-kV Digiray Shielded Cabinet Reverse Geometry Radiography System.

4.2.3 Stereoscopic Radiography.

A stereo radiography option is available for the RGX system. In this mode, dual X-ray detectors are positioned next to each other at a distance approximately equal to that between two human eyes to produce 3D images within seconds. The operator wears special Polaroid glasses designed to view two rapidly alternating offset images on a special shuttered monitor. This feature may be useful for the radiographic determination of flaw depth or crack orientation.

The system also has dual-angle imaging capabilities. The two detectors normally used to integrate depth perception in three-dimensional imaging can be set to instantaneously produce two images taken at small angular differences. This can resolve image interpretation ambiguities caused by the overlap of objects in different planes.

4.3 PRESENT APPLICATIONS.

At present most applications are in the areas of aerospace, aircraft, electronics, and pyrotechnics.

4.4 AIRCRAFT APPLICATIONS.

Because the Digiray system is fairly new, not all of its potential applications have been fully investigated. In general, it is applicable to the inspection of most aerospace components that can be radiographed with a 100-kV X-ray machine. In addition, the RGX system has some potentially unique applications that cannot be performed by film and conventional non-film radiography.

Traditional applications, as evidenced by customer hardware being tested in Digiray's Applications Laboratory, include the successful inspection of a wide variety of airframe, engine, and aerospace hardware. Representative samples include metal matrix and graphite epoxy composites; aluminum and composite honeycomb; castings; turbine blades; fasteners; rubber parts; plastic components; aircraft structural parts, both new and aged; and a wide variety of electronic hardware, including multilayer circuit boards and chip packages.

Representative sample RGX images of some parts of interest to the aircraft transportation industry are shown in Figures 4-5, 4-6, and 4-7.

Stereo radiography with the RGX system is performed by placing two small radiation detectors, separated by a small distance, in the cabinet and rapidly alternating their respective images on a special display monitor. This has generated some interest in the circuit board and microelectronic fabrication industry. Three-dimensional viewing enables the operator to perceive individual planes in multilayer printed circuit boards and also to obtain a better image of critical solder joints. Other stereoscopic applications for RGX imaging include the location of fiber breakage in metal matrix composites and the location of subsurface corrosion and material loss.

4.5 TECHNICAL CONSIDERATIONS.

4.5.1 Discussion.

For the RGX technology to be useful to the aircraft industry, its components must be modularized outside the shielded cabinet. In this configuration, the shielded X-ray tube would

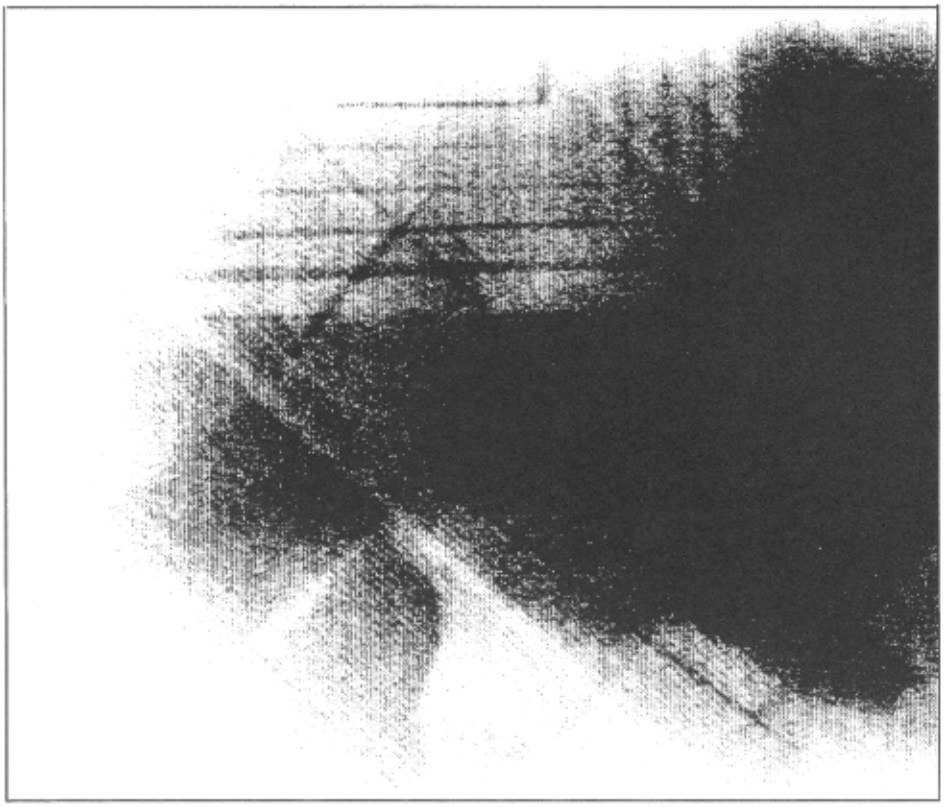

Figure 4-5. RGX Radiograph of a 1/2-Inch-Thick Low-Radar-Visibility Composite Showing the Composite Weave Throughout, Adhesive Density Variations, and a Repair Patch.

Figure 4-6. RGX Radiograph of a 3/4-Inch-Thick Composite Honeycomb Imaging Resin-Rich Cells and Some Water Entrapment (the Long Irregularity Running Along the X-axis). These defects are much more apparent with RGX imaging.

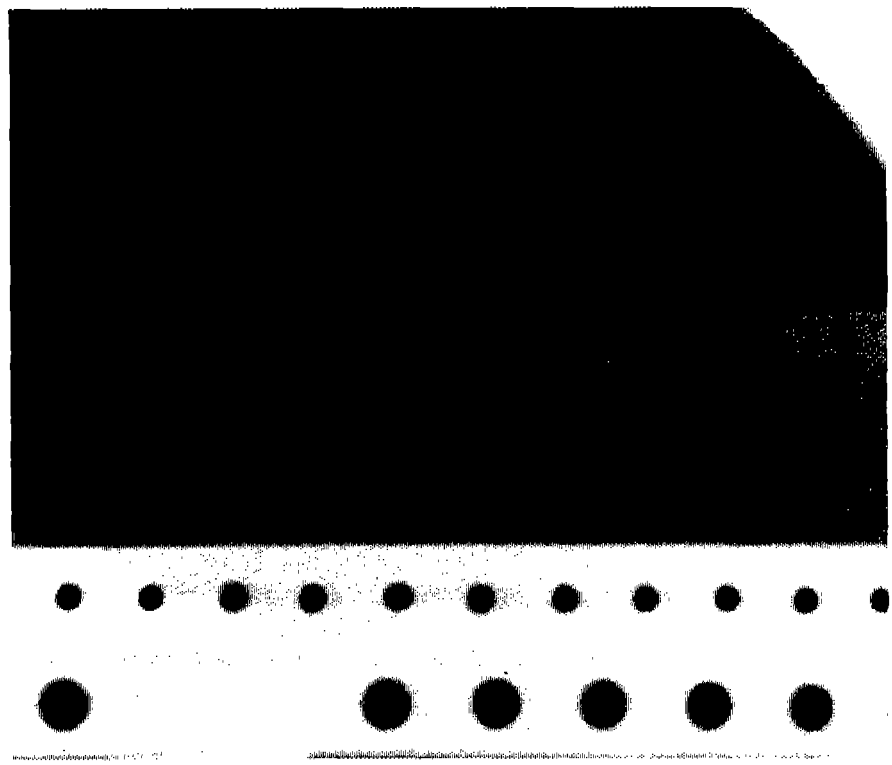

Figure 4-7. RGX Radiograph of the Aluminum Wing Skin of an F-111 Showing Extensive Corrosion and Exhibiting Both Metal Loss (Dark Irregular Images) and the Buildup of Corrosion By-Products (Irregular-Shaped, Brighter Regions).

be mounted on a mobile positioner (tripod) or gantry and the radiation detector would be miniaturized and connected to the CPU through a long cable. The detector, possibly as small as a fiber optic cable, could be snaked into tight places on the aircraft or engine to perform single-wall reverse geometry radiography with a higher flaw detection sensitivity than is achievable with normal radiographing through materials twice as thick. One can also position a detector inside the airplane and place the RGX tube outside the fuselage to inspect the aircraft skin, stringers, and frames for corrosion that may escape detection with conventional NDI techniques. The image of the skin and its underlying support structure will remain in focus, whereas intervening structures near the detector will not be imaged.

4.5.1.1 X-ray Spectrum.

The transmission target X-ray spectrum from RGX tubes is similar to that of a heavily filtered X-ray spectrum obtained from a conventional X-ray reflection source. The thickness of the thin transmission target is optimized for a maximum operating energy of the tube. Operating the tube at lower than the optimized voltage results in a rapid reduction in X-ray intensity because (1) X-ray production is proportional to the accelerating voltage, and (2) more of the X-rays will get absorbed inside the target to harden the X-ray spectrum (average X-ray energy is closer to the peak X-ray energy). This X-ray beam hardening effect coupled with differences between film and radiation detector quantum detection efficiencies can explain image contrast differences obtainable with the two techniques. For example, RGX image contrast can decrease as the kilovolt level is lowered.

The X-ray scintillation detector used in the RGX system is energy sensitive and could be used as a spectrometer. By running the detector signal through a pulse height or energy discriminator, it is possible to rapidly obtain radiographic images of select energies. This capability, although not demonstrated yet, would be extremely useful in enhancing small differences in image density for improved corrosion detection. Similarly, with the availability of multiple digital image memories, one could employ multi-energy radiographic image subtraction techniques in near real-time to enhance flaw detection or to simplify image interpretation.

4.5.1.2 Geometry Effects.

As in conventional radiography, the reverse geometry radiographic process displays similar image distortions and geometrical unsharpness effects (image blur). The image distortion is more pronounced near the outer edge of the image area and, like in conventional radiography, is proportional to the source-to-detector distance. Also, in RGX the depth of focus decreases (geometrical image becomes less sharp) as the object is moved away from the source. This decrease in image sharpness can be minimized by tighter collimation of the radiation detector.

4.5.2 Advantages.

Some of the technical advantages of reverse geometry digital X-radiography for airplane inspection have already been mentioned. These include the ability to image small changes in density or thickness in aluminum and composite structures that may be missed with conventional radiography or other NDI techniques. Although this has been demonstrated in the laboratory with test panels and plates of uniform thickness, the applicability of RGX inspection of complete airframes on the maintenance hangar floor remains to be evaluated. Before this can happen, the RGX system components must be modularized with additional X-ray-shielding materials to minimize personnel radiation exposures. The other proposal, radiographing the airplane fuselage with the RGX tube positioned against the skin and with the detector inside the cabin, also requires some equipment modifications before it can be demonstrated.

Other advantages of RGX when compared to conventional film radiography include:

- The digital image obtained with the RGX system lends itself to rapid computer storage and retrieval of images and to on-line quantitative image analysis with image processing software to measure, for example, metal thinning.
- The RGX system can image a wide range of aircraft material thicknesses (latitude) with a high contrast sensitivity in a single exposure. The system has a wide dynamic range, acquiring up to 4096 levels of gray. The RGX system therefore allows the user to manipulate a track ball to "tint roll" through selected density levels in either black and white or false color. This technique can dramatically highlight such defects as corrosion or water entrapment.
- RGX can provide a spatial resolution that is comparable to that achievable with microfocus X-ray real-time imaging systems using projection magnification radiographic techniques.
- By reducing the diameter of the point radiation detector from 1 in. to 1/8 in., many additional applications, including on-wing engine inspections, may be feasible. For example, replacing bulky film with a very small radiation detector would make it possible to snake the RGX detector into many locations that are inaccessible to film in airframes, wings, and engines to perform radiographic evaluations.

4.5.3 Disadvantages.

Like all inspection systems, reverse geometry radiography has limitations. Some of these, such as the limited image area (10 in. diameter maximum) and maximum radiographic energy (100

kV) are inherent in the current design but may be overcome by the manufacturer. Others, such as the decrease of spatial resolution with increasing object-to-source distance, or the geometric image distortion near the edge of the image area, can be mitigated by changes in the radiographic setup.

In RGX-radiography the image area is limited to the size of the X-ray tube. This may or may not be a problem to a customer since RGX imaging is fairly rapid and large areas can be radiographed with multiple exposures. The energy limitation of the tube, however, can be a problem, especially if one wants to radiograph thick-section components. Since most of the radiographic aircraft applications fall into the other extreme, this may not be a severe limitation; however, the present unavailability of RGX tubes with different peak radiographic energies may preclude its application for certain inspections.

Radiography systems that are radiation-detector based, like the RGX system, exhibit the best flaw detection sensitivity when the product of the material linear attenuation coefficient times its thickness falls into the 1 to 3 range. Since the RGX tube with its transmission target is designed to operate efficiently over a narrow energy band, optimum radiographic results will be obtained only for a limited density-times-thickness range for a given material. It is predicted that an RGX tube designed to operate at lower energies will exhibit even better performance characteristics than the 100-kV tube shown in Figure 4-1 when radiographing thin composites or aluminum structures less than 0.12 in. thick.

Another area where the RGX system's applicability may be limited is in the radiography of explosive devices. Safe-handling procedures for most explosive components do not permit high-voltage equipment in the vicinity required for RGX-radiography. Although this may be a problem in the inspection of military and space hardware, it presents no problem for the inspection of commercial airplanes because they contain no explosive components.

4.6 STATUS.

4.6.1 Present.

The reverse geometry radiographic system is just emerging as a viable NDI tool for the aircraft industry. In its present state of development it appears to compete with real-time microfocus radioscopy systems for some applications, including stereo radioscopy. Although it appears to have advantages over conventional radiography for thin-section radiography and the inspection of materials with a high X-ray scattering probability such as composites, plastics, and adhesives, industry acceptance has been slow.

4.6.2 Future.

The RGX system exhibits some desirable radiographic imaging characteristics that make it a useful tool for the inspection of modern plastic and composite materials. Because it can reject image-degrading scattered radiation, the RGX system is capable of producing digital radiographs of very small density or material thickness changes that are difficult or impossible to detect with conventional radiographic techniques. This makes the RGX inspection system particularly suitable for the inspection of thin and low density materials that are widely used in the transportation industry. Other desirable imaging characteristics, such as the capability for stereoscopic (3D) viewing for flaw depth or orientation determination and the capability of performing image energy slicing for enhanced corrosion detection, contribute to the value of the RGX system as a valuable new tool for ensuring the quality of aged aircraft and extending its future life.

4.7 REFERENCES.

4-1. John Bond, "Reverse geometry X-ray produces clear images," *Test & Measurement World*, September 1991, p. 177.

4-2. Richard Albert, Thomas Albert, and Joseph Fjelstad, "SMT inspection: Another Choice," *Circuits Assembly*, December 1991, pp. 34-36.

4-3. Richard Albert and Thomas Albert, "New Geometry for Large Area, Real-Time, High Resolution Radioscopy," presented at American Society for Nondestructive Testing 1993 Fall Conference, Chicago, IL, November 21, 1992.

4-4. Richard Albert, Ken Bakes, Thomas Albert, "Reverse Geometry X-ray Imaging: A Novel NDT Modality," presented at the 41st DoD Working Group on Nondestructive Testing, Tucson, Arizona, November 17, 1992.

4-5. Thomas M. Albert and Douglas A. Froom, "High Throughput Technology for Aircraft NDE," *Nondestructive Inspection of Aging Aircraft*, SPIE Vol. **2001**, July 1993, pp. 20-36.

4-6. Thomas M. Albert, "X-Ray System Applications Using Reverse Geometry for High Sensitivity," *Materials Evaluation*, September 1993, pp. 1020-1027.

4-7. E. A. Birt, F. R. Parker, and W. P. Winfree, "Quantification of Corrosion Damage in Aircraft Skin Using a Novel X-ray Radiography System," presented at 20th Annual Review of Progress in Quantitative NDE (Center for Nondestructive Evaluation, Iowa State University), held in Brunswick, ME, August 2, 1993.

5. ADVANCED ELECTROMAGNETICS.

The two techniques discussed in this section are magneto-optic eddy current imaging (MOI) and advanced eddy current techniques. The very distinct nature of these techniques makes it appropriate to cover each of them in a separate section: Section 5A for the MOI and Section 5B for the advanced eddy current techniques.

5A. MAGNETO-OPTIC EDDY CURRENT IMAGING (MOI).

5A.1 SUMMARY.

To ensure the continued airworthiness of today's commercial aging aircraft fleet during its extended operational life, the airline industry needs good NDI techniques and sensors. One such emerging NDI technique is the magneto-optic eddy current imager (MOI), which does real time imaging of airframe fatigue cracks and corrosion. Unlike conventional aircraft eddy current NDI in which an accept/reject decision is based on the movement of a meter needle or the interpretation of differences in impedance plane diagrams, the MOI yields visual images corresponding to flaws.

Evaluation of the MOI by both airplane manufacturers and airlines has shown that (1) inspection of large areas for cracks and corrosion is rapid, (2) the inspection can be reliably performed through paint and airline decals (it is insensitive to lift-off effects), (3) the inspection results can be easily videotaped for test documentation, (4) interpretation of the results is fairly intuitive, (5) the instrument is portable, the hand-held sensor is light-weight and easy to use on airplanes, and more important (6) NDI inspectors require little training to become proficient in its use.

Inspection limitations of the MOI include (1) its inability to inspect concave surfaces and rivets that are not flushly mounted (i.e., universal or button heads), and (2) a loss of flaw detection sensitivity near ferrous fasteners. Laboratory probability of crack detection data have indicated that the MOI is at least as reliable as existing eddy current techniques, and it has been recently approved by Boeing, McDonnell Douglas, and Lockheed for the inspection of some riveted joints on their airplanes.

5A.2 TECHNICAL BACKGROUND.

5A.2.1 Introduction.

The MOI instrument, shown in Figure 5A-1 being used by an aircraft technician for lap joint inspection, consists of a hand-held imaging scanner head, TV monitor and power unit, and 30 feet of interconnecting flexible cables. The light-weight (~3-pound) imaging head contains the eddy-current inducing system, a magneto-optic sensor element, and a TV camera.

The MOI images result from the response of the Faraday magneto-optic sensor to weak magnetic fields that are generated when eddy currents induced by the MOI interact with defects in the inspected material. Images appear directly at the sensor and can be viewed directly or imaged by a small CCD TV camera located inside the imaging unit for remote

viewing. The operator views the image on the video monitor while moving the imaging head continuously along the area to be inspected.[5A-1]

The MOI produces video images in real time that show flaw-induced irregularities and inconsistencies in the inspected material. In contrast to conventional eddy current methods, the slightly enlarged images resemble the defects that produce them, making the interpretation of the results more intuitive than the interpretation of traces on a CRT screen. Rivet holes, cracks, and subsurface corrosion are readily visible. Since the image is in a video format, it is easily recorded for inspection documentation.

The instrument is capable of inducing currents in a frequency range of 1.6 to 102.4 kHz. For typical aircraft aluminum, the depth of penetration for these frequencies is 0.12 to 0.015 in., respectively. At the higher frequencies, the MOI can image and detect small, tight fatigue cracks near rivets in the outer surface of aluminum aircraft skins. At lower frequencies, the instrument can image and detect subsurface cracking and corrosion in aluminum.

The advantages of this visually based inspection technique include increased inspection speed, more intuitive and easily interpreted inspection information, a reduction in false calls, and the

Figure 5A-1. Airline Technician Using the Commercial MOI to Examine an Aircraft Fuselage Lap Joint for Fatigue Cracks. (Note: The TV monitor, which is facing out in this figure, would normally be turned toward the operator.)

elimination of the need for paint and decal removal. Unlike other eddy current inspection systems, the MOI is relatively insensitive to lift-off effects.

5A.2.2 Imaging Technology.

The present implementation of the magneto-optic/eddy current imaging technology uses a 3-in.-diameter sensor and is designed to provide images of a relatively large area compared to that covered by an eddy current probe. Present eddy current lap joint inspections are performed rivet by rivet, whereas with the MOI it is possible to capture several rivets in one image. This capability makes the technology appropriate for large, flat or convex, relatively unobstructed areas and ideal for examination of an airplane fuselage, wings, and control surfaces.[5A-2,5A-3]

The MOI technique is relatively insensitive to the effects of lift-off, so paint removal is not necessary. However, maintaining contact with the test surface helps achieve the highest quality images. Test inspections have indicated that in some cases crack images can be seen through nonconductive material that is thicker than any conceivable paint layer(s). Very tight fatigue cracks, as small as 0.02 in. in length, have also been imaged and detected at the higher frequencies. At lower frequencies the instrument has been able to image simulated corrosion regions through more than 0.1 in. of aluminum skin.

Figure 5A-2 illustrates schematically how MOI images are formed. Images are formed when defects or other obstructions such as rivets or holes divert the otherwise uniform flow of induced electric currents near the surface of the test piece. This diversion of eddy currents creates weak magnetic fields perpendicular to the surface of the test piece. These weak magnetic fields are readily imaged in real time by the magneto-optic eddy current imager. Since alternating current is used to excite the inspection area, only half of the image is generated during each half of the cycle of applied current, as shown in Figure 5A-2. The current-switching process occurs so rapidly that the image appears as one to the inspector. The images of rivets and holes appear as slotted screws.

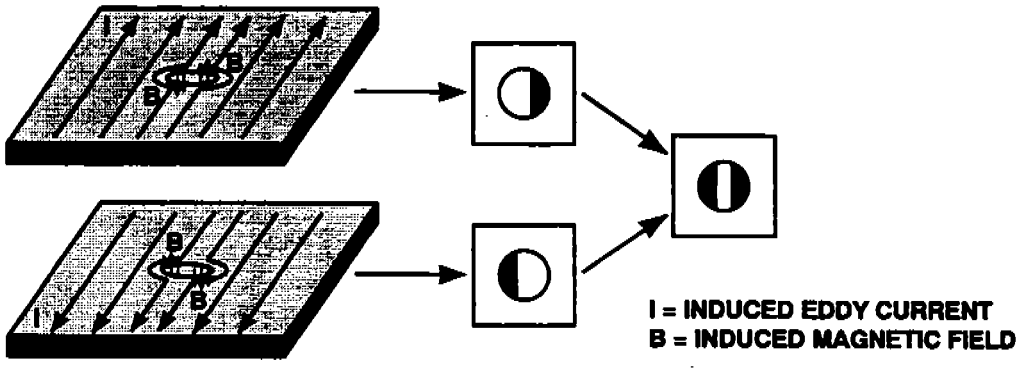

Figure 5A-2. MOI-Formed Images. Note the slotted-screw-like appearance of the MOI images.

Surface cracks. Figures 5A-3, 5A-4, and 5A-5 show MOI images of various samples. It is clear from these figures that the magneto-optic/eddy current imager produces crack images that resemble the crack. Crack images are images of the magnetic fields surrounding the actual crack or rivet, which includes a halo region approximately one eddy current skin depth in width.[5A-3] An estimate of the actual crack length may be obtained by subtracting the skin depth (frequency dependent) from the observed defect length (taking into consideration scale changes on the monitor). Clearly this method will begin to break down when the actual crack length is equal to or less than the skin depth (Figure 5A-6). The estimate of length also varies somewhat as the image-level setting is varied. An alternative method for estimating crack length is to compare the cracks to MOI images of rivets or holes with a known size. These techniques for estimating crack lengths have not been extensively tested for accuracy.

Extended cracks. Extended cracks may not generate continuous images, as is apparent in Figure 5A-5. Because the sensor images the magnetic fields surrounding an extended crack, a nonuniform current flow around such a crack leads to a nonuniform image. Typically, the center portion of the image of a very long crack will be weaker than that at the ends because of nonuniform current flow near the center. The ends of these types of cracks are usually quite obvious and easily detectable.

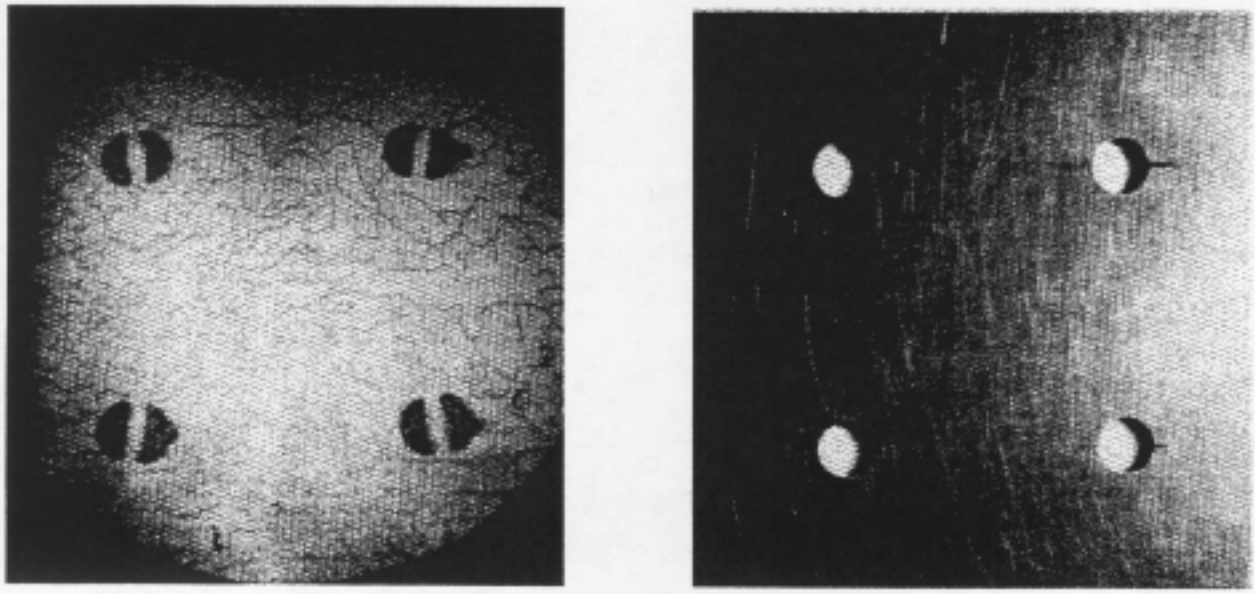

(a) (b)

Figure 5A-3. MOI Image (a) and Photo (b) of Holes in Aluminum Test Panel. The 0.060-in.-thick aluminum panel contains four 0.025-in.-diameter holes with EDM notches emanating from them in lengths of 0.020, 0.040, 0.060, and 0.080 in. The order is counterclockwise beginning with the 0.02-in.-long EDM notch in the upper left corner of (a) and (b).

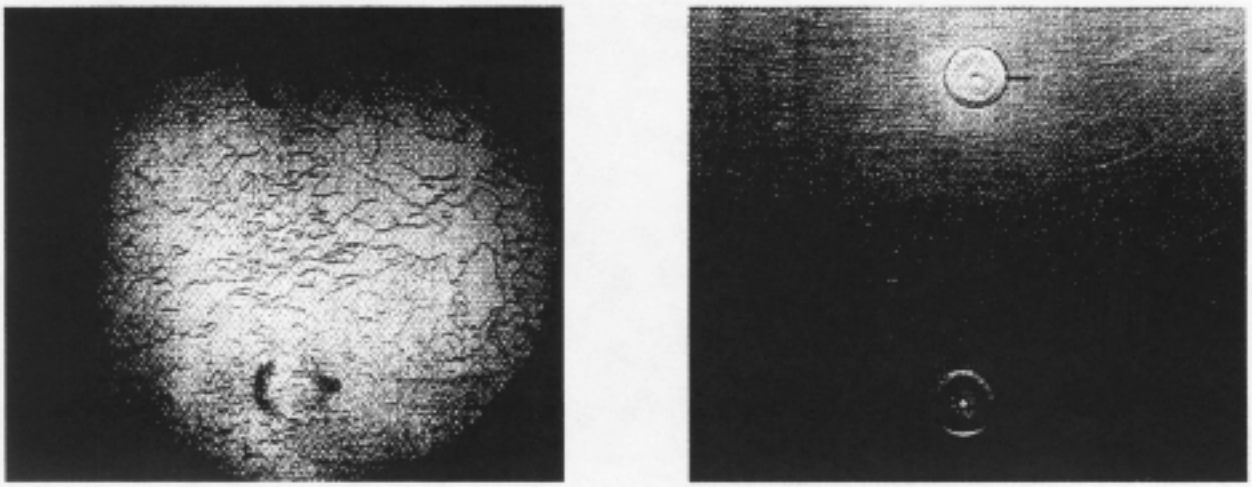

(a) (b)

Figure 5A-4. MOI Image (a) and Photo (b) of Test Piece Made Up of Two Aluminum Panels Riveted Together. The top panel is 0.09 in. thick and the bottom panel is 0.05 in. thick with various-length EDM notches emanating from the rivet hole shanks. The upper notch in (b) extends 0.18 in. from the rivet head while the lower notch extends 0.12 in. from the rivet head.

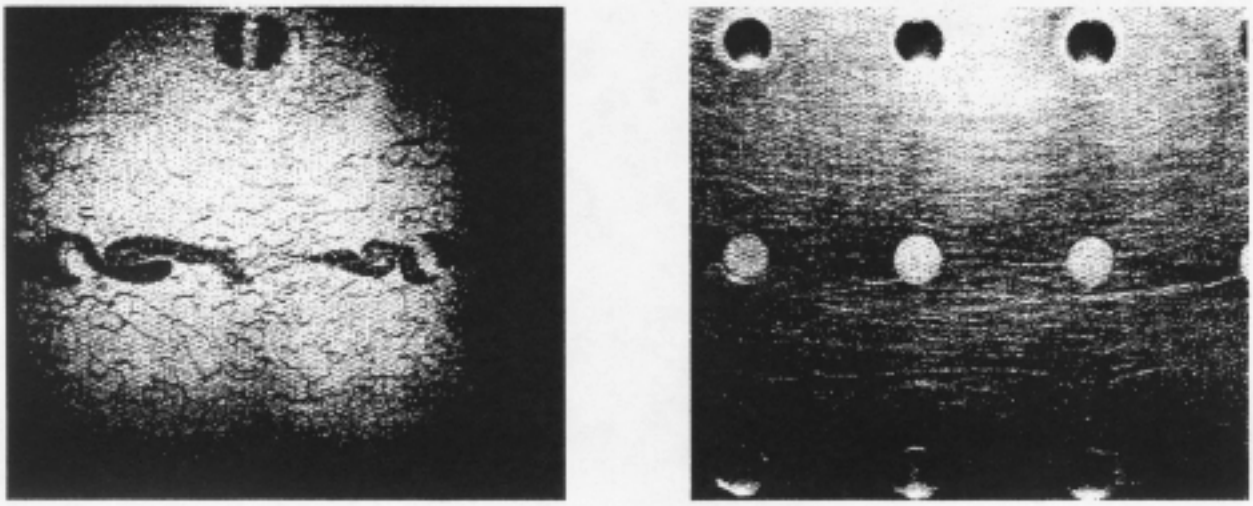

(a) (b)

Figure 5A-5. MOI Image (a) and Photo (b) of an Extended Crack In a Riveted Aluminum Lap Joint Test Sample. The extended crack was generated during a fatigue test. Note the scalloped- shape similarities of the crack and its MOI image.

Second-layer cracks and corrosion. Defects which are not near the surface may also be detected, provided that the eddy current skin depth is at least as great as the depth of the defect. Defects deeper in material than one skin depth usually produce very weak magnetic fields that are difficult or impossible to image. Thus, the instrument's settings of 25.6, 51.2 and 102.4 kHz are used for imaging near-surface defects, while the lower frequency settings (1.6 to 12.8 kHz) can penetrate deeper for imaging second-layer cracks and corrosion. Inspection at lower frequencies is accompanied by a loss of resolution and a reduction in flaw detectability.

The eddy current skin depth as a function of excitation frequency for various conductors is shown in Figure 5A-6. Figure 5A-7 is an image of EDM notches in the second layer of a DC-9 test standard. The images of these deeper defects are more diffuse and less sharply defined than surface cracks. This occurs because the magnetic fields associated with these defects are weaker and more diffuse.

Figure 5A-8 shows an image of a corroded region in a panel removed from an older commercial airplane. The image is a mirror image of the actual component because it was obtained from the opposite, non-corroded side.

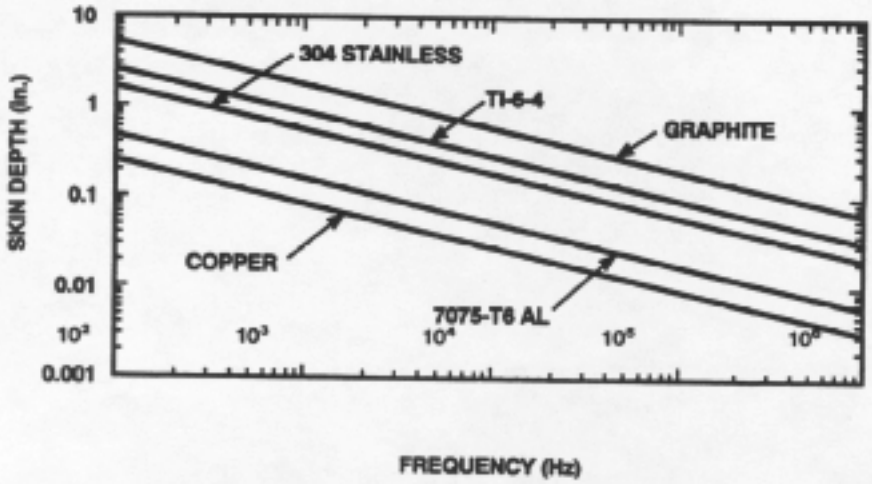

Figure 5A-6. Eddy Current Penetration Depth as a Function of Excitation Frequency for Select Materials.

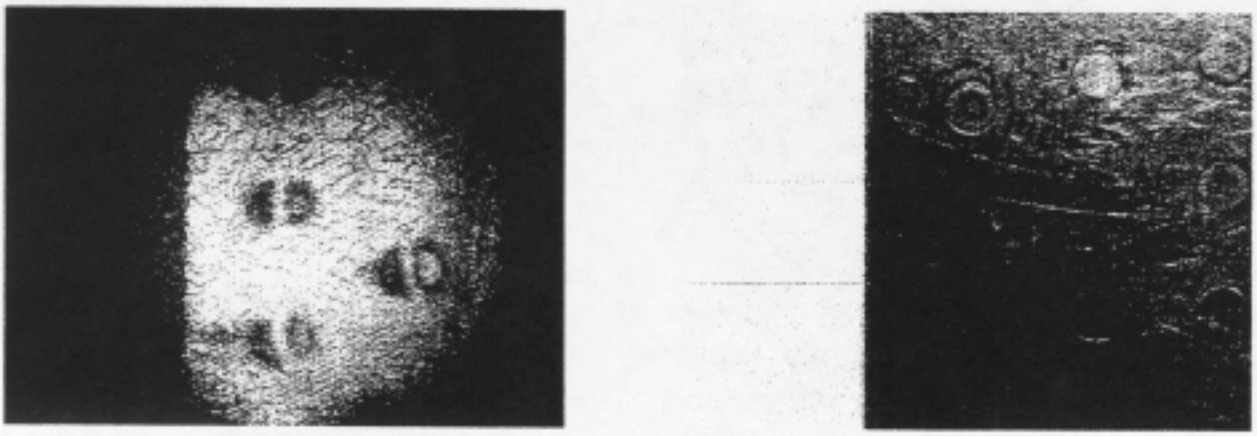

Figure 5A-7. MOI Image (a) and Photo (b) of a Second-Layer EDM Notch in a DC-9 Eddy Current Test Standard. Note that the images of deeper flaws are more diffuse and less sharply defined than surface flaws shown in Figures 5A-3, 4, and 5.

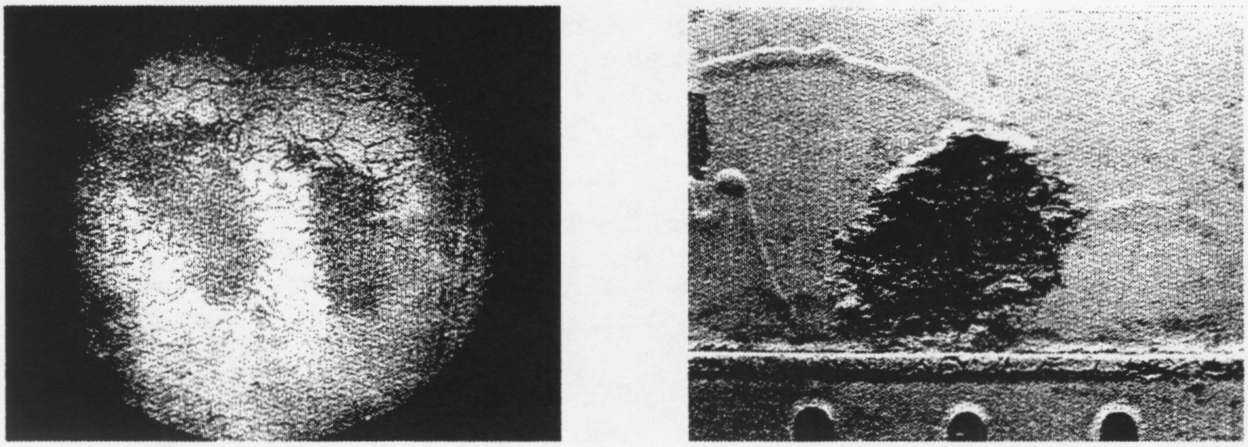

(a) (b)

Figure 5A-8. MOI Image (a) of a Corroded Region In an Aluminum Panel Removed from a Commercial Airplane and the Corresponding MOI Image (b) Taken from the Side Opposite the Corrosion.

In conventional eddy current inspections involving thickness measurements of a test piece, phase information from the complex impedance vectors can provide a quantitative measure of thickness. Thickness information can also be estimated from MOI images. By varying the excitation frequency throughout its range and knowing the corresponding standard depth of penetration for the material being inspected, estimates of depth may be obtained. For example, if a second layer crack is observed at 12.8 kHz, but not at 25.6 kHz, then its depth would be somewhat greater than the skin depth at 12.8 kHz. The depth contour of a region of corrosion can be similarly estimated.[5A-4]

To evaluate the MOI for corrosion detection, the Volpe National Transportation Center, under FAA Technical Center sponsorship, conducted a joint feasibility demonstration of the MOI with Boeing and Physical Research, Inc. (PRI).[5A-5] The study indicated that thinning less than 10 percent of base metal thickness would be hard to detect with the MOI. Quantitative estimates of residual thickness were also harder to make with the MOI than with eddy current scanning. However, it was reported that the MOI visualization of the extent of corrosion is simple and free of the labor intensive point-by-point mapping required by eddy current scanning.

Ferromagnetic fasteners. Residual magnetism in ferromagnetic (i.e., steel) fasteners may obscure the magnetic fields generated by defects in the vicinity of the fastener. Severe image distortions caused by the residual magnetism in a fastener will mask flaw images and preclude their detection. However, demagnetizing the fastener prior to inspection permits the MOI to image defects in the vicinity of steel fasteners. Magnetized fasteners can be easily degaussed with a small hand-held AC yoke commonly used in the magnetic particle inspection process. The image of a properly degaussed fastener will look like a slotted screw, whereas magnetized fasteners appear as dark, often distorted, spots.[5A-6,5A-7] The magnetized fasteners will also be imaged even when the excitation eddy current is turned off.

5A.2.3 Evaluation of AANC Sample Defect Library Specimens.

In January 1992, personnel at Sandia National Laboratories, Albuquerque, NM, had the opportunity, with the assistance of a PRI Instrumentation representative, to inspect a number

of the aged aircraft specimens in their sample library with a MOI. The MOI test instrument was PRI's latest version (Model 301-1), which had an eddy current frequency range of 1.6 to 102.4 kHz. The accessible surfaces of all aluminum specimens, large or small, were scanned with the MOI operating at various frequencies in order to detect both corrosion and fatigue cracks (simulated and real).

Some of the samples that contained both surface and subsurface flaws (ultrasonic test specimens) were too thick (>0.125 in.) to be analyzed for internal flaws with the MOI. The simulated surface cracks were easily imaged. When the specimens were covered with 0.010-in.-thick paper to simulate thick paint, the MOI could detect all of the visible surface flaws. The MOI personnel who scanned large Boeing 737 skin panels were able to detect some previously unknown cracks. Of particular interest were the commercially fabricated multilayered eddy current laboratory reference test samples simulating DC-9 riveted structures containing very small machine-simulated cracks. The cracks emanating from rivet holes were as short as 0.100 in. With the MOI, it was possible to readily detect the 0.100-in. surface cracks even when covered with 0.010-in.-thick paper to simulate paint. One multilayered specimen contained simulated second-layer cracking around rivets in a 0.050-in.-thick aluminum sheet covered with an unflawed 0.071-in.-thick top skin. The randomly distributed rivet hole cracks in the second layer ranged in length from 0.125 in. to 0.250 in. With the MOI operating at 1.6 kHz, it was possible to detect all of the second-layer cracks that were >0.1875 in. in length. There was also some indication of the 0.125-in.-long crack, but interpretation was more difficult.

Some of the specimens exhibited corrosion, which was also evaluated with the MOI. Much of the corrosion was cosmetic and the metal thinning was insufficient to be detected (i.e., <5 percent–10 percent reduction in thickness). However, other areas of corrosion were readily detected, especially where the corrosion-induced metal loss left a sharp, jagged, or well-defined edge in the aluminum skin. It appears that corrosion detection with the MOI is related to both the depth and shape of the remaining metal cavity after metal removal by the corrosion process. Corrosion was most easily detected when there was a sharp thickness transition in the MOI's 3-in.-diameter image area. It also appeared that large-area corrosion with little or uniform metal removal was very difficult to detect. These findings are consistent with the ones presented in the FAA Technical Note.[5A-5]

In general, MOI appears to be more sensitive for the detection of fatigue cracks than corrosion. Its corrosion detection performance characteristics could not be evaluated objectively with the available test specimens. This determination requires a more precise laboratory evaluation with well characterized corrosion samples. Several ongoing studies are investigating the capabilities of the MOI to detect corrosion.

5A.3 PRESENT APPLICATIONS.

The MOI instrument was designed for aircraft inspection. (See Section 5A.4.)

5A.4 AIRCRAFT APPLICATIONS.

The tedious nature of inspections carried out using a conventional pencil probe and a template, which requires paint removal to ensure that fasteners are visible, has prompted several airlines and manufacturers to investigate the use of MOIs. The following paragraphs contain information from American Airlines, Cessna, Tower Air, and Boeing which was excerpted from internal reports and communications between the users and PRI Instrumentation, Inc.

American Airlines. American Airlines inspection personnel first used the MOI to detect fatigue cracks in section 41 of Boeing 747s. The MOI was used without paint removal. American also used MOI in two other applications. They inspected the upper row of fasteners on skin lap joints of stringers 4 and 10 of a Boeing 727 and were able to detect cracks through the paint and decals 360° around the fasteners with a single setup. This inspection was previously done using a sliding probe. Due to the nature of the sliding probe, the center of the probe has to be over the center of the fastener, and cracks off axis 30° or more could go undetected. Moreover, the skin lap joint on stringer 10 has either paint or decals covering fasteners, making the sliding probe inspection even more difficult.

American also tried the MOI on a Douglas DC-10, searching for cracks in the lower wing skin panels. The equipment was able to image successfully without paint removal.

In general, some inspectors at American Airlines felt that the MOI inspections are better, easier, and faster to use than conventional eddy current inspection methods. Other inspectors using the MOI to inspect lower wing panels felt that it was too bulky and tiring.

Cessna Aircraft. Cessna Aircraft Company performed a pressure cycle test to evaluate the structural integrity of four cabin skin butt joints, various stringers, window doublers, and frames at fastener locations on a 10-foot-long fuselage test assembly. NDI was to be performed every 5,000 pressure cycles between 36,000 and 119,000 cycles. The original inspection technique was to have been done using a conventional surface eddy current pencil probe and template, but because of the large number of fasteners to be inspected (about 2,000) and the planned frequency of the inspections (once per day), the conventional inspection method was abandoned in favor of MOI.

The first MOI inspection at 36,000 cycles was completed in 3 man-hours, compared to an estimated 24 man-hours using the pencil probe and template method. At 85,000 cycles (about four aircraft lifetimes) five cracks were detected. These had lengths of approximately 0.02 in. (two cracks), 0.07 in. (two cracks), and 0.05 in. (one crack). The test was continued to 119,900 cycles (about five aircraft design lifetimes). At this time, a total of 40 cracks were detected, the longest of which was approximately 0.19 in.

Cessna concluded that the MOI equipment was easy to operate and that crack images were easily interpreted. Cessna's experience indicated that the MOI is capable of routinely detecting surface-breaking cracks 0.05 in. and longer. It is estimated that 336 man-hours were saved by using the MOI rather than the conventional eddy current test method.

Tower Air. The Quality Control Supervisor at Tower Air used the MOI to perform a required eddy current inspection on three recently repainted 747 aircraft. Stripping and repainting would have added both time and expense to the job. They found the sensitivity of the unit to be good and located one indication, which was validated with an eddy current pencil probe. After paint and fastener were removed from the area, they were able to see with a magnifying glass a very small static discharge burn on the edge of the rivet countersink.

Boeing's Probability of Detection. To evaluate how well the instrument performs, the Boeing Commercial Airplane Group Quality and Assurance (QA) R&D department generated crack probability of detection (POD) curves for the MOI unit and three other conventional eddy current test methods. Their results for the MOI and the sliding probe test method are shown in Figures 5A-9 and 5A-10. These results were generated by having different inspectors evaluate a number of representative lap joint samples containing EDM notches to simulate cracks. These flawed specimens were developed by Boeing for the specific purpose of testing such devices and techniques. Each point on the graphs represents the proportion of the inspectors detecting one particular manmade flaw.

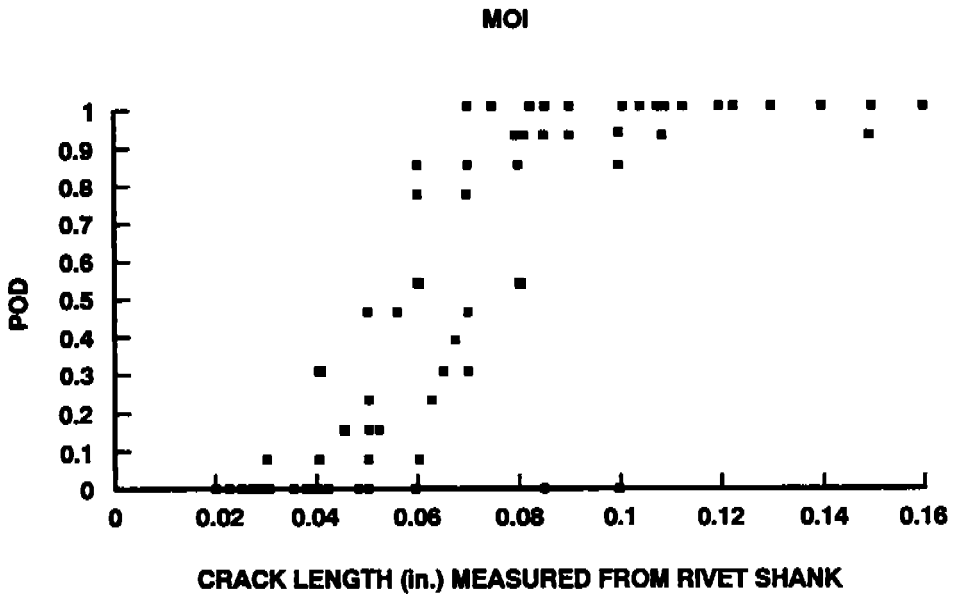

Figure 5A-9. A Plot of Probability of Detection Versus Crack Size for the MOI. Each plotted point is the proportion of 12 inexperienced MOI inspectors detecting a particular crack. The crack detection probability rises rapidly to 1 at about the 0.1-in. crack length and remains at this high level as crack size increases.

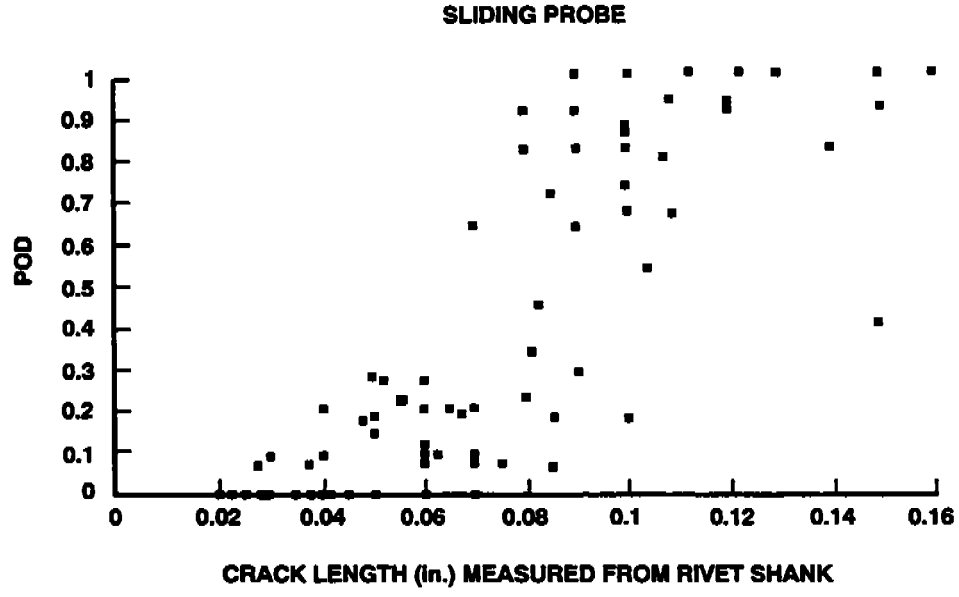

Figure 5A-10. A Plot of Probability of Detection Versus Crack Size for the Sliding Probe Eddy Current Method. Each plotted point is the proportion of inspectors with various degrees of training detecting a particular crack. The crack detection probability does not rise nearly as rapidly as for the MOI and does not approach 1 very closely even as crack size increases.

Figure 5A-9 shows the POD plot based on the evaluations by 12 inspectors using the magneto-optic/eddy current imager. All of the inspectors using this device were experienced inspectors but without formal training on the MOI, yet the data approaches a high POD at a crack length of about 0.1 in.

Figure 5A-10 shows the POD plot for the sliding probe eddy current method. In general this technique is insensitive to off-angle cracks, such as the 0.15 in. one showing about a 50 percent POD.

Several points of qualification should be mentioned. First, the exact length of these cracks is not known with certainty, since this would require destructive testing, which would destroy the test samples. Crack lengths were determined with dye penetrant and optical means. For example, it is uncertain that the crack shown at about 0.085 in. on the plots actually exists. Second, the crack about 0.1 in. long, which is not detected by the MOI, was in a geometric location not accessible to the imager. Other than these points, the estimated POD for large cracks (>0.08 in.) approaches and remains near 1.0, which is the desired characteristic for any technique.

Boeing, Wichita. Along with the Boeing Commercial Airplane Group's study, the military side of Boeing has evaluated the MOI for the purposes of inspecting B-52G/H pressure cabin side skins.[5A-8] They concluded that the detectable crack length using the MOI is approximately the same as with surface eddy current inspections, but the speed of the inspection and the subsequent attentiveness and enthusiasm of the operator was improved. They report that the template-guided surface eddy current inspections of pressure cabin skins that took 32 hours to complete were completed using the MOI in 3-1/2 hours.

Use of MOI at aircraft maintenance facilities. In addition to Boeing evaluation of the MOI, numerous hangar inspections of aging aircraft have been performed at Alaska Airlines in Seattle, American Airlines in Tulsa, the Dee Howard maintenance facility in San Antonio, Texas, Japan Airlines in Tokyo, and McCord Air Force Base, Tacoma, to name a few. These inspections have shown that rivets and cracks on aircraft can be imaged even through relatively thick layers of paint and have demonstrated that the device can image cracks and corrosion on in-service aircraft with a good probability of detection and a low probability of false calls.

Conclusion. In general, users have concluded that the MOI is fairly easy to use even with very little training. Typically, training consists of a 1- or 2-day in-house course covering theory of operation and practical hands-on training using flawed aircraft specimens. The operation of the MOI requires only the selection of the power and frequency level, and the equipment requires less setup and calibration time than other eddy current techniques. Its large 3-in. inspection area and its ability to perform the inspection in real time are other advantages. Several evaluators thought that the imaging head would tend to get heavy after prolonged periods of inspecting the underside of a fuselage or wing.

5A.5 TECHNICAL CONSIDERATIONS.

5A.5.1 Advantages.

The major advantages of MOI are listed below:

- Both fatigue cracks and corrosion can be detected. High frequency scanning is used for surface fatigue cracks. Low frequency scanning is used for subsurface cracks and corrosion.
- Flaw detection is relatively insensitive to lift-off.

- Rivet inspections can be performed through decals and heavy coats of paint. Rivets do not have to be visible to the inspector since the MOI images all rivets in a 3-in.-diameter field of view.
- Tests have shown that in some cases crack images can be seen through nonconductive material that is thicker than any conceivable paint layer(s). Very tight fatigue cracks, as small as 0.02 in. in length, have been detected at higher frequencies. At lower frequencies simulated corrosion regions have been detected through more than 0.1 in. of aluminum skin.
- Large-area inspection capability makes it possible to reduce inspection times. Inspection times have been reported to take 1/8 to 1/10 the time needed for eddy current inspections. Reduced inspection time should reduce operator fatigue.

5A.5.2 Disadvantages.

- Residual magnetism in steel fasteners can interfere with image interpretation and must be removed by degaussing. This can be done with a small hand-held AC yoke commonly used in the magnetic particle inspection process.
- Contact with the test surface must be maintained to achieve the highest quality images through decals and paint.
- The operator may become fatigued from holding the MOI imaging head for very long inspections. This is especially true when the operator is required to inspect positions above shoulder height.
- The MOI equipment is bulkier and more difficult to maneuver than the comparable eddy current devices used for the same inspections. This can lead to using procedures that call for two-person teams. One person concentrates on the image-head scanning and the other person watches the video image and makes the flaw call.
- To detect flaws at any orientation, the MOI head must be rotated 90 degrees for each inspection site. This means that two passes are necessary for each row of rivets that is examined.
- Inspection surfaces must be convex and relatively flat. Thus the MOI cannot be used on or immediately around button-head rivets. Rivet sites next to patches would also be inaccessible to the MOI.
- As with any video image, a relatively dark environment for the monitor is needed. Images on a video monitor are hard to view in bright daylight.

5A.6 STATUS.

5A.6.1 Present.

MOI procedures have been developed by both Boeing and McDonnell Douglas for use on their aircraft. Boeing published an all-model procedure in March 1992 and has included it in their aircraft NDI manuals.[5A-9] The final procedures from McDonnell Douglas are soon to be published. Lockheed is currently involved in writing procedures. The military has also been interested in developing procedures for use of the MOI. A Technical Order is currently being written for B52s. Efforts will soon begin on other military aircraft.

Extensive laboratory inspections by personnel from PRI Instrumentation, Boeing Commercial Airplane Group, McDonnell Douglas, Lockheed, NASA, the FAA (Galaxy Scientific Co.) and a

number of others over the past three years have demonstrated the ability of the MOI to detect cracks both in prepared samples and in samples extracted from aging aircraft.

The field performance of the MOI is currently being evaluated in airline maintenance facilities as part of an FAA-sponsored aircraft lap splice experiment being fielded by Sandia National Laboratories. The experiment will evaluate the field performance characteristics of the MOI along with the capabilities of currently approved eddy current techniques in airline maintenance and inspection facilities. The objective of the experiment is to make reliability assessments for high-frequency eddy current inspections of lap splice joints, as those inspections are currently performed in the aircraft maintenance and inspection industry. It takes into account such variables as facility differences (human factors considerations), inspector training, and equipment.

5A.6.2 Future.

Technical evaluation of the MOI instrument by the airline transportation and manufacturing industry is continuing. It is anticipated that the MOI will also play an important role in the airworthiness assurance of the commuter fleet. The primary reasons for this are (1) the skin panels, stringers, and frames are thinner in the commuter aircraft, and the MOI could achieve a greater reliability in detecting first- and second-layer flaws in these airplanes when compared to that achievable in the transport fleet, (2) it allows rapid inspection of large areas without paint or decal removal, and more important (3) the NDI inspectors require little training before becoming proficient and confident.

Since the MOI's output format is a video image, it can be easily analyzed or enhanced with a wide variety of cost-effective off-the-shelf image-processing and analysis software and hardware. Preliminary work by the Photonics Group at NASA Ames Research Center has demonstrated the feasibility of performing real-time image processing on MOI images. They have digitized videotape outputs of corrosion around rivets and have processed these to produce enhanced, easily interpreted images clearly delineating the affected areas. It is anticipated that this work by NASA and others will lead to the development of an MOI system with alarms and the possibility of automated inspections.

Both NASA Langley and PRI Instrumentation have demonstrated the feasibility of building a multidirectional magneto-optic imager that would automatically switch the direction of the induced eddy currents and preclude the need to physically rotate the MOI head and to perform the inspection twice on each row of rivets, as must now be done with the commercial MOI. Development of such a multidirectional imager could speed up the inspection process, thereby reducing operator fatigue.

The multidirectional MOI would also be the ideal real-time robotic NDI sensor for the inspection of aged aircraft. In addition to its already established attributes of (1) being able to detect fatigue cracks in aircraft skin panels without the removal of paint or decals, (2) the rapid inspection of large areas, (3) being easy to set up and calibrate, (4) video signal output that can be readily recorded for inspection documentation, and (5) video signal output which lends itself to the application of off-the-shelf image processing/analysis software and automatic defect recognition systems, the multidirectional MOI will require only a single scan to nondestructively inspect a long row of rivets for cracks independent of their angular orientation. Additional attributes that would make the multidirectional MOI an ideal robotic NDI sensor include (1) the MOI's large-area imager (3-in.-diameter area), (2) being able to detect flaws at speeds up to 1 in. per second without objectionable blurring of motion, and (3) being relatively insensitive to eddy current lift-off effects. These desirable robotic NDI

sensor features of the multidirectional MOI would permit it to be used with contour-following scan robotics, with less stringent requirements for positional accuracy, in the aircraft maintenance/repair facility environment.

5A.7 REFERENCES.

5A-1. Jin-Yong Kim and J. C. Moulder, "Kerr Magneto-optic Eddy Current Imaging," *Review of Progress in Quantitative Nondestructive Evaluation,* Vol. **10A,** pp. 575-580, Plenum Press, NY, 1991.

5A-2. D. K. Thome et al., "Aircraft Inspection With The Magneto-optic/Eddy Current Imager—A New Technology," presented at ATA NDT Forum, September 10-12, 1991, Long Beach, CA, PRI Instrumentation, Torrance, CA, 1992.

5A-3. G. L. Fitzpatrick and D. K. Thome, "New Magneto-optic Eddy Current Inspection Methods for Aging Aircraft," presented at the 1989 U.S. Air Force Structural Integrity Program Conference, San Antonio, TX, December 6, 1989, WRDC-TR-90-4051, p. 608.

5A-4. W. Shih, "Airframe Fatigue Crack and Corrosion Detection," presented at the 1992 American Society for Nondestructive Testing Spring Conference, Orlando, Florida, March 31 - April 2, 1992.

5A-5. S. Bobo, "Magneto-optic Imaging Inspection of Selected Corrosion Specimens," DOT/FAA/CT-TN92/20, July 1992.

5A-6. G. L. Fitzpatrick, "Imaging Near Surface Flaws in Ferro-Magnetic Material Using Magneto-optic Detectors," in *Review of Progress in Quantitative Nondestructive Evaluation,* ed. D. O. Thompson and D. E. Chimenti, Plenum Publishing Corp., 1985.

5A-7. G. L. Fitzpatrick, "Flaw Imaging in Ferrous and Nonferrous Materials Using Magneto-optic Visualization," U.S. Patent 4,625,167 and 4,755,752.

5A-8. "Magneto-optic Eddy Current Inspections of B-52G/H Pressure Cabin Side Skin Determination of Detection Reliability," Enclosure A to Boeing Letter Y-7W16-129-164-1130.

5A-9. Boeing Nondestructive Test Manuals; MOI usage is incorporated into Part 6: "Eddy Current."

5B. ADVANCED EDDY CURRENT TECHNIQUES.

5B.1 SUMMARY.

New advances in eddy current techniques employ multiple-frequency and pulsed eddy current techniques. These techniques increase inspection capabilities for fatigue crack and corrosion detection, particularly in subsurface or second-layer structures. Computerization and signal processing of eddy current signals are advancing the interpretation of low-level signals and pulsed-signal responses by providing C-scan or waterfall maps that allow detection of cracks and corrosion that is impossible to detect by manual techniques alone. Eddy current C-scan imaging is becoming available through the use of encoded manual scanners. Commercial equipment is available that uses multiple-frequency and pulsed eddy current techniques. Since multiple layers can be inspected at the same time, using these techniques, the reduced inspection time presents a cost savings.

5B.2 TECHNICAL BACKGROUND.

Eddy current techniques are applied on conductive materials to detect cracks and corrosion in aircraft skins and structural elements. Basic principles and equipment used for eddy current testing are discussed in Reference 5B-1. Multiple-frequency and pulsed eddy current techniques, which were not included in Reference 5B-1, will be discussed here. Dual- or multiple-frequency techniques and pulsed eddy current techniques are emerging as viable, cost-effective methods to detect cracks and quantify corrosion in single- and multi-layered metal skins.

An alternating electrical current flowing in a wire-wound coil induces a changing magnetic field around the coil. Placing the coil next to a conductor induces eddy currents within the near surface of the conductor, and these induced eddy currents create a magnetic field that opposes the applied field. The overall effect is an impedance change measured in the coil. Flaws or thickness changes of the test-piece influence the flow of eddy currents and change the impedance of the coil accordingly. Instruments record the impedance changes either through impedance plane plots or by needle deflections of a microampere meter.

The depth of penetration of eddy currents is inversely proportional to the square root of the product of magnetic permeability, electrical conductivity, and frequency of the inducing currents. Therefore, eddy current tests are most sensitive to discontinuities on the surface next to the coil, which makes them very effective for detecting fatigue cracks in the near surface. High frequencies (above 10 kHz) are generally used to detect near-surface flaws. Low frequencies (100 Hz to 10 kHz) are used to detect inner flaws or corrosion. Eddy currents deeper in the material are weaker and lag in phase compared to the currents near the surface. By measuring the phase, one can determine whether the defect is near the surface or at the inner wall.

Single-frequency eddy current measurements can be used effectively to determine corrosion of a single-layer skin. However, the use of single-layer techniques to assess corrosion in a two-layer skin fails because a variable gap between the skins produces a signal that cannot be distinguished from a corrosion signal.

The response from a variable gap is suppressed by simultaneously mixing eddy current signals for two or more test frequencies. The primary frequency chosen is the one most sensitive to the

flaw of interest (cracks or thickness changes by corrosion). The secondary frequency chosen is the one more sensitive to the gap variation but less sensitive to the flaw of interest. Digitally combining the two signals by using a mixing algorithm produces an output signal that optimizes or enhances the flaw response and minimizes or suppresses the undesirable gap response. The result is reliable detection of second-layer corrosion.

An extension of the advantages of multiple-frequency eddy current testing is provided by pulsed eddy current testing. A pulse provides essentially an infinite range of frequency excitations. The lower-frequency components of the pulse propagate slower and are less attenuated than the high-frequency components. The relationship of time delay and depth of penetration can be used to gate the response signal to extract information on flaw depth location. Lift-off variations are reduced and a deeper magnetic field penetration is obtained due to the wide-band frequency excitation pulse.

A pulsed eddy current inspection technique has been developed for fatigue crack detection at fasteners in aircraft skins and structures. The technique uses a square wave pulse applied to a coil and a broad-band Hall effect sensor for detection purposes. The original work on the technique was done by David Harrison of the Royal Aircraft Establishment.[5B-2] Campbell and Gibbs developed a commercial scanner based on Harrison's work.[5B-3] The scanner rotates the eddy current probe above and around the circumference of the fastener head. Algorithms are used to process the response signal, which varies due to the rotation of the probe. From the processing, a target and cross-hair display is generated on the instrument screen, and the scanner is moved laterally until it is centered over the fastener and the target and cross hair are visually aligned.

Figure 5B-1 shows a schematic of the basic construction of the rotating Hall effect sensor and coil. As the scanner spins the probe, a pulser drives the coil with a square-wave voltage pulse. A horizontal trace of the Hall effect sensor response can be made on the instrument screen that represents the full 360° rotation of the probe. Gating the response signal at different time delays from pulse excitation and generating a waterfall plot of successive gated signals provides a "map" of inspection data that represents "slices" down through layers of the structure. Figure 5B-2 shows an example of a map where the location and depth of the flaw can be determined from the waterfall plot. In the figure, a straight horizontal line indicates no flaw whereas a bump or curve in the line indicates a flaw.

In recent years, PC-compatible data acquisition systems have been developed to process eddy current data. C-scan images (2D pictures) of eddy current inspection data over an area of a test-piece can be made using digital encoders attached to a manual scanning apparatus. Low-cost systems can be made using portable PC-compatible computers and manual scanners that attach easily to the test-piece. Encoded x-y position data along with signal data acquisition, signal processing, and image display can improve inspections significantly. Two examples of C-scan pseudocolor images of eddy current inspection data are seen in Figure 5B-3. These images were recorded using a Mobile Automated Scanner.[5B-4] The Mobile Automated Scanner can also be used for ultrasonic data acquisition and C-scan display. (A photograph of the scanner can be seen in Figure 7-7 of Section 7, Advanced Ultrasonics.)

A two-dimensional color image showing variations of the eddy current response signal over a test-piece area is an integration of a very large single-point data set. Since the large data set is viewed at one time, the ability to identify certain types of flaws is fast, more intuitive, and more reliable than single-point evaluations. Quantitative measurements of crack length or contour maps of percent corrosion can be made in a timely manner from the images. One two-dimensional examination of a layered structure with data acquisition of the eddy current

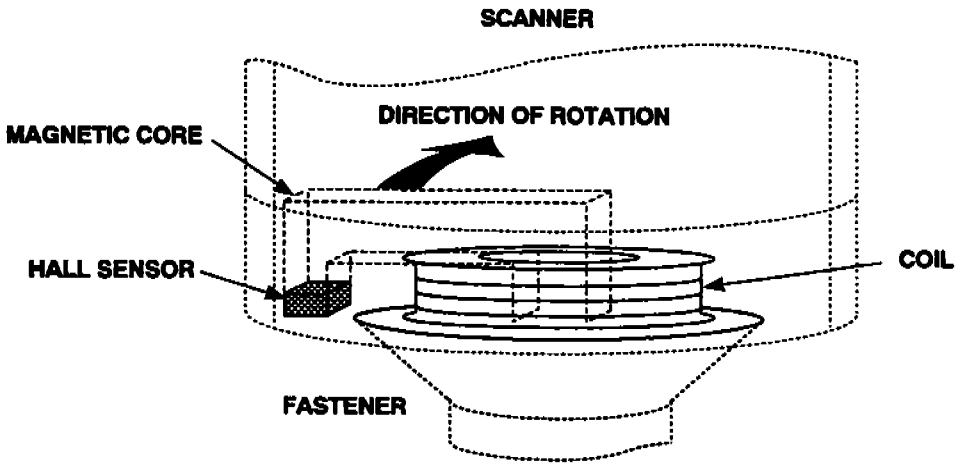

Figure 5B-1. Basic Configuration of Scanner with Rotating Hall Effect Sensor and Eddy Current Coil. [Source: Stavely Instruments, Inc., Kennewick, Washington. Reprinted by permission from Stavely Instruments.]

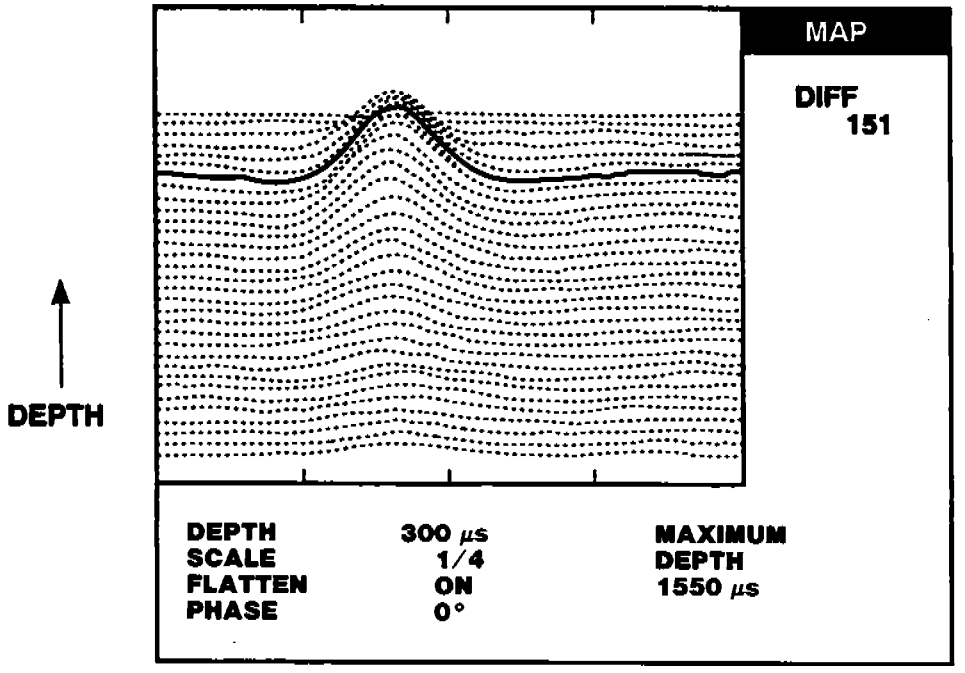

Figure 5B-2. Eddyscan Map of 2-mm EDM Notch in Third Layer of a Riveted Al-Ti-Al Sandwich 4.5 mm Deep at 140° Rotation. [Source: Stavely Instruments, Inc., Kennewick, Washington. Reprinted by permission from Stavely Instruments.]

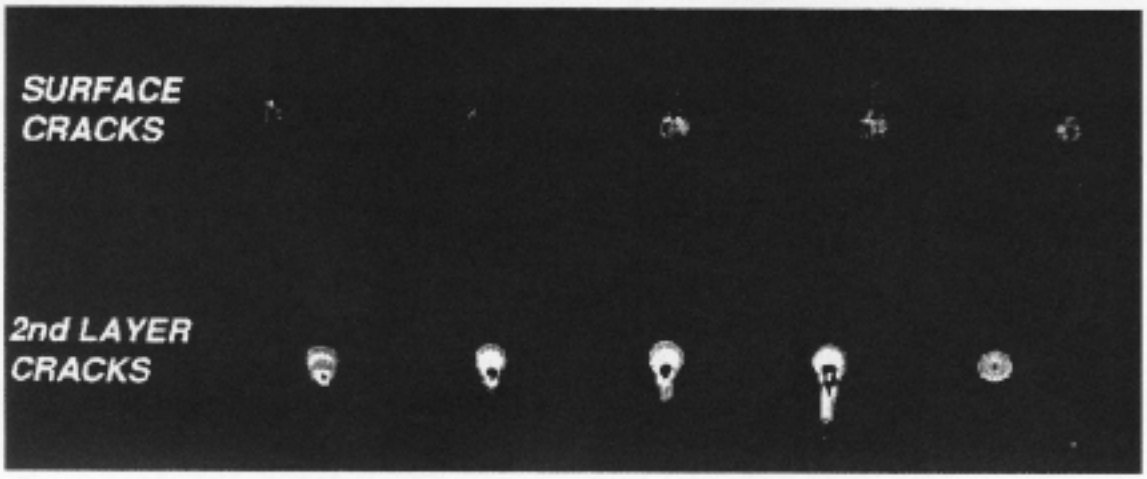

(a)

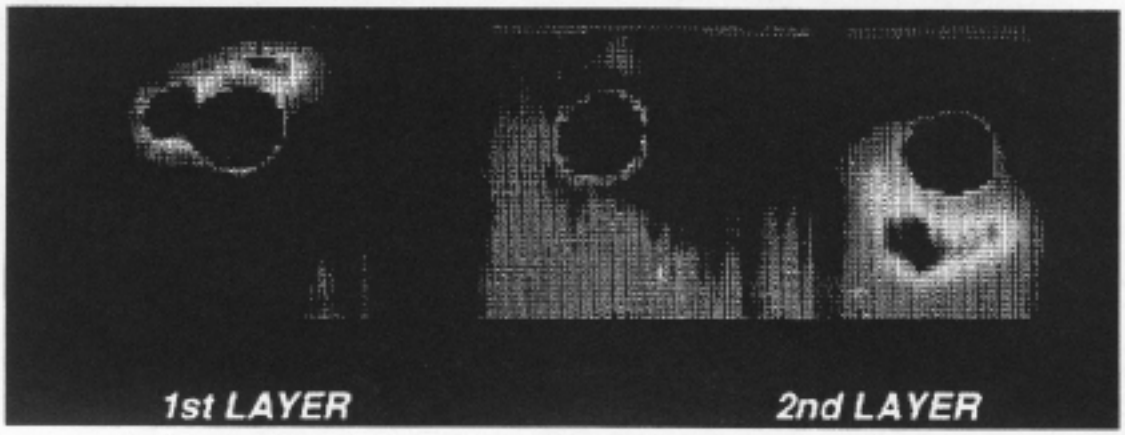

(b)

Figure 5B-3. Pseudocolor C-scan Images of Eddy Current Data for (a) First and Second Layer Cracks at Fasteners and (b) First and Second Layer Corrosion at Fasteners. [Source: McDonnell Aircraft Company, St. Louis, MO. Printed by permission from McDonnell Aircraft.]

response in a pulsed mode can be used to form separate images of cracks and corrosion for the multiple-layered skins. This process eliminates the cost of making different single- or multiple-frequency inspections. Scans using an array of eddy current probes instead of a single probe can decrease the inspection time significantly.

Artificial neural networks could also be trained with a computer system, and C-scan mappings of flaw classifications could be made to further reduce reliance on operator interpretation of inspection results.

5B.3 PRESENT APPLICATIONS.

Multi-frequency eddy current techniques have been developed for detecting cracks in heat exchanger tubing of steam generators in nuclear power plants. Mixing a low inspection

frequency, which is most sensitive to the tubing support plates, with a higher inspection frequency, which is most sensitive to cracks in the tubing, allows a clear display of crack signals adjacent to and under the support plates.

5B.4 AIRCRAFT APPLICATIONS.

For both top-layer and second-layer corrosion of lap splices, 10 percent corrosion loss is the maximum allowable before repairs must be made. Ten percent top-layer corrosion can be determined successfully by using single-frequency techniques. Ten percent second-layer corrosion (which represents only 5 percent of the combined thickness) has been reliably detected only with dual frequency-mixing techniques.[5B-5] Two other applications where dual frequency-mixing has been beneficial are in the detection of surface cracks at a changing radius where lift-off varies and in the detection of cracking under fasteners in first- and second-layer skins.[5B-6]

The Nortec 30 Eddyscan pulsed system has demonstrated its ability to find cracks and corrosion in fastener holes through several skin layers with the fastener in place.[5B-3]

Eddy current C-scan imaging as displayed in Figure 5B-3 has the potential to improve inspections for many aircraft applications that require quantitative information of crack length and corrosion assessment.

5B.5 TECHNICAL CONSIDERATIONS.

Dual-frequency eddy current techniques increase the signal-to-noise ratio of desired flaw signals significantly. This cannot be done with single-frequency techniques. The increased signal-to-noise ratio has allowed 10 percent second-layer corrosion to be detected. Instruments that incorporate the dual-frequency mixing techniques are easy to use and they can reduce the inspection time by providing inspection of two layers simultaneously.

Pulsed eddy current techniques offer many advantages over conventional single-frequency techniques: Lift-off effects are reduced, and simultaneous sensitivity to various thicknesses is possible. With the availability of low-cost portable computers, data acquisition of the dynamic time-base eddy current response with signal processing could provide flaw characterization information not possible with single-frequency methods. Initial cost of the equipment could be up to five times that of normal eddy current testers. Training required to operate the equipment is not expected to be more extensive than would be required for conventional equipment.

Two-dimensional C-scan images of any analog eddy current signal can provide fast, reliable, easy-to-interpret, documented inspection results. Such inspection results are not feasible with point-by-point manual inspections.

5B.6 STATUS.

Multi-frequency and pulsed eddy current instruments are on the market. The development stage of the instruments is such that they can be implemented in the field immediately after applications are identified and procedures developed to fully realize their capabilities.

5B.6.1 Present.

Pulsed eddy current techniques for corrosion assessment could be developed and ready for field use in two or three years. Research in eddy current flaw characterization continues to be done

in nondestructive evaluation. Eddy current modeling and flaw characterization techniques have been developed.[5B-7 to 5B-9] For example, C-scan eddy current images of cracks are blurred (see Figure 5B-3a) because of the large-radius nonlinear response of the transducer. For such images, a restoration technique was recently developed that produces accurate flaw size estimates from the eddy current images.[5B-10]

Recently, a field-ready commercial manual scanner with a PC-compatible data acquisition and display system using a dual-frequency eddy current technique for corrosion detection was demonstrated on a panel section of the AANC 737 airplane.[5B-11] Figure 5B-4(a) is the eddy current C-scan image obtained over the inspected area where the light color indicates corrosion damage around the tearstrap, stringer, and frame locations. Figure 5B-5 shows the portable R-Theta manual scanner attached to the aircraft and the C-scan image being developed on the CRT screen of the portable computer. A second C-scan image of the same general location of the AANC aircraft is shown in Figure 5B-4(b). The image of Figure 5B-4(b) was generated using a single frequency for detection of corrosion in the outer skin layer using an automated X-Y portable scanner, data acquisition, and display system that is commercially available.

5B.6.2 Future: Estimated Time to Field

Implementation of dual frequency techniques and pulsed eddy current techniques for quantitative corrosion assessment could be developed and ready for aircraft inspections in the mid to late 1990s. Implementation of the manual and automated C-scan imaging techniques can take place as soon as procedures and calibration standards are established. Procedures for each specific aircraft application with appropriate calibration standards and calibration procedures need to be developed before the C-scan systems can be used with confidence by airline inspectors.

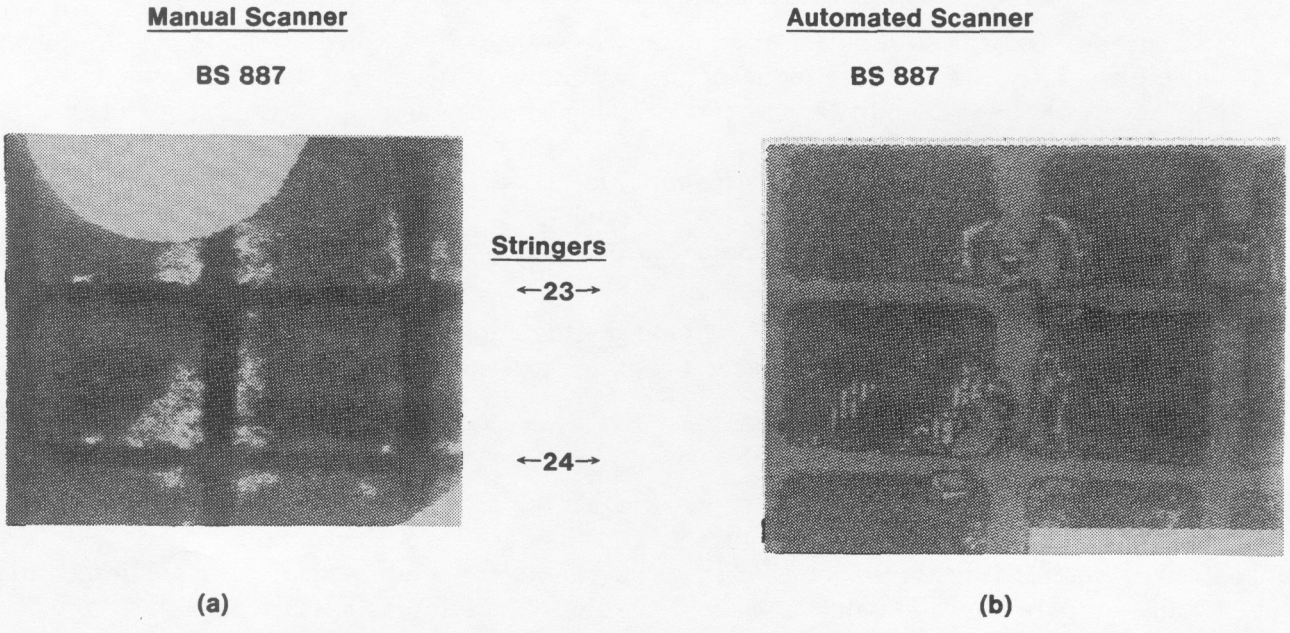

Figure 5B-4. Eddy Current C-Scan Images Obtained on the AANC 737 Airplane In the Area Aft of the Rear Cargo Door.

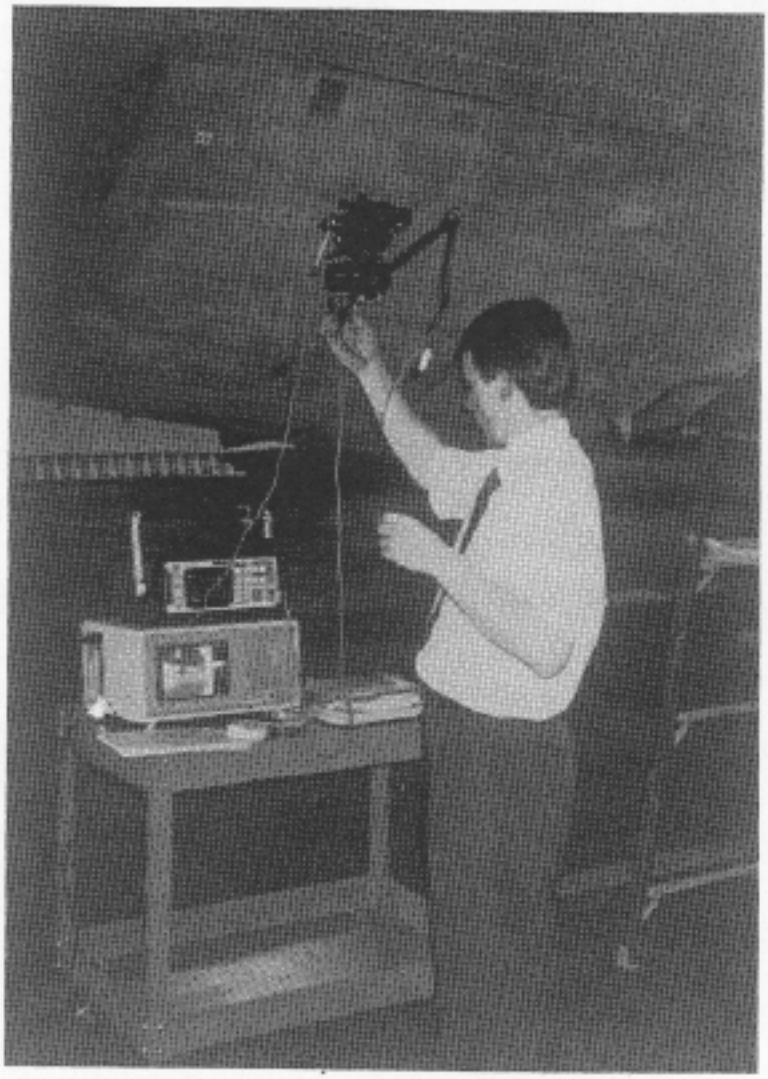

Figure 5B-5. Manual Scanner Attached to AANC 737 Airplane for Eddy Current C-scan Imaging of Corrosion in the Outer Skin Layer.

5B.7 REFERENCES.

5B-1. U.S. Department of Transportation, Federal Aviation Administration Report, *Current Nondestructive Inspection Methods for Aging Aircraft,* DOT/FAA/CT-91/5 June 1992.

5B-2. D. J. Harrison, "The Detection of Cracks under Installed Aircraft Fasteners by Means of a Scanning Eddy-Current Method," in *Review of Progress in Quantitative Nondestructive Evaluation,* ed. D. O. Thompson and D. E. Chimenti, 1987, Vol. **6A** pp 1053.

5B-3. J. Campbell and M. Gibbs, "Portable Flaw Imaging for Aging Aircraft," in *Review of Progress in Quantitative Nondestructive Evaluation,* ed. D. O. Thompson and D. E. Chimenti, 1991, Vol. **10B** pp. 2061-2068.

5B-4. "Mobile Automated Scanner II," Automated Testing Systems, McDonnell Aircraft Company, St. Louis, MO 63166-0516.

5B-5. J. G. Thompson, "Second Layer Corrosion Detection Using Dual Frequency Eddy Current Techniques," Boeing Commercial Airplane Group, Seattle Washington, Paper presented at 1992 ATA NDT Forum, Cincinnati, Ohio, 1992.

5B-6. D. Jankowski, "Multiple Frequency Eddy Current Inspection of Aircraft Components," Krautkramer Branson/Hocking, Lewistown, PA., Private communication.

5B-7. L. D. Sabbagh and H. A. Sabbagh, "Eddy-Current Modeling and Flaw Reconstruction," in *J. Nondestr. Eval.*, Vol **7**, 1988, pp. 95-110.

5B-8. B. A. Auld, S. R. Jefferies, and J. C. Moulder, "Eddy-Current Signal Analysis and Inversion for Semielliptical Surface Cracks," in *J. Nondestr. Eval., 1988, pp. 25-34.*

5B-9. R. E. Beissner, "Approximate Model of Eddy-Current Probe Impedance for Surface-Breaking Flaws," *J. Nondestr. Eval.*, 1988, pp. 79-94.

5B-10. B. R. Groshong, G. L. Bilbro, W. E. Snyder, "Eddy Current Image Restoration by Constrained Gradient Descent," in *J. Nondestr. Eval.*, Vol. **10**, No 4, 1991, pp. 127-57.

5B-11. The 737 airplane is housed in the Federal Aviation Administration/Aging Aircraft NDI Development and Demonstration Center (FAA/AANC) hangar facility, Albuquerque, NM.

6. COHERENT OPTICS.

6.1 SUMMARY.

For the purpose of this section, "coherent optics" will include holographic interferometry (holometry), electronic speckle-pattern interferometry (ESPI), and shearography. These are all "wide area" interferometric imaging techniques that are capable of detecting micron-sized displacements of the surface of an object such as the skin of an aircraft. For these techniques to be used in flaw detection, the object under test must be stressed in a manner that causes the surface to deform in an anomalous way when a flaw is present. These techniques are particularly useful for detecting debonds or delaminations, which can be caused to bulge by heating or applying a vacuum. Flaws which tend to cause only in-plane deformations, such as cracks under tension, are the most difficult to detect using coherent optical techniques.

Film-based holometry has been in laboratory use, and in limited use in production inspection, for over twenty-five years. The inconvenience of wet film processing and the need for automated data reduction techniques have limited its use. ESPI and shearography are newer techniques that use electronic imaging, and due to the convenience of electronic imaging over film, they are experiencing rapid growth. Shearography is a clear choice over holometry for field inspections due to its relative insensitivity to object motion.

Several production inspections in the aerospace industry currently use these techniques. Time-average holometry is ideally suited for modal analysis of turbine blades and wheels. United Technologies Pratt & Whitney currently use both ESPI and shearography to inspect gas turbine compressor tip seals. In 1990, Laser Technology Incorporated (LTI) fielded a three-series laboratory experiment on full-sized panels which simulated Boeing 727 and 737 fuselage construction. The object was to evaluate the flaw detection capability of shearography. Weak rivets, cracks, and lap joint debonds were easily detected. The lap-joint images contained a lot of information, but were complex to interpret. To rectify this problem, significant operator training is needed, and sophisticated data analysis techniques are being actively researched. In a 1991 LTI comprehensive field demonstration on selected portions of a Boeing 737 fuselage, twenty percent of the candidate area was covered in the available 24-hour period, and thirty-one debonds were detected. Based on this demonstration and the assumption that shearographic inspection would eliminate the need for extensive internal visual inspection, it was estimated that when the data interpretation and sensitivity issues are resolved, shearography could substantially reduce inspection costs.

6.2 TECHNICAL BACKGROUND.

Several good references on holometry and ESPI are in the open literature. Charles M. Vest authored a complete college text on the subject that includes full mathematical analysis on fringe formation, fringe localization, and data reduction from fringes.[6-1] The *Metals Handbook* is an applications-oriented treatment that has sections on laser selection, optical equipment, and applications.[6-2] Erf's *Speckle Metrology*, although somewhat dated, gives the basics of speckle interferometry and ESPI.[6-3] Y. Y. Hung has written several papers explaining the principles of shearography.[6-4]

The objective of this section is to give, using a minimum of mathematics, a physical feel for why coherent optics techniques work and to relate their use to aging aircraft inspection. First, the conventional diffraction-based explanation of holometry is given. Next, since the electronic recording used in ESPI and shearography is based on fringes rather than diffractive reconstruction, an explanation based on fringes in the hologram itself is given. Last, a discussion is presented on applications of the techniques in the aerospace industry and their application to aging aircraft inspections in particular.

6.2.1 Optical Interference Concept.

The concept of optical interference is fundamental to all the implementations of all the inspection techniques presented in this section; therefore, a few points should be made about this process.

If two light beams of the same wavelength λ and intensities I_1 and I_2 intersect at a detector, the resulting intensity is given by

$$I = I_1 + I_2 + 2\sqrt{I_1 I_2}\,\cos(\phi) \qquad (1)$$

where the phase ϕ is the relative phase difference between the two beams. The information of interest is carried in this phase term. The observable quantity is the intensity I, which being a cosine function of ϕ, is periodic. This means that a single measurement of I can only determine ϕ within the range 0 to 2π, or in a "modulo 2π" sense. Other information, such as multiple measurements of I coupled with counting the number of cycles of the cosine function, must be employed to fully determine the phase.

6.2.2 Holographic Interferometry (Holometry).

Film-based holography: recording the hologram. Figure 6-1 shows the basic idea of hologram construction. The diffusely scattering object is illuminated by coherent light from a laser, and each point on the object scatters a spherical wave of light, part of which hits the photographic film that will become the hologram. (In this model, a "point" on the object is an area whose size is dictated by the aperture intercepted by the hologram. The size of the point is usually on the order of a few wavelengths of light.) The light from each point on the object interferes with that from every other point, creating the familiar speckle pattern. This speckle pattern is typically considered to be a noise component, usually the major one, in holographic imaging. Since light obeys the superposition principle, a single object point can be considered for this discussion.

The film is also illuminated by a reference beam, which must be coherent with the light scattered from the object. In practical terms, this means that both the object light and the reference light must be derived from the same laser, separated by a beamsplitter, and then travel roughly the same distance before they recombine at the film plane. The two path lengths must be the same to within the coherence length of the laser, which is the distance the light can travel and still have a predictable phase. The following are typical coherence lengths: for helium-neon lasers, ~20 cm; for Ar-ion lasers with an etalon, a few meters; and for diode-pumped, frequency-doubled YAG lasers, tens of meters.

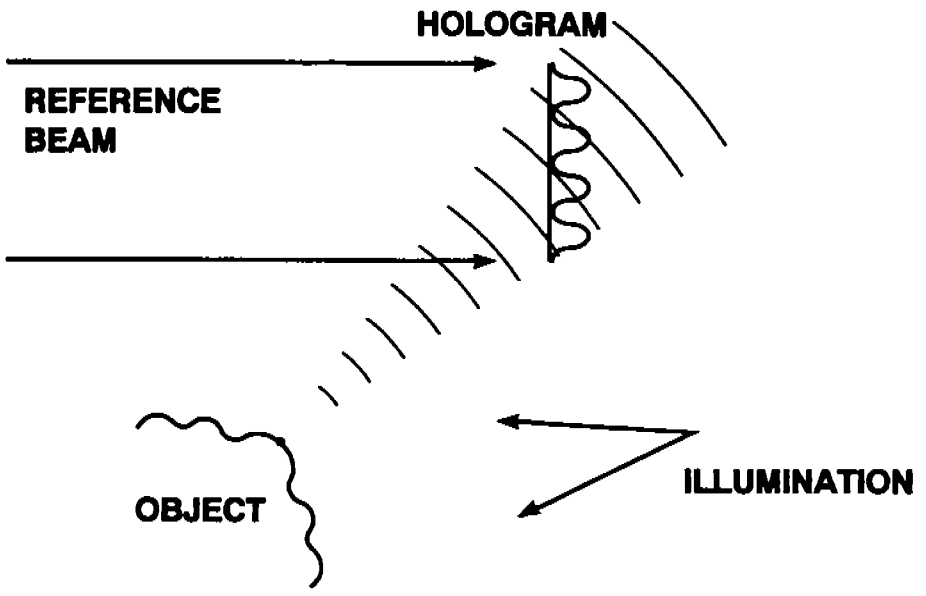

Figure 6-1. Hologram Construction Process. Light from object interferes with reference beam to form intensity pattern which is recorded at hologram plane.

At the film plane, the reference wave and the object wave interfere to form a grating structure, which is recorded by the film. The key concept to holography is that while the film responds only to light *intensity,* the *phase of* the object light, relative to the reference beam, is recorded in the spatial phase, or position, of the intensity grating recorded on the film. When the film is developed, it contains a superposition of these gratings from each point on the object, all with the correct phase relative to one another. This film is the hologram.

Film-based holography: diffractive reconstruction. To reconstruct or replay a hologram in the conventional way, a duplicate of the reference beam is used to illuminate the hologram. Each grating on the film diffracts light, some of which exactly duplicates the original light wave from the object, as shown in Figure 6-2. Since the hologram reconstructs the wave from each point on the object (and all waves have the correct relative phase), the total diffracted wave exactly duplicates the object wave that would have been scattered from the original object. Thus, the hologram stores and reconstructs the entire object wave, including both amplitude and phase. If an observer, such as the eye or a camera, is placed in the reconstructed wave, an image of the object is reconstructed as indicated by the dotted lines in Figure 6-2. This image has all the optical characteristics of the original object, including depth of focus and parallax, which result in the familiar three-dimensional imaging capability of holograms. This three-dimensional characteristic is incidental to holometry. What makes holographic interferometry possible is the fact that the phase of each scattered wave is recorded.

Film-based holographic interferometry. The holographic image can be used in several ways to make measurements of displacement. Figure 6-3 is a diagram of *double exposure* holometry. In this technique, two holographic images of the same object are sequentially recorded on a single film. Between recording the first and the second image, a stress is applied that causes the object to move. When the hologram is reconstructed, both images are superimposed and interfere on a point-by-point basis. At a particular object point, the total optical path from the illumination point to the scattering point to the observer is I-P-O in

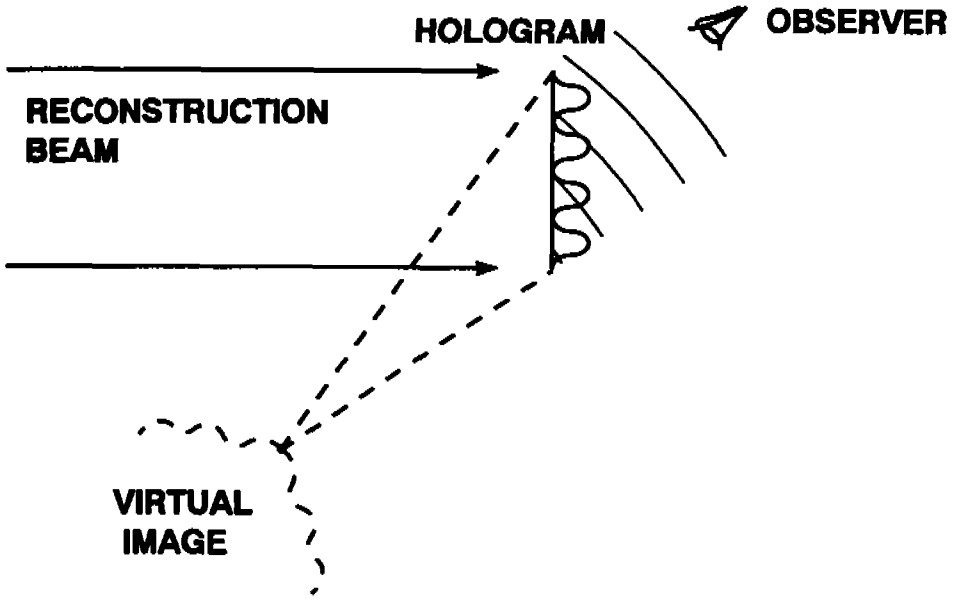

Figure 6-2. Diffractive Reconstruction of Film-Based Hologram. Part of the reconstruction beam is diffracted by the hologram, reconstructing original object wave.

Figure 6-3. In the second image, this path becomes I-P′-O due to displacement of point P. These waves strike the detector simultaneously and interfere according to equation (1). In this case, the phase $\phi = 2\pi\Delta/\lambda$, where Δ is the difference in optical paths. If these paths differ by an integral number of waves (including zero), the two image waves interfere constructively at the observing detector ($\cos\phi = 1$), and the point appears bright. If the paths differ by an integral number plus half a wavelength, the light waves interfere destructively ($\cos\phi = -1$), and the point appears dark. The result is an image of the object that is covered with a pattern of interference fringes of cosinusoidal intensity, as predicted by equation (1). Each fringe is the locus of an equal change in optical path, and the image is essentially a contour map of change in path length. Figure 6-4 is an example of a holographic interferogram. In this case, the object was a thin spherical shell, stressed by internal pressurization (4 psi). The object had a thin spot, which is indicated by the "bulls-eye" pattern.

Two other common modes of holometry in use are *real-time* and *time-average*. In real-time (or live-fringe) holometry, a single holographic image is superimposed on the actual object, which is also illuminated. The object wave interferes with the image in a fashion similar to the double exposure case, but here the object can be stressed and the fringes observed in real time. In time-average holometry, the object is moved, typically by vibration, during the hologram exposure. The resulting image is an integral over all the object positions during the exposure. If the motion is simple harmonic vibration, the resulting fringe pattern in the image has an intensity that is mathematically expressed as a Bessel function of the vibration amplitude. Because a part that is vibrating sinusoidally spends most of its time at the two extremes of its motion, this Bessel fringe pattern is similar to the pattern that would result from a double-exposure interferogram with exposures taken at both extremes. It is helpful to keep this in mind when interpreting time-average interferograms. In particular, the nodes, which do not move at all during the exposure, reconstruct brightest. This version of holometry is often used for modal analysis.

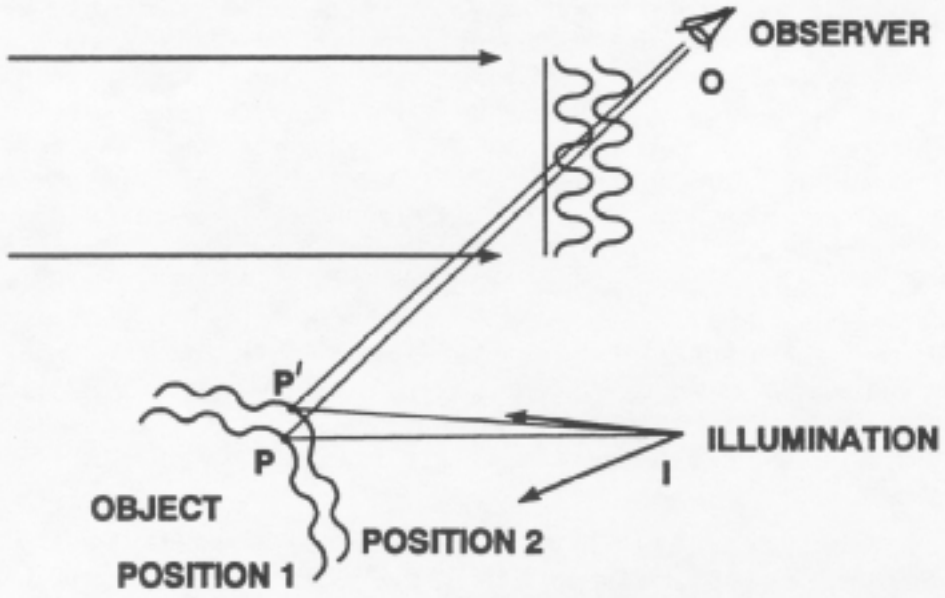

Figure 6-3. Holometry with Diffractive Reconstruction. Two diffracted image waves interfere, giving information on path-length difference.

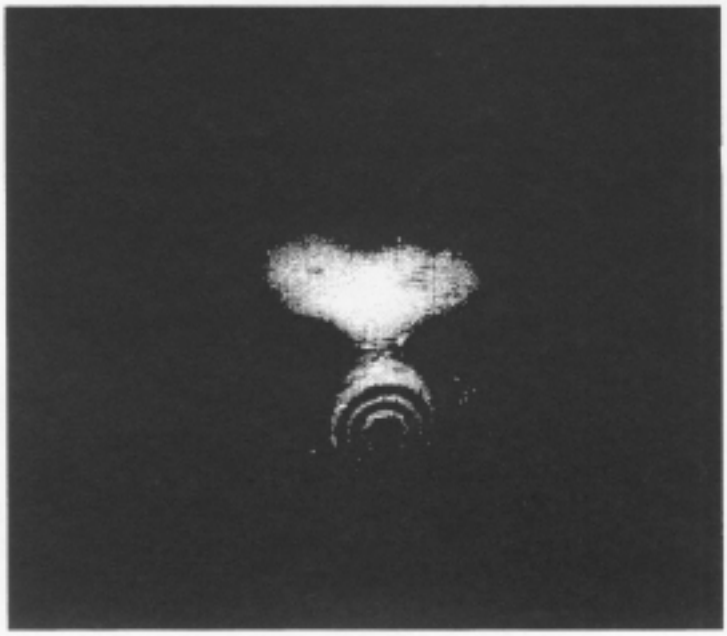

Figure 6-4. Holographic Interferogram of an Aluminum Shell Stressed by Pressurization. Shell is 0.3 m in diameter and 0.5 mm thick, with 4-psi pressure difference between holographic exposures.

Electronic speckle-pattern interferometry. If the film is replaced by an electronic detector such as a CCD camera, the experiment becomes electronic holography, or electronic speckle-pattern interferometry. In practice, some changes to the layout depicted in Figure 6-1 are necessary, as shown in Figure 6-5. One change is dictated by the detector resolution. In film holography (Figure 6-1) a large angle (typically 45° to 90°) can be used between the object and reference beams, and the intensity grating has a line spacing on the order of a wavelength, which is a fraction of a micron. This requires a film with a resolution of several thousand line pairs per millimeter. Since typical CCD cameras have a face-plate resolution on the order of tens of microns, the reference beam must be nearly collinear with the object beam. This is typically done with a beamsplitter and additional optics, as shown in Figure 6-5. Another fundamental difference is that the resulting holograms are recorded electronically and cannot be reconstructed optically as shown in Figure 6-2. For this reason, the object is typically imaged onto the detector and an *image plane* hologram is formed. While this can also be done in film holography, it is typically not necessary—the imaging is done by the detector, whether it is the eye or a camera.

Because the image is not reconstructed by diffraction, there are no image waves to interfere and the model described under "Film-Based Holography" does not hold. However, there is an equivalent explanation based on the fringes at the hologram plane. In Figure 6-3, if the two diffracted image waves are in phase, then the gratings in the hologram are in phase also, and the hologram has a strong grating at that point. This grating diffracts image light toward the observer, and the image point appears bright. If the gratings in the hologram are out of phase, they cancel at that point—the hologram contains no grating, and diffracts no image light from that point with the result that the image appears dark there. ESPI relies on an electronic comparison of the intensity gratings to give the interferometric information. If the "before stress" and "after stress" images are subtracted, a similar result occurs. Where the two gratings were originally in phase, the image appears dark, whereas if they were out of phase, a bright

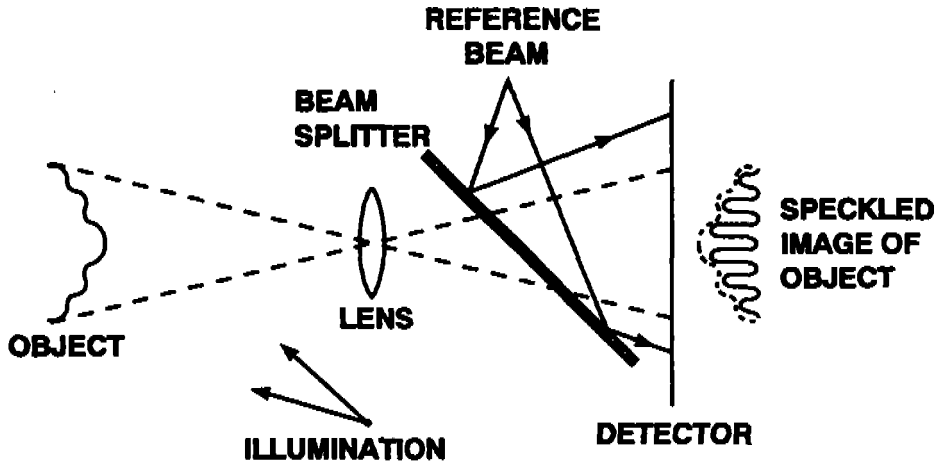

Figure 6-5. ESPI with In-Line Reference Beam. Similar to Figure 6-1. Differences are ***that object is imaged*** onto detector, and reference beam ***is*** nearly collinear with object light.

image (of the grating, or speckle pattern) appears. The result is the same as in film holography, that is, an image of the object with a fringe pattern superimposed. Since the resolution of the camera is much lower than that of film, the speckles are much larger, and ESPI images tend to be much more grainy in appearance than film holometry images.

In the case of time-average ESPI, subtraction cannot be performed because the continuously moving image integrates, or adds, during the exposure of a single video frame. Areas where the integrated fringe pattern tends to cancel have a constant bias value, and areas where they reinforce have a grating or speckle pattern superimposed on a bias. This is usually handled by a high-pass filtering operation to remove the bias term.

6.2.3 Shearography.

In shearography, as in holography, an interference pattern is recorded at the hologram plane. However, instead of interference occurring between an object and reference beam, as in holography, the interference occurs between two nearby points on the object surface. To make this happen, a shearing element, such as a prism, is introduced into the imaging optics so that two images, slightly displaced, appear at the detector plane, as shown in Figure 6-6. The images interfere on a point-by-point basis, creating a speckle pattern. The intensity at each point depends on the phase relationship between the waves scattered from the two object points superimposed at the image, which is in turn determined by the difference between the two optical paths I-P_1-O and I-P_2-O. Shearography, like holography, can use either film or an electronic detector.

As in holometry, shearography is implemented by comparing two interference patterns, typically before and after an object motion. If the motion causes changes in the optical path difference of an integral number of wavelengths, the "before" and "after" speckle patterns are identical. If the path difference changes by an integer plus half wavelength, the speckle patterns differ. These images can be compared by subtraction or other algorithms to obtain an image of the object with fringe patterns superimposed. Since shearography measures differential motion of closely spaced object points, it is often said that "shearography measures strain directly." This is true, but in a fairly complex way. In the most typical shearography experiment, the surface is viewed from a nearly normal direction, in which case the measurement is out-of-plane motion Δz, divided by an in-plane shift Δy. This scalar quantity gives only one element of the strain tensor, and an off-diagonal one at that. By viewing the surface at an angle to the normal, a portion of the in-plane strain element can be measured. Several scalar measurements must be combined to measure in-plane strains.

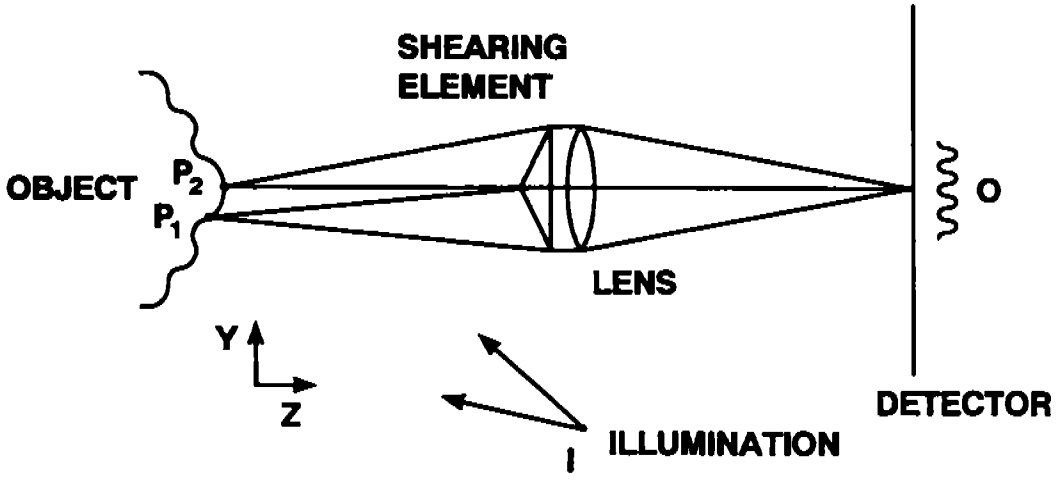

Figure 6-6. Shearography. Shearing element causes light from P_1 and P_2 to interfere at detector.

Shearography's major advantage is its insensitivity to rigid-body object motion. In holography, the first order interference fringes (the ones that construct the hologram) result from interference between an object and reference beam. This means that during hologram exposure, relative motion between the object and the optical system must be less than a fraction of a wavelength. This is a severe restriction, and typically holography must be done with the object and optics on a rigid, vibration-isolation table.

In shearography, both interfering beams scatter from nearby points on the object, following almost identical paths throughout the experiment. Rigid-body motions introduce the same phase difference in each path, and these differences cancel when the beams interfere. This makes shearography much more suitable than ESPI or holography for field environments. The limit on relative motion between the object and the optical system in shearography is the correlation of the "before" and "after" speckle patterns. The object cannot move between exposures more than the size of the speckle. If it does, "speckle decorrelation" results, unrelated speckle patterns are subtracted, and all interferometric information disappears. This motion limitation is typically on the order of a millimeter, as opposed to a micron for ESPI.

6.2.4 Experimental Techniques and Data Interpretation.

Stress methods. As mentioned above, all of the coherent optical inspection techniques involve a comparison of surface positions of a particular part in different stress states. Any stress that causes a deformation is valid, and certain applications have a "natural" stress method, such as pressurization for pressure vessels and application of a voltage for capacitors. For flaw detection in various materials, three types of stress have been widely applied: thermal, pressure reduction, and vibration. Since the coherent optical techniques measure a *surface* deformation, the actual manifestation of a subsurface flaw will depend strongly on material properties, flaw depth and size, and stress method.

Thermal stress, applied by oven, heat gun, or heat lamps, is convenient since it is non-contact and requires relatively simple apparatus. In the case of a debond or delamination, the thermal conductivity at the flaw site is typically reduced by the flaw, causing the material over the flaw to expand slightly more than the surrounding part. This results in an out-of-plane bulge which can be easily detected.

Pressure reduction, applied either in a totally enclosed vacuum chamber or by a one-sided suction chamber applied to the part, tends to cause debonds, delaminations, or weak spots to bulge outward more than the surrounding material. This technique requires somewhat more complex equipment than thermal stress, but tends to apply a more even stress field. It does rely on residual internal pressure inside the flaw, so if the flaw is open to the vacuum, such as a debond in the edge of a lap seam, pressure reduction will not detect it.

Vibration, applied either by a contact transducer or air-coupled horn, tends to excite the material over a debond into a higher amplitude vibration than the surrounding material. Either a swept frequency, or a broad-band white noise is used to attempt to resonate the debonded area. This usually requires a significant amount of acoustic energy and hence is inconvenient, especially in the audio frequencies, because it can be quite loud.

In an experiment carried out by United Technologies Pratt & Whitney, all three of these stress techniques were applied to a composite test panel, and shearography was used to detect delaminations. Figures 6-7(a) through 6-7(c) show the results for a particular flaw. Although all three stress methods detected the various flaws in the panel, the actual size and shape of the indication varied by about 25 percent.

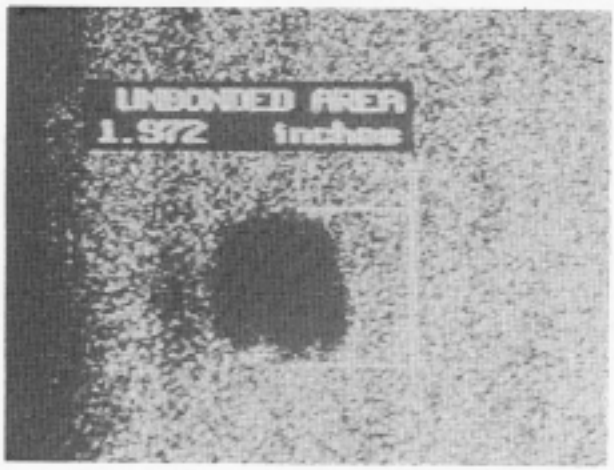

(a)

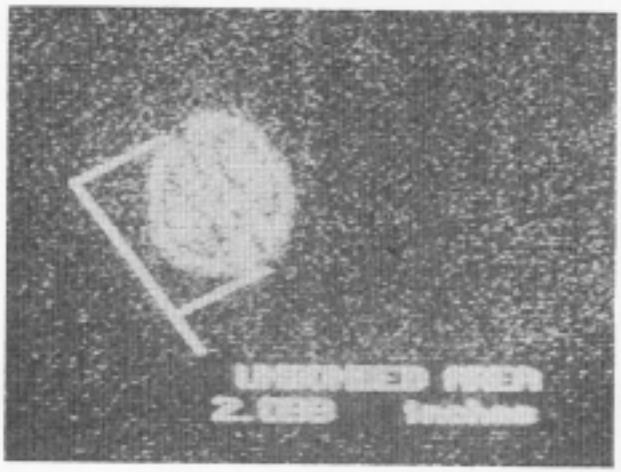

(b)

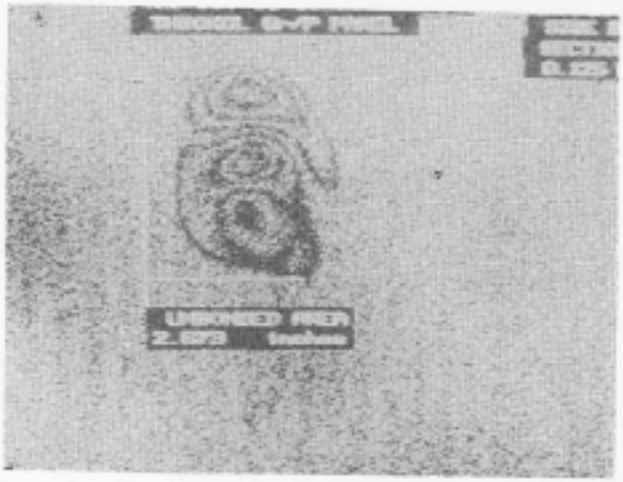

(c)

Figure 6-7. Composite Panel with Delaminations Visualized by Shearography. (a) Acoustic stress, 4000 to 8000 Hz random noise. (b) Thermal stress. (c) Pressure reduction, 0.125. [Source: United Technologies Pratt & Whitney, *Electronic Holography/Shearography NDE System.* Reprinted by permission from Pratt & Whitney.]

Data interpretation. The interferometric data can be interpreted in several ways. The methods vary in complexity and in the amount of information extracted. The simplest method, and certainly the most prevalent for flaw detection, is simply to look for anomalies in the expected fringe pattern. This requires some experience or training to recognize "expected" versus "anomalous" patterns. However, in many cases these anomalies are dramatic and hence easily recognized. In Figure 6-4, for instance, the "bulls-eye" indicating a weak spot in the pressure vessel stands out and is easily recognized. In Figure 6-7, the object is a nominally uniform composite plate, and because no fringes are "expected," any indication of a surface slope represents a potential flaw. Discontinuities in fringes typically indicate a discontinuity in surface displacement, which can indicate a crack.

Quantitative information can also be obtained from holographic interferograms or shearograms by several methods. Each fringe in the image represents a change in *optical path* of one wavelength between the two beams being compared. There is usually a known geometrical relationship between these changes in optical path and the *displacement vector,* which describes actual motion of each point on the object. The relationship can be complex and typically varies across the image. The optical path length change is a *scalar* quantity, resulting from the projection of the local surface displacement vector on the illumination and observation vectors. To measure full three-dimensional *vector* displacement, at least three observations must be made. Sometimes these observations can be made from a single hologram by varying the observation point, and sometimes three holograms may be required. This is governed by the hologram aperture, recording quality (signal to noise), and desired resolution. Because the fringes are cyclic, ambiguities are possible. Some analysis algorithms require the zero order (no displacement) fringe to be known, and that is not always easy (or indeed possible) to identify.

In some experiments, variables can be eliminated to simplify the process. For example, if only the out-of-plane component of displacement is needed, and if the interferogram is illuminated and viewed nearly normal to the surface, the interferogram becomes a contour map, with each fringe representing an out-of-plane displacement of one-half the wavelength of the light used. In general, however, interferogram fringe analysis can be extremely complex.

Various techniques other than fringe counting are used to determine the relative phase. One popular technique is known as "phase stepping" or "phase shift" interferometry. In this technique, several interferograms are taken with a known phase shift introduced between interfering beams for each interferogram. At least three, and possibly many, interferograms are taken with the same optical geometry. At each point, the intensity of each interferogram is read, and multiple equations can be solved to give the absolute phase shift as a function of these intensities. Most of the algorithms used for phase stepping give the phase only in modulo 2π form due to the cyclic nature of the intensity fringes. A separate "phase unwrapping" operation is needed to resolve the modulo 2π information into absolute path-length difference. Also, these techniques still give a scalar piece of information at each point, so if vector information on displacement or its derivatives is needed, independent viewing/illumination directions must be utilized. Development in the area of interferogram interpretation is still quite active.

6.3 PRESENT APPLICATIONS.

Since its introduction in 1965, holometry has been applied to a variety of industrial inspections. Detection of out-of-plane motions is somewhat easier than detection of in-plane motions, because for out-of-plane motions the optical beams can be nearly perpendicular to the surface. Thus these techniques have been particularly useful for detection of features that have a predominant out-of-plane deformation. Examples of such deformations are debonds or delaminations in composite or layered structures like skinned honeycomb, bonded or coated

structures, and complex layered objects such as rubber tires. Holometry has also been useful for modal analysis of structures such as turbine blades, and automotive components including engines and body panels. References 6-1 to 6-3 contain many application examples. The Society of Photometric Instrumentation Engineers (SPIE) has several conferences each year that have sessions on holographic and speckle techniques.[6-5] The Society for Experimental Mechanics has also sponsored conferences on coherent optical inspection.[6-6] These conference proceedings describe many current applications.

Because of the strict vibration-isolation requirements and inconvenience of film processing, film-based holometry has been used mainly for development testing in a laboratory environment. There have been a few examples of production inspection by film holometry. Perhaps the most well-known of these is the tire tester originally developed by GCO, Inc. This device, shown in Figure 6-8, has a vacuum chamber which subjects each tire to a partial vacuum. Debonds show as fringe concentrations. This device can be economically justified for high-value tires with strict quality requirements, such as aircraft tires.

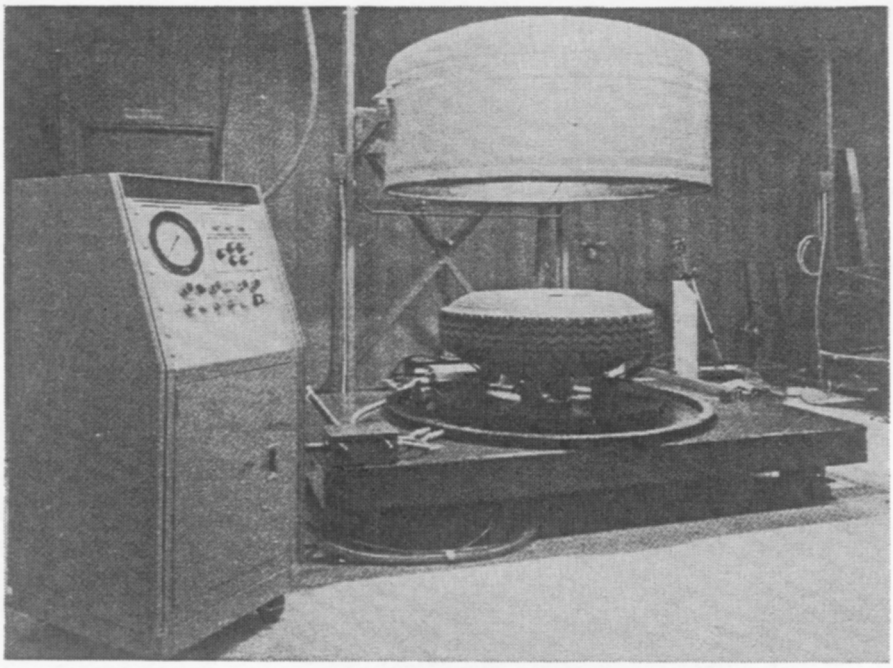

Figure 6-8. GCO, Inc. Tire Tester. [Source: Gordon W. Brown, "Pneumatic Tire Inspection," *Holographic Nondestructive Testing*, R. K. Erf, ed., Academic Press, New York, 1978. Reprinted by permission from Academic Press.]

6.4 AIRCRAFT APPLICATIONS.

Because high quality and reliability are necessary in many aircraft components, the complexity of coherent optical measurements has been justified in many cases of design and production inspection. The following examples from jet engine manufacturing, component design, and materials properties measurement illustrate these uses.

6.4.1 Turbine Blade Modal Analysis.

Time-average holometry is ideally suited for modal analysis of turbine blades, as shown in Figure 6-9, or entire turbine wheels. These techniques are applied in two ways, often sequentially. First, a real-time technique can be used to find interesting resonance frequencies quickly. An initial exposure is taken of the object without any acoustic driving force applied. This image is used as a reference image when the part is driven acoustically with a variable frequency. While resonance conditions can be detected by electronically monitoring (or for lower frequencies, audibly monitoring) the vibration frequency at one or a few points, the entire image can be viewed to select interesting or troublesome mode shapes. Usually the entire frequency range of interest can be swept in a few minutes.

By modulating the optical reference beam, the bright areas of reconstruction (the nodal lines in the unmodulated case) can be manipulated so they appear at the locus of a particular phase and amplitude of surface vibration. This technique can be used to obtain quantitative amplitude information, or relative phase of the nodal areas, during the real-time interferometric inspection.

After the interesting frequencies are detected, time-average interferograms are taken at these frequencies, producing higher resolution, higher contrast images than is possible in the real-time mode. These images can be used simply to visualize mode shapes, since the nodal lines appear brightest. Flaws can be localized by anomalies in the expected or normal fringe pattern. The interferograms can also be quantitatively analyzed to measure vibration amplitude, which can be related to wall thickness and other design and manufacturing properties such as cooling channel location and integrity.

6.4.2 Abradable Seal Integrity.

United Technologies Pratt & Whitney have been using both ESPI and shearography to inspect gas turbine compressor tip seals. These abradable seals are either a brazed-fiber metal or a plasma-sprayed layer. The object of the inspection is to determine the integrity of the bond between this layer and the engine compressor case. Figure 6-10 shows the results of using holometry with broad-band acoustic excitation to detect bonds in this assembly.

6.4.3 Aging Aircraft Inspection.

Several demonstration experiments have recently been performed to assess the capability of shearography to detect the major flaw categories—debonds, cracks and corrosion—targeted by aging aircraft inspection. Both laboratory experiments and field trials on full-sized aircraft have been run.

In 1990, Laser Technology Incorporated (LTI), under contract to the Department of Transportation's Volpe National Transportation Systems Center, fielded an experiment to demonstrate and evaluate the flaw detection capability of shearography in a laboratory environment, on actual-sized test specimens.[6-7] These 6- by 10-foot specimens were fabricated

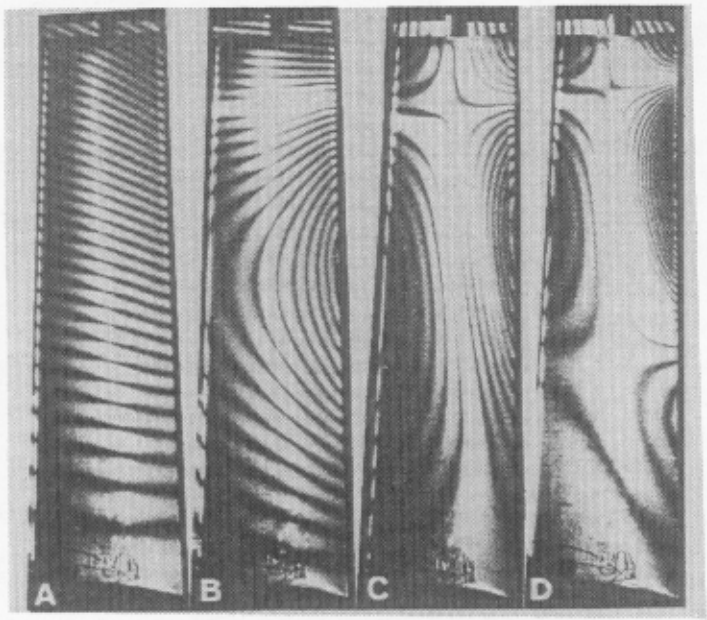

Figure 6-9. Turbine Blade Holometry Showing Various Resonant Modal Structures. Bright areas represent nodes. [Source: Robert K. Erf, "Turbine Blade Inspection," *Holographic Nondestructive Testing*, R. K. Erf, ed., Academic Press, NY, 1978. Reprinted by permission of Academic Press.]

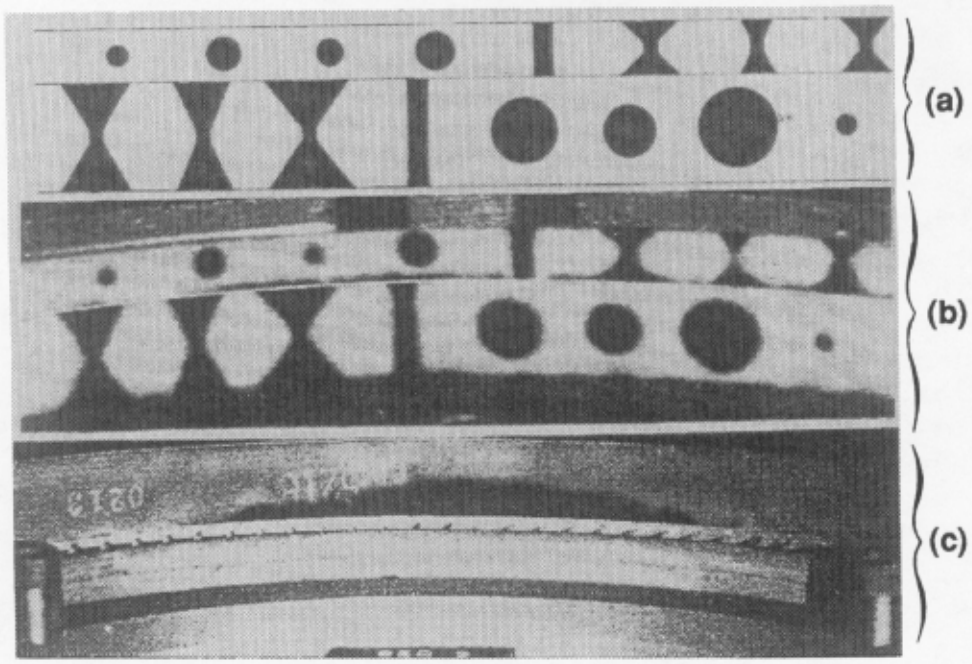

Figure 6-10. Abradable Seals In Gas Turbine Engines. (a) Map of programmed debonds in technique verification sample. (b) Image indicating location of debonds in test master. (c) Production part with large debond. [Source: United Technologies Pratt & Whitney, *Electronic Holography/Shearography NDE System*. Reprinted by permission from Pratt & Whitney.]

to resemble the fuselage structure of Boeing 727 and 737 aircraft and had various programmed flaws machined into them. They were stressed by pressurization that simulated flight conditions on the FAA Aircraft Panel Test Facility, which was operated under separate contract by Foster-Miller, Inc.

Although the first panel was a control panel with no known flaws, shearography found one unplanned weak rivet by detecting a strain concentration in the skin surrounding it. For the second test series, a 10-inch-long slice was cut in the panel and the ends of the crack were sharpened by fatigue cycling. This large crack was easily detected with an application of a differential pressure between exposures of only 0.005 psi.

The third test series looked at lap joint debonds. A 737 panel section was built with an intentional debond 30 inches long in the lap seam. This was inspected with a series of 11-inch by 14-inch views, covering about 4 feet of lap seam. The pressure differential used was 0.04 psi. The inspection took about 30 minutes. Figure 6-11 shows two of the 11-inch by 14-inch views. In these two images the lap seam is vertical.

See Reference 6-7 for a complete description of these images—they are included here only to illustrate a few key points. First, and perhaps most obvious, is that these images can be quite complex. Either a fairly skilled operator or sophisticated analysis software, or perhaps both, may be required to allow shearography to become a routine inspection tool. This problem is being addressed currently by analysis software development efforts. Research is also under way to optimize the stress method to selectively excite the flaw in question and to minimize sensitivity to unrelated structure. These efforts are directed toward making shearography more "user friendly."

The second key point is that there is a lot of information in these images. The waviness of the fringes in Figure 6-11(b), indicates strains in the skin surrounding the rivets. This implies that the rivets are taking the load, and the bond is not. Other fringe features are related to the bond integrity of the tear straps.

Several field trials of shearographic inspection have also been conducted. One comprehensive demonstration was conducted by LTI in August 1991. Selected portions of a Boeing 737 fuselage were inspected with shearography at a USAir repair station in Winston-Salem, NC.[6-8] A tripod-mounted, variable-field-of-view shearography system was used for lap seams accessible from floor level, and a fixed-field, vacuum-cup-mounted system was used for upper seams. In the available 24-hour period, approximately twenty percent of the candidate inspectable area was covered. In the area inspected, thirty-one debonds were discovered by shearography. Based on this demonstration and the assumption that shearographic inspection would eliminate the need for extensive internal visual inspection (and the associated internal tear-down), it was estimated that use of shearography could save $72K for each aircraft inspected, not counting equipment cost. If the equipment were rented at current rates, net savings per inspection would be about $40K.

(a)

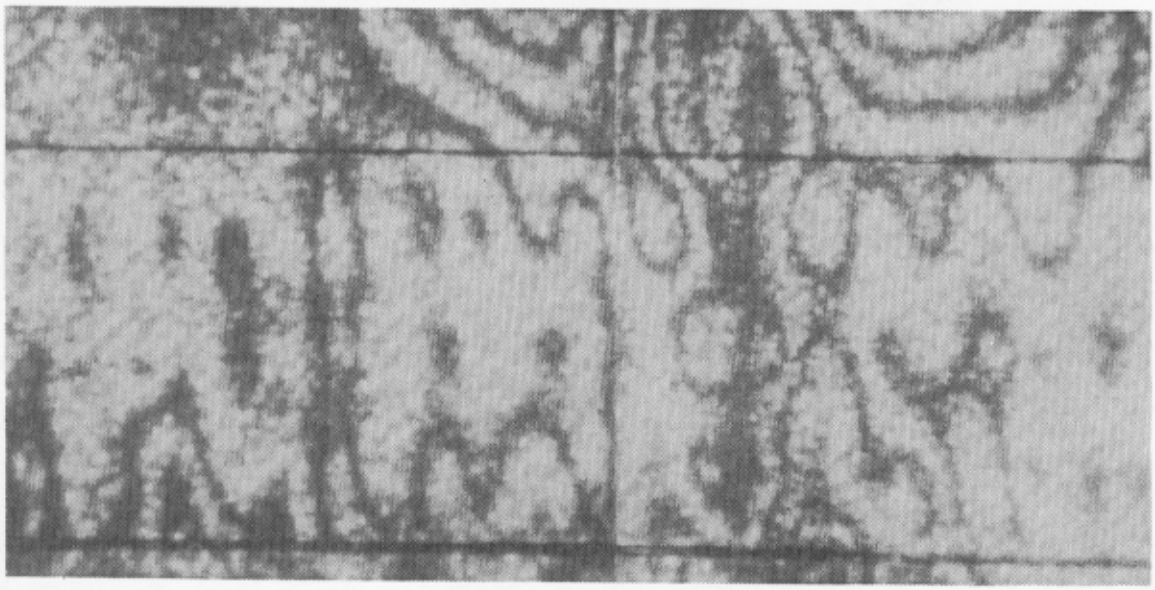

(b)

Figure 6-11. Shearography Image of a Disbonded Lap Seam In a Simulated 737 Fuselage Panel Section. The actual lap joint is denoted by the black lines. Figure 6-11(a) is a bonded region, and 6-11(b) is unbonded. Note the fringing around the rivets in 6-11(b), indicating the rivets are taking the load. [Figure courtesy Laser Technology Incorporated.]

6.5 TECHNICAL CONSIDERATIONS.

6.5.1 Advantages.

The major advantages of flaw detection methods based on the coherent optical techniques are that they:

- are wide-area imaging techniques, hence fairly rapid
- allow for essentially non-contact inspections
- are very sensitive to small deformations
- are single-side access.

6.5.2 Disadvantages.

The major disadvantages include the following:

- for film holometry, inconvenience of film processing
- possible need for vibration isolation
- need to stress the object in some way
- difficulties in image interpretation
- possible laser safety considerations.

6.5.3 Discussion.

All the techniques considered in this section are imaging techniques in the sense that they inspect an area without employing scanning. Image sizes are governed by desired spatial resolution, detector sensitivity, and available laser power. Typical range is a few centimeters square when inspecting for small cracks to a meter square when inspecting for debonds of a few centimeters in size. Although film holometry has a much greater potential spatial resolution than the electronic methods, this advantage is offset by two factors: First, wet-chemistry film processing in the field is inconvenient. Second, the only practical technology available for automated image analysis and archiving is video, and this limits the useful resolution. A thermoplastic holographic recording system that eliminates the need for chemical film processing is available, but most field applications today use either ESPI or electronic shearography for their convenience.

The interferometric imaging process itself is non-contact. However, the object being inspected needs to be perturbed in some way. First, since the fundamental quantity being measured is a motion or displacement, some stress needs to be applied to cause this displacement. Typical stress methods for aircraft are internal pressurization of the fuselage, external application of partial vacuum, thermal stress applied by air gun or heat lamp, or vibration (either air-coupled or contact-coupled to the structure). Second, many aircraft skins are shiny, possibly polished. This can cause a specular reflection of the laser light, which creates highlights or saturation problems in the detector. A solution to this problem is to apply a diffuse reflective coating to the surface. Often a dye penetrant developer is used since it is easy to apply and remove.

The sensitivity of these techniques to surface displacements on the order of microns is both an advantage and a disadvantage. On the plus side, very small stresses are required to cause detectable deformations. On the minus side, environmental effects such as noise, ambient

vibrations, and temperature shift can cause sufficient motion to invalidate the measurement. This problem exists particularly in holometry and ESPI, which measure absolute surface motion. These two techniques are difficult or impossible to apply in the field, although there are "tricks," such as attaching the reference mirror to the object under test, which make them barely fieldable. Shearography has the clear advantage here because it measures relative surface motion and is less sensitive to gross object motions. Even with shearography, it has been necessary to stop other operations on the aircraft, especially repairs or similar "high impact" operations, to avoid speckle decorrelation problems during shearographic inspections. Some techniques for attaching the optics to the skin of the aircraft have been developed that tend to help, but ambient motions are still a problem and the search for the "best" solution remains ongoing.

Data interpretation is another area of active research. As exemplified by Figure 6-11, the images can be complex, and application of these flaw-detection techniques may require significant operator training in some cases. Some of the more sophisticated data analysis techniques could help alleviate this problem, but this too is an area of ongoing research.

6.6 STATUS.

6.6.1 Present.

The NDI method of coherent optical inspection using holometry, ESPI, and shearography has been in use in the laboratory for about twenty-five years and has been in limited use in industrial inspection for most of that time. NDI systems, the NDI equipment and technique applied to inspection activities, are commercially available and are in use in several industrial production inspections. At least one formal military standard inspection process has been written at Boeing. This process defines level I, II, and III inspector requirements for shearographic inspection of the SRAM II missile case.

In the arena of aging aircraft inspection, these techniques and systems are in the "preliminary design" phase: Tests have been conducted on laboratory samples, and some field demonstrations have been conducted. Although at least one demonstration test included data on inspection time, no statistically designed experiments have been conducted, nor have inspector requirements (training, physical condition, etc.) been formally defined.

6.6.2 Future: Estimated Time to Field Use.

It will be several years before the above-mentioned problems of image interpretation and sensitivity to vibration and object motion are solved in a general sense. Some specific inspections, such as inspection of composite surfaces for impact damage, are now undergoing field trials, and the process of seeking FAA approval and certification for these specific inspections has begun. Coherent optical systems may be in limited use in about 1994 or 1995, and in more general use in the mid to late 1990s.

6.7 REFERENCES.

6-1. Charles M. Vest, *Holographic Interferometry,* John Wiley & Sons, New York, 1979.

6-2. Joseph R. Davis, et al., *Metals Handbook,* ninth edition, Vol. **17,** ASM International, Metals Park, Ohio, 1989.

6-3. Robert K. Erf, ed., *Speckle Metrology,* Academic Press, New York, 1978.

6-4. Y. Y Hung, "Shearography: A Novel and Practical Approach for Nondestructive Inspection," *Journal of Nondestructive Evaluation,* Vol. **8,** No. 2, 1989.

6-5. The SPIE has several annual meetings that contain sessions on coherent optical techniques. Proceedings, such as *San Diego, 1991, SPIE,* Vols. **1554A** and **1554B,** give many applications.

6-6. *Proceedings: SEM Conference on Hologram Interferometry and Speckle Metrology, November 5-8, 1990, Baltimore, MD,* ISSN: 1046-6797.

6-7. *Inspection of Fabricated Fuselage Panels Using Electronic Shearography,* Department of Transportation report no. DOT/FAA/CT-TN92/26, July 1992.

6-8. *Shearographic Inspection of a Boeing 737,* Department of Transportation report no. DOT/FAA/CT-TN92/19, July 1992.

7. ADVANCED ULTRASONICS.

7.1 SUMMARY.

Advanced ultrasonic techniques include two nonconventional ways to generate and detect ultrasonic waves: laser ultrasonic methods and methods that use electromagnetic acoustic transducers (EMATs). The development of laser pulse generation and laser beam detection methods has reached the stage that both methods can be applied to inspection of aircraft structures, and both are non-contact and remote—features that lend themselves to fast and wide-area scanning. EMATs, by their very nature, can only be used on conductive materials. The various EMAT designs make it possible to generate a wide variety of wave propagation modes that are not available with conventional transducers.

From the variety of wave propagation modes available, the inspection technique most sensitive to detection of the particular type of flaw or defect of interest in a specific aircraft structure can be chosen. Three advanced ultrasonic methods have been investigated in the laboratory for the generation and detection of plate waves: leaky Lamb wave techniques, oblique incident wave techniques, and acousto-ultrasonic techniques. A problem with using leaky Lamb wave methods to inspect aircraft structures is that this method requires that a substantially thick coating be applied to the surface of the structure. Oblique incident and acousto-ultrasonic methods are feasible with dry couplant roller transducers.

Advanced ultrasonic signal-processing techniques that resolve ultrasonic pulse echoes between very thin interfaces, such as those present in the skin-bonded joints of aircraft, can be used to good advantage in aircraft inspections. Frequency domain analysis can extract flaw echoes from normal material noise echoes. In many cases it can also make the ultrasonic flaw inspection of composites feasible. The extraction of features of ultrasonic signals in the time and frequency domain has made it possible to distinguish echoes produced by flaws from those produced by normal, unflawed material. Software using artificial neural network techniques has also been developed to classify ultrasonic signals into flawed or unflawed types.

Portable computer systems for ultrasonic data acquisition, processing, and image display have recently become available. These portable systems can be applied to aircraft NDT inspections to increase reliability and effectiveness.

7.2 TECHNICAL BACKGROUND.

High-frequency ultrasonic waves can be used to measure material properties and detect flaws in elastic solids, and many types of ultrasonic wave modes can be used for the ultrasonic inspection of materials and structures. Important considerations in the development of advanced NDT inspections for the detection of flaws in aging aircraft structures are knowledge of the different wave types and their uses. Different ultrasonic inspection techniques take advantage of the properties of the particular wave mode that is most sensitive or that optimizes the detection capability of certain flaws; for example, for the generation and detection of flaw signals, evaluation of bond interface integrity requires completely different techniques from detection of fatigue cracks.

In some cases the flaw signal is buried in "normal" scattered signals (noise signals), as from grain boundaries or multiple interface layers of a composite. The flaw signal can be detected by applying signal processing techniques. The use of portable computers has increased the availability of flaw imaging capabilities by automated scanning systems using both time/amplitude and frequency domain information in the flaw signal. This section considers the advanced generation, detection, and signal processing techniques that presently comprise state-of-the-art in optimizing ultrasonic inspection capabilities.

Two types of ultrasonic waves are possible in the bulk solid material: longitudinal (compression) waves and shear (transverse) waves. When the solid is bounded by surfaces, many more wave types are possible, such as Rayleigh (surface) waves, Love (2nd type surface) waves, Lamb (plate) waves, Stoneley (interface) waves, head waves, creeping waves, and leaky Lamb waves.

Each wave type or mode has its own propagation velocity and wave motion which are characterized by the vibration mode or displacement motion of the particles of the solid with respect to the wave propagation direction. Bulk longitudinal waves are approximately twice the velocity of bulk shear waves. Surface wave velocities are approximately 90 percent of the bulk shear wave velocity. Plate and interface wave velocities are usually multi-valued and depend on the material properties, the ultrasonic frequency (dispersion), the thickness, and the boundary conditions of the test-piece. At a given frequency more than one mode of plate waves may exist for layered structures, and for some ultrasonic techniques two may be present at the same time.

Longitudinal wave motion is characterized by particle motion that is parallel to the direction of propagation. Shear wave particle displacement is perpendicular to the direction of propagation. Surface waves are characterized by an elliptical particle motion resulting from a combination of longitudinal and shear displacements. Plate waves and interface waves exhibit complex particle motions to form two basic types of plate wave motion: symmetrical (dilatational) and antisymmetrical (bending). Figure 7-1 shows a schematic of the particle motions with respect to the direction of wave propagation for longitudinal, shear, and surface waves. Figure 7-2 shows a schematic of the particle motions and wave propagation directions for symmetric and antisymmetric plate waves. The infintesimal "real structure" particle motions are greatly exaggerated in the figures for easy visibility.

Figures 7-1 and 7-2 illustrate the generation of ultrasonic waves using conventional piezoelectric transducers, which are normally used for NDT inspection purposes. The pulses of high-frequency sound waves interact with defects or flaw interfaces within the solid, and portions of the energy of the pulse are reflected back to the transducer, where they are detected, amplified, and displayed on a CRT screen of an oscilloscope. Figure 7-3 illustrates the application of a surface wave transducer and the detected signal from a surface crack in a plate as it appears on the CRT screen. The time-of-flight of the detected crack signal depends on the surface velocity of the wave in the plate. The ultrasonic signal can be viewed as an oscillatory pulse (rf pulse) or as a rectified pulse showing only the amplitude envelope of the rf pulse, as is seen on most ultrasonic flaw detector instruments.

The interaction of ultrasonic waves with defects depends very much on the wave mode and frequency. For NDT inspection purposes, defects of a certain nature can be optimally detected by selecting advanced ultrasonic techniques that apply the appropriate wave mode and frequency. In a number of practical applications, as in aircraft structures, the advanced techniques to generate and detect the appropriate wave modes may not be optimized or known. Therefore, appropriate techniques must be developed and tested in the laboratory before they can be applied in the field.

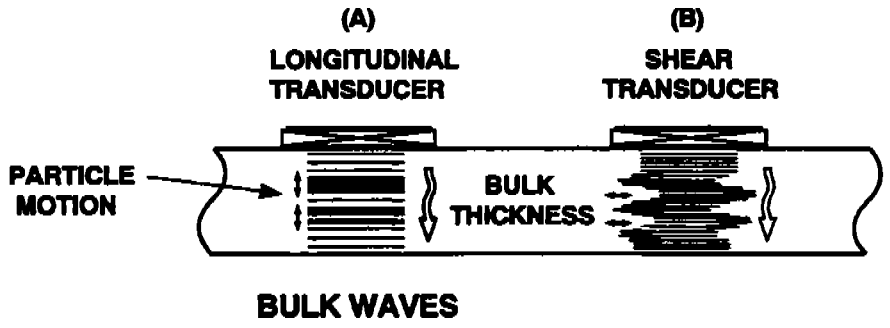

(a) Longitudinal wave. Material particles undergo a succession of compressions and expansions as the wave travels through the bulk material.

(b) Shear wave. Material particles undergo sidewise displacements as the wave travels through the bulk material.

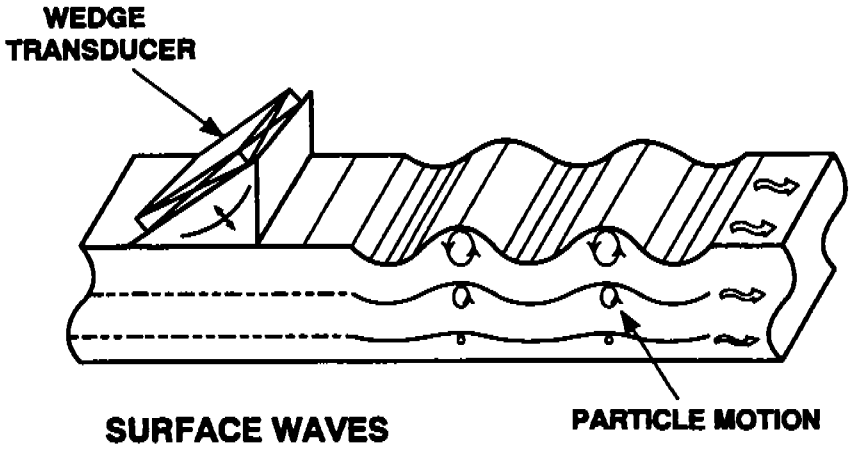

(c) Rayleigh (surface) wave. Material particles undergo elliptical displacements as the wave travels along the surface; displacements vanish at a depth of two wavelengths.

Figure 7-1. Modes of Acoustic Wave Propagation In Solids.

For composite materials and anisotropic materials, wave propagation velocities depend on the propagation direction in the material. Two velocities for the same wave mode are possible and are designated as the phase velocity or the group velocity. The phase velocity is the propagation velocity of a point-of-constant phase of the wave. The group velocity or energy velocity is the propagation velocity of the modulation envelope of the wave packet. For anisotropic media, the group velocity direction may be skewed to the phase velocity direction. These wave modes are described as quasi-longitudinal and quasi-transverse. For inspection purposes, both for composites and plates, the group or energy velocity of the wave packet is normally detected. Development of inspection methods for composites and bonded plates will require specific knowledge of all the wave mode characteristics.

Ultrasound is the propagation of stress waves through the material. Based on a generalization of Hooke's Law in terms of stress and strain tensors, the phase velocity of wave modes can be

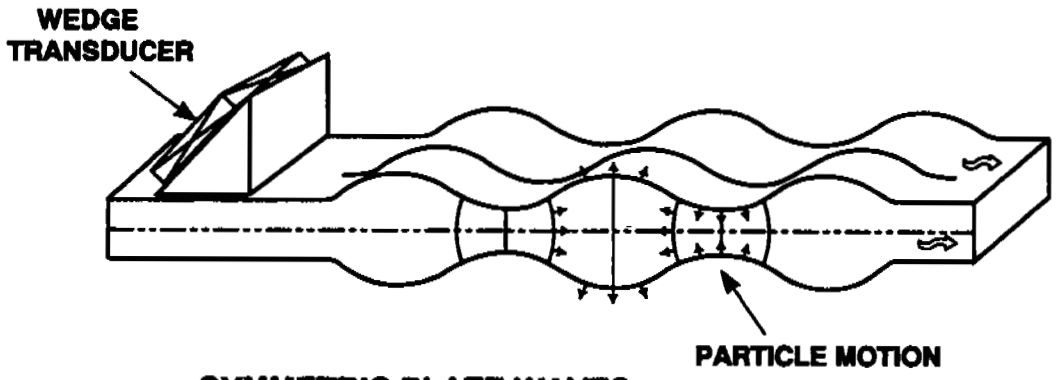

SYMMETRIC PLATE WAVES

(a) Symmetric Lamb (plate) waves. Material particles undergo longitudinal and shear displacements which are symmetric about the midplane of the plate.

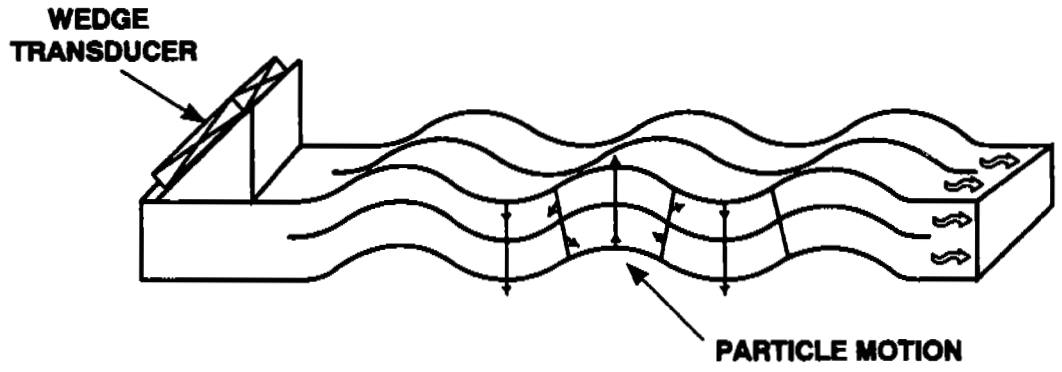

ANTISYMMETRIC PLATE WAVES

(b) Antisymmetric Lamb (plate) waves. Material particles undergo longitudinal components of opposite sign about the midplane of the plate whereas shear components are of the same sign.

Figure 7-2. Modes of Acoustic Wave Propagation in Thin Plates.

written in terms of the stiffness constants or elastic constants of the material. Phase velocities or group velocities of the ultrasonic waves can be measured experimentally and from those measurements effective elastic constants or elastic moduli can be calculated. The strength of a material in the absence of defects is related to the effective modulus of the material. Therefore, by noting decreases in values over time, plate-wave velocity measurements can provide a means of evaluating changes in the strength of composites or adhesive bonded joints used in aircraft structures.

Current ultrasonic techniques and inspection methods used for aircraft applications are described in Reference 7-1. The aspects of new and advanced ultrasonic techniques appropriate for aging aircraft inspections include advanced ultrasonic wave generation and detection techniques; advanced evaluation techniques of bond interfaces using surface, plate, or interface waves; acousto-ultrasonic techniques; frequency and time domain signal-processing techniques;

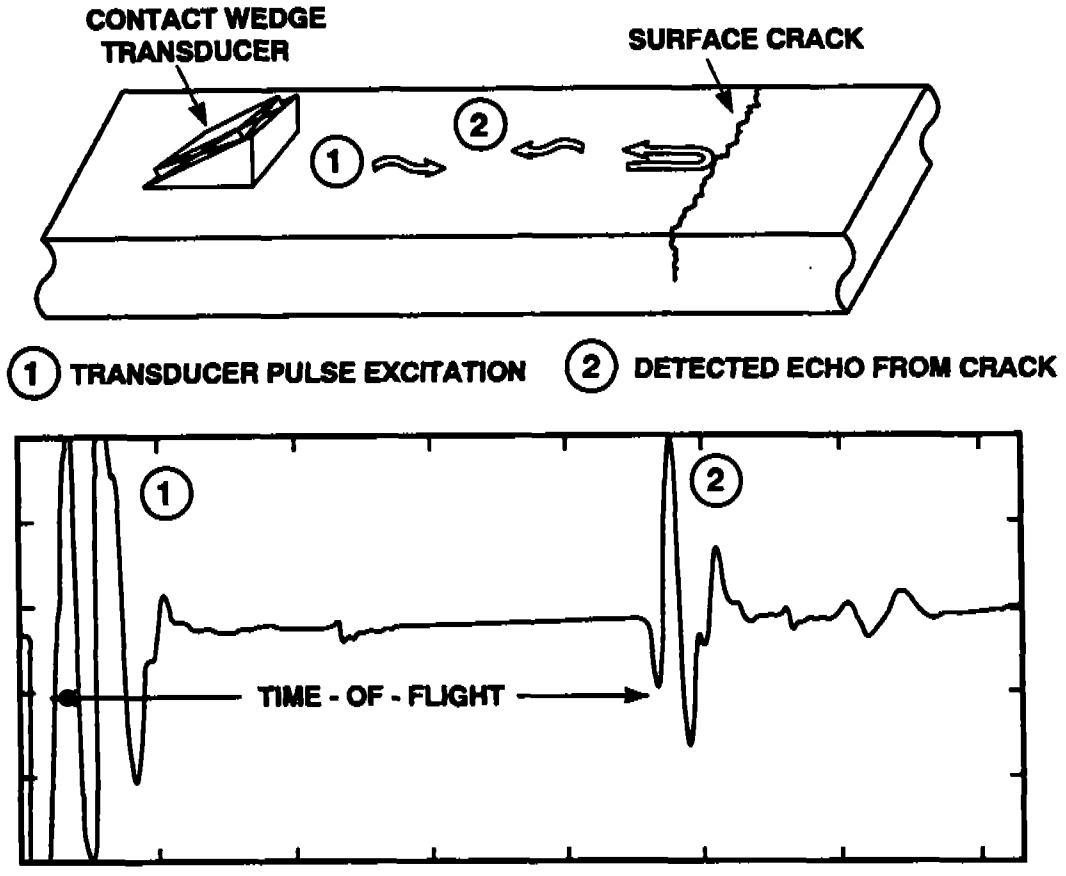

Figure 7-3. Conventional Surface Wave Generation and Detection of a Crack In a Plate As Observed On An Oscilloscope Screen.

and computerized data acquisition and flaw imaging techniques. Because of the magnitude of topics covered, only the most pertinent aspects of each are discussed here. For a more comprehensive treatment, see the cited references.

7.2.1 Advanced Ultrasonic Wave Generation and Detection Techniques

Pulse-echo ultrasonic testers normally consist of a stress wave generator and a stress wave detector coupled with amplifiers and a visual display unit, such as an oscilloscope screen, to observe the signal waveform. Conventional ultrasonic pulse generators use a high-voltage pulse applied to a piezoelectric transducer element. The same or a similar transducer element is used to detect the stress wave after internal reflections from flaw interfaces occur within the test-piece. The transduction principles, basic equipment, and conventional A-scan, B-scan, and C-scan displays are described in Reference 7-1.

In conventional contact transducer applications, a liquid or viscous couplant must be applied between the contact transducer and the inspection surface to ensure adequate transmission of the high frequency sound waves across the transducer-to-work-piece interface. The surface must be quite smooth and free of dirt and obstructions. Lack of consistency in thickness of the coupling medium can greatly influence the inspection results. The inability to maintain a consistent coupling during fast manual or automated scanning techniques can impair the

inspection process significantly. It is also difficult to find compatible coupling mediums for some materials sensitive to oils, solvents, and water or for ones that can be used in high-temperature applications. For these reasons, there has been an increasing interest in using non-contact generation and detection of stress waves in solids.

Two non-contact ultrasound transduction methods are currently available which might be used for aircraft NDI inspections: laser generation and optical detection methods, and electromagnetic acoustic transducer (EMAT) methods.

7.2.1.1 Laser Generation and Optical Detection of Ultrasonic Stress Waves.

In 1963, R. M. White demonstrated laser generation of acoustic waves in a solid.[7-2] Since that time, especially in the 1980s, significant work has been done that resulted in laboratory systems which may eventually find use in practical engineering NDT applications and aircraft inspections. Laser generation and detection of ultrasonic waves is both non-contact and remote. The remote aspect has the advantage of directing the laser beam with mirrors and lenses to quickly scan a large test-piece that may have curved and irregular surfaces of complex geometry, such as in aircraft structures. However, a great amount of work must still be done before laser systems advance from the laboratory to field applications.

A basic laser generation and detection system is schematically shown in Figure 7-4. Figure 7-4 actually consists of two systems, (1) the laser acoustic wave generation system and (2) a laser-beam interferometer system.

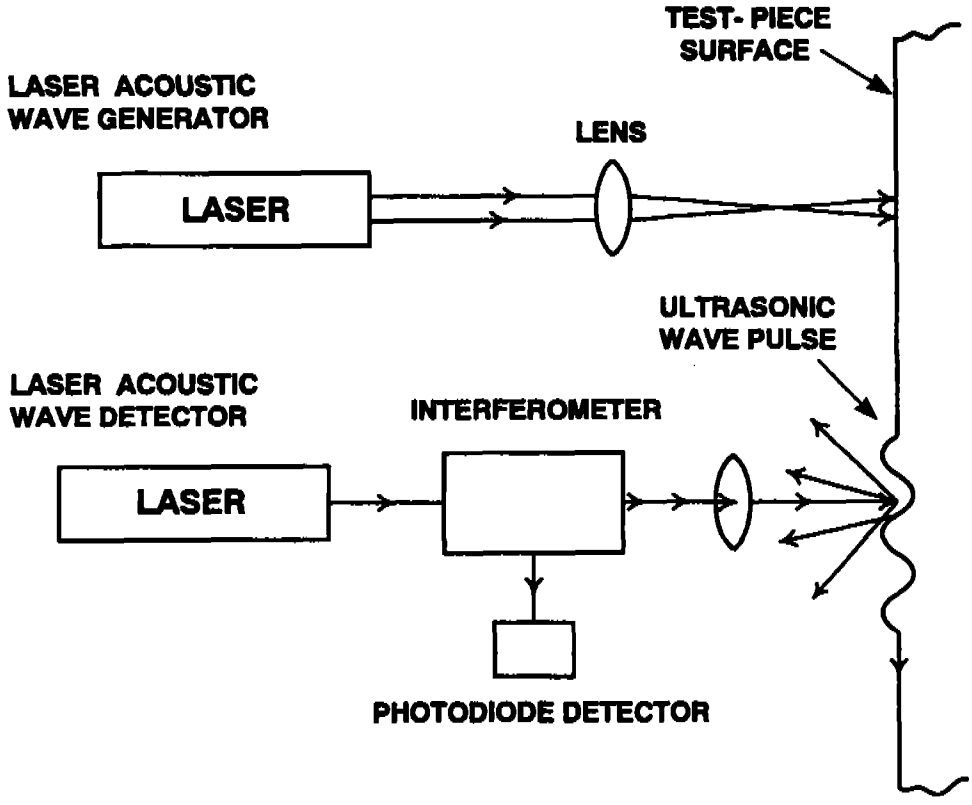

Figure 7-4. Basic Laser Generation and Optical System for Ultrasonic Testing.

Ultrasonic generation with lasers has the ability of generating longitudinal waves, shear waves, surface waves and, consequently, plate and interface waves.[7-3 to 7-10] The source of the elastic waves is by thermal expansion at the point of laser energy deposition (thermoelastic effect) where a shear wave and surface wave are favored under low energy conditions. Increasing the laser power density to cause evaporation of the surface material (ablation effect) favors generation of a longitudinal wave primarily perpendicular to the surface.[7-3] To prevent surface damage by ablation when a longitudinal wave is desired for inspection, a sacrificial coating (oil film) may be applied to the test-piece. Beam patterns and beam-forming techniques have been developed to improve the conversion of laser energy into acoustic energy of the wave type of interest.[7-7]

The laser-beam interferometer system uses a small focused spot (several microns in diameter) on the surface of the test-piece to record the infinitesimal displacements of the surface as the acoustic pulse travels through the spot area. The acoustic stress waves can be detected by either of two interferometer methods coupled with photodiode detection of the light intensity. One design employs optical heterodyning techniques based on the Michelson interferometer.[7-3,7-4,7-7,7-8,7-10] A second design consists of a confocal Fabry-Perot interferometer as the optical detector.[7-5,7-6] The Michelson interferometer technique uses the test-piece surface as one leg of the interferometer and is sensitive to surface out-of-plane displacements caused by the wave motion passing the point of illumination. The Fabry-Perot interferometer is sensitive to the surface velocity of the displacement because it detects the Doppler shift in the frequency of the scattered light from the point of illumination on the surface of the test-piece. A modification of the Michelson interferometer technique has been designed to include a dual-probe detection capability where two points of detection at some distance apart from each other are recorded simultaneously on the surface of the test-piece.[7-10]

7.2.1.2 Electromagnetic Acoustic Transducer.

EMATs offer another non-contacting transduction method for the generation and detection of elastic waves in conductors. Alers [7-11] and Maxfield[7-12] describe many practical EMAT designs which have been successfully used in commercial applications. Hutchins[7-3] compares EMAT techniques with laser techniques.

The fundamental principles of construction of an EMAT are illustrated in Figure 7-5. A radio-frequency transmitter coil is placed close to a conducting surface of a test-piece in the presence of a strong magnetic field. A pulsed rf current I in the coil induces an eddy current density J in the conductor. The interaction of J with the magnetic field B produces the Lorentz force F on the moving electrons. Resulting electron-ion interaction within the conductor generates ultrasonic waves which propagate into and along the surface of the test-piece. An ultrasonic stress wave is detected by a pickup coil (which can be the same as the transmitter coil) where motion of the electron displacements due to the wave causes an induction of a current in the pickup coil.

When the field B is normal to the surface, the Lorentz forces are parallel to the surface as shown in Figure 7-5 and a shear acoustic wave is generated. When the field B is tangential to the surface, the Lorentz forces are perpendicular to the surface and longitudinal acoustic waves predominate. Sensitivity of the transducer does depend on the proximity of the coil and magnet to the surface since generation and detection falls off exponentially with the air gap width. Clearly, proximity is desired but lift-off distances of 3 mm and more can be tolerated. In this respect, the transducer is not remote as is the case for laser transduction, but the technique can still be considered contactless since no couplant is needed between the air gap for operation.

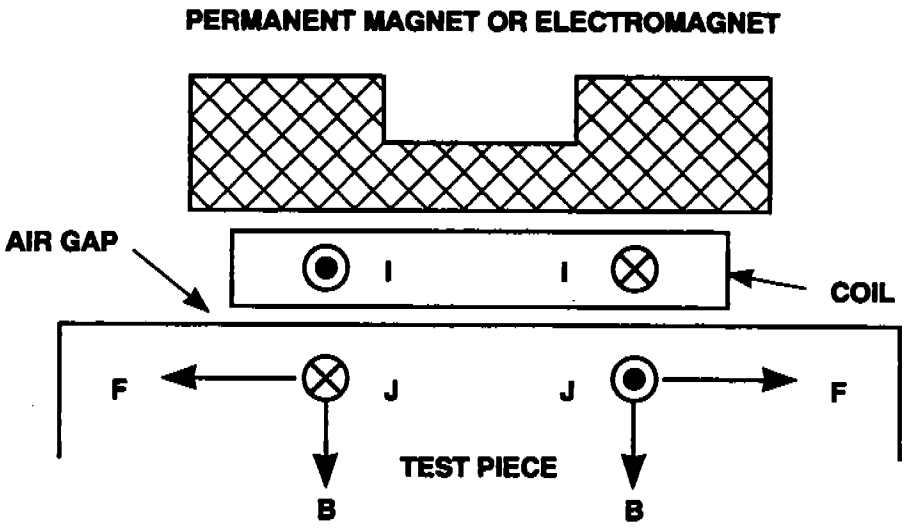

F = LORENTZ FORCE
J = PULSED EDDY CURRENT DENSITY
B = STATIC MAGNETIC FLUX DENSITY
I = PULSED CURRENT IN EDDY CURRENT PROBE COIL

Figure 7-5. EMAT Transduction Geometry and Physical Principles.

7.2.2 Ultrasonic NDE Techniques for Adhesive Bond Integrity of Plates and Composites.

The integrity of adhesive bonded joints in many aircraft structures is important for the safe and continued operation of the aircraft. A few examples of bonded structures are bonded lap joints, layered composite structures, and bonded repair patches where the reliable operation of the aircraft depends on the integrity of interfacial bonds. Advanced ultrasonic nondestructive evaluation techniques are being developed in the laboratory for use in assuring the in-service performance of bonded joints in aircraft.

At present a variety of ultrasonic tranducer resonance techniques, some utilizing sweeping frequencies below 500 kHz, are available on the market for bond evaluations. They operate on the principle that the resonant frequency of ultrasonic waves interacting between the thickness of the bonded structure and the applied transducer are dependent on the quality of the bonded joint at that spot. For detecting debonds, these instruments work fairly well, but for many of the more subtle evaluations of bond quality, such as bond weaknesses, they are not effective. Advanced techniques utilizing shear waves, surface waves, Lamb waves (plate waves), and Stoneley waves (interface waves) show promise for interrogating defects and for evaluating the effective elastic properties of bond interfaces. These properties include deteriorating bond strength and kissing bond (touching but not adhering to one or both surfaces) conditions. A state-of-the art review of the nondestructive evaluation of adhesive bond quality up to 1989 is given by Light and Kwun.[7-13]

Bondline interrogation using Stoneley waves has been shown to be sensitive to changes in the interfacial conditions of the adhesive.[7-14] In laboratory experiments, Rokhlin et al. have shown that an effective shear modulus calculated from an interface shear wave velocity was related to

adhesive bond strength.[7-15] Yew has shown that characteristics of horizontal shear waves (SH waves) in a bonded plate are dependent on the bonding stiffness of the adhesive.[7-16] For plate waves, the dispersion curves (phase velocity versus wave frequency) have been found to be a sensitive measure of assessing defects and elastic properties of adhesively bonded plates and fiber-reinforced composites.[7-17 to 7-19]

There are many methods to generate and detect longitudinal, shear, surface, plate, and interface waves for bonded materials. The three most successful methods in laboratory experiments and those which may find application on aircraft structures are the leaky Lamb wave (LLW) method, the oblique incidence method, and the acousto-ultrasonic method. Figure 7-6 shows the basic transducer configuration for the three methods. In Figures 7-6(b) and 7-6(c), a pitch-catch transducer configuration is shown for both local and global (at a distance) interrogations.

7-2.2.1 Leaky Lamb Wave Method.

Figure 7-6(a) shows for LLW methods a transmitter and receiver transducer positioned at an angle to the surface of the test-piece, which is immersed in a fluid (water). When the angle and frequency of the transmitting wave is correct to excite a LLW, the reflected field consists of two lobes with a local minimum or null zone between them. The minima occur only at conditions for LLW generation. Varying the frequency or angle allows excitation of the different modes of plate waves. The phase velocity for each mode can be calculated from Snell's law and the angle of incidence. Plots of the phase velocity versus frequency (or frequency times plate thickness) establish the dispersion curves for the structure. By setting the angle and frequency to the plate mode generation that is most sensitive to bond material properties (e.g., particle motion that produces shear stress on the bond interface and within the bond thickness), features related to the frequency content and reflection amplitude at a single location in the bonded test-piece can be used to characterize the bond quality or elastic properties of the bonded structure at that location. Chimenti and Martin have shown results with this technique in C-scan format by developing a scanning technique for inspecting a multi-ply graphite-epoxy composite with two 5-MHz transducers in tandem over the surface of the composite plate.[7-20] Seeded defects representing delaminations, porosity, ply gaps, induced damage, foreign matter, and changes in fiber volume fraction were detectable.

7-2.2.2 Oblique Incidence Methods.

Rose et al. describe how oblique incidence measurements, Figure 7-6(b), can be used to generate subsurface longitudinal, shear, and Rayleigh waves and to determine their wave velocities for calculating certain elastic properties of composites.[7-21] Pilarski and Rose demonstrated in laboratory experiments that the sensitivity of transverse waves at oblique incidence is significantly better than the sensitivity of longitudinal waves at normal incidence for the local interrogation and detection of weak adhesion strength of an aluminum-epoxy interface. Their conclusion was that this method can be used as a tool for measuring interfacial weaknesses in adhesively bonded structures.[7-22]

Jiao and Rose have presented a model for solving the adhesive weakness evaluation problem.[7-23] For the oblique incidence analysis of waves traveling across the interface of aluminum-epoxy, they selected the best frequency range for the appropriate shear wave mode which is most sensitive. The higher sensitivity of shear waves with a measurable dependence of transmission factors on the frequency and angle of incidence was demonstrated for different interfacial

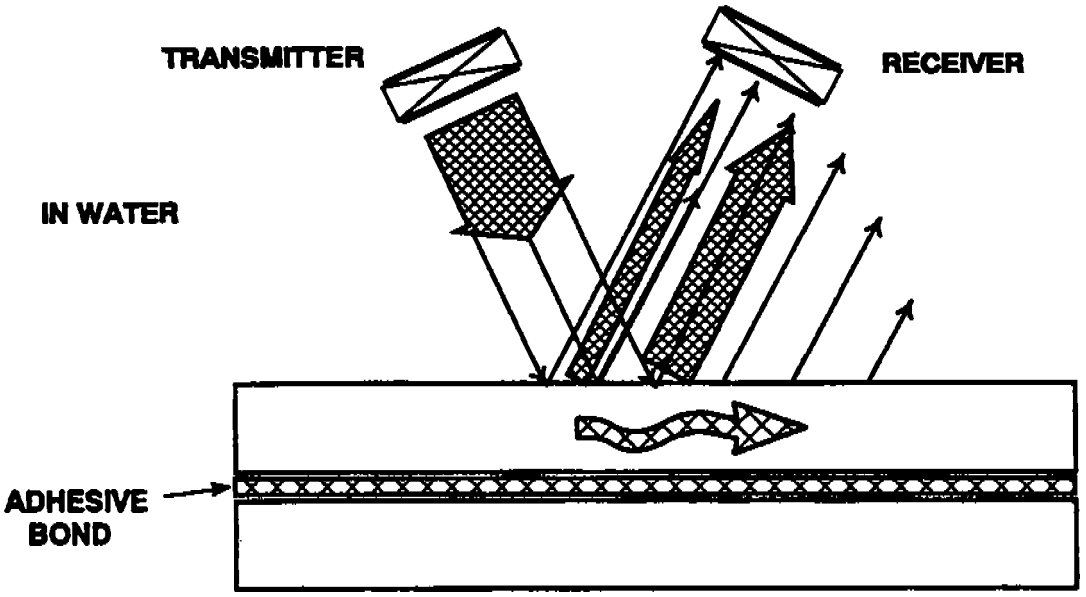

(a) Leaky Lamb wave interrogation technique.

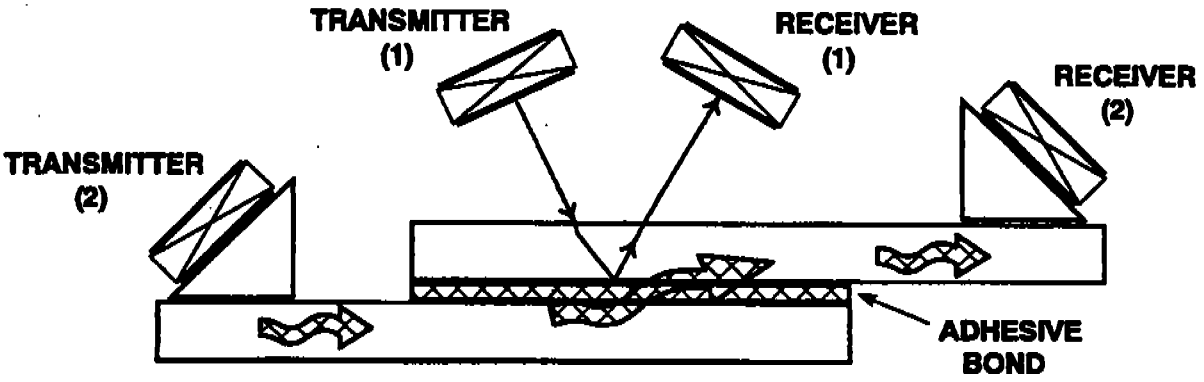

(b) Oblique incidence pitch-catch. (1) Local and (2) Global interrogation techniques.

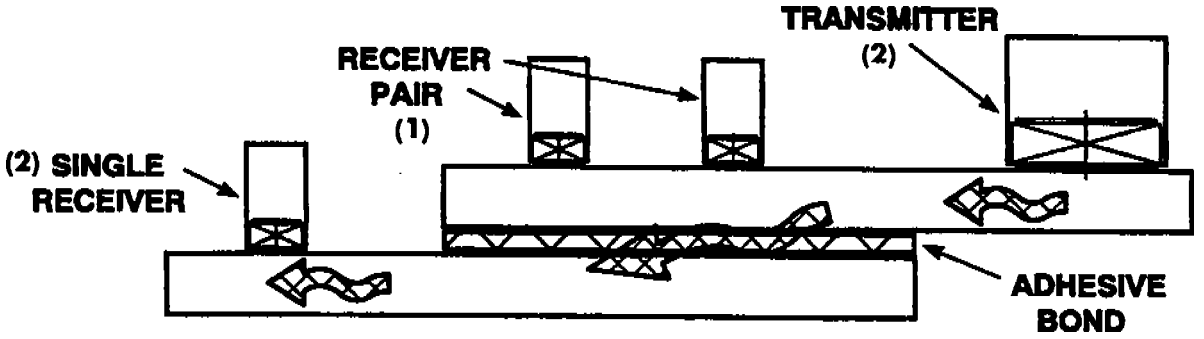

(c) Acousto-ultrasonic techniques

Figure 7-6. Three Inspection Methods for Generation and Detection of Plate Waves.

conditions. Wang and Rokhlin have also shown how an oblique angle beam technique can be used for the evaluation of interfacial properties of adhesive joints in aluminum plates.[7-24] The technique in Reference 7-24 was based on measurement of the frequency response of obliquely incident waves selected in such a way that only transverse waves exist in the aluminum plate and undergo interference in the adherent-adhesive bond layer.

7-2.2.3 Acousto-Ultrasonic Methods.

Acousto-ultrasonics (AU) was introduced by Vary.[7-25] The method combines the advantages of conventional ultrasonics with the detection techniques developed for acoustic emission. Figure 7-6(c) shows the transducer arrangement where a broad-band transmitter is coupled directly to the test-piece and the resultant waves are detected with acoustic emission sensors at some distance away. The transmitting transducer injects longitudinal waves normal to the surface. Longitudinal and mode-converted stress waves are produced which travel parallel to the plane of the plate in all directions. As a result, Lamb waves of the lowest symmetric and antisymmetric modes are generally excited. Acousto-ultrasonics (also known as the stress-wave-factor technique) measures the relative efficiency of the energy transmission of the stress waves propagating in a given direction in the test-piece. AU techniques can be used to assess integrated effects of subcritical flaw conditions that collectively influence the strength or mechanical properties of the structure.

Kautz and Lerch show AU results detecting composite damage from tensile and thermal loads.[7-26] The technique was also observed to be sensitive to certain interface characteristics. Tang and Henneke used a modified AU method to evaluate composite damage by placing a pair of receiver transducers at a small distance from each other, but the pair is placed at a larger distance from the transmitter.[7-27] The modified method improved the efficiency of obtaining experimental data by not having to move the receiver to obtain velocity data. In this study, by measuring the plate wave velocities, the dispersion curve (velocity versus frequency) of the lowest antisymmetric mode changed significantly with respect to a stiffness reduction (strength) of a composite laminate.

7.2.3 Ultrasonic Flaw Data Signal-Processing Techniques.

Portable PC-based systems with high speed digitizers and processors make it possible for signal-processing techniques to be integrated into ultrasonic test equipment. Enhanced C-scans, B-scans, time-of-flight (TOF) images, feature mapping, and neural network mapping become possible in near real-time processing as the test-piece is being inspected. Computerization allows efficient data collection and storage and digital signal processing of large data sets. Digital image enhancement can greatly improve the ability of an inspector to distinguish defects from normal background noise that appears in inspection images. Depth and lateral resolution of C-scan and B-scan images can be greatly improved by deconvolution techniques. Spectrum analysis, feature and pattern recognition analysis, and neural network techniques have become available for an enhanced interpretation of the inspection data set that leads to expert system techniques (automated flaw classification).

The ultrasonic pulse-echo, through transmission or pitch-catch A-scan signals, represents the stress wave responses in amplitude and time (time domain). The received signal can also be analyzed in the frequency domain by Fast Fourier Transform (FFT) analysis. Because the interaction of stress waves with flaws is frequency dependent, FFT analysis allows information about the frequency content of the received signal to be calculated. Ultrasonic spectroscopy

(frequency domain analysis) has been investigated as a NDE tool for many flaw detection applications.

Newhouse has shown that flaw detection was enhanced in noisy large-grain echoes by split-spectrum processing.[7-28] Since flaw echoes may display a downward shift in their frequency content as compared with natural-grain echoes, which display an upward shift in frequency content, a robust flaw detection filtering technique can be developed by processing the data in frequency bands. Similar techniques are appropriate for processing ultrasonic flaw data in the inspection of composites. However, a long processing time associated with the filtering process would limit this technique for field applications. Aussel has shown how a more efficient decomposition method based on finite impulse response filtering in the time domain can be implemented in real-time using tapped delay lines.[7-29]

Sin and Chen describe the application of deconvolution techniques for ultrasonic NDE signals.[7-30] O'Brien et al. investigated a high-resolution deconvolution technique for improving temporal resolution of ultrasonic signals.[7-31] Kishoni and Pietsch describe a correlation technique to overcome low signal-to-noise ratio in inspection data.[7-32] Singh and Udpa have described digital signal processing techniques that have produced useful information for improved defect characterization.[7-33] The application of a number of these techniques may be useful in resolving bond interface echoes for the NDT characterization of bond quality.

Feature mapping (F-map) techniques are used to characterize defects by considering a large number of time and frequency domain parameters extracted from a received ultrasonic signal.[7-34] These parameters are mapped into a smaller dimensional feature space. A pattern recognition technique is then applied using the feature space mapping to classify the defect as to type. Flaw types can then be identified for evaluation and possible repair. C-scan representation of F-map results (classifications) provides an image of the defect area. Subjective interpretation ambiguities of a flaw echo by an inspector may be eliminated by the F-map technique.

Software using artificial neural network (ANN) techniques has also been developed to classify ultrasonic flaw signals for composites.[7-35] Artificial neural networks imitate the process that the living brain uses to recognize patterns, make decisions, and draw conclusions from complex and noise-contaminated data. The technique works fast in its ability to be trained, generalize, and associate features that allow classifications of signals to be made. The ANN computation can be thought of as a mapping of n-dimensional input vectors to n-dimensional output vectors. A useful neural network computation is done when the input vectors (ultrasonic signal measurements) and output vectors (flaw classification label) represent meaningful robust quantities that can be used to recognize the flaw type. C-scan imaging of the flaw classification label provides area images of the defects. The network is trained by using representative samples containing known flaw types.

The open literature contains a large number of papers concerning signal processing methods, but in this section reference is made to a only a few of the more recent papers in which general references to the subject can be found.

7.2.4 Automated Data-Acquisition and Flaw-Imaging Systems.

Portable PC-based systems for ultrasonic data acquisition, signal processing, and image display have increased substantially in speed, memory, and performance in the last few years.

Field-ready inspection systems are emerging that have the potential to become widely used for aircraft applications. C-scan format of ultrasonic inspection data is available in real-time, which assists the inspector in making reliable decisions of flaw detection. Voluminous data can be archived and retrieved for postprocessing and hard-copy output.

Many of the more complex inspection problems, such as corrosion assessment and adhesive bond integrity of plates, composites, and repair patches, may be solved with computerized C-scan systems. A variety of manual scanning devices to provide position information with digitized ultrasonic gated-signal amplitudes, time-of-flight values and signal waveforms are becoming available for PC systems. Signal processing and image processing software for PC systems is also available.

7.3 PRESENT APPLICATIONS.

7.3.1 Laser Ultrasonics.

To date, the applications for laser-generated and detected ultrasonic tests have been limited to laboratory experiments. These experiments have demonstrated the generation of the different ultrasonic wave types. The ability to detect surface-breaking cracks and to characterize electroplated metal coatings is discussed in References 7-7 and 7-8. Characterizing material properties by velocity determinations at ambient temperatures and at elevated temperatures is discussed in References 7-6 and 7-36.

7.3.2 Electromagnetic Acoustic Transducers.

EMATs have been used in many commercial applications where inspection techniques at high speeds and at elevated temperatures were needed. Inspection of corrosion in gas pipe lines was performed at speeds approaching 30 mph.[7-11] Inspection of aluminum plate thickness and detection of defects have been performed for hot-rolled aluminum at speeds of 10 in./s (Ref. 7-12).

7.3.3 Advanced Ultrasonic Bond Evaluation Methods.

Applications of advanced bond evaluation techniques are still in the laboratory stage. Mal and Bar-Cohen discuss how ultrasonic spectroscopy and leaky Lamb waves[7-37] have potential applications for the nondestructive determination of bond quality. A strong dependence of the first symmetric Lamb mode was observed in its dispersion curve characteristics for a bonded aluminum plate.

Balasubramaniam and Rose show how plate waves and dispersion curves can be used for nondestructive evaluation of composites.[7-38] They show laboratory results obtained on a unidirectional graphite epoxy specimen. The global transducer arrangement in which the transmitter and the receiver are spaced apart and the wave travels some distance through the plate, as shown in Figure 7-6(b), is suggested as a practical method of inspection in the field. Bendec et al. successfully used the global transducer arrangement shown in Figure 7-6(b) for Lamb waves to evaluate the quality of the spot-welded zone in joining two overlapping plates.[7-39]

Acousto-ultrasonic techniques have been used to evaluate the strength of bonded joints in aluminum, fiber glass composites, and rubber sheets bonded to steel. Wegman and Mitchell

used a commercially available instrument based on the AU technique with dry-coupled rolling probes, and data were presented showing its capability to assess the bond strength of adhesively bonded aluminum panels.[7-40]

7.3.4 Signal-Processing Methods.

McRae has applied deconvolution techniques to the ultrasonic examination of adhesive joints in the laboratory.[7-41] Real-time processing was accomplished to produce improved C-scan images. Resch and Karpur used split-spectrum processing to improve detection of fatigue cracks in aluminum with surface wave methods.[7-42] Karpur et al. reported that in a demonstration of the effects of Wiener filtering for image enhancement of impact-damaged graphite-epoxy composites, the resolution of C-scan images showed significant improvement.[7-43] Dewen et al. show how cepstral processing, which is a deconvolution technique, was able to resolve ultrasonic echoes from the bond interface of thin aluminum plates.[7-44] These methods can readily be put to use in automated data acquisition systems as the need for them arises in aircraft NDT inspections.

7.3.5 Automated Data-Acquisition and Flaw-Imaging Systems.

A number of both manual and mechanized scanning bridges, combined with computerized data acquisition, have been used in industrial applications. For example, the P-scan system has been used for field inspections of service-induced defects in piping and pressure vessel welds in nuclear power plants.[7-45] Field inspections have also been made on welds of storage tanks and wind turbine rotors. The oil and gas industry has used the equipment to detect hydrogen or stress corrosion cracking as well as corrosion assessment in piping and vessels.

7.4 AIRCRAFT APPLICATIONS.

7.4.1 Laser Ultrasonics.

The potential exists to use laser-generated and optical detection techniques for non-contact wide-area scanning applications on aircraft surfaces. The non-contact and remote features lend themselves to scanning methods that use mirrors and lenses for beam steering and collection of the scattered light. The dual-beam interferometer technique[7-10] may have possibilities for fast scans of lap joints, doubler bond interfaces, and corrosion assessment of thin plates. The characterization of composite overlays of boron fiber epoxy by laser ultrasonics has been proposed for assessment of adhesive bond strength.[7-36] Since laser-generated acoustic waves are extremely short pulses, their broad-band feature makes them valuable for potential ultrasonic inspection of thin ceramic coatings used on turbine blades and other engine components.

7.4.2 Electromagnetic Acoustic Transducers.

EMATs have many potential inspection applications for aircraft structures. EMATs can be designed to be efficient generators and detectors of surface waves and plate waves that can be used for bond evaluations of lap joints and doublers. Because the transduction mechanism takes place within the skin depth of the test-piece, EMATs can be used over coats of paint and decals. This eliminates the cost to remove these materials for timely inspections of lap joints and butt joints for debonding or fatigue crack detection. EMATs are well suited to fast automated scanning methods of inspection.

7.4.3 Advanced Ultrasonic Bond Evaluation Methods.

Scanning techniques using the leaky Lamb wave method, as in Refence 7-20, need to be developed for aircraft applications. A fieldable scanning technique would make inspection of bonded metal plates and composite repair patches possible on aircraft structures. Similar techniques for the detection of various forms of corrosion in aircraft structures would also be possible.[7-46]

Presently being developed is a prototype global pitch-catch arrangement with roller transducers. This method will be applied to aircraft lap joint evaluation using specific Lamb wave modes and dispersion curve analysis for improved inspection sensitivities.[7-23] Local pitch-catch oblique incidence scanning techniques could also be developed to provide C-scan imaging of bonded joints and bonded repair patches.

Acousto-ultrasonic techniques have been used to evaluate impact damage and the effect of hydrothermal aging in composites; this has direct applications to aircraft structures. Stress wave propagation efficiency can be related to many (material bond integrity) parameters affected by aging and in-service operating conditions of aircraft. These parameters may be measurable from acousto-ultrasonic techniques using time and frequency domain analysis.

7.4.4 Signal-Processing Methods.

Many of the signal-processing techniques can be applied in ultrasonic inspections of aircraft structures, which require very sophisticated techniques. In the future, many of the signal processing techniques will be necessary for implementation of robotic and expert systems.

7.4.5 Automated Data-Acquisition and Flaw-Imaging Systems.

A computerized manual scanner with automated data acquisition of position and ultrasonic data has been developed specifically for in-service aircraft applications of composite and bonded structure inspections.[7-47] A hand-held fast scanner with a data acquisition system that uses a UNIX workstation environment has been developed to inspect debonds and corrosion in bonded joints of aircraft skins and impact damage or delaminations in aircraft composite structures.[7-48] The hand-held scanner (Mobile Automated Ultrasonic Scanner) shown in Figure 7-7 mechanically oscillates a set of four transducers which can cover a test area of 4 by 8 inches in about 30 seconds. This rapid coverage makes inspection rates of up to 100 sq ft/hr possible. The Mobile Automated Scanner can also be used with eddy current probes (see section 5.2 for C-scan images of eddy current data). Similar C-scan images are obtained for ultrasonic data.

Manual scanning equipment with automated data acquisition and display can be used for inspections from exterior as well as from interior surfaces of the aircraft. Applications include skin-lap and butt-joint evaluations, doubler bonds from the interior or exterior surface, in-service defects of repair patches, and corrosion assessment of skin structures. Recently, two commercially available portable eddy current and ultrasonic automated scanning systems were demonstrated on the AANC 737 aircraft.[7-49] Figure 7-8 shows one of the scanners attached to the skin panel aft of the rear cargo door. Figure 7-9 is a C-scan image of ultrasonic inspection data taken at that location where a delaminated tearstrap is clearly imaged. Two comparable eddy current C-scan images of the same area are shown in section 5B, Figure 5B-4, where corrosion is clearly detected at the tearstrap. Figures 7-9 and 5B-4 are complementary since the delamination area of the tearstrap extends beyond the area of the detected corrosion. The

second portable automated scanner is shown in Figure 7-10 where C-scan images of the lap splice joint were being recorded.

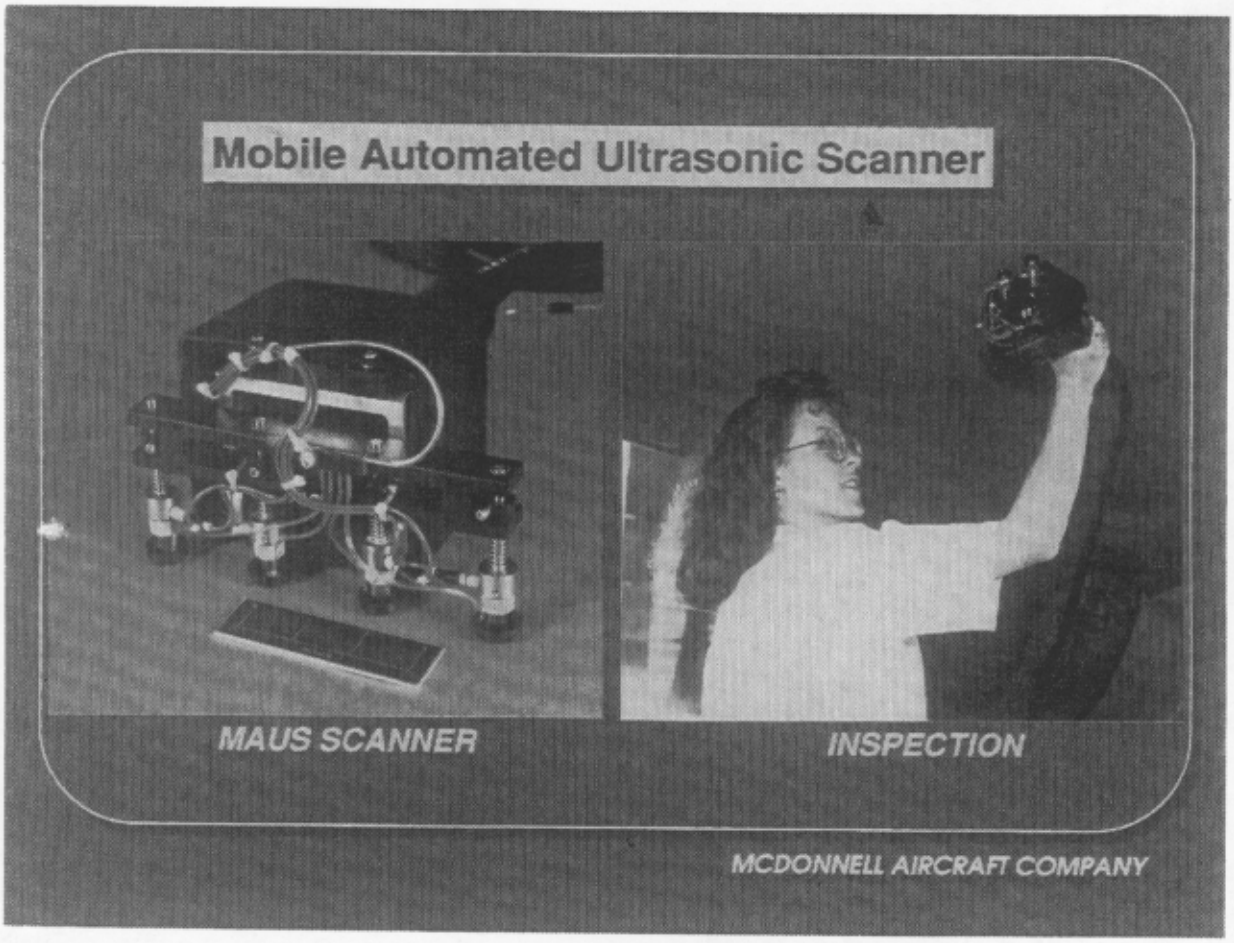

Figure 7-7. Mobile Automated Ultrasonic Scanner for C-scan Imaging of Ultrasonic Inspection Data of Aircraft Structures. [Source: McDonnell Aircraft Company, St. Louis, MO. Reprinted by permission of McDonnell Aircraft.]

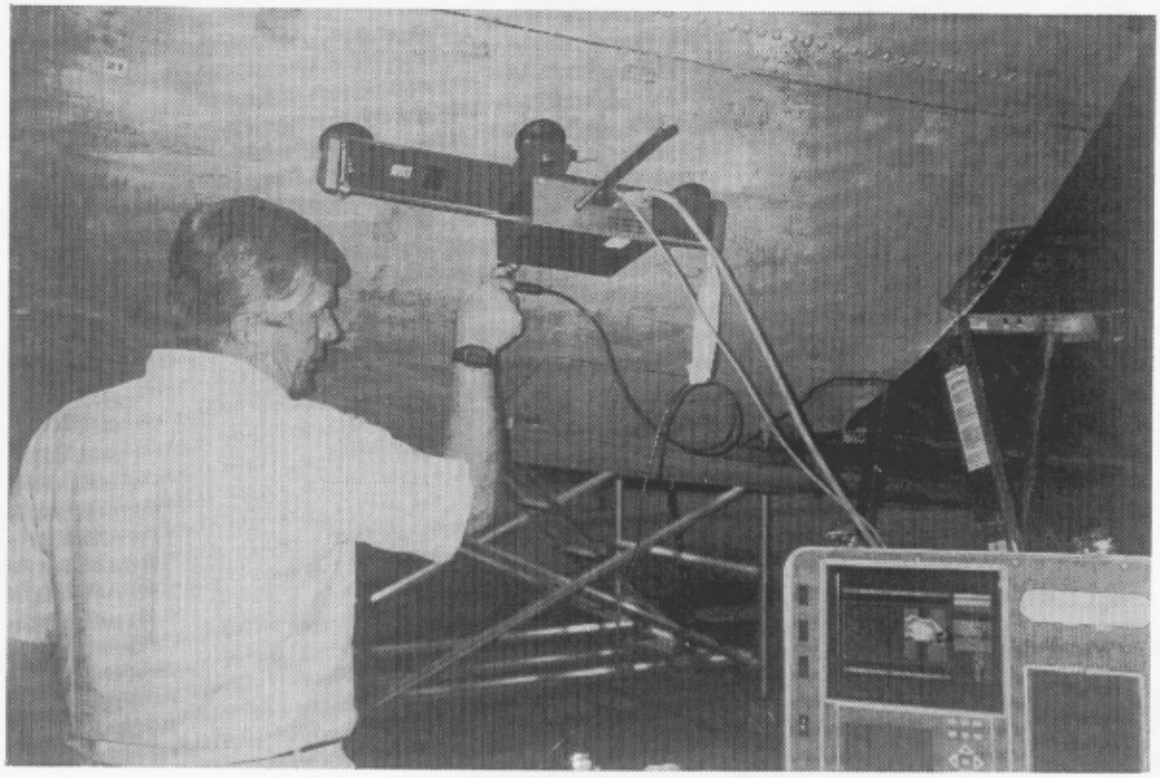

Figure 7-8. A Portable Automated Eddy Current or Ultrasonic Scanner Is Shown Attached to the AANC 737 Airplane Aft of the Rear Cargo Door.

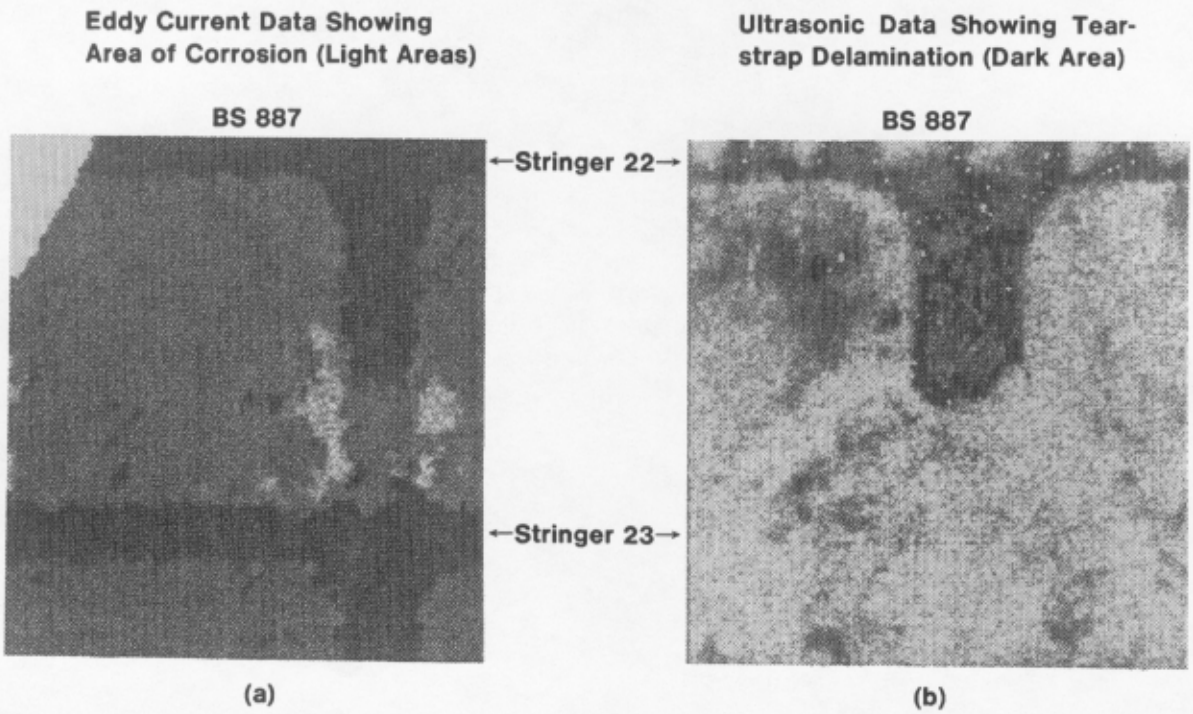

Figure 7-9. C-scan Image of Ultrasonic Inspection Data Showing the Presence of a Delaminated Tearstrap Compared with the C-scan Image of Eddy Current Inspection Data at the Same Location.

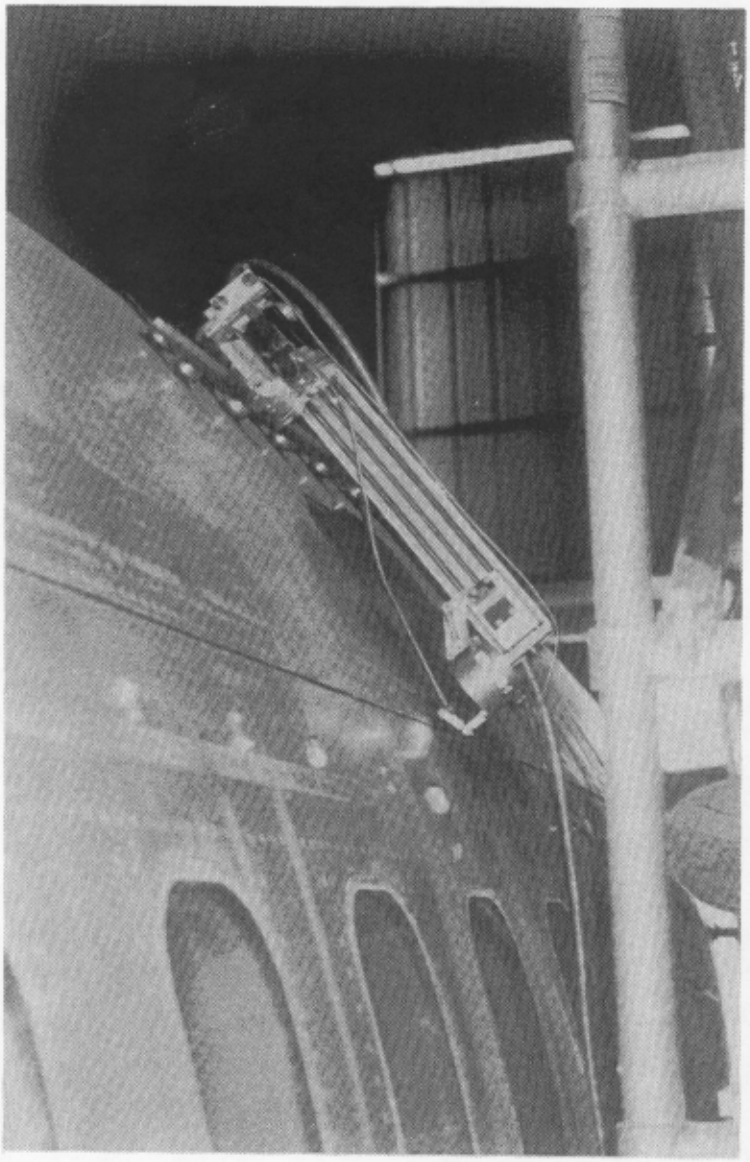

Figure 7-10. A Portable Automated Scanner for Eddy Current or Ultrasonic Inspection Data Acquisition and C-scan Display is Shown Recording Data on a Lap Splice Joint.

7.5 TECHNICAL CONSIDERATIONS.

7.5.1 Laser Ultrasonics.

Methods of improving the generation and detection efficiencies of laser ultrasonics are still under development. Recently the rapidly scanned laser technique to efficiently generate surface acoustic waves has been shown to enhance the amplitude and sensitivity of the generated waves. The reproducible elastic waves generated at low laser power levels have no irreversible effect on the surface of the test-piece, even as the laser power is increased and approaches the ablation regime, where slight surface evaporation (less than 0.00005 in.) occurs.

Advantage

- The nature of the acoustic pulse generated makes it particularly attractive for resolving echoes within thin plates as might be necessary for assessing the extent of corrosion or the inspection of thin ceramic coatings used as oxidation and wear inhibitors on turbine blades and other engine components.

Disadvantages

- Efficiency of thermoelastic transduction is several orders of magnitude lower than piezoelectric transduction, giving low signal-to-noise ratio.
- The surface of the test-piece must be smooth and polished for adequate signal-to-noise ratios using the Michelson interferometer. However, the Fabry-Perot interferometer has been used successfully on rough, diffuse reflecting surfaces.

7.5.2 Electromagnetic Acoustic Transducers.

EMATs have a lower power conversion efficiency than piezoelectric transducers, but since coils have less inherent noise than piezoelectric devices, the signal-to-noise ratio is comparable. For some aircraft applications on rough surfaces, where the laser interferometry detection is limited, a hybrid system using laser generation and EMAT detection modules might be developed to optimize the technical advantages of each module.

Because of the versatile design of an EMAT, many different elastic wave modes can be generated by adjusting the direction of the magnetic field and changing the geometry of the transmitter.[7-11] Some of these modes are not possible with the piezoelectric transducers. Some of the modes possible with EMATs are longitudinal and shear waves perpendicular to the surface; longitudinal and shear vertical waves at some angles to the surface; angle-beam shear horizontal waves at all angles; surface and plate waves (Rayleigh, Lamb, shear horizontal plate modes); and torsion tube waves.[7-12] Future inspection problems in aging aircraft may be solved by considering the use of a number of wave modes.

Advantages

- EMATs can be used effectively on rough, unclean, or coated surfaces.
- EMATs can be used in fast scanning conditions on complex geometries.
- The versatile design of EMATs makes them attractive in difficult-to-solve inspection problems.

Disadvantage

- EMATS operating at frequencies in excess of 5 MHz lose efficiency rapidly due to lift-off effects.

7.5.3 Advanced Ultrasonic Bond Evaluation Techniques.

The practical use of all three advanced ultrasonic bond evaluation techniques described in section 7.2.2 depends on implementing them for scanning capabilities over a large area of an aircraft structure. The leaky Lamb wave method requires the test-piece to be immersed in a fluid. In some cases, a captured water column technique may solve this problem. The oblique-angle methods and the acousto-ultrasonic methods can be implemented by using plexiglass variable-angle-beam wedges or even dry-couplant roller transducers. The use of EMATs is also a viable alternative for these two methods on conductors. All have the advantage of accessing the structure from one side.

A major difficulty with these methods may be obtaining quantitative reproducible results under field conditions. Analysis of plate wave signals is not straightforward, nor is it presently manageable for field use. Reproducibility and interpretation problems may be alleviated by employing signal-processing techniques. Signal-processing techniques can be used to eliminate the effect of couplant variations on the amplitude of the received signal as well as to uncouple the frequency components of multiple-plate wave velocities and modes. The success of implementing these techniques depends on the speed of full waveform capture with a computerized data acquisition system. Fast signal processing techniques and algorithms need to be developed so that inspection results can be obtained during scanning.

Advantage

- All three of the techniques described in section 7.2.2 have the advantage of accessing the structure from one side.

Disadvantages

- The leaky Lamb wave method may be difficult for field use because the method requires that the test piece be immersed in a fluid. In some cases, a captured water column technique may solve this problem.
- Obtaining quantitative reproducible results under field conditions may be difficult. Analysis of plate wave signals is not straightforward, nor is it presently manageable for field use. (See discussion above.)

7.5.4 Signal-Processing Methods.

Effective inspections of aircraft require timely identification of defects in the principal structural elements. Signal-processing techniques can assist the NDE inspector to properly identify flaws or defects which compromise the safety of the aircraft. The availability of signal and imaging processing quantifies the inspection data and makes it more reliable by presenting to the inspector definitive information about the nature of the flaw. Flaw signals that are small (within noise signals) and difficult to discern can be imaged separately with signal-processing techniques thus presenting the possibility of detecting damage at an early stage.

Advantages

- Signal and imaging processing techniques can quantify the inspection data and make it more reliable, giving the NDE inspector more definitive information for determining the nature of the flaw.
- Very small flaw signals (within flaw signals) which are difficult to discern can be imaged separately, presenting the possibility of detecting damage at an early stage.

Disadvantages

(Not applicable)

7.5.5 Automated Data-Acquisition and Flaw-Imaging Systems.

Automated systems afford many advantages over conventional point-by-point manual scanning methods.

Advantages

- Extensive training or skill above present practices is not required because data collection is similar to conventional methods.
- Automated systems provide real-time C-scan images of single-point A-scan waveforms into an area mapping of the inspection surface. These area views provide the inspector with easier-to-use and more reliable data with which to recognize flaw patterns.
- The area mapping capability significantly reduces the time required to perform on-site examinations.
- Examinations are more repeatable and effective than with point-by-point manual scanning methods. They provide programmable test procedures, thus assuring that proper setup, calibration, and scanning requirements are met.
- The systems provide long-term archival data storage and hard copy plot capability. Stored A-scan data can be post-processed to enhance flaw characterization and assist the inspector in making objective decisions.
- Human factors are improved. An inspector observes proof of an effective examination from the quantitative content of the C-scan image. Viewing the trends and spatial relationships of patterns as they are created on the viewing screen keeps the inspector's interest high and reduces inspector fatigue.
- PC-based manual scanning systems are modest in cost.
- Procedures for scanning aircraft structures could be developed within a year using commercial equipment presently available.

Disadvantages

(Not applicable)

7.6 STATUS.

Most advanced ultrasonic inspection techniques are still being investigated in the laboratory. However, as implementation of computerized systems for aircraft inspections are realized, many of the advanced ultrasonic techniques can be applied immediately in the field.

7.6.1 Laser Ultrasonics.

Commercial instrumentation for the laser generation and detection of acoustic waves is available as laboratory equipment. Scanning designs for wide-area scanning have not been

developed. The equipment is expensive and requires highly trained and skilled personnel to operate. Field use of a practical system is estimated to occur in the late 1990s.

7.6.2 Use of Electromagnetic Acoustic Transducers in Aircraft Inspections.

EMAT equipment is commercially available and has been used for many applications outside the aircraft industry. Portable units have been designed. Once development of aircraft inspection techniques for corrosion, fatigue cracks, and bond evaluations is initiated, field use could be expected within the following two-year period. Equipment expense, operator training, and operator skill are comparable to those required for conventional piezoelectric transducer techniques.

7.6.3 Advanced Ultrasonic Bond Evaluation Techniques.

Limited equipment is presently available for field implementation of advanced ultrasonic bond evaluation techniques. Manual scanning methods with computerized data acquisition are now becoming available commercially, making these methods practical. Equipment expense is modest, but operator training and skill would need to be at a level higher than presently required for bond testers. Development of field procedures for their use needs to be initiated. If this occurs, practical field equipment could be available in the next two years.

7.6.4 Ultrasonic Signal-Processing Techniques.

Commercial software is available to perform visualization and resolution enhancement by digital signal processing on the entire volume of 3D ultrasonic inspection data sets. Neural network processing software is also available commercially. As portable PC-based ultrasonic systems become available for aircraft inspections, more classification problems for flaw signals will be solved with the use of feature analysis and neural nets. Software costs for signal processing methods are modest for most applications. The training and skill levels of the field inspector are estimated to be minimal since the computation process will be transparent to the collection of data. Some techniques can be implemented immediately for certain applications as they are identified. Development of techniques and procedures for more complex inspection problems need to be established by experienced investigators. Field use could then be implemented within the following one or two years.

7.6.5 Automated Data-Acquisition and Flaw-Imaging Systems.

Commercial equipment is presently available from a number of different sources. Many of the present systems may not be optimized for aircraft inspections. Some of the systems may be implemented immediately for some aircraft applications and procedures to use the equipment for those applications could be written in a year's time.

7.7 REFERENCES.

7-1. U.S. Department of Transportation, Federal Aviation Administration, in *Current Nondestructive Inspection Methods for Aging Aircraft*, Report DOT/FAA/CT-91/5 June 1992.

7-2. R. M. White, "Elastic wave generation by electron bombardment of electromagnetic wave absorption," *in J. Appl. Phys.*, Vol. **34**, 1963, pp. 2123-24.

7-3. D. Hutchins, J. Hu, and K. Lundgren , "A comparison of laser and EMAT techniques for noncontact ultrasonics," in *Materials Evaluation*, Vol. **44**, 1986, pp. 1244-53.

7-4. R. J. Dewhurst, C. E. Edwards, A. D. W. McKie, and S. B. Palmer, "Comparative Study of Wide-band Ultrasonic Transducers," in *Ultrasonics*, Vol. **25**, November 1987, pp 315-21.

7-5. J.-P. Monchalin and R. Heon, "Laser ultrasonic generation and optical detection with a confocal Fabry-Perot interferometer," in *Materials Evaluation*, Vol. **44**, 1986, pp 1231-37.

7-6. K. L. Telschow, J. B. Walter, and G. V. Garcia, "Laser ultrasonic monitoring of sintering," in *J. Appl. Phys.*, Vol. **68**, 1990, pp. 6077-82.

7-7. P. Cielo, F. Nadeau, and M. Lamontagne, "Laser generation of convergent acoustic waves for materials inspection," in *Ultrasonics*, March 1985, pp. 55-62.

7-8. X. Maldague, P. Cielo, and C. K. Jen, "NDT applications of laser-generated focused acoustic waves," in *Materials Evaluation*, Vol. **44**, 1986, pp. 1120-24.

7-9. C. M. Scala and P. A. Doyle, "Time and frequency-domain characteristics of laser-generated ultrasonic surface waves," in *J. Acoust. Soc. Am.*, Vol. **85**, 1989, pp. 1569-76.

7-10. J. Huang and J. D. Achenbach, "Dual-probe laser interferometer," in *J. Acoust. Soc. Am.*, Vol. **90**, 1991, pp. 1269-74.

7-11. G. A. Alers and L. R. Burns, "EMAT designs for special applications," in *Materials Evaluation*, Vol. **45**, 1987, pp. 1184-89.

7-12. B. W. Maxfield, A. Kuramoto, and J. K. Hulbert, "Evaluating EMAT designs for selected applications," in *Materials Evaluation*, Vol. **45**, 1987, pp. 1166-83.

7-13. G. M. Light and H. Kwun, "Nondestructive evaluation of adhesive bond quality," in *State-of-the-Art Review*, NTIAC-89-1, Southwest Research Institute, 6220 Culebra Road, San Antonio, TX 78284, 48 pages, June 1989.

7-14. R. O. Claus, "Adhesive bondline interrogation using Stoneley wave methods," in *J. Appl. Phys.*, Vol. **50**, 1979, pp. 8066-69.

7-15. S. I. Rokhlin, M. Hefets, and M. Rosen, "An ultrasonic interface-wave method for predicting the strength of adhesive bonds," in *J. Appl. Phys.*, Vol. **52**, 1981, pp. 2847-51.

7-16. C. H. Yew, "Using ultrasonic SH waves to estimate the quality of adhesive bonds: A preliminary study," in *J. Acoust. Soc. Am.*, Vol **76**, 1984, pp. 525-31.

7-17. P. B. Nagy, A. Jungman, and L. Adler, "Measurements of backscattered leaky Lamb waves in composite plates," in *Materials Evaluation*, Vol. **46**, 1988, pp. 97-100.

7-18. J. L. Rose and A. Pilarski, "Surface and plate waves in layered structures," in *Materials Evaluation*, Vol. **46**, 1988, pp. 597-605.

7-19. M. R. Karim, A. K. Mal, and Y. Bar-Cohen, "Inversion of leaky Lamb wave data by simplex algorithm," in *J. Acoust. Soc. Am.*, Vol. **88**, 1990, pp. 482-91.

7-20. D. E. Chimenti and R. W. Martin, "Nondestructive evaluation of composite laminates by leaky Lamb waves," in *Ultrasonics*, Vol. **29**, 1991, pp. 13-21.

7-21. J. L. Rose, J. J. Ditri, Y. Huang, D. P. Dandekar, and S. Chou, "One-sided ultrasonic inspection technique for the elastic constant determination of advanced anisotropic materials," in *J. Nondestructive Evaluation*, Vol. **10**, 1991, pp 159-66.

7-22. A. Pilarski and J. L. Rose, "Ultrasonic oblique incidence for improved sensitivity in interface weakness determination," in *NDT International*, Vol. **21**, 1988, pp. 241-46.

7-23. D. Jiao and J. L. Rose, "An ultrasonic interface layer model for bond evaluation," in *J. Adhesion Sci. Technol.*, Vol. **8**, 1991, pp. 631-46.

7-24. W. Wang and S. I. Rokhlin, "Evaluation of interfacial properties in adhesive joints of aluminum alloys using angle-beam ultrasonic spectroscopy," in *J. Adhesion Sci. Technol.*, Vol. **5**, 1991, pp. 647-66.

7-25. A. Vary, "Acousto-ultrasonic characterization of fibre reinforced composites," in *Materials Evaluation*, Vol. **40**, 1982, pp. 650-62.

7-26. H. E. Kautz and B. A. Lerch, "Preliminary investigation of acousto-ultrasonic evaluation of metal-matrix composite specimens," in *Materials Evaluation*, May 1991, pp. 607-12.

7-27. B. Tang and E. G. Henneke, II, "Lamb-wave monitoring of axial stiffness reduction of laminated composite plates," in *Materials Evaluation*, Vol. **47**, 1989, pp. 927-34.

7-28. V. L. Newhouse, N. M. Bilgutay, J. Saniie, and E. S. Furgason, "Flaw-to-grain echo enhancement by split-spectrum processing," in *Ultrasonics*, March 1982, pp. 59-67.

7-29. J. D. Aussel, "Split-spectrum processing with finite impulse response filters of constant frequency-to-bandwidth ratio," in *Ultrasonics*, Vol. **28**, 1990, pp. 229-40.

7-30. S. K. Sin. and C. H. Chen, "A comparison of deconvolution techniques for the ultrasonic nondestructive evaluation of materials," in *IEEE Trans. on Image Processing*, Vol. **1**, 1992, pp. 3-10.

7-31. M. S. O'Brien, A. N. Sinclair, and S. M. Kramer, "High resolution deconvolution using least-absolute-values minimization," in *IEEE Ultrasonics Symposium Proc.*, Vol. **2**, 1990, pp. 1151-56.

7-32. D. Kishoni and B. E. Pietsch, "Ultrasonic correlator versus signal averager as a signal to noise enhancement instrument," in *ISA, 1989*, paper #89-0019, pp. 195-99.

7-33. G. P. Singh and S. Udpa, "The role of digital signal processing in NDT," in *NDT International*, Vol. **19**, 1986, pp. 125-32.

7-34. J. L. Rose, J. B. Nestleroth, and K. Balasubramaniam, "Utility of feature mapping in ultrasonic nondestructive evaluation" in *Ultrasonics*, Vol. **26**, 1988, pp. 124-31.

7-35. J. J. Thomsen and K. Lund, "Quality control of composite materials by neural network analysis of ultrasonic power spectra" in *Materials Evaluation*, May 1991, pp. 594-600.

7-36. C. M. Scala and P. A. Doyle, *Characterization of Composite Overlays by Laser Ultrasonics*, NDT 91, Australian Institute for Nondestructive Testing, Melbourne, August 1991.

7-37. A. K. Mal and Y. Bar-Cohen, "NDE of strength related properties of adhesive joints," *in Advances in Fracture Research (ICF7)*, Vol. **5**, 1989, pp. 3197-3204.

7-38. K. Balasubramaniam and J. L. Rose, "Physically based dispersion curve feature analysis in the NDE of composites," *in Res. Nondestr. Eval.*, Vol. **3**, 1991, pp. 41-67.

7-39. F. Bendec, M. Peretz, and S. I. Rokhlin, "Ultrasonic Lamb wave method for sizing of spot welds," *in Ultrasonics*, March 1984, pp. 77-84.

7-40. R. Wegman and J. R. Mitchell, "Evaluation of adhesive bond strength by nondestructive testing," in *21st Intnat. SAMPE Tech. Conf., September 1989*, pp. 196-209.

7-41. K. I. McRae, "Deconvolution techniques for ultrasonic imaging of adhesive joints," in *Materials Evaluation*, November 1990, pp. 1380-84.

7-42. M. T. Resch and P. Karpur, "Split spectrum processing of backscattered Rayleigh wave signals to improve detectability of fatigue microcracks," Cyclic Deformation, Fracture, and Nondestructive Evaluation of Advanced Materials, in *ASTM STP 1157*, M. R. Mitchell and O. Buck, eds., ASTM Philadelphia, 1992, pp. 323-33.

7-43. P. Karpur, B. G. Frock, and P. K. Bhagat, "Wiener filtering for image enhancement in ultrasonic nondestructive evaluation," in *Materials Evaluation*, November 1990, pp. 1374-79.

7-44. P. N. Dewen, T. P. Pialucha, and P. Cawley, "Improving the resolution of ultrasonic echoes from thin bondlines using cepstral processing," in *J. Adhesion Sci. Technol.*, Vol. **5**, 1991, pp. 667-89.

7-45. N. Thomsen, "Modern ultrasonic weld inspection," in *Welding Rev. International*, August 1991, pp. 173-75.

7-46. A. K. Mal, private communication.

7-47. D. R. Hamlin, B. M. Jacobs, R. H. Peterson, W. R. Van der Veer, and R. L. Spinks, "A real-time ultrasonic imaging system (ARIS) for manual inspection of aircraft composite structures," in *Revue of Progress in Quantitative Nondestructive Evaluation*, Vol. **7B**, ed. D. O. Thompson and D. E. Chimenti, 1987, pp. 1653-60.

7-48. "Mobile Automated Scanner II," Automated Testing Systems, McDonnell Aircraft Company, St. Louis, MO 63166-0516.

7-49. The 737 airplane is housed in the Federal Aviation Administration/Aging Aircraft NDI Development Demonstration Center (FAA/AANC) hangar facility, Albuquerque, NM.

7-50. Kazushi Yamanaka, Yoshihiko Nagata, and Toshio Koda, "Generation of surface acoustic waves by rapidly scanned laser beam," in *Nondestr. Test. Eval.*, Vol. **7**, pp. 137-48.

8. ADVANCED VISUAL INSPECTION.

8.1 SUMMARY.

Several emerging optical technologies that may aid in the visual inspection of aircraft are *moiré and structured-light-based optical profilometry, Diffracto Sight, and video image enhancement analysis* as applied to video borescopes and other video-based observations. Moiré and structured light are methods to visualize and quantify surface height irregularities, Diffracto Sight is a surface-slope visualization technique, and video image processing is a computer-based methodology for enhancing and analyzing video images for flaw detection or other properties either on-site or at remote locations.

The most promising applications of *moiré* are in the detection and classification of surface irregularities such as corrosion-induced paint liftoff, and pillowing induced by corrosion between faying surfaces; in the identification of damage sites such as dents and dings; and in detecting surface damage in composite materials. Moiré also has potential for the detection of bending or twisting of structural members such as ribs and spars. A non-contact profilometer based upon structured light was developed by General Electric for use on jet engine turbine blades to locate such defects as nicks, pits, cracks, and dents. The profilometer uses two optical wavelengths to correct for variations in surface reflectivity. Boeing has developed a structured-light system to measure the depth of scratches on aircraft skins.

Diffracto Sight is a patented technique developed by Diffracto, Ltd., of Windsor, Ontario, Canada. Several companies have investigated its use to detect flaws. Douglas Aircraft studied it as an inspection tool for impact damage, the extent of the damage, and the quality of repairs for carbon/epoxy composites. A test performed by Komorowski, using D Sight showed buckling in the skin of a commuter aircraft and pillowing in a transport jet lap-joint repair. The reported rate of inspection was 18 m^2/hr. Boeing Aircraft also has investigated the use of D Sight.

Video image enhancement and analysis of fiber-optic borescopes transmitted to a remote location permits supervisory personnel at that location to make maintenance and repair decisions about an aircraft that is being inspected. This capability was demonstrated at an Olympus-sponsored event in which video engine inspection was demonstrated to a remote audience. Borescopes permit inspection of inaccessible areas and areas that would traditionally require disassembly, such as interiors of aircraft engines, landing gear struts, and cabins. Boroscopy of engines is a highly developed discipline in which manufacturers of borescopes and manufacturers of engines cooperate closely in the development of inspection kits and procedures for solving specialized problems. Boeing has combined machine vision, including neural network processing methods, with video borescope observation for the measurement of faying surface gaps for subsequent shim fabrication, which demonstrates the use of automated measurements for production applications. Similar applications will undoubtedly be found in aircraft maintenance and repair.

8.2 TECHNICAL BACKGROUND.

8.2.1 Moiré Interferometry.

Moiré interferometry is a family of techniques that visualize surface irregularities. Many variations are possible, but the three main implementations are (1) in-plane moiré method for stress and strain measurements, (2) shadow, or projection moiré for surface height determination, and (3) reflection moiré for surface slope measurements. [A method related to reflection moiré is called moiré deflectometry.[8-1]] The most popular application for moiré has been in the experimental mechanics field, particularly in stress and strain visualization measurements, in which the in-plane method is usually employed; however, moiré-based contouring and profilometry have attracted increased attention in recent years.

Basic principles. The moiré effect is often observed in the world when two nearly regular screens, such as window screens or picket fences, are superimposed. The name moiré derives from a French word describing a type of fabric made by pressing two layers of cloth together to produce a wavy pattern. As far back as the late 1800s, Lord Rayleigh first indicated that the principle of moiré could potentially be applied to metrology because he recognized that the effect could be used to detect differences between regularly ruled structures, such as diffraction gratings.[8-2]

The basic principle of moiré metrology is that when one finely ruled grating, or nominally uniform pattern of straight lines, is superimposed on a similar grating a fringe pattern, called a moiré, develops. This pattern is the mathematical product of the two grating patterns, where local variations in the spacing of the grating yield transmission variations. If the gratings are identical and perfectly aligned, then the transmission across the two gratings is perfectly uniform. However, if one grating is slightly misoriented or slightly distorted relative to the other, then there is transmission of light in some places, but not others. For example, in the case of a grating with a ruling frequency that is slightly different from the other grating, the observed pattern contains a beat, or difference, frequency between the two grating frequencies. If one grating is perfectly uniform in straightness and spacing of rulings and the other grating moderately departs from regularity, then the superposition of the two gratings results in a fringe pattern of light and dark lines. This fringe pattern represents a contour map of grid nonuniformity, as illustrated in Figure 8-1. A linear, constant-spaced grating is shown in (a); in (b), the grating is superimposed over a slightly rotated copy of itself, producing the four dark straight fringes; and in (c), the grating is superimposed over a distorted grating (actually a section of a grating consisting of evenly spaced radial spokes), producing curved fringes.

The sensitivity of the moiré method is largely a function of the amount of distortion of one grating relative to the average grating pitch. A displacement of one-half of a grating pitch changes the fringe pattern from light to dark. In many applications, changes of a small fraction of a fringe can be detected. For gratings with pitches of a few microns, submicron motion is detectable. Indeed the method is employed in high-resolution incremental encoders, and various optomechanical displacement gauges.

Because a grating may be distorted through a number of mechanisms, interpretation of the fringe field will be affected. For example, in in-plane moiré, physical distortion of a grating yields a stress map, and in shadow moiré, an out-of-plane surface distorts the projected image of a grating, yielding a contour map of the surface.

Moiré can be described as a geometrical equivalent to holography (discussed in Section 6). In fact, many holographic and interferometric principles, such as shearography, can be explained with a moiré analogy.

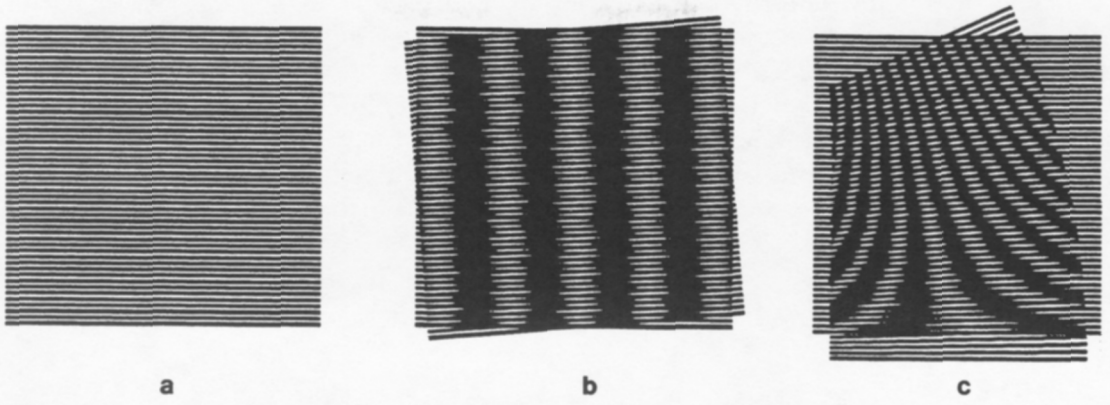

Figure 8-1. Generation of Moiré Fringes. (a) Linear, constant-spaced grating; (b) Grating superimposed over a slightly rotated copy of itself; and (c) Grating superimposed over a distorted grating (actually a section of a grating consisting of evenly spaced radial spokes), producing the curved fringes.

In-plane moiré. In the in-plane *moiré* method, a ruled grating is embossed, printed, or otherwise bonded to the surface to be measured, and a rigid reference grating is optically superimposed over the surface grating. The surface and attached grating are then deformed by an applied stress. When viewed through the reference grating, the subsequent moiré fringe pattern represents a contour map of the in-plane strain field of the surface.[8-3] The process has also been used to measure propagation of crack tips,[8-4] and to test the integrity of various lap bonds, splices, patches, and other repairs, and it has been applied to microprocessor-based strain gauges with high sensitivity.[8-5]

The in-plane method has been used primarily in materials research studies and development programs rather than for field diagnostics. The disadvantage of using this approach for monitoring fielded surfaces is that a grating must remain part of the surface during its entire service life—and obviously, a precision grating cannot be cleaned or painted over. For this reason, in-plane moiré is probably not a practical technique for routine aircraft inspection.

Most researchers using in-plane moiré apparently prefer to build their own holographic cameras because the only known commercially available in-plane moiré camera has been produced by the Photoelastic Division of the Measurement Group, Inc. Raleigh, NC. This instrument is essentially a $\times 1$ magnification view camera equipped with a ruled grating at the ground-glass screen image plane. A flexible grating is bonded to the part to be stressed. The resulting fringe pattern can be recorded with a camera viewing the screen. Adjustments are provided for aligning the ruled grating to the image grating.

Shadow moiré. The shadow moiré method is used to measure variations in surface height. In its simplest implementation, a fine-line grid on a flat, transparent substrate is held close to the surface being tested, and a collimated light source is projected at an angle through the grid. This casts a shadow of the grid onto the surface. If one views the shadow of the grid through the original grid, but at a different angle, departures from flatness show up as contour lines of equal height. This is because the shadow of the grid is distorted by the non-flat surface and then is multiplied by the original grid. The vertical sensitivity of the measurement is a function of the grid spacing and of the projection and viewing angles.

The concept of shadow moiré is illustrated in Figure 8-2. A grating with spacing d is superimposed over the surface. (In actuality it is held in close contact.) A light source with angle θ_i illuminates the surface. The grating allows slits of light to impinge the surface. When viewed at angle θ_v, the image of the light slit is displaced from nominal by an amount Δd. Depending upon the height h of the surface from a plane parallel to the grating, the light slits are either transmitted through a grating ruling or are intercepted. It can be shown that the resulting contour pattern due to the superposition of a grating and its shadow has a contour interval C, given by

$$C = \frac{d}{(\tan\theta_i + \tan\theta_v)}$$

Depending on grid spacing, viewing angle, and field of view, contour intervals on the order of 1 mm or less can be generated, with resolution better than 0.010 mm possible.

Examples of practical applications for shadow moiré have included the mapping of post-buckled composite surfaces,[8-6] various non-topographic photogrammetric applications,[8-7] and medical measurements on human subjects, particularly in the diagnosis of scoliosis.[8-8]

A hand-held moiré test system has been developed by the Naval Air Development Center (NADC), Warminster, PA, for field inspection of possible damage sites in composite structures on naval aircraft.[8-9] The device, called the Shadow Moiré Out-of-Plane Interferometric (SMOOPI) Damage Detector, is a hand-held instrument consisting of a 4-inch by 4-inch moiré screen, a battery-powered illuminator, and a pistol grip. The SMOOPI is currently being marketed by Strainoptic Technologies of North Wales, PA who has licensed the NADC design. Figure 8-3 shows the SMOOPI being used to evaluate impact damage on a surface.

A major drawback to shadow moiré is that the size of the moiré screen must equal the area to be contoured. Ideally the light source that illuminates the screen should be collimated, necessitating a large optical component. However, a divergent point source can be used, although it is not as desirable. The divergent light corrupts the uniformity of the contour interval slightly and must be corrected. A second drawback is that if the surface being examined has a non-flat component, such as on a cylindrical fuselage section, the departure from flatness is manifested as increasing numbers of contour fringes, which become too close together to

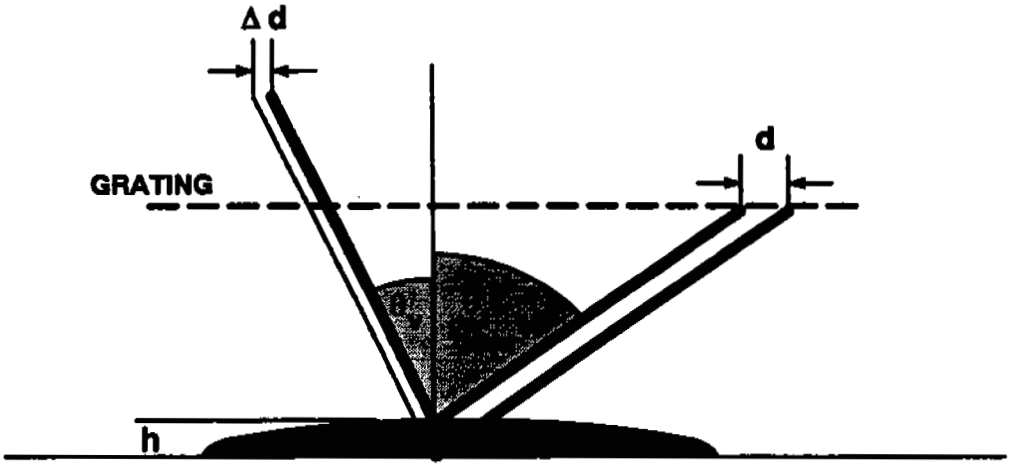

Figure 8-2. Shadow Moiré Geometry.

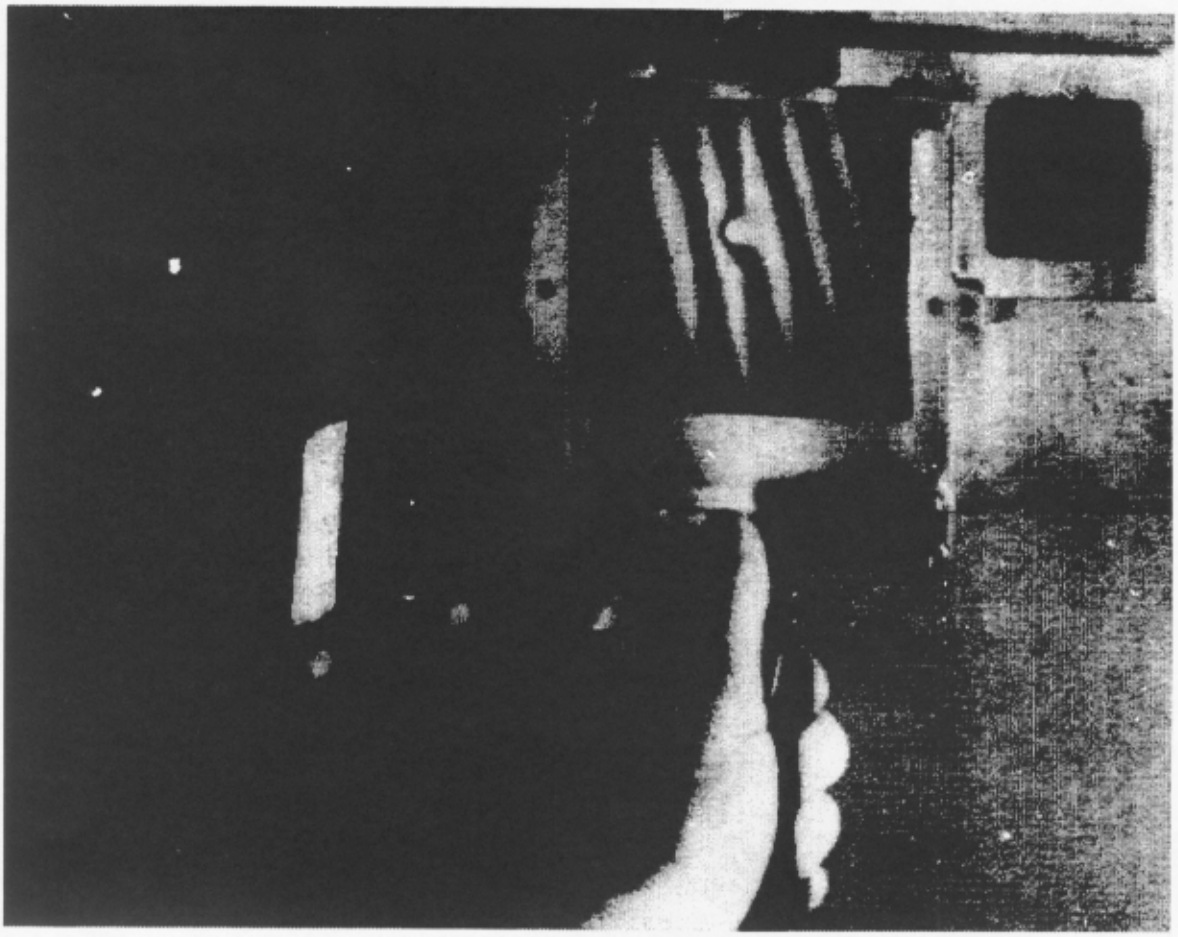

Figure 8-3. SMOOPI Interferometer Examining a Dented Surface. [*Source: A. E. Scotese, A Low Cost Shadow Moiré Device for the Nondestructive Evaluation of Impact Damage in Composite Laminates,* Report No. NADC-90011-60, Naval Air Development Center, Warminster, PA, 1 March 1990, Reprinted with permission of Naval Air Development Center.]

resolve. Finally the grating must be in fairly close contact with the surface—otherwise the shadows tend to blur out due to the finite size of the incident light source.

Projection moiré. A variation of shadow moiré is projection moiré, in which a fine grid is projected on the part to be inspected. The resulting image is viewed through an imaging device that contains a grid on the image plane. Again, a multiplication of the distorted pattern by the image plane grid results in the contour lines. The image plane grid can be a physical grating, or it can be defined within an electronic imaging system, such as a CCD video camera.

The optical system must transmit high-resolution fringes to the image plane without geometric distortion in order for the method to work. The fringe projection can be generated in a number of ways, including using a high-resolution slide projection of a ruled grating or generating the fringes with a laser interferometer.

A projection moiré system built and marketed by WYKO Corp. of Tucson, Arizona, generates fringes interferometrically and uses a fringe shift algorithm to compute the surface contour. In this system the reference grid is the CCD camera pixel spacing itself. This system was advertised as having a height resolution that is better than 1/1000 of the length of the object

being contoured. In other words, an object whose greatest dimension being observed is 10 inches will have a height resolution of 0.010 inch. This value should improve as higher-resolution CCD cameras become available. Figure 8-4 shows a number of applications for the WYKO system. A similar system has been developed by the Air Gauge Company of Livonia, MI.

An alternate approach is to photograph static fringes as projected on a part, and reconstruct the surface topography using a quasi-holographic technique.[8-10] However, this approach is not real time and would not lend itself well to on-line inspection.

Reflection moiré. Reflection moiré has been used to detect slope variations in nominally flat, reflective surfaces. This method involves viewing a moiré grid as reflected by a nominally flat mirror-like surface. If the surface is not truly flat, the grid is distorted. Comparison to an undistorted grid yields moiré fringes that are contours of constant slope. Spatial integration of the slope measurements yields height information. This technique has been developed by Phase Shift Technology of Tucson for the sheet aluminum industry to measure flatness of test samples of rolled aluminum sheet.[8-11] Like the WYKO system, it employs a fringe shift algorithm to calculate the surface profile. The current system has a measurement-height resolution of 0.001 inch for samples that are 96 by 64 inches in size. Currently the method is useful on flat samples, but probably can be adapted to curved surfaces as well. Figure 8-5 shows an interferogram generated from a measurement of an aluminum sheet.

8.2.2 Structured Light.

The structured light technique is geometrically similar to projected or shadow moiré methods. A plane or sheet of light, or multiple spot source,[8-12] is projected at an angle onto the surface of interest. By mapping the positions of the spots or line as seen by a vision system from a different angle, the surface profile or distance to a surface can be determined. The light sheet can be easily generated by a laser and a cylindrical lens, or by using diffraction or holographic gratings to generate multiple spots.

The geometry is virtually identical to projection moiré. However, instead of fringe contours being the resultant observation, the departure from straightness of a line is the observable, as seen in Figure 8-6. Using image processing techniques, the surface profile can be calculated. Alternatively, an observer could compare the straightness of the line to a scale and derive an indication of the non-flatness of the specimen. In this way, structured light could be used as an optical straight edge.

A variation of structured light is in the use of highly grazing incidence lighting on an object.[8-13] At extreme angles, edges and shadows become enhanced and more visible.

8.2.3 Diffracto Sight.

Diffracto Sight™ is a patented technique developed by Diffracto, Ltd, of Windsor, Ontario, Canada. D Sight, as it is also called by its developers, has the potential to map areas of surface waviness, as well as to identify cracks, depressions, evidence of corrosion, and other surface anomalies. D Sight is a method by which slope departures from flatness of an otherwise smooth surface are visualized as shadows. It can be used in direct visual inspection, or combined with photographic or video cameras and computer-aided image processing.

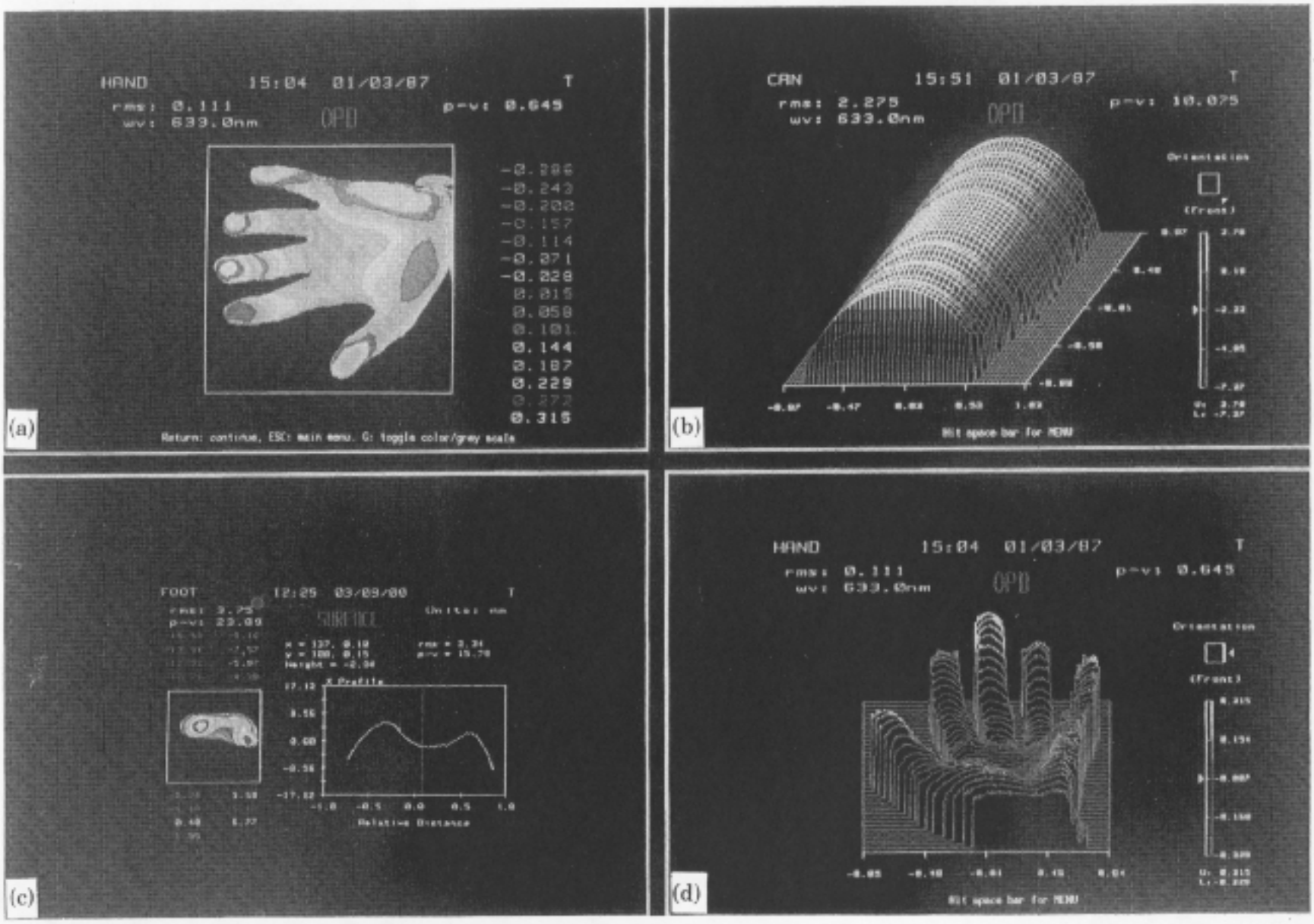

Figure 8-4. Applications of the WYKO Moiré Interferometer System. (a) Hand contour. (b) Can isometric. (c) Foot contour. (d) Hand isometric. [Reprinted by permission from J. C. Wyant, WYKO Corporation.]

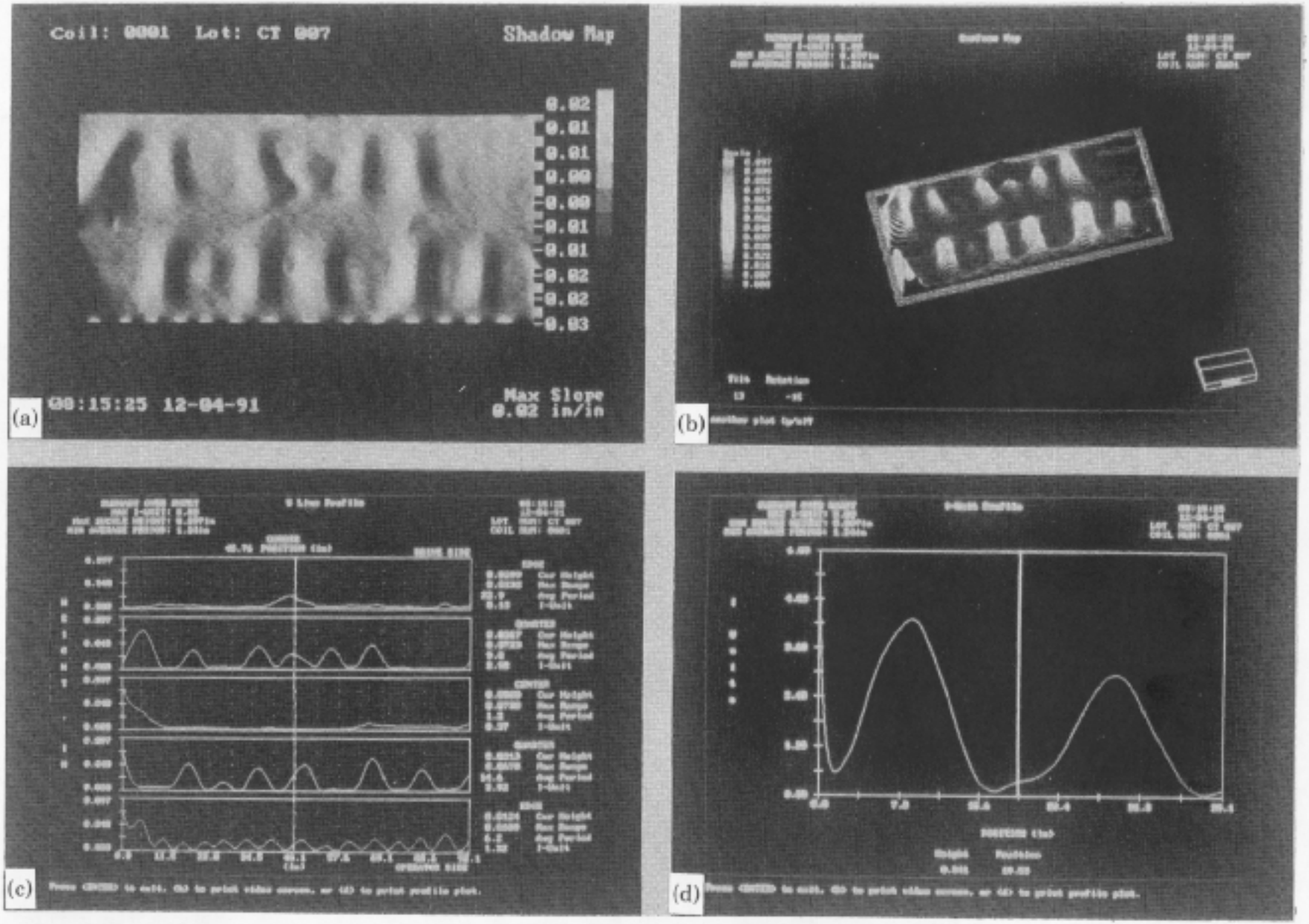

Figure 8-5. A Reflection Moiré Interferogram of an Aluminum Sheet Processed with the Phase Shift Technologies System. (a) Shadow map. (b) The processed surface map. (c) Line profiles. [*Source:* C. L. Koliopoulos, "Rapid measurement of sheet flatness in a production environment," *7th International Aluminum Sheet and Plate Conference on Rolling Emissions and Gauge/Shape/Profile Technology, Nashville, TN, June 23-26, 1992,* Reprinted with permission of C. L. Koliopoulos, Phase Shift Technologies.]

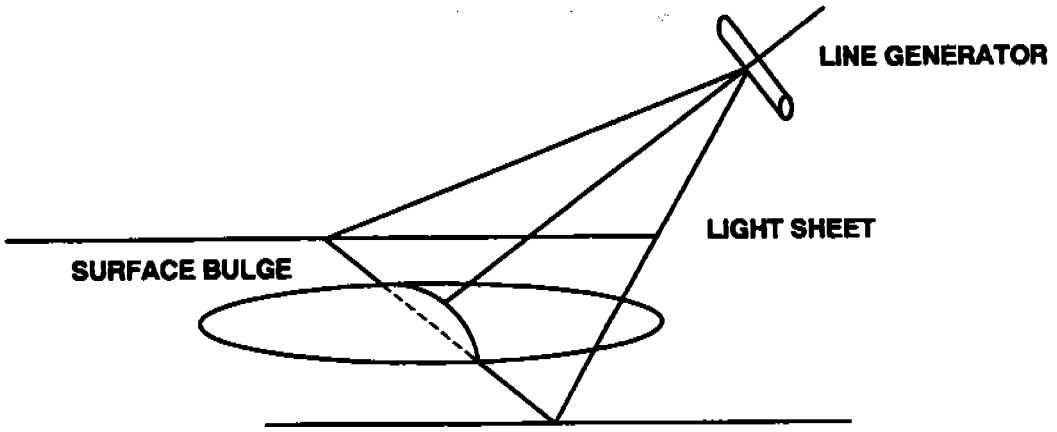

Figure 8-6. Principle of Structured Light.

The concept of D Sight is related to the schlieren method for visualizing index of refraction gradients or slopes in an optical system. It can be very simple and easy to implement with fairly low-cost materials. A schematic is shown in Figure 8-7. An incandescent light source and a large retroreflective screen, such as ScotchLite™ (the material used in highway signs), are located on either side of the surface region being inspected at an angle of about 60° from the surface normal. An observer positions his eye or a camera above the light source. The surface being examined must be fairly specularly reflective. If the surface is not polished or otherwise shiny, reflectivity can be enhanced by wetting the surface with water, oil, or some other fluid. Light from the source reflects from the surface and onto the retroreflective screen. The retroreflective screen attempts to reverse the light along the original path. Because the screen is not a perfect retroreflector, the return light is actually scattered into a cone, rather than along a single ray. The intensity of the cone is brightest along the nominal ray path, but falls off as light departs from that central ray. Because the observation point is offset slightly from the source, the brightness of the image of the surface is reduced from what one would see exactly at the source position. Light striking a surface defect is deviated at an angle from the main ray bundle. Thus, the surface brightness at a point is a function of the surface slope at that point relative to the average surface slope. The result is that a positive surface slope appears darker, and a negative slope appears brighter, than the surrounding surface. The net effect is the same as if a flashlight were used to illuminate a surface at grazing incidence, except that with D Sight the illumination is more controlled.

D Sight has been shown to visualize surface anomalies greater than 0.020 mm, including dents and ripples in surfaces (Figure 8-8), corrosion-induced pillowing (Figure 8-9), corrosion associated with fasteners, including exfoliation corrosion around steel fasteners (Figure 8-10), surface cracks, and barely visible impact damage on composites. D Sight can be coupled to a video image processing system for documentation, enhancement, and interpretation of observed defects.

One possible problem with D Sight is that the technique shows virtually every deviation on the surface, regardless of whether it is a defect or a normal result of manufacture. Depressions associated with rivet installation show up clearly and could be confused with corrosion-induced pillowing. Scratches, and even fingerprints on the surface, can also show up and possibly confuse the inspector. Further research must be performed to control the sensitivity of the observation and add the appropriate interpretations to observations. Characterization against calibrated samples should be performed.

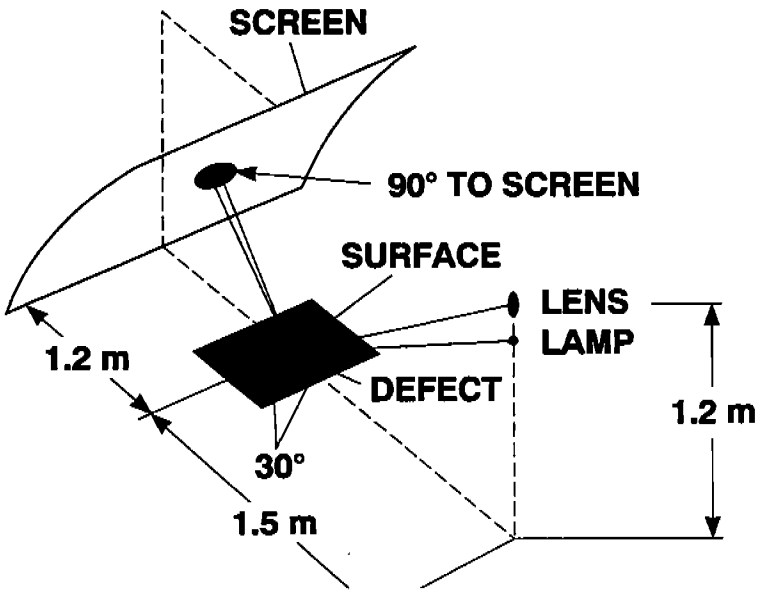

Figure 8-7. Principle of D Sight. [*Source:* J. P. Komorowski, et al., "Recent progress in the application of Diffracto Sight to inspection of aircraft structures," presented at *1992 USAF Structural Integrity Conference*, 1-3 December 1992, San Antonio, Texas. Reprinted with permission of J. P. Komorowski, National Research Council, Canada.]

8.2.4 Video Image Enhancement.

Image processing is the ability to modify images that have been converted to a digital format to extract additional information from the scene. Rather than depending upon a visual interpretation of a scene, an inspector or analyst can gain information about objects of interest, including the number, the size, and the orientation of objects of interest. With processing, images can be boosted or enhanced so that marginally identifiable objects become more detectable, or perhaps, even automatically detected and identified.

Any instrument that can acquire an image with a video camera can benefit from image enhancement. Recent advances in miniature video cameras as well as fiber-optic borescopes have made it possible to obtain permanent images of regions previously accessible only by the unaided human eye, if at all. Although human observers have visual acuity that is as good as any detector, as well as a remarkable ability to detect and interpret even threshold visual data, they suffer from subjective judgment that can impair a decision about an inspection site. For example, poor lighting, a poor observation angle, or a momentary distraction can hide a possible defect from detection. Image processing permits the freeze-frame capture, enhancement, and display of an image, along with the application of algorithms that could identify, measure, and classify defects or objects of interest.

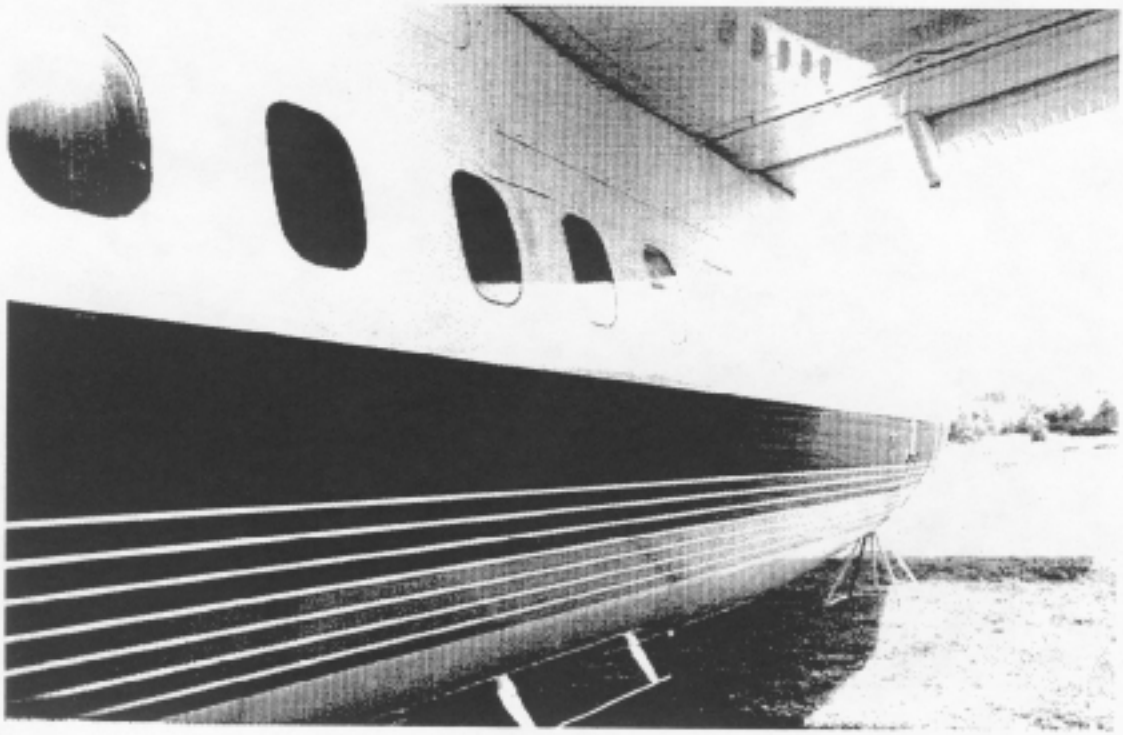

AMBIENT

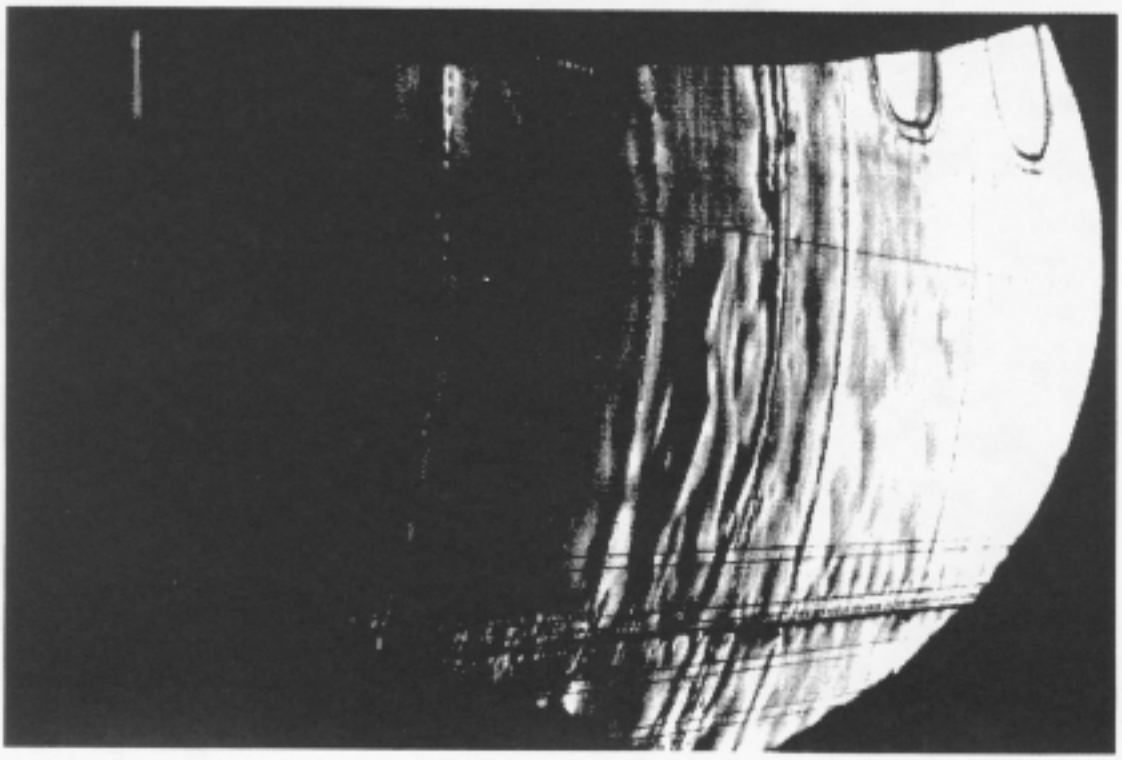

D SIGHT

Figure 8-8. A Center Fuselage Section of a Commuter Aircraft. D Sight image demonstrates large surface area inspection capability. [*Ibid.* Reprinted with permission of J. P. Komorowski, National Research Council, Canada.]

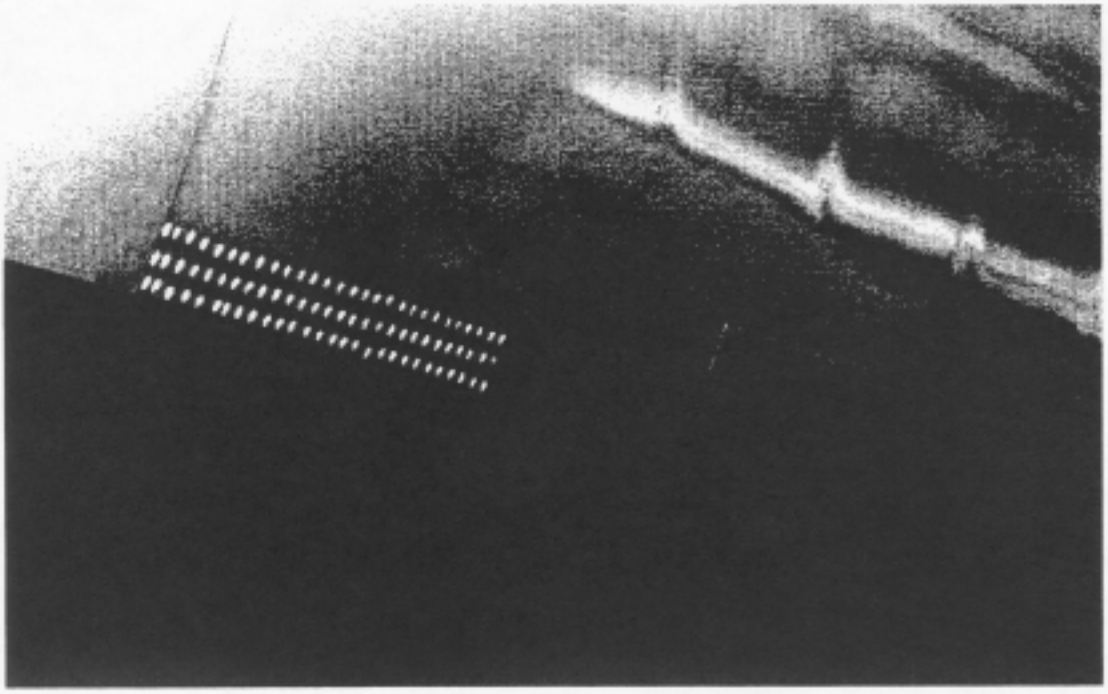

AMBIENT

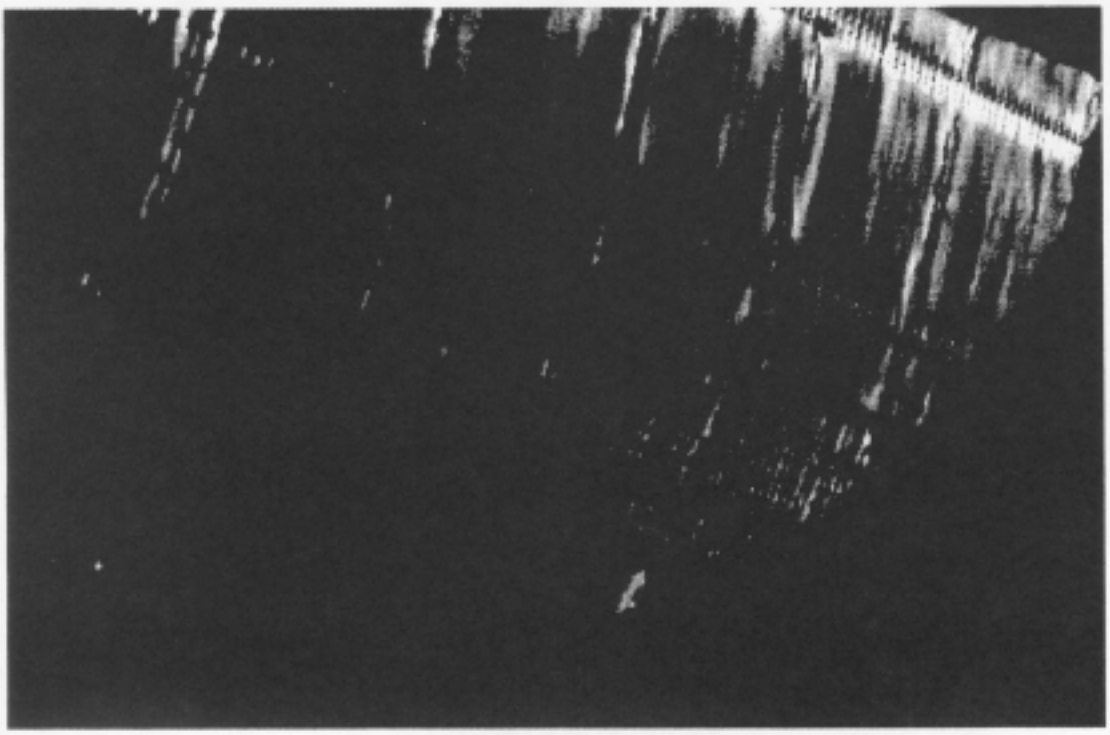

D SIGHT

Figure 8-9. A Jet Transport Horizontal Lap Joint. Note "pillowing" outside the patch repair indicative of corrosion. [*Ibid.* Reprinted with permission of J. P. Komorowski, National Research Council, Canada.]

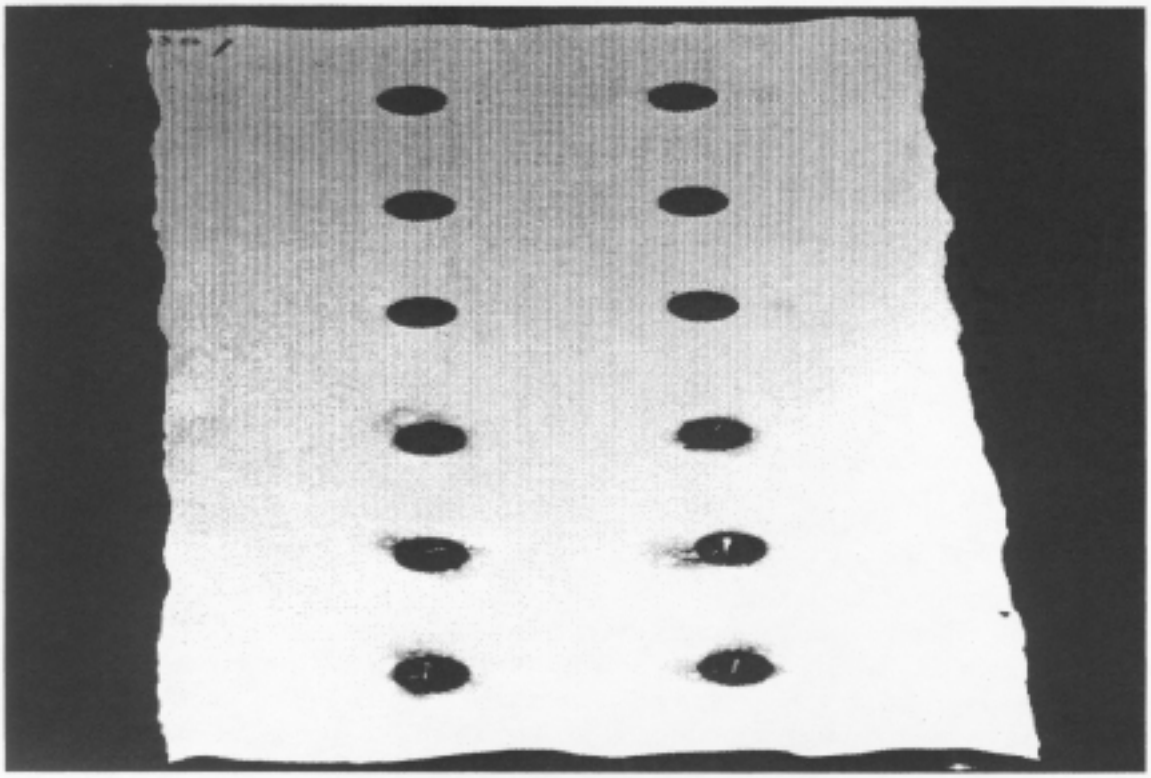

AMBIENT

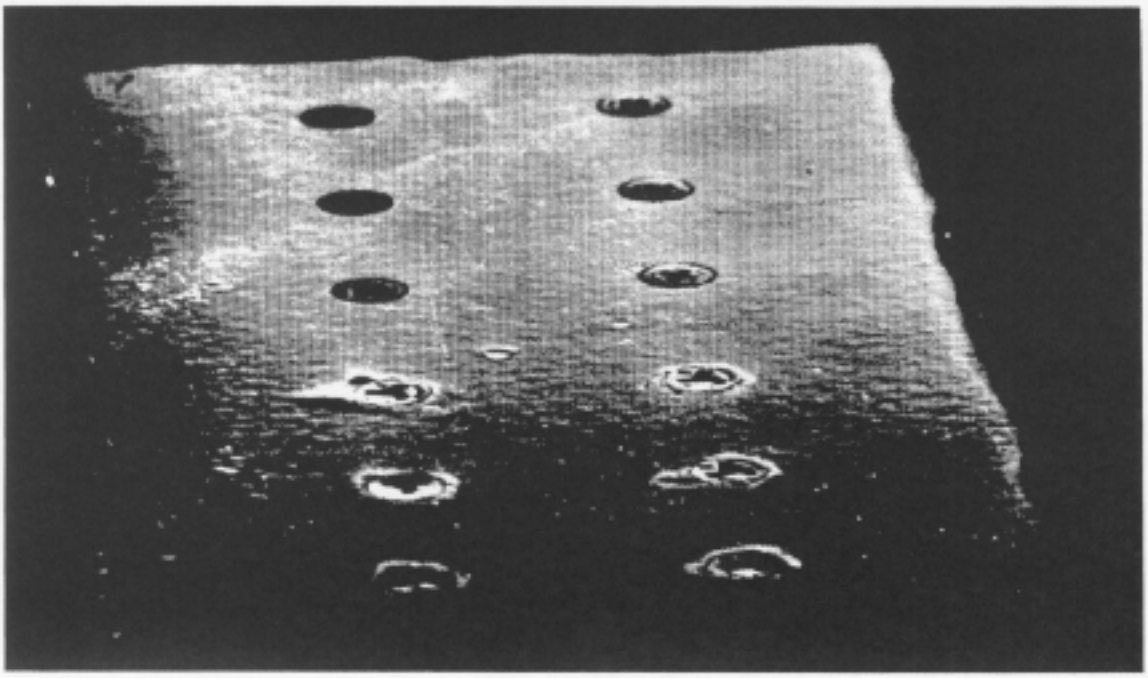

D SIGHT

Figure 8-10. A Corrosion Specimen with Two Types of Fasteners. Corrosion can be observed on the D Sight image around the lower six fasteners. [*Ibid.* Reprinted with permission of J. P. Komorowski, National Research Council, Canada.]

Image processing includes a wide variety of tasks. Among these tasks are image acquisition, contrast enhancement, geometric transformation, spatial and statistical filtering, and feature measurement and identification. For image acquisition, systems are available that can grab single or multiple frames of video data, or in the more sophisticated systems can process data in real time. In the contrast enhancement phase, an image can be altered with a number of algorithms, including histogram equalization and linearity (gamma) correction, to produce an image that reveals more information than gained by the unaided eye. With geometric transformation, images can be rotated, flipped, zoomed, or distorted according to desired rules to remove camera deficiencies or present the image from a different apparent viewpoint. With filtering techniques, edges of images can be sharpened or smoothed to enhance particular features of interest. To increase ease of feature measurement and identification, images can be colorized according to particular rules to code the scene.

Because image processing has moved to the PC environment only recently, the marriage of image processing and boroscopy is still in its infancy. Until a few years ago, most image processing was done on relatively large, expensive, mainframe computer platforms, and the imagery was generally not acquired and processed in real time. Hence, the use of image processing technologies for real-time inspection was not very practical, except perhaps in a factory assembly line environment. The development of inexpensive but fairly sophisticated frame-grabber cards and image-processing software for personal computers is now making portable image processing practical and affordable. One can take a desktop or laptop computer, complete with frame grabber and monitor, to an inspection site such as an aircraft interior and perform image manipulations in real or near-real time. As computers continue to shrink in size and cost and become even more portable, there will be even more opportunities for real time inspection and image processing.

8.2.5 Borescopes and Image Processing.

The major problem with borescope systems is that direct dimensional measurements of objects cannot be made readily. Often, the size of a defect is important when one must determine if a replacement is required. The borescope is a short-focal-length lens system that has a relatively large amount of linear distortion even for objects that are viewed end-on, and for extended three-dimensional objects there is a large amount of parallax distortion. Often the viewing geometry is unknown. If an object lies at an oblique angle to the line of sight there is no obvious scale with which to size the image.

Another problem is that, depending upon the distance of the borescope probe to the object under examination and the reflectivity of the object, the viewed image can vary in degree of illumination, especially when the object covers a large depth of field. These wide variations in illumination can mask subtle defects.

8.3 PRESENT APPLICATIONS.

8.3.1 Moiré Interferometry.

Most of the applications of moiré have been limited to research tools, particularly the use of in-plane moiré in fracture mechanics, composite bond strength, and crack tip propagation studies. Most researchers apparently build their own apparatus, unique to their requirements. Shadow moiré has even been used by the orthopedic and chiropractic communities to detect and diagnose scoliosis and other posture-related medical conditions.

Several commercial moiré instruments have been produced. The WYKO and CADEYES systems have been designed for computer-aided design and manufacturing applications, including "reverse engineering" of previously manufactured parts. The WYKO projection moiré system has been sold to a number of foot specialists for designing orthopedic shoes. The CADEYES system, developed by the Air Gage Company,[8-14,8-15] uses a moiré technique for 3D non-contact inspection and coordinate measurement of small parts. The Phase Shift Technologies reflection moiré system was developed for the aluminum can industry to be used in the flatness inspection of sheet aluminum stock. The shadow moiré system known as SMOOPI[8-9] has also seen limited use in surface damage inspection of composite materials in aircraft. The system has probably not seen its full potential yet. Other companies that have produced moiré measurement systems and components include Dolan-Jenner and Gradient Lens Corporation. Principal applications have been for on-line machine vision and measurement systems in manufacturing inspection.

8.3.2 Structured Light.

The most prevalent use of structured light has been in robotic and machine vision applications. A common application has been as a proximity sensor for a robot arm, whereby a known distance from an object is reached when the image of the structured light pattern reaches a designated part of a detector surface.

Structured light has been incorporated into a measuring video borescope manufactured by Welch-Allyn, called the ShadowProbe. This instrument projects a shadow, rather than a line, on a part being viewed through the video borescope head. The shadow defines an oblique plane in space. By observing the displacement of the shadow from the nominal, a depth measurement is made.

A system for measuring smooth, featureless surfaces such as aircraft wings was reported by Yeung. This system projects an array of 32 by 32 spots on a surface.[8-16]

A variation on structured light topography was available some time ago in the form of the "light section" microscope. In this system, a slit of light is projected onto a surface through an objective at an oblique angle. It is not known if this instrument is still available.

8.3.3 D Sight.

D Sight has been used by the automobile industry for the inspection of body panels and metal-working dies.[8-17] It is an alternative for the inspector who must otherwise squint at a surface at grazing incidence under poor or uncontrolled illumination to search for irregularities in the panel, such as paint drips, dents, or poor-quality stampings.

8.3.4 Video Image Enhancement.

Until a few years ago, most image processing was done on relatively large, expensive computer platforms, and the imagery was generally not acquired and processed in real time. Hence, the use of image-processing technologies for real-time inspection was not very practical, except perhaps in a factory assembly line environment. The development of fairly sophisticated frame-grabber cards and image-processing software for personal computers is now making portable image processing practical and affordable. One can take a desktop or laptop computer,

complete with frame grabber and monitor, to an inspection site such as an aircraft interior and perform image manipulations in real or near-real time. As computers continue to shrink in size and cost and become even more portable, there will be even more opportunities for real-time inspection and image processing.

8.3.5 Borescopes and Image Processing.

Olympus markets a video image analyzer system, the IW-1, that addresses the measurement problems discussed in paragraph 8.2.5: linear distortion, parallax distortion, and variance in illumination. The operator can input into the system a wire frame model of a known part to be measured. The operator superimposes the image of the wire mesh over a stored image by manipulating cursor keys. The system uses this match to calibrate the image orientation and magnification. Measurements of linear dimensions of interest along a surface can then be made on the image.

The system also has a frame-grabbing and frame-storage capability. The system allows contrast manipulation of the image, as well as comparison of the image to stored images by using a digital zoom capability. Also, an internal modem permits transmission of images to remote locations for viewing and inspection by personnel not on site.

Welch-Allyn markets a competing video borescope-based processor that is used primarily to measure dimensions, but that can also handle depth measurements. This instrument, called the ShadowProbe, uses a structured illumination approach to measurement. It projects a line shadow from the illuminator at an oblique angle to the line of sight of the camera lens. The relative position of the shadow in the image is a measure of the distance to the surface. Depth of a site such as a scratch or groove is then manifest as a departure from straightness of the shadow. Measurements are made by manipulating cursors and reading the indicated display. Instrument Technology, Inc., markets a videoscope with image enhancement capabilities that include freeze frame, contrast enhancement, digital zoom, and split screen viewing from multiple cameras.

8.4 AIRCRAFT APPLICATIONS.

8.4.1 Moiré Interferometry.

To date, development of moiré methods for use in routine aircraft inspection has been limited, although there have been numerous applications of moiré to aircraft structural problems. As of 1988 the SMOOPI was to have been field-tested at Navy depots for composite damage assessment. It was also to have been incorporated in the McDonnell Douglas MAUS system.[8-9]

Aircraft inspection applications for which Moiré methods have the greatest potential are in the detection and classification of surface irregularities such as corrosion-induced paint liftoff, pillowing induced by corrosion between faying surfaces, and identification of potential damage sites, such as dents and dings and surface damage in composite materials. Moiré methods also have potential for use in detecting bending or twisting of structural members such as ribs and spars.

8.4.2 Structured Light.

General Electric developed a non-contact profilometer based upon structured light for use on jet engine turbine blades. This system locates such defects as nicks, pits, cracks, and dents. It

uses two optical wavelengths in order to correct for variations in surface reflectivity. Boeing has developed a structured light system for measuring the depth of scratches on aircraft skins.[8-18] This system generates a line with a laser and a cylindrical lens at normal incidence and images the line with a microscope objective and CCD camera at 45° to the normal. A microcomputer processes the acquired image and calculates the feature depth.

8.4.3 D Sight.

Douglas Aircraft studied D Sight as an inspection tool for the detection of impact damage, extent of damage, and quality of repairs for carbon/epoxy composites.[8-19] A test by Komorowski[8-20] shows buckling in the skin of a commuter aircraft, as well as pillowing in a transport jet lap-joint repair. Boeing Aircraft has also investigated the use of D Sight.

The results of using a portable D Sight system to inspect a 727 transport and a deHavilland Dash 8 in broad daylight were reported at the 1992 USAF Structural Integrity Program Conference.[8-21] The system contains a video camera and image processor. Using a 0.3 m^2 inspection area, the inspection team could cover an aircraft at a reported rate of 18 m^2/hr.

8.4.4 Video Enhancement of Borescopes.

Borescopes have been used to inspect the interiors of aircraft engines, as well as otherwise inaccessible regions such as the interiors of landing gear struts. In fact, boroscopy of engines is a highly developed discipline, with much cooperation between the engine manufacturers and borescope manufacturers in the development of inspection kits and procedures for specialized problems. Borescopes could also be used to look for corrosion in aircraft regions such as cabin interiors where traditional inspection has been performed by disassembly or removal of interfering panels or structures. Image processing would permit enhancement, measurement, and documentation of these areas.

Remote transmission of images can permit supervisory personnel to make maintenance and repair decisions when an aircraft is at a distant location. This capability was demonstrated at an Olympus-sponsored event in which video engine inspection was demonstrated to a remote audience.[8-22]

Boeing has combined machine vision, including neural network processing methods, with video borescope observation to measure faying surface gaps for subsequent shim fabrication.[8-23] This application demonstrates the use of automated measurements for production applications. Similar applications will undoubtedly be found in aircraft maintenance and repair.

8.5 TECHNICAL CONSIDERATIONS.

8.5.1 Moiré Methods.

Advantages

- Is a wide-area imaging technique—can allow relatively rapid screening of large areas of surface at once as a purely visual (non-automated) inspection tool.
- Can give absolute surface height measurement.
- Can be non-contact.

- Has variable sensitivity, based upon grating line spacing, illumination, and viewing angles. Sensitivity can be appropriate to the size of the expected surface defects.
- Can be automated.

Disadvantages

- Measurement may be dependent upon surface treatment (rough or smooth, painted or unpainted, etc.)
- Requires somewhat sophisticated software for fully automated analysis.

Discussion

Moiré has been claimed by some to be a difficult technique to implement for general inspection applications. One problem is that when the two grids are multiplied together, the original grid, as well as the contour grid of interest, remains in view. This original grid can reduce the contrast of the contour fringes of interest and introduce additional fringes that add to the difficulty of interpretation. Also, mathematically, there are higher order components to the spatial frequency of the grating. The multiple-frequency fringe problem can be eliminated by judicious spatial filtering, that is, by limiting the resolution of the final imaging system.

A second problem is that if the surface has much curvature, such as a cylinder has, the contour fringes quickly run together, making an accurate measurement or visualization of the features of interest difficult. This has traditionally been the problem when using either the projection moiré or conventional single-screen techniques. The problem can be eliminated with a pre-distorted grating. In projection moiré, for example, the projected grating lines could be plotted to correct for the expected nominal curvature. The resulting moiré pattern would then automatically compensate for the curvature. Similar concepts for shadow moiré are also possible.

Vibration sensitivity has been another concern. Motion of approximately one grating spacing will move the resulting fringe pattern by one fringe spacing. In shadow moiré, there must be constant spacing between the object and the gratings; otherwise the resulting fringe contours will move. However, a pure lateral movement of the grating is actually beneficial because the high-frequency fringes blur out, but the contour fringes remain constant in position. In projection moiré, there must be stability in both lateral and vertical dimensions. But in both instances, the stability requirement translates to that fraction of a contour interval that is of interest. Also, with the development of CCD cameras with electronic shutters, even moving fringe patterns can be captured adequately.

Another problem with moiré has been that the interpretation of the contour fringes was difficult. In particular, establishing whether a contour represented an increase or decrease in surface height was difficult; however, this problem has been corrected. A method has been developed for automated reading of fringes that eliminates the ambiguity and interprets the fringes. As has been demonstrated with optical interferometry for optical component testing applications, one can learn how to interpret fringes with minimal training. However, if required, image processing (including the use of neural net processing)[8-24] can be implemented for automated measurement, feature extraction, and defect identification.

The non-flat, variable-reflectivity metal surfaces typical of aircraft skins have also been an impediment to the use of moiré in aircraft inspection. Although surfaces that are painted with diffuse paint are ideal for examination by moiré, a perfectly polished specular surface presents

a problem because a shadow does not form. Normal dimpling in the surface caused by rivets and other fasteners, which could be confused with corrosion-induced pillowing, presents another problem. Also, surface protuberances, such as rivets and other fasteners, can prevent close contact between a shadow moiré grating and the surface. However, there are undoubtedly solutions to these problems. The reflection moiré system of Phase Shift Technologies, in fact, *requires* a reflective surface for operation.

8.5.2 Structured Light.

Advantages

- Is non-contact.
- Permits rapid visualization of surfaces.
- Can be automated for quantitative height measurements.

Disadvantages

- Sampling is limited to number of spots or lines projected on surface.
- Spot/line measurement requires excellent resolution in imaging detector.

8.5.3 D Sight.

Advantages

- Is a wide-area technique.
- Permits rapid visualization of surface condition.

Disadvantages

- Requires reflective surface treatment (polish or oil coating).
- Shows all surface features, such as scratches, which may or may not be relevant.
- Absolute feature height measurement has not yet been demonstrated.

8.5.4 Video Boroscopy and Image Processing.

Advantages

- Internal inspection sites can be accessed without major disassembly.
- Feature heights can be measured through image processing.
- Images under difficult lighting conditions can be enhanced.

Disadvantages

- It is essentially a point measurement technique.

8.6 STATUS.

Most of the methods described are still in a laboratory development phase, although a few commercial devices have been marketed. The video-based borescope systems are probably the

most advanced and sophisticated, having developed a proven market base in the realm of jet engine inspection. The other techniques described still have to prove their utility as diagnostic tools for specific applications which have yet to be fully demonstrated.

8.6.1 Present.

Most of the methods described are still in a laboratory development phase, although a few commercial devices have been marketed. The video-based borescope systems are probably the most advanced and sophisticated. They have developed a proven market base in the realm of jet engine inspection. The other techniques still have to prove their utility as diagnostic tools for specific applications that have yet to be fully demonstrated. None of the techniques described is currently being used for routine airframe inspection by the aircraft maintenance industry. Specific inspection sites and procedures still must be developed. D Sight, moiré, and structured light all appear to have the potential for use as screening techniques (that is, they indicate to an inspector that a more detailed or confirmatory inspection is required) rather than as absolute, quantitative indicators of airframe integrity.

8.6.2 Future.

Video-based borescopes offer the most positive near-term enhanced visual aid. The technology itself is very mature, although the size and weight of the equipment that must be moved to an inspection site will undoubtedly be improved. However, specific applications to airframe inspection, in particular the economics of using the video borescopes over current methods, will have to be demonstrated. Since video borescope systems are expensive, the cost-savings over the current inspection methods will have to be proved. Current methods require the total disassembly of aircraft interiors and inspection with flashlight and mirror. Video borescopes will permit inspection of areas that are difficult to access with minimal teardown of assemblies and interiors.

Moiré, structured light, and D Sight will probably continue to serve as indicators of potential problems, rather than as absolute diagnostic techniques. The utility of D Sight will probably be demonstrated in FY 94 through an FAA-funded study by the National Research Council–Canada.

8.7 REFERENCES.

8-1. O. Kafri and I. Glatt, *The Physics of Moiré Metrology,* John Wiley, 1990, p. 89.

8-2. Lord Rayleigh, *Philosophical Magazine,* **47**, 81, 1874.

8-3. F. P. Chiang, "Moiré methods of strain analysis," in *Manual on Experimental Stress Analysis,* 3rd. ed., A. Kobayashi, editor, Society for Experimental Stress Analysis, Westport, Conn., 1978.

8-4. Y. Y. Wang, F. P. Chiang, R. S. Barsoum, and S. T. Chou, "Study of displacement and residual displacement field of an interface crack by moiré interferometry," *Proceedings SPIE **1554B,*** 1991.

8-5. F. P. Chiang, C. L. Yuan, R. Krishnamurth, "Moiré strain gauge with high sensitivity," *Optical Eng.* **27,** No. 3, p. 231, March 1988.

8-6. T. S. Gates, "Photogrammetry as a means of mapping postbuckled composite surfaces," *Proceedings of 1985 Spring Conference on Experimental Mechanics.*

8-7. H. Takasaki, "Moiré topography," *Appl. Opt.* **9,** p. 1467, 1970.

8-8. B. Drerup, W. Frobin, and E. Hierholzer, eds., *Moiré Fringe Topography and Spinal Deformity,* Gustav Fischer Verlag, Stuttgart, 1983.

8-9. A. E. Scotese, *A Low Cost Shadow Moiré Device for the Nondestructive Evaluation of Impact Damage in Composite Laminates,* Report No. NADC-90011-60, Naval Air Development Center, Warminster, PA, 1 March 1990.

8-10. R. N. Shagam, "Heterodyne interferometric method for profiling recorded moiré interferograms," *Optical Engineering* **19**, No. 6, 1980, p. 806.

8-11. C. L. Koliopoulos, N. W. H. Sufi, "Rapid measurement of sheet flatness in a production environment," *7th International Aluminum Sheet and Plate Conference on Rolling Emissions and Gauge/Shape/Profile Technology, Nashville, TN, June 23-26, 1992.*

8-12. H. G. Maas, "Automated photogrammetric surface reconstruction with structured light," *Proc. SPIE* **1526** *Industrial Vision Metrology,* 1991, p. 70.

8-13. J. J. Lumia, "Grazing-incidence lighting techniques for machine vision inspection," *Proc. SPIE* **1614** *Optics, Illumination, and Image Sensing for Machine Vision VI,* 1991.

8-14. L. H. Bieman, K. G. Harding, and A. Boehnlein, "Absolute measurement using field shifted moiré," *Proc. SPIE* **1614** *Optics, Illumination, and Image Sensing for Machine Vision VI,* 1991, p. 259.

8-15. A. Prabala, L. H. Bieman, "From Electronic Imaging to CAD: Reverse Engineering Now," *Advanced Imaging,* November 1991, p. 16.

8-16. K. K. Yeung, P. D. Lawrence, "A low cost three-dimensional vision system using space-encoded spot projections, *Proc. SPIE* **728** *Optics, Illumination, and Image Sensing for Machine Vision,* 1986, p. 160.

8-17. R. L. Reynolds and O. L. Hageniers, "Optical enhancement of surface contour variations for sheet metal and plastic panel inspection," *Proc. SPIE* **95** *Optical Testing and Metrology II,* 1988.

8-18. D. P. Sarr, "Scratch measurement system using machine vision: Part II, *Proc SPIE* **1708** *Applications of Artificial Intelligence X:" Machine Vision and Robotics,* 1992, p. 811.

8-19. D. J. Hagemaier, "Nondestructive testing developments in the aircraft industry," *Materials Evaluation,* Vol. **49,** No. 12, December 1991, p. 1470.

8-20. J. P. Komorowski, D. L. Simpson, and R. W. Gould, "Enhanced Visual Techniques for Rapid Inspection of Aircraft Structures," *Materials Evaluation,* Vol. **49,** No. 12, December 1991, p. 1486.

8-21. J. P. Komorowski, R. Gould, D. Simpson, and O. Hageniers, "Recent progress in the application of Diffracto Sight to inspection of aircraft structures," presented at *1992 USAF Structural Integrity Program Conference, 1-3 December 1992, San Antonio, Texas.*

8-22. *Proceedings of Remote Visual Inspection of Aircraft,* 2nd International Symposium, August 27, 1992, Cincinnati, OH.

8-23. D. P. Sarr, T. W. Jurick, "Faying surface-gap measurement of aircraft structures for shim fabrication and installation," *Proc. SPIE* **1469** *Applications of Artificial Neural Networks II,* 1991.

8-24. B. G. Grossman, F. S. Gonzalez, J. H. Blatt, and J. A. Hooker, "Detection, location and quantification of structural damage by neural net processed moiré profilometry," *Proc. SPIE* **1614,** *Optics, Illumination, and Image Sensing for Machine Vision VI,* 1991, p. 194.

9. INFRARED THERMOGRAPHY.

9.1 SUMMARY.

The temperature distribution on an aircraft skin or component can be measured optically by the radiation that it produces at infrared wavelengths. Several techniques have been developed that use this temperature information to characterize the thermal properties of the sample being tested. Many defects affect the thermal properties of those materials. Examples are corrosion, debonds, cracks, impact damage, panel thinning, and water ingress into composite or honeycomb materials. By the judicious application of external heat sources, these common aircraft defects can be detected by an appropriate infrared survey. Several organizations have demonstrated techniques for infrared structural inspection of aircraft in field tests at maintenance facilities. However, none of these techniques is currently in widespread use in the aviation field. Use of thermography techniques currently range from laboratory investigations to fielded equipment. The more advanced systems are in the prototype stage, and their design and operational feasibility for use on transport aircraft are being evaluated.

9.2 TECHNICAL BACKGROUND.

All objects with a temperature above absolute zero radiate energy as described by Planck's radiation equation.[9-1] An object radiating exactly as predicted by this equation is referred to as a *blackbody*. The spectral output of a near-room-temperature blackbody in the wavelength band of 1 to 20 μm is shown by the dashed curves of Figure 9-1. Commercial infrared devices typically operate in the 2-to-5 or 8-to-12 μm wavelength band. These wavelengths are commonly referred to as mid-infrared or simply infrared (IR). Several existing IR wavelength regions afford good atmospheric transmission. The unbroken curve of Figure 9-1 is a plot of the relative spectral transmission of 1 km of standard sea-level air. For room-temperature objects, the 8-to-12 μm band contains more usable energy because the radiated energy is higher and the air attenuation is less. Either the 2-to-5 or 8-to-12 μm band can be used if enough infrared signal is available.

The temperature of a radiating surface can be measured optically by comparing its thermally emitted energy to that predicted by Planck's equation. A plot of the spectral emission of most radiating surfaces will have a shape similar to that predicted by Planck's equation, but the total emitted power will be less. The ratio of actual emitted power to ideal emitted power is the emissivity (ϵ) of the surface. A surface having spectral output that resembles a blackbody but emissivity that is less than unity is described as a *graybody* radiator. The temperature of objects with emissivity that varies with optical wavelength and/or temperature (non-graybody radiators) can still be determined optically by using an appropriate emissivity function. Apparent temperature resolution of much less than 1°C for high-emissivity surfaces is possible with nearly all commercial systems whether they be spot thermometers or imaging systems. Absolute accuracy of these temperature measurements depends on accurate determinations of emissivity.

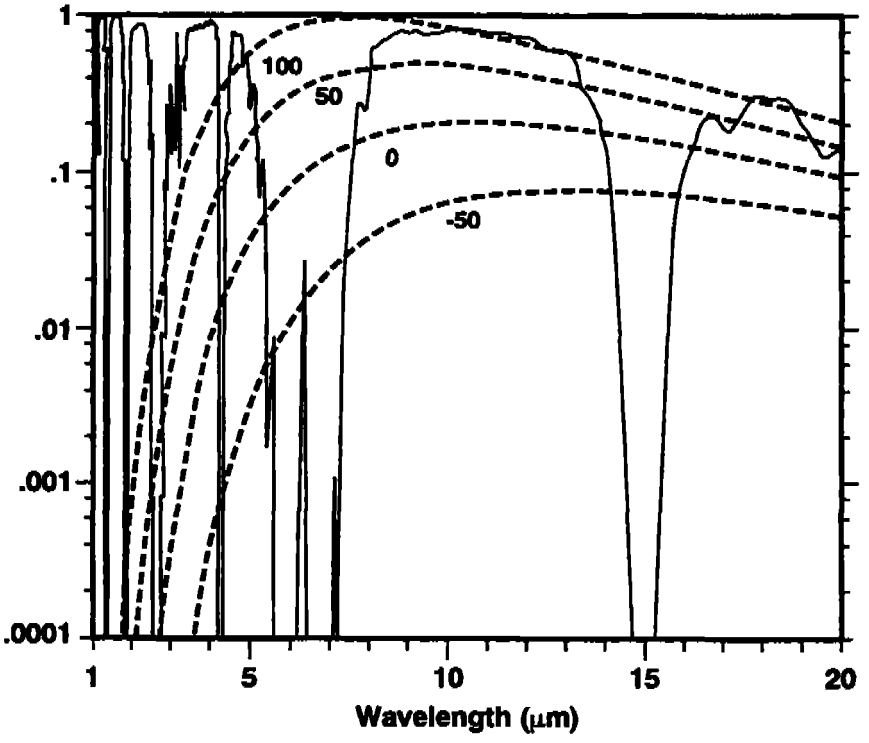

Figure 9-1. Blackbody Relative Spectral Irradiance vs. Temperature (°C) (dashed line) and Relative Transmission of 1 km of Sea-Level Air (solid line), Both Plotted as a Function of Wavelength in Microns.

The transmission (t), reflectivity (r), and emissivity (ϵ) of an object are related by the expression:

$$t + r + \epsilon = 1.$$

Most aircraft surfaces of interest for nondestructive inspection (NDI) are opaque ($t = 0$), which reduces this relationship to:

$$\epsilon = 1 - r.$$

Infrared measurements of highly reflective surfaces present a problem for two reasons. Reflected energy from adjacent sources creates interference, and the radiated thermal energy is reduced. Either of these factors can cause erroneous measurements of surface temperature.

This radiation theory is used in a variety of instruments, ranging from hand-held, remote-sensing thermometers that measure a single point to infrared imaging systems that produce two-dimensional (2D) temperature maps of a surface. Thermography normally describes systems that produce 2D thermal images, although the theory can be applied to any infrared measurement system. Commercial aircraft inspection systems will, almost certainly, produce 2D images because of the visual interpretation power provided by an image.

An IR image of an unheated object in thermal equilibrium will normally reveal little information that cannot be detected by a visual inspection of its surface. Most thermography used for materials NDI will apply heat to the object and observe the resultant temperature differences. This heat can be from nearly any source: hot air, electrical resistance heaters, lasers,

heat lamps, large optical flashlamps, etc. The properties of the material (for example, thermal conductivity, heat capacity, and thickness) determine what spatial and temporal temperature distribution will be produced by a particular heat input. Defects in the materials under test that alter these thermal properties can be detected by measuring deviations from the expected temperature patterns. Sufficient heat is needed to overcome the inherent background noise of the system. However, there is a practical upper limit because the applied heat must not damage the surface.

The unprocessed IR image data typically forms a gray-scale video image in which shades of gray represent different IR energy levels. Images with spatial resolution roughly equivalent to commercial TV broadcasts are the current standard. Several systems produce commercial video output signals and can be recorded and reproduced with commercial VCRs. Other systems require more specialized recording equipment. However, all systems can be electronically recorded for later retrieval or data archival. Data processing and image enhancements by computer software are routinely used. It is also common to colorize the images, replacing the shades of gray with contrasting colors. This colorization visually enhances the data but provides no additional sensitivity.

9.3 PRESENT APPLICATIONS.

Many different thermography applications with widely varying levels of sophistication exist. The simplest methods measure temperature distributions that occur during normal use; no additional energy source is needed. Examples of current use of these simple methods include detection of overloaded or defective electrical power distribution equipment, heat loss surveys of buildings to detect wet or missing insulation, and inspections of steam systems to detect leaks or defective components.[9-2]

Other methods that are only slightly more sophisticated measure temperature patterns that are enhanced by mechanical means such as artificial heating or a mechanical excitation that produces heat. These methods usually analyze near-static heat patterns and use little, if any, computation. An example of one of these methods is applying a heat source and then using an IR imager to view the surface to detect debonds buried in a structure.[9-3] If proper sensitivity can be achieved, these simpler methods are preferred. A difficulty with these simple systems is that aircraft skin made of aluminum has a high thermal diffusivity which dissipates small temperature gradients quickly. Reference 9-3 reports that buried debond detection by simple heating was more difficult if "material with a thermal diffusivity near that of aluminum" was involved.

The methods being used for aircraft structural inspections rely heavily upon theory and computational power to enhance the data and extract information not otherwise evident. These advanced techniques analyze transient thermal phenomena produced by dynamic thermal excitation. Major efforts are aimed at not only enhancing IR measurement sensitivity but at providing systems that produce accurate, quantitative results. Various thermographic evaluation efforts exist to detect corrosion, metal thinning, cracks, and lap-joint debonds. These efforts range from laboratory investigations to actual aircraft field tests. Previous work at Johns Hopkins University on the assessment of the integrity and thickness of coatings has recently been applied to the analagous problem of detecting aircraft corrosion.[9-4] This method shows promise, but to date has been limited to laboratory samples. Lawrence Livermore National Laboratory[9-5] has demonstrated the use of terrestrial data from both the 2-to-5 μm and 8-to-12 μm IR wavelengths to minimize the emissivity problem inherent in all infrared systems. Work is under way to extend this two-wavelength approach to aircraft maintenance applications.

9.4 AIRCRAFT APPLICATIONS.

Many aerospace companies (for example, General Electric,[9-6] Pratt & Whitney, Lockheed, Martin Marietta, McDonnell Douglas) use various thermal techniques to evaluate components for engine and aircraft manufacture. At this time, thermography is not widely used in aircraft maintenance hangars. Thermography equipment was purchased by the U.S. Air Force (Military Airlift Command) in 1989 for inspections of pressurization and thermal duct leaks, structural delaminations, and leading-edge de-icing systems on C-130 and C-141 aircraft.[9-7] British Airways uses similar imager systems (shortly after aircraft landing) to detect ice from water ingress into the composite rear horizontal stabilizer of their L1011's.[9-8] Another typical application is detection of overheated bearings or brake assemblies. These examples are analogous to the simplest thermography uses discussed in the previous paragraph. They are available and being used on a limited scale.

More technically advanced uses of thermography for structural inspection have been developed by AEA Technology,[9-9] NASA Langley Research Center,[9-10] and Wayne State University.[9-11] These major efforts are aimed at applying thermography to maintenance inspection of commercial aircraft. They have all demonstrated their thermographic capabilities on transport aircraft and continue to refine their techniques. Work with a variety of systems has been documented, but in general AEA and Wayne State concentrate on high-power flashlamp heat sources, and NASA uses intermittent excitation from incandescent quartz-lamp heaters.

A hypothetical thermography system in use at a military maintenance facility is illustrated in Figure 9-2. The major change needed when the fighter aircraft is replaced with a transport plane would be a larger hangar; the IR system would be almost identical. Figure 9-3 illustrates the components that such a system might contain. The heat source may vary depending upon the technique; the important factor is delivery of the appropriate heat energy to the surface. The induced temperature rise is a few degrees and dissipates quickly after the heat input is removed. The IR camera records the infrared patterns during and shortly after the heating sequence. The image temperature data are processed to provide more quantitative information, and the resultant patterns are displayed on the computer terminal. Currently, a human operator analyzes the screen and determines whether or not a defect has been detected. The ideal system would automate this decision-making process to remove the uncertainty of human interpretation.

An example of a typical processed aircraft thermographic image is shown as Figure 9-4. The darker shades of gray represent bonded areas, and the lighter (or white) areas represent lack of bonding. (The different colors that normally represent the varying shades of gray were omitted from the figure to facilitate the copying of this report.) Pertinent data patterns can be printed or recorded digitally for documentation or analysis purposes.

9.5 TECHNICAL CONSIDERATIONS.

9.5.1 Advantages.

- Since thermography is an optical measurement, it can be done without physical contact. A 2D image of the inspected surface helps the operator visualize the location and extent of any defects. Depending upon the spatial resolution of the IR camera and the size of the expected flaw, each image can be of a relatively large area. (Inspection areas of one square meter are currently attainable.) Non-contact imaging of relatively large areas holds the potential for rapid inspection of large surface areas.

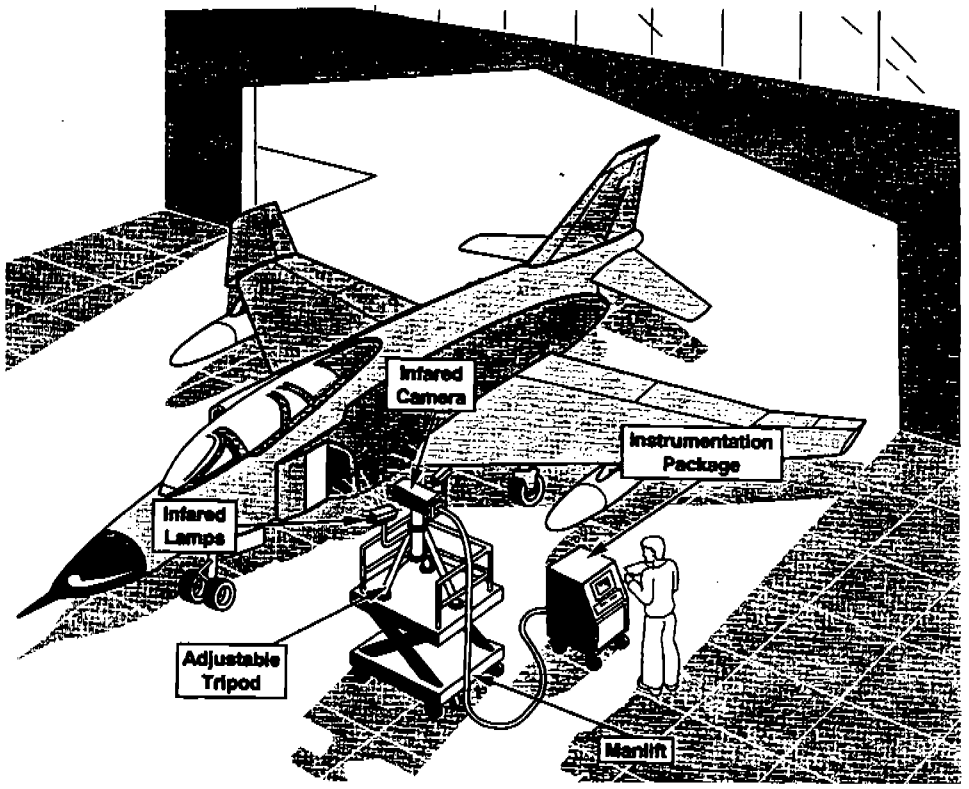

Figure 9-2. Possible Arrangement of a U.S. Air Force Thermography Inspection System. [Source: Southwest Research Institute, *Large-Area Nondestructive Inspection Scanner*, Project 17-3205. Reprinted by permission from Frank Iddings. See Reference 9-12.]

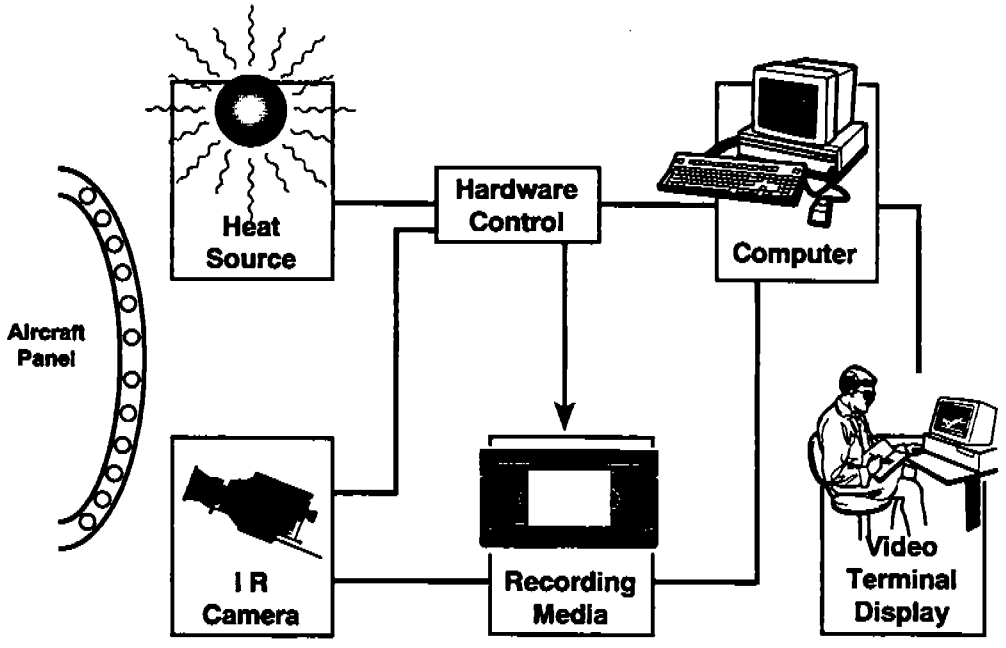

Figure 9-3. Typical Components Needed for an Advanced Infrared Inspection System.

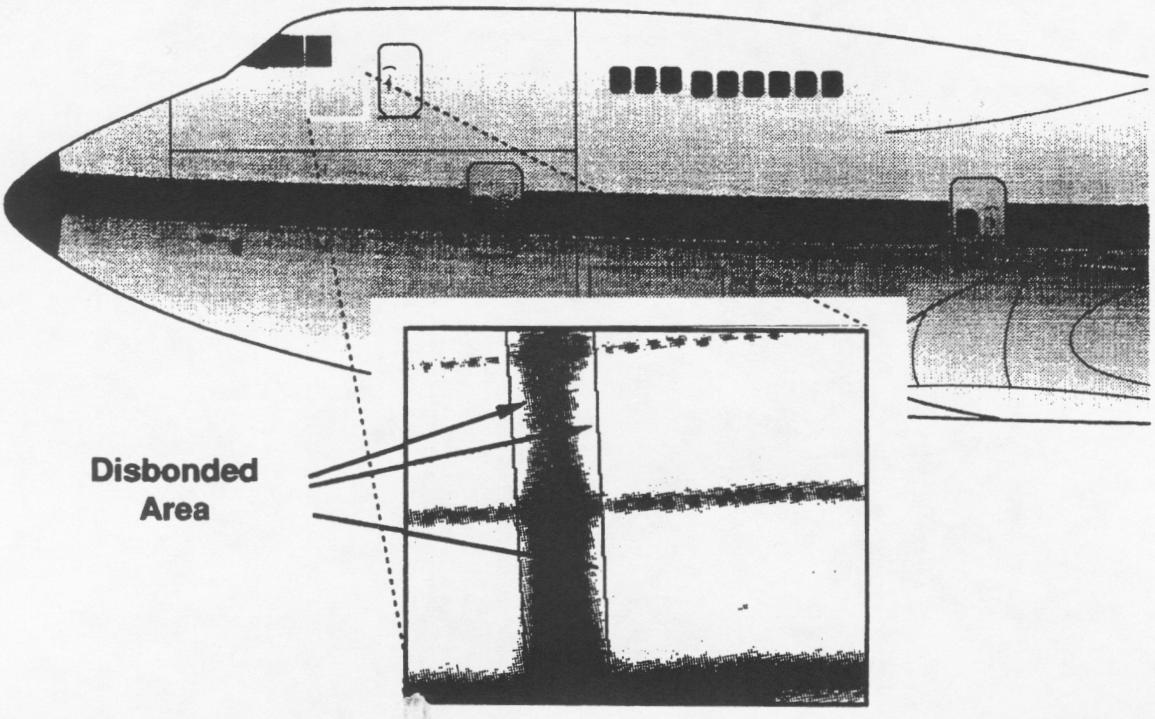

Figure 9-4. Typical Output of Advanced Thermographic Inspection System. (Courtesy of NASA Langley Research Center. Images are similar to those of Reference 9-10.)

- Neural networks applied to the IR image data have possible application for automated recognition of defects; however, no reports of field use of this technique have been published. Electronic recording of the image data holds possibilities for rapid inspection that can be followed by more thorough data analysis while other maintenance activities are being performed. Unlike X-rays, the heat sources (when properly handled) are not a hazard to nearby workers.
- Thin coats of paint conduct heat fairly well and are not a great obstacle if their presence is taken into consideration. (Different colors of paint have different emissivities.)
- Nonmetallic materials usually can be inspected more easily than metals because of a difference in thermal properties.

9.5.2 Disadvantages.

- Because of their low emissivity, bare metal surfaces are usually not good IR radiators, and they present reflection problems. Surface coatings and contaminants can also cause problems. To overcome either of these difficulties, a temporary high-emissivity coating can be applied and removed after testing. Black washable paints and black "contact paper" have been used successfully for this purpose.
- Prior knowledge of the structure being inspected is commonly needed to interpret thermography results; calibration samples similar to the area being inspected may be required for highest accuracy. This, however, is not uncommon for other technologies and is not judged to be a major impediment.
- Although the current systems can be moved about the hangar, such movement is not a one-man operation. At present, the largest elements are the computer system, the camera, and

the heat source. Since electronic systems continue to shrink in size, eventually every element except the heat source should become smaller.

- With any of these systems the nonuniformity of the applied heat as well as variations in surface emissivity make interpretation of raw data difficult. Even with sophisticated mathematical analysis to minimize these effects, temperature differences and patterns tend to be more important than actual temperature. Damage to layers deep within a structure is more difficult to assess than damage to surface layers because the larger mass of metal tends to dissipate the applied heat energy.
- The high cost of advanced thermal imaging systems could inhibit industry interest. The typical IR camera system, without additional data capture and processing equipment, costs from $50K to $100K. It must be proven that the results are worth the cost.

9.6 STATUS.

9.6.1 Present.

Thermography for simple imaging evaluations of aircraft parts is available now to those willing to buy an IR imaging system. These systems are commercially available from a variety of sources and can be obtained with a variety of capabilities. The prices are in the multiple tens of thousands of dollars. Current cost considerations have no doubt limited the application of the systems. Although British Airways thought it worth the price, many others have not. As with most NDI systems, image interpretation requires an understanding of the physics of the techniques.

The more advanced thermography systems have much greater capabilities at the expense of being more complex and costly. NASA and Wayne State University continue to develop and demonstrate their systems on transport aircraft. Wayne State has used their system on 727 aircraft at Northwest Airlines in Minneapolis, on the AANC's 737 in Albuquerque, and on the aircraft corrosion coupons in Tinker Air Force Base experiments (Oklahoma City). NASA has tested its own 737 aircraft, visited Northwest Airlines to test 747 aircraft on more than one occasion, and is also planning a trip to the AANC 737. Both systems are capable of generating reduced data in the hangar in a matter of minutes. Thermal anomalies can be identified rapidly with either system. The accuracy with which these areas can be classified as corrosion or debonds is not yet as high as either group would like. Work continues on improving this accuracy as well as on efforts to miniaturize the systems and make them more suited for hangar use. Companies such as AEA Technologies, and to a lesser extent Bales Scientific, are more commercially oriented and are capable of materials inspection and even limited aircraft inspections. Any of these systems are highly specialized and require very highly trained operators to properly apply the techniques and interpret the results.

An advanced thermographic NDI system can be purchased directly or assembled from components purchased from a variety of sources. The price for such a system will be in the $100K to $300K region. Because of the high price and the lack of original equipment manufacturer (OEM) and regulatory approval for the use of these methods, sales for aircraft maintenance inspections have been limited.

9.6.2 Future.

In a study for the U. S. Air Force, Southwest Research Institute[9-12] included flashlamp-excited infrared thermography as one of the promising candidate technologies for potentially providing

rapid, large-area, nondestructive inspection of military aircraft. Similar arguments can be made for commercial aircraft. Whether flashlamp excitation, heat-lamps, lasers, or some other source will provide superior data is still uncertain. Researchers have demonstrated good results for each. Each may have its own best applications. If the utility of systems now under development can be demonstrated to the industry, it is possible that they could be used in maintenance hangars within the next five years.

Advances in IR detector technology include the recent introduction of closed-cycle detector cooling (replacing liquid nitrogen) and the replacement of scanned single-point detectors with detector arrays. Limited examples of these technologies are now available and more systems will be using them. Someday uncooled detectors may be available.

The emphasis of much of the work related to aircraft NDI is on producing IR inspection techniques that are more quantitative and easier to use. The goal is to produce systems that can be operated by maintenance personnel with training similar to that currently given to NDI technicians.

Both NASA and Wayne State hope to transfer their technology into the marketplace in the near future. NASA has made and will continue to make their various infrared technologies available through the NASA technology transfer process. A small Wisconsin firm is combining their technology with that of NASA to develop a "Forced Diffusion Thermography" system that exploits the thermoelastic effect of materials to locate defects. A commercial company has been formed by Wayne State with the intention of marketing an infrared inspection system based on the "Thermal Wave Imaging" principles developed by Wayne State.

9.7 REFERENCES.

9-1. *The Infrared Handbook*, revised edition, W. L. Wolfe and G. J. Zissis, ed., Environmental Research Institute of Michigan/Office of Naval Research, 3rd printing, Ch. 1, 1989.

9-2. J. M. Garner, "IRS-Infrared Research Services vs. $$$—The Bottom Line," *Thermosense XIV*, SPIE Vol. **1682**, p. 23, 1992.

9-3. M. T. Quinn, J. R. Hribar, R. L. Ruiz, and G. F. Hawkins, "Thermographic Detection of Buried Debonds," *Review of Progress in QNDE*, Vol. **7B**, p. 1117, Plenum Press, 1988.

9-4. J. W. Maclachlan Spicer, W. D. Kearns, L. C. Aamodt, and J. C. Murphy, "Characterization of Hidden Airframe Corrosion by Time-Resolved Infrared Radiometry (TRIR)," to be published in *Review of Progress in QNDE*, Vol. **12**, 1993.

9-5. N. Del Grande, "Airborne Detection of Buried Minefields," *Energy and Technology Review*, Lawrence Livermore National Laboratory, p. 9, December 1991.

9-6. R. Burkel and J. Murphy, "Infrared Imaging Systems Automate Aircraft Engine Inspection at General Electric," *Industrial Engineering*, p. 28, April 1989.

9-7. "Air Force to Use Infrared for Aircraft Maintenance," *The Infrared Scanner*, Vol. **3**, No. 1, p. 1, Inframetrics Inc., Winter 1989/1990.

9-8. J. H. Daymond, "The Introduction of Thermography as an Inspection Tool in the Operational Aerospace Environment," British Airways, presented at the ATA NDT Forum, Denver, CO, August 26-28, 1986.

9-9. C. Hobbs, D. Kenway-Jackson, and J. Milne, "Quantitative Measurement of Thermal Parameters Over Large Areas Using Pulse Video Thermography," *Thermosense XIII*, SPIE Vol. **1467**, p. 264, 1991.

9-10. H.I. Syed, W.P. Winfree, K.E. Cramer, "Processing Infrared Images of Aircraft Lapjoints," *Thermosense XIV*, SPIE Vol. **1682**, p. 171, 1992.

9-11. L. D. Favro, T. Ahmed, X. Wang, Y. X. Wang, H. J. Jin, P. K. Kuo, and R. L. Thomas, "Thermal Wave Detection and Analysis of Adhesion Disbonds and Corrosion in Aircraft Panels," to be published in *Review of QNDE*, Vol. **12**, 1993.

9-12. *Large-Area Nondestructive Inspection Scanner*, Southwest Research Institute Project 17-3205. Prepared for San Antonio Air Logistics Center, Kelly AFB, TX, under U.S. Air Force Contract #F4606-89-D-0039-SA-01, October 1991.

10. Conclusions.

One of the major technical concerns currently facing the civil aviation community is that of ensuring the continued integrity and safety of structures, both airframe and engines, as these systems age. As a result, the FAA is directing a significant effort, through its National Aging Aircraft Research Program (NAARP), toward developing and identifying additional inspection methods that will enable earlier and more reliable detection of conditions in aging aircraft structures.

Emerging technologies reported on in this document are acoustic emission testing, X-ray computed tomography, backscatter radiation, reverse geometry X-ray, the advanced electromagnetic techniques of magneto-optic imaging and advanced eddy current techniques, coherent optics, advanced ultrasonics, advanced visual, and infrared thermography. Several of these technologies have already gained acceptance and approval by the airline industry, while others require further development and evaluation to prove their potential.

The FAA is actively addressing these emerging technologies in order to keep pace with inspection needs prompted by the aging fleet. As the promising techniques discussed in this document mature, their acceptance and approval for use by the airline industry will ultimately depend on whether they can provide reliable, cost effective alternatives to the inspection methods used today.